Graduate Theses and Dissertations   Graduate School

2010

Theoretical and experimental simulation of passive vacuum solar flash desalination

Mohammad Abutayeh
University of South Florida

Follow this and additional works at: http://scholarcommons.usf.edu/etd

Part of the American Studies Commons

Scholar Commons Citation

Theoretical and Experimental Simulation of Passive Vacuum Solar Flash Desalination

by

Mohammad Abutayeh

A dissertation submitted in partial fulfillment
of the requirements for the degree of
Doctor of Philosophy
Department of Chemical & Biomedical Engineering
College of Engineering
University of South Florida

Major Professor: D. Yogi Goswami, Ph.D.
Elias K. Stefanakos, Ph.D.
Scott W. Campbell, Ph.D.
John T. Wolan, Ph.D.
Thomas L. Crisman, Ph.D.

Date of Approval:
March 23, 2010

Keywords: Solar Energy, Seawater Separation, Desalting, Distillation, Evaporation

DEDICATION

To the loving memory of my brother, Hussein

ACKNOWLEDGEMENTS

TABLE OF CONTENTS

LIST OF TABLES

LIST OF FIGURES

xi

LIST OF SYMBOLS

Nomenclature

A	area (cm^2) / enthalpy parameter
B	enthalpy parameter
BPE	boiling point elevation (°C)
C	enthalpy parameter
CV	flow coefficient
D	diameter (cm) / enthalpy parameter
DL	disturbance loop transfer function
E	energy flow (J/min) / enthalpy parameter
f	fanning friction factor
F	heat removal factor / counter–current departure correction factor
g	gravity acceleration (cm/s^2)
h	heat transfer coefficient (W/cm^2–°C)
$\underline{H}$	molar specific enthalpy (J/mol)
H	specific enthalpy (J/g)
HC	Henry's constant (bar)
HF	Henry's coefficient (°C)
I	solar insolation (W/cm^2)
k	thermal conductivity (W/cm–°C)
K	vapor–liquid equilibrium distribution coefficient / gain
L	length (cm)
M	flow rate (g/min)
MW	molecular weight (g/mol)
n	molar amount (mol)
N	molar flow rate (mol/min) / number of vertical rows
NEA	non–equilibrium allowance (°C)

P	pressure (bar)
PA	saturated pressure coefficient
PB	saturated pressure coefficient
PC	saturated pressure coefficient
PD	nominal pipe diameter (cm)
PEC	prime energy consumption
PL	equivalent pipe length (cm) / process loop transfer function
Q	heat input rate (J/min)
r	correlation coefficient
R	universal gas constant (bar–cm^3/mol–°C)
Re	Reynolds number
S	counter–current departure parameter
s	Laplace domain frequency (1/sec)
SG	specific gravity
T	temperature (°C)
t	time (min)
TIC	temperature controller transfer function
U	overall heat transfer coefficient (W/cm^2–°C)
V	volume (cm^3)
W	work output rate (J/min)
x	mole fraction in concentrated brine
XA	cross sectional area (cm^2)
y	mole fraction in flashed vapor
Z	level or elevation (cm)
z	mole fraction before flash
α	relativity factor / absorptance
γ	activity coefficient
δ	thickness (cm)
ΔP	pressure drop (bar)
Δt	time increment (min)
ΔTm	logarithmic mean temperature difference (°C)

ε	Error
ζ	non–equilibrium allowance correlation parameter
η	efficiency (%)
μ	viscosity (Poise)
μA	viscosity coefficient
μB	viscosity coefficient
μC	viscosity coefficient
μD	viscosity coefficient
ξ	non–equilibrium allowance correlation parameter
ρ	density (g/cm^3)
ρA	density coefficient
ρB	density coefficient
ρC	density coefficient
σ	diffusion conductance parameter (g–°C$^{\frac{1}{2}}$/bar–min–cm^2)
τ	transmittance / time constant (sec)
φ	mass fraction in streams
ψ	gas phase molecular content correction factor
Ω	diffusion resistance parameter (bar)
ω	mass fraction in sea salt

Subscripts

0	dead time
Ar	argon
B	brine water tank
BO₃	borate
BP	bubble point
Br	bromide
C	condenser / controller
Ca	calcium
Cl	chlorine
CO₂	carbon dioxide

CT	condenser tube
CV	condenser vacuum
D	derivative
DL	disturbance loop
DP	dew point
E	flashed vapor
EV	evaporator vacuum
F	fluoride / fresh water tank
H	heater
H_2O	water
HCO_3	bicarbonate
HT	heater tube
I	integral
j	representative stream
K	potsium
Mg	magnesium
N_2	nitrogen
Na	sodium
NCG	representative non–condensable gas
O	orifice
O_2	oxygen
P	pump
PL	process loop
R	recovery
S	seawater tank
Salt	sea salt
SC	solar collector
SO_4	sulfate
Sr	strontium
T	thermal
V	vacuum

W	evaporator
X	seawater preheat

Superscripts

a	accumulating
C	condensed vapor
d	diffusing
i	initial / inside
id	inside dirt
in	entering
L	latent
o	reference state / outside
od	outside dirt
out	existing
sat	saturated
W	concentrated brine
w	wall

THEORETICAL AND EXPERIMENTAL SIMULATION OF PASSIVE VACUUM

SOLAR FLASH DESALINATION

Mohammad Abutayeh

ABSTRACT

Experimental and theoretical simulations of a novel sustainable desalination process have been carried out. The simulated process consists of pumping seawater through a solar heater before flashing it under vacuum in an elevated chamber. The vacuum is passively created and then maintained by the hydrostatic balance between pressure inside the elevated flash chamber and outdoor atmospheric pressure.

The experimental simulations were carried out using a pilot unit built to depict the proposed desalination system. Theoretical simulations were performed using a detailed computer code employing fundamental physical and thermodynamic laws to describe the separation process, complimented by experimentally based correlations to estimate physical properties of the involved species and operational parameters of the proposed system setting it apart from previous empirical desalination models.

Experimental and theoretical simulation results matched well with one another, validating the developed model. Feasibility of the proposed system rapidly increased with flash temperature due to increased fresh water production and improved heat recovery. In addition, the proposed desalination system is naturally sustainable by solar radiation and gravity, making it very energy efficient.

CHAPTER 1. INTRODUCTION

1.1 Overview

Fresh water demand is persistently increasing both as populations around the world keep growing and as existing fresh water reserves keep declining due to consumption and pollution. Figure 1 shows the estimated water consumption of US counties for 2000 [1]. Marine waters represent an infinite water source since 98 % of all global water is present in oceans; therefore, seawater desalination is the logical approach to meet rising fresh water demand.

Energy demand is also continually increasing due to relentless global industrialization. Oil and gas remain the primary sources of energy for most of the world; however, their reserves are dwindling, production is peaking, and consumption is harming the environment. Figure 2 illustrates the estimated energy consumption per capita of US states for 2001, while Figure 3 compares energy consumption per capita of Florida to the rest of the country for the past forty years [1]. Renewable energy sources are continually replenished by cosmic forces and can be used to produce sustainable and useful forms of energy with minimum environmental impact.

Serious economic and social disruptions are unfolding over the finite water and energy resources; hence, securing fresh water supply and employing renewable energy sources will help avoid catastrophic conflicts, continue modern lifestyles, and circumvent global warming and environmental pollution [2].

Desalination can be accomplished by separation techniques developed over the years to produce potable water. The most widespread desalination methods are given in CHAPTER 2. Momentous amounts of energy are required in all desalination processes; therefore, reducing energy demand, as well as employing renewable energy, is imperative to developing viable desalination processes. Various desalination systems driven by renewable energy have been developed over the last few years; nonetheless, most have not yet been commercially implemented due to high capital cost associated with utilizing renewable energy.

Solar radiation is a very appealing source of energy because it is available at no cost; furthermore, exploiting it has no notable adverse effect on the environment. Plenty of research and development have been undertaken to utilize this free form of energy to develop more efficient sustainable processes such as water desalination and power generation. Figure 4 illustrates the US share of solar radiation [3]. Solar energy is intermittent and requires storage; however, maximizing its use alongside developing energy efficient processes can greatly diversify energy resources, save the environment, and reduce imposed social cost [4].

Solar desalination is essentially a small–scale duplicate of the natural hydrologic cycle that produces rain, which is the primary source of fresh water worldwide. Solar insolation is preferred over other renewable energy sources to drive desalination systems because its thermal energy can be directly applied to thermal desalination schemes without adverse energy conversion requirements that usually entail certain energy losses. In addition, thermal desalination schemes are more suitable than mechanical desalination schemes for large–scale applications as will seen later.
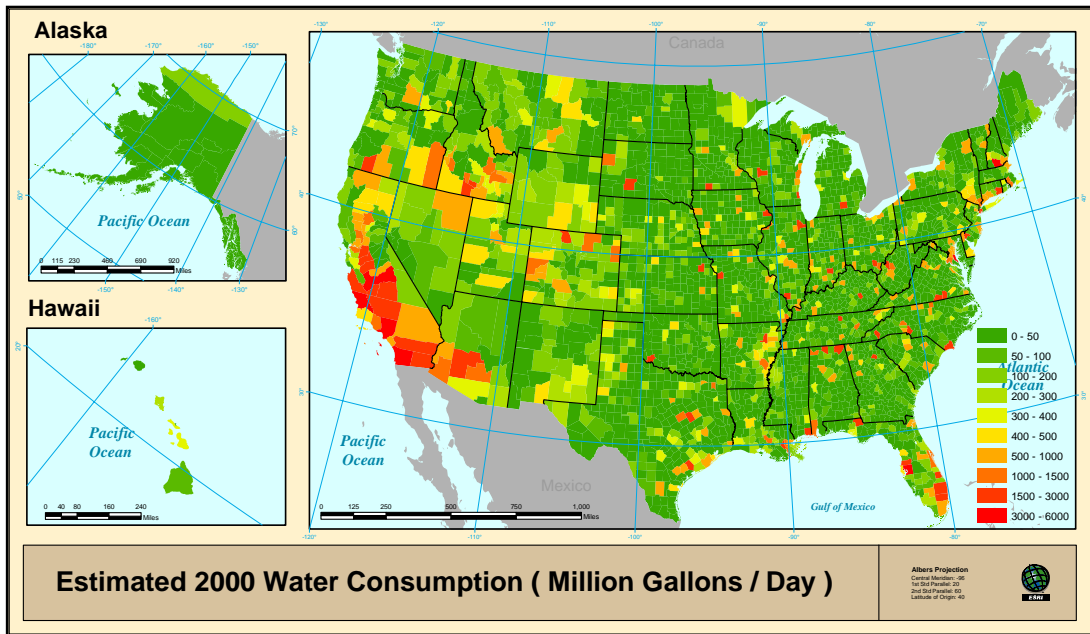
Figure 1. Estimated water consumption of US counties for 2000 [1]
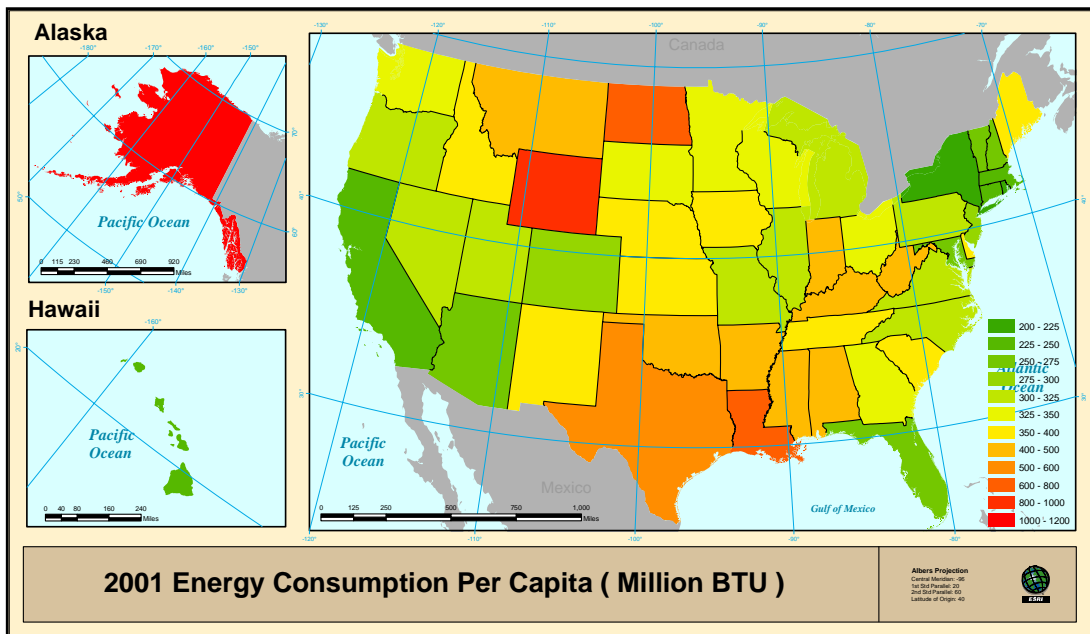
Figure 2. Estimated energy consumption per capita of US states for 2001 [1]
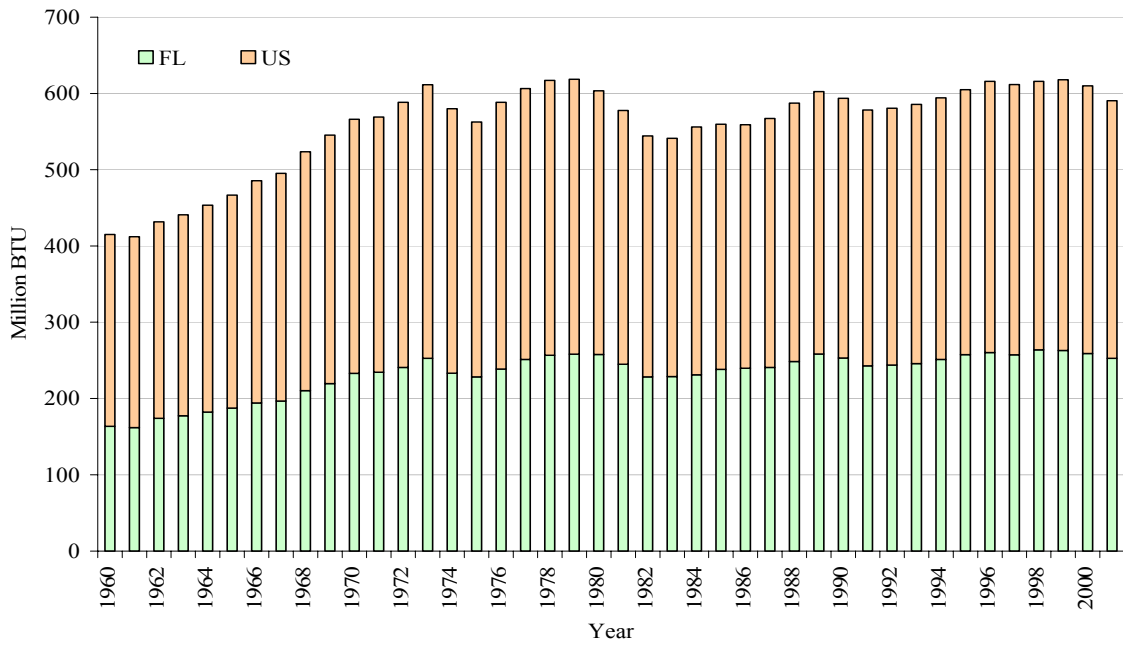
Figure 3. Estimated energy consumption per capita of Florida and the US [1]
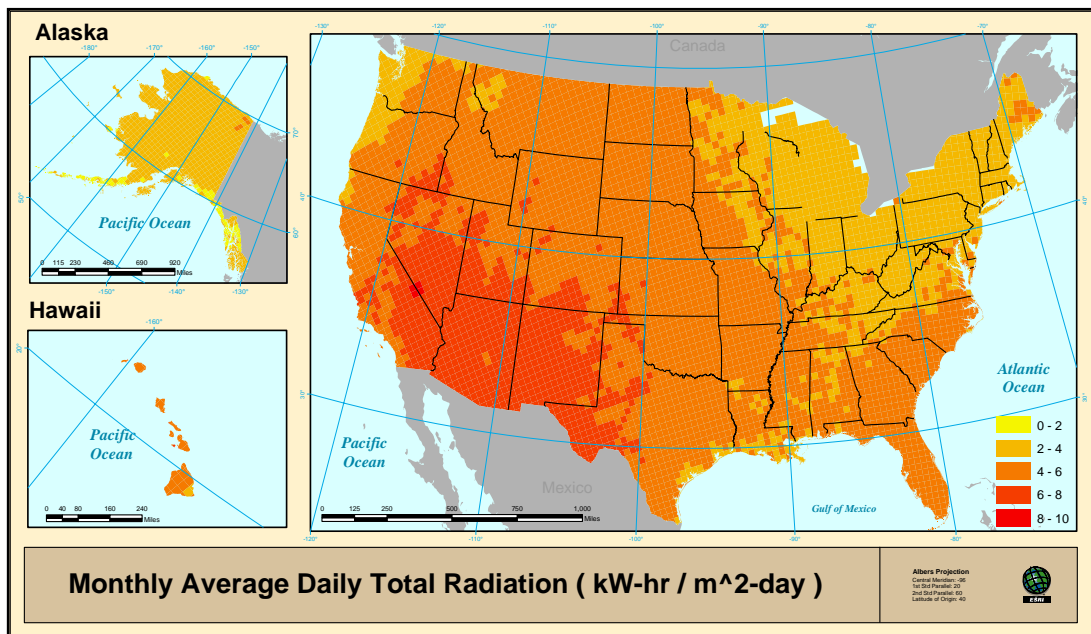
Figure 4. Monthly average daily solar insolation in the US [3]

1.2 Objective

Developing an economically–viable and environmentally–friendly desalination system involves lowering its energy demand and employing renewable energy to drive its operation. In this study, the most common desalination technique, multi–stage flash, will be modified to have its system vacuum created passively and to have its thermal energy requirements drawn from solar insolation. The proposed modifications are expected to further the feasibility and broaden the applicability of the desalination process.

Creating vacuum conditions above liquids will increase their evaporation rates. This phenomenon can be integrated into a practical continuous desalination process by repeatedly flashing seawater in vacuumed chambers to produce water vapor that will be condensed to produce fresh water. Gravity can be used to balance hydrostatic pressure inside the flash chambers with the outdoor atmospheric pressure to maintain that vacuum, while low grade heat or solar radiation can be used to heat seawater before flashing it.

The objective of this study is to simulate theoretically and experimentally a solar flash desalination process under a hydrostatically sustained vacuum and analyze its controlling variables. Theoretical simulation is accomplished by a rigorous computer code employing fundamental physical and thermodynamic relationships to describe the process complimented by reliable empirical correlations to estimate physical properties of the involved species and operational parameters of the proposed system. Experimental simulation is realized by constructing a pilot unit depicting the proposed desalination system. Theoretical and experimental simulations will be run under various analogous conditions, and their results will be compared and analyzed both to validate the developed model and to examine the feasibility of the proposed system.

CHAPTER 2. DESALINATION

2.1 Conventional Desalination

Desalination is very energy intensive and requires costly infrastructure; therefore; several desalination processes have been developed over the years to produce fresh water from seawater economically. These can be classified according to the applied separation scheme into thermal, physical, and chemical processes.

Thermal desalination processes produce a fractional phase change of liquid seawater to either vapor or solid. The new phase is then separated from the bulk brine water producing fresh water, while the latent heat of phase change is reclaimed. Multiple effect evaporation, multi–stage flash, vapor compression, and indirect contact freezing are examples of thermal desalination processes.

Physical desalination processes extract fresh water from seawater by applying pressure or electric potential across a membrane. Either fresh water or solute ions travel through the semi–permeable membrane due to the mechanically induced gradient yielding the desired separation. Reverse osmosis, electro–dialysis, and nano–filtration are examples of physical desalination processes.

Chemical desalination processes extract fresh water from seawater by precipitating its salts due to chemical reactions. These processes are less common because they are usually too expensive to produce fresh water. Ion exchange, gas hydrate, and liquid–liquid extraction are examples of chemical desalination processes.

Selecting a suitable desalination process requires several design considerations such as: start–up time, seawater quality, seawater supply, maintenance requirements, energy efficiency, capital cost, operating cost, and other site specific factors [2]. Global distribution of these processes is illustrated categorically in Figure 5 and geographically in Figure 6 as percentages of total installed capacity [5].

Selecting a particular desalination process also requires knowledge of its specific design limitations. Discussing the design limitations of different desalination processes is beyond the scope of this study, but such discussions are widely available in academic and business literature [6]. A brief summary of these limitations is provided here.

The energy needed to recover fresh water from seawater increases with increased salinity; therefore, limiting recovery rates is one way to optimize the desalination process. Also, increasing process efficiency usually involves increasing equipment size, which entails capital cost increase. Optimum design of desalination plants generally includes analyzing the tradeoff between energy and capital costs to minimize production costs. In addition, scaling is a major issue in desalination because it fouls mass and heat transfer surface areas, reducing both capacity and efficiency. Scaling can be minimized by reducing the saturation limit of saline water via dropping the operating temperature and limiting the recovery rates in addition to chemical pretreatment and lime soda softening. Finally, desired water quality directly influences which desalination path to take [6].

Desalination is a continually evolving field with many of its processes under research and development. In addition, a wide variety of cost effective hybrid processes are proposed as alternatives to the rather expensive common commercial processes. A brief discussion of the major desalination processes is provided next.
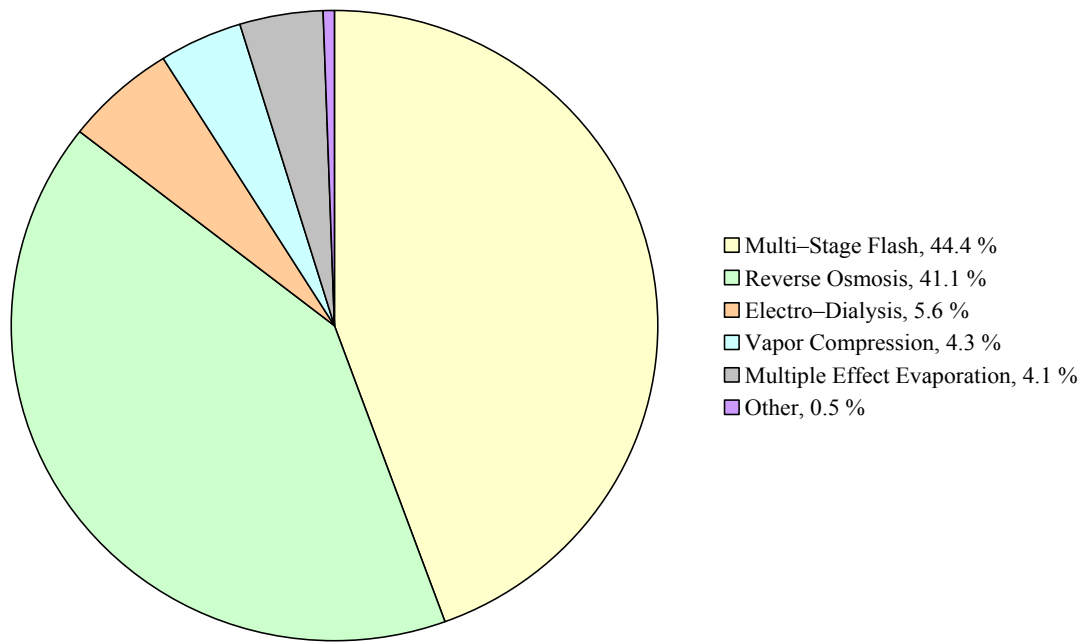
Figure 5. Global distribution of installed desalination capacity by technology [5]

- Multi–Stage Flash, 44.4 %
- Reverse Osmosis, 41.1 %
- Electro–Dialysis, 5.6 %
- Vapor Compression, 4.3 %
- Multiple Effect Evaporation, 4.1 %
- Other, 0.5 %
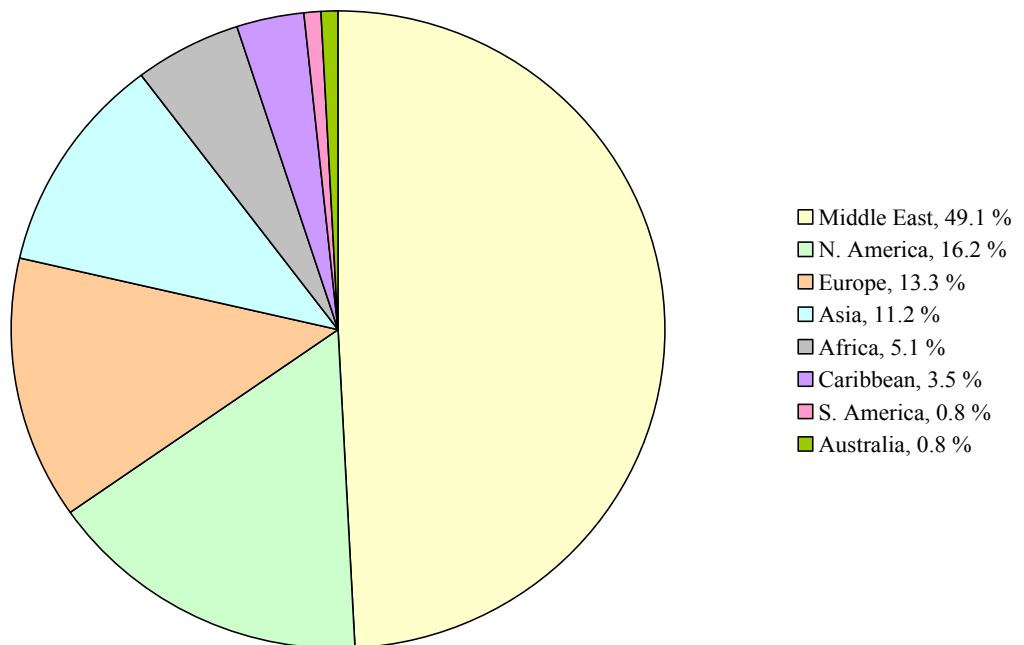
Figure 6. Global distribution of installed desalination capacity by region [5]

- Middle East, 49.1 %
- N. America, 16.2 %
- Europe, 13.3 %
- Asia, 11.2 %
- Africa, 5.1 %
- Caribbean, 3.5 %
- S. America, 0.8 %
- Australia, 0.8 %

2.1.1 Multiple Effect Evaporation

Originally developed in the 1820s for concentrating sugar in sugar cane juice, multiple effect evaporation was used for desalination in the 1950s, making it the oldest desalination process still in operation. Multiple effect evaporation has been combined with other desalination methods, such as vapor compression, to increase its efficiency.

Seawater is distributed to a sequence of vacuumed vessels, known as effects, held at successively lower pressures. External heat is supplied to the first effect, and the generated vapor of each effect supplies its latent heat of condensation to the next. Condensed vapor of each effect is then collected as the fresh water product.

Multiple effect evaporation has a relatively good thermal performance since external heating is only required for the first effect, but its heat transfer tubes are very susceptible to scaling, making it a less attractive desalination option. Figure 7 provides a simple process flow diagram of the multiple effect evaporation desalination process [6].
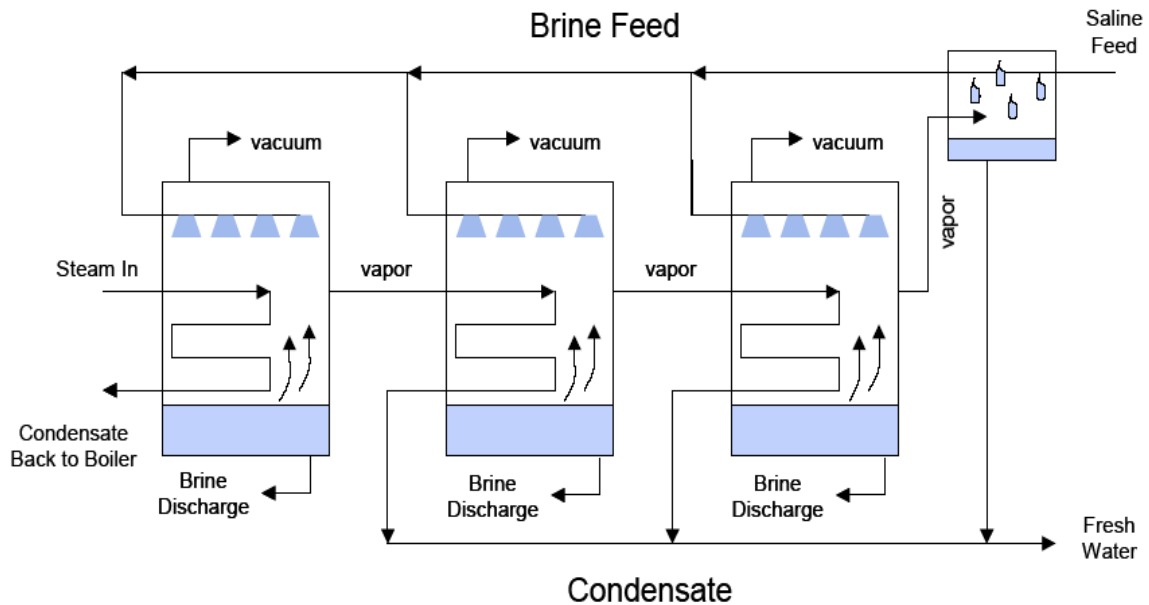
Figure 7. Multiple effect evaporation

9

2.1.2 Multi–Stage Flash

Multi–stage flash is the most common desalination technique, accounting for over 40 % of the global capacity [5]. It has been coupled with other processes, such as solar heating and steam turbine power generation, to increase its efficiency.

Seawater is moved through a sequence of vacuumed vessels, known as stages, held at successively lower pressures, where it is preheated. External heat is then supplied, heating the seawater to above its saturation point. Seawater is then successively passed from one stage to the next, where a small amount of water flashes to steam in each stage, and the remaining brine is forwarded to next stage for further flashing. The flashed steam of each stage condenses by losing its latent heat of condensation to the entering seawater. The condensed vapor of each stage is then collected as the fresh water product.

Multi–stage flash has a relatively low thermal performance due to bulk heating of seawater, but its heat transfer tubes are less susceptible to scaling because of that bulk heating, making it a more attractive desalination option. Figure 8 provides a simple process flow diagram of the multi–stage flash desalination process [6].
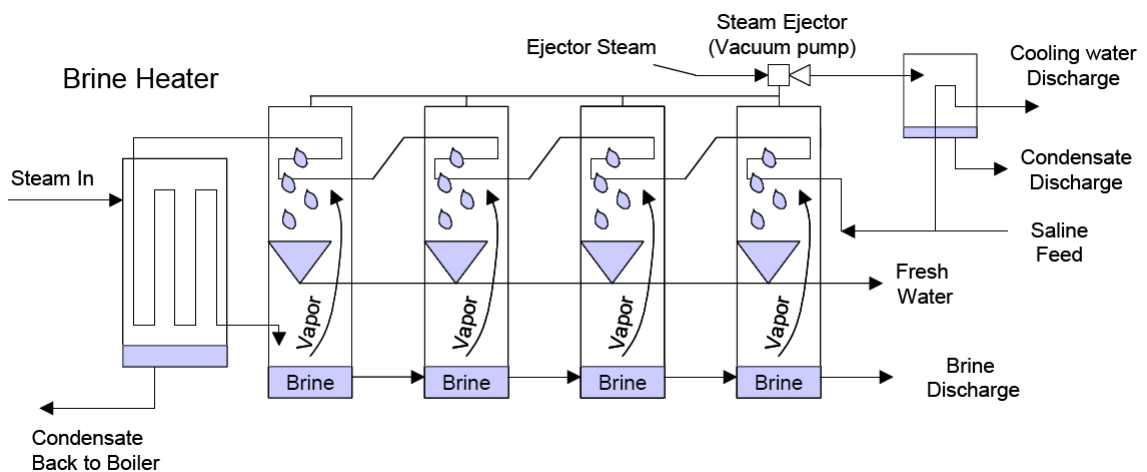
Figure 8. Multi–stage flash

2.1.3 Vapor Compression

Seawater is preheated before entering a vacuumed vessel to be partially vaporized by the latent heat of a condensing steam obtained via compressing vaporized water. The process is dubbed mechanical vapor compression if steam compression is done by a compressor or thermal vapor compression if steam compression is done by an ejector.

Vapor compression has a relatively high thermal performance and can be applied in the desalination of extremely concentrated brines. Vapor compression is generally employed in small and medium capacity applications. Figure 9 provides a simple process flow diagram of the mechanical vapor compression desalination process [6].
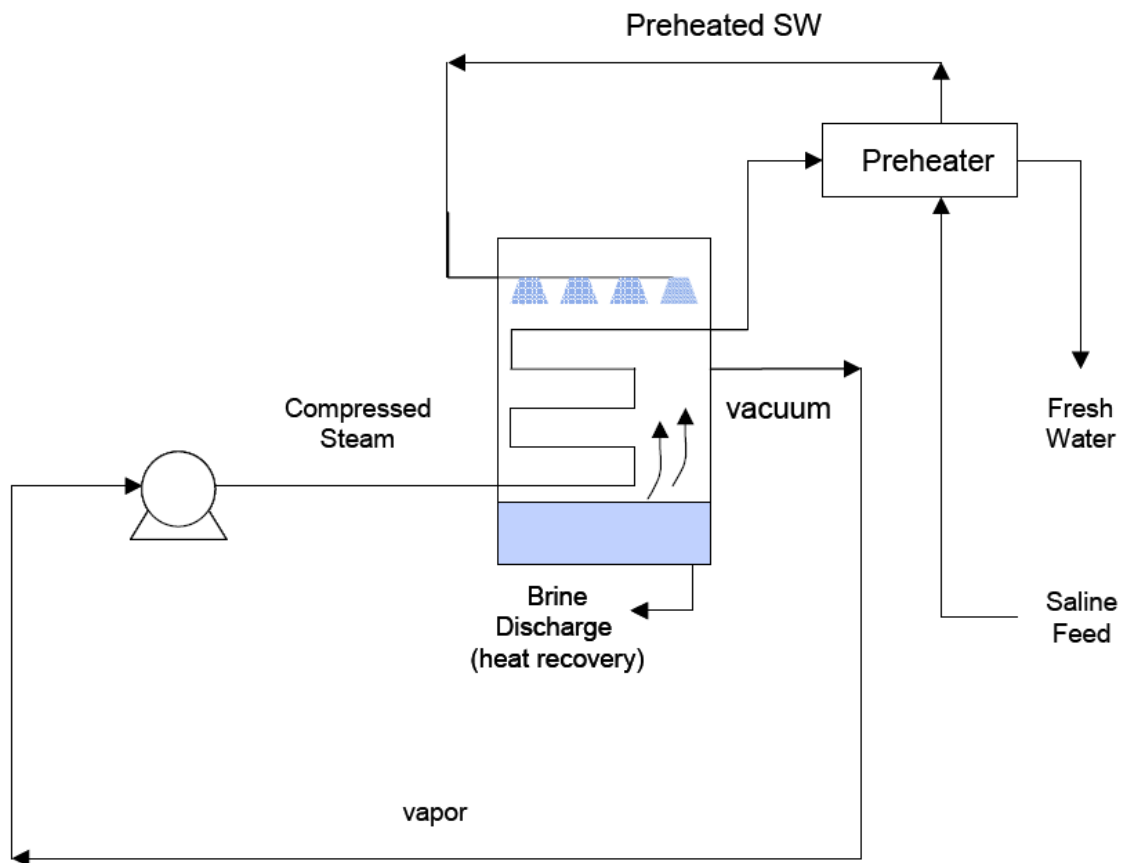
Figure 9. Mechanical vapor compression

2.1.4 Indirect Contact Freezing

Seawater is cooled by cold outgoing fresh water and brine before it enters the evaporator of a separate refrigeration cycle, known as the freezer, where it is partially frozen by evaporating refrigerant. Crystallized ice is separated from the brine before it enters the condenser of the refrigeration cycle, known as the melter, where it melts by extracting its latent heat of fusion from condensing refrigerant. Cold outgoing fresh water and brine streams are used to cool the entering seawater in a heat exchanger.

Indirect contact freezing has a relatively high thermal performance and is less susceptible to scaling and corrosion due to its low temperature operation, but problems arise both from controlling solids handling operations and from the uncertain reliability of refrigerant compressors due to increased risk of oil slugging at low pressures. Figure 10 provides a simple schematic of the indirect contact freezing desalination process [6].
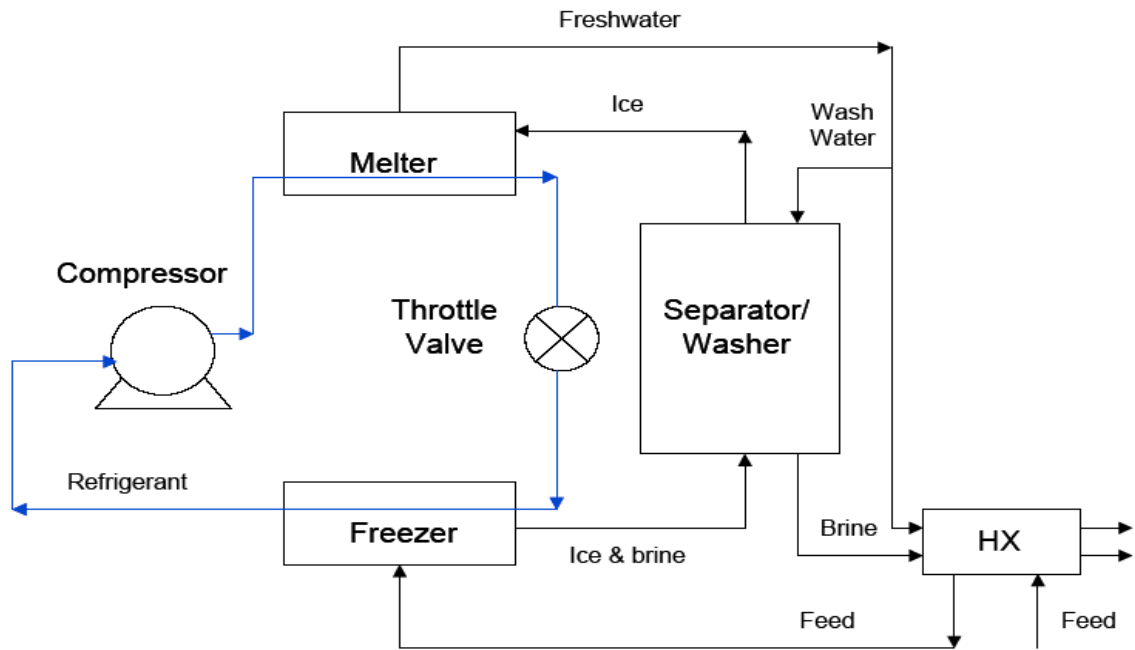
Figure 10. Indirect contact freezing

2.1.5 Reverse Osmosis

Reverse osmosis is the most common desalination process nationally and the second most common internationally in terms of capacity. It is best used for brackish water and is usually combined with other filtration methods to increase its efficiency.

Seawater is initially treated to adjust its pH and to free it from particulates that negatively impact the membrane structure. Seawater is then pumped to a network of semi–permeable membranes, separating fresh water from concentrated brine. Seawater pressure is raised above its natural osmotic pressure, typically 25 bars, but is kept below the membrane tolerance pressure, typically between 60 and 80 bars, forcing pure water molecules through the membrane pores to the fresh water side. Separated water is then treated and collected as the fresh water product, while the concentrated brine is rejected.

Reverse osmosis is very efficient because the mechanical compression energy can be reclaimed from the rejected concentrated brine with a suitable turbine. Figure 11 provides a simple process flow diagram of the reverse osmosis desalination process [6].
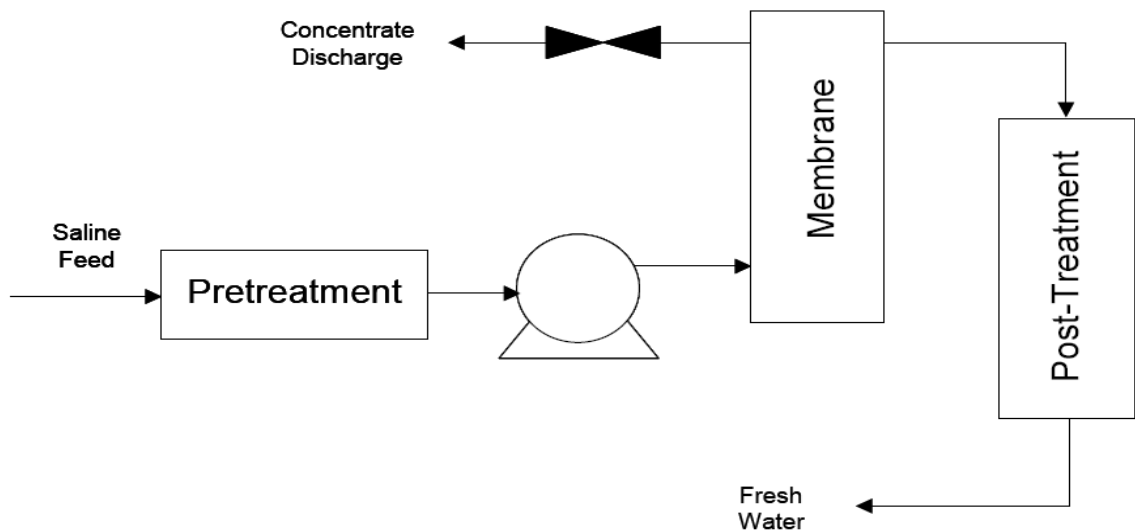
Figure 11. Reverse osmosis

2.1.6 Electro–Dialysis

Seawater is passed through an electro–dialysis stack consisting of alternating layers of cationic and anionic ion exchange membranes in an electrical field. Cations and anions then migrate in opposite directions through ion selective membranes and away from the saline feed in response to applied voltage across the electro–dialysis stack, producing fresh water in the intermediary channels.

The electro–dialysis stack can be arranged in series to increase purification and in parallel to increase output. Electro–dialysis is best used in brackish water applications and is usually combined with other filtration methods to increase its efficiency. Figure 12 provides a simple process flow diagram of the electro–dialysis desalination process [6].
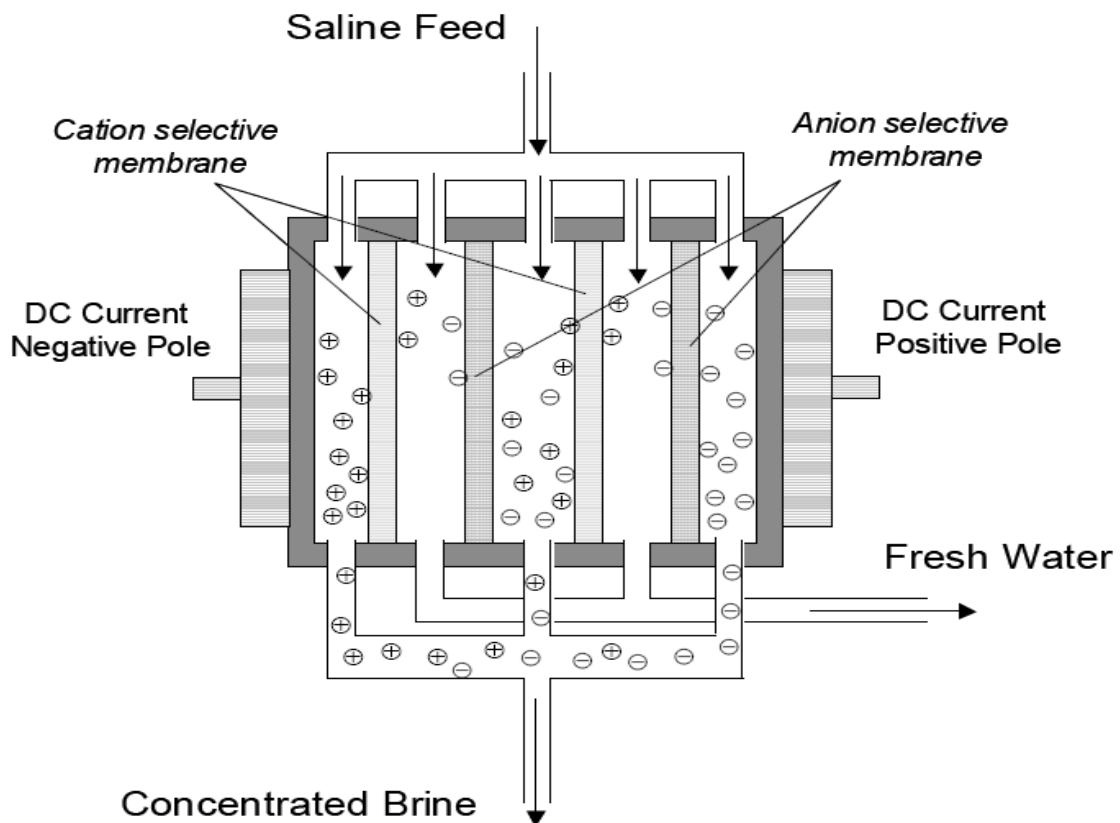
Figure 12. Electro–dialysis

14

2.2 Solar Desalination

Extracting fresh water from seawater requires a great deal of energy, both thermal and mechanical, as detailed in Table 1 [7]. Renewable energy driven desalination is becoming more viable despite its expensive infrastructure because it employs free natural energy sources and releases no harmful effluents to the environment. Solar insolation is usually chosen over other renewable energy sources because its thermal energy can be directly applied to drive desalination systems without irreversible energy conversion that involves inevitable energy loss according to the second law of thermodynamics.

Solar desalination systems are classified into direct and indirect processes depending on the energy path to fresh water. Direct solar desalination systems combine solar energy collection and desalination in one process producing fresh water distillate by directly applying collected solar energy to seawater. Solar distillation using a solar still is an example of direct solar desalination. Indirect solar desalination systems comprise two sub–systems: a solar collection system and a desalination system. The solar collection sub–system is used either to collect heat using solar collectors and supply it via a heat exchanger to a thermal desalination process or convert heat to electricity using photovoltaic cells to power a physical desalination process. The desalination sub–system can be any of the previously mentioned conventional desalination systems.

Table 1. Energy consumption of desalination systems [7]

Process	Heat Input (kJ / kg of product)	Power Input (kJ / kg of product)	Prime Energy Consumption (kJ / kg of product)
MEE	123	8	149
MSF	294	9–14	338
VC	—	29–58	192
RO	—	18–47	120
ED	—	43	144

2.2.1 Solar Distillation

Seawater is placed in a blackened basin inside an air tight transparent structure where it evaporates due to absorption of solar radiation then condenses on the sloping structure by losing its latent heat of condensation to the surroundings. Condensed droplets run down the cover to accumulating troughs to be collected as fresh water.

Solar distillation is a small scale hydrological cycle, and its efficiency is significantly dependent on meteorological limitations such as solar radiation, sky clearness, wind velocity, ambient temperature, and many others. Solar distillation requires large collection areas to maximize insolation and is usually combined with other desalination methods to increase its efficiency. Figure 13 provides a simple process flow diagram of the solar distillation desalination process [6].
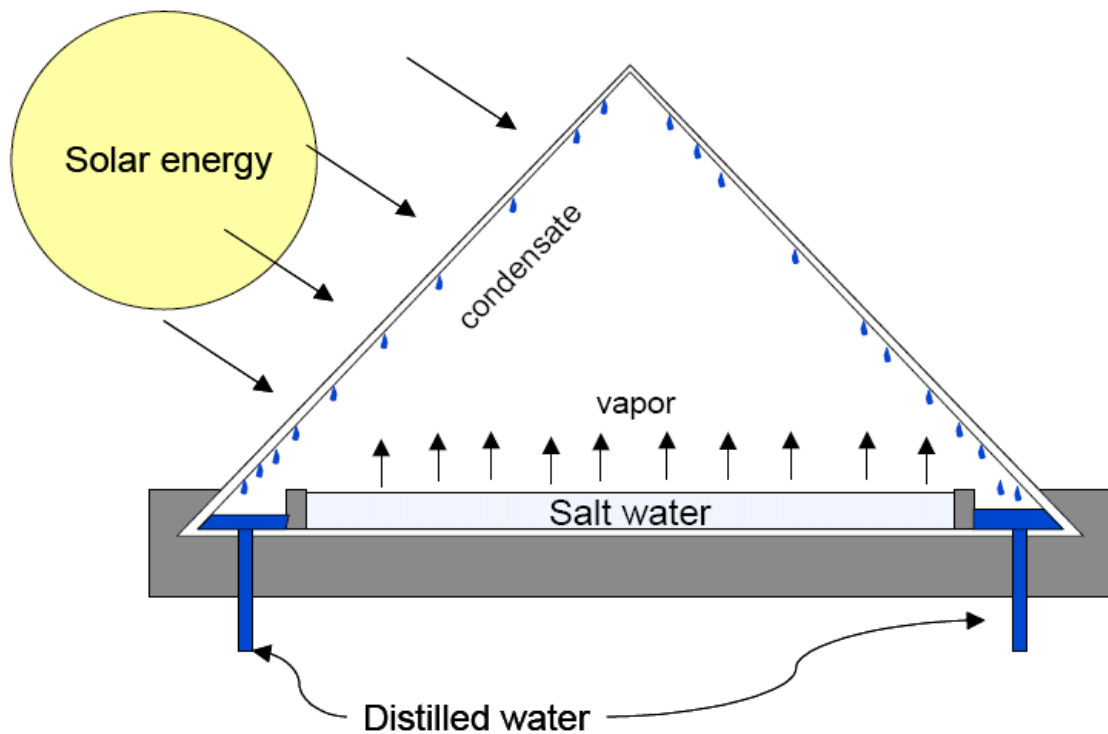
Figure 13. Solar distillation

2.2.2 Solar Collectors

The solar collection sub–system of an indirect solar desalination system is essentially a solar collector that absorbs incident solar radiation and transfers heat to a fluid flowing through it. The working fluid of the collector can either be a medium to transfer heat to the process or to a thermal energy storage reservoir, or it can be the seawater itself before going through a thermal desalination system. Solar collectors can be either stationary or tracking. Tracking solar collectors can be designed to go after the rays of sunlight by moving around either a single axis or double axes.

Solar collectors can also be classified as concentrating and non–concentrating types. The concentration ratio of a solar collector is the relative amount of the solar flux on the receiver to flux on the aperture. Concentrating collectors have a highly reflective surface to reflect and concentrate solar radiation onto a receiver or an absorber, while non–concentrating collectors have a highly absorptive surface with low emittance to maximize heat transfer to the working fluid. Solar collectors are chosen according to the desired process temperature. Table 2 includes an extensive list of solar collectors and their operational temperature ranges [7].

Table 2. Solar collectors [7]

Tracking	Collector Type	Absorber	Concentration Ratio	Operational Range
Stationary	Flat plate	Flat	1	30–80 °C
	Evacuated tube	Flat	1	50–200 °C
	Compound parabolic	Tubular	1–5	60–240 °C
Single–axis	Compound parabolic	Tubular	5–15	60–300 °C
	Linear Fresnel	Tubular	10–40	60–250 °C
	Parabolic trough	Tubular	15–45	60–300 °C
	Cylindrical trough	Tubular	10–50	60–300 °C
Double–axis	Parabolic dish	Point	100–1000	100–500 °C
	Heliostat field	Point	100–1500	150–2000 °C

2.2.3 Thermal Energy Storage

Thermal energy storage in various solid and liquid media is used to synchronize energy supply and demand due to the intermittent nature of solar energy. Energy can be stored as sensible heat, as shown in Table 3, or as latent heat, as shown in Table 4 [8]. Thermal storage design depends on the temperature range of the solar collection and desalination systems, charge and discharge rates, space, corrosivity, and many others.

Table 3. Sensible heat storage material [8]

Medium	Range (°C)	ρ (kg / m^3)	Cp (J / kg-°C)	K (W / m-°C)
Water	0–100	1000	4190	0.63
Water – 10 bar	0–180	881	4190	—
50 % ethylene glycol	0–100	1075	3480	—
Dowtherm A®	12–260	867	2200	0.12
Therminol 66®	-9–343	750	2100	0.11
Draw salt	220–540	1733	1550	0.57
Molten salt	142–540	1680	1560	0.61
Liquid sodium	100–760	750	1260	67.50
Cast iron	Up to 1150	7200	540	42
Taconite	—	3200	800	—
Aluminum	Up to 660	2700	920	200
Fireclay	—	2100–2600	1000	1.0–1.5
Rock	—	1600	880	—

Table 4. Latent heat storage material [8]

Medium	MP (°C)	ΔH^L (kJ / kg)	ρ (kg / m^3)		Cp (kJ / kg-°C)		k (W / m-°C)
			Solid	Liquid	Solid	Liquid	
$LiClO_3 \cdot 3H_2O$	8.1	253	1720	1530	—	—	—
$Na_2SO_4 \cdot 10H_2O$	32.4	251	1460	1330	1.76	3.32	2.25
$Na_2S_2O_3 \cdot 5H_2O$	48	200	1730	1665	1.47	2.39	0.57
$NaCH_3COO \cdot 3H_2O$	58	180	1450	1280	1.90	2.50	0.50
$Ba(OH)_2 \cdot 8H_2O$	78	301	2070	1937	0.67	1.26	0.65 (ℓ)
$MgNO_3 \cdot 6H_2O$	90	163	1636	1550	1.56	3.68	0.61
$LiNO_3$	252	530	2310	1776	2.02	2.04	1.35
$LiCO_3 / K_2CO_3$	505	345	2265	1960	1.34	1.76	—
$LiCO_3 / K_2CO_3 / Na_2CO_3$	397	277	2300	2140	1.68	1.63	—
n–Tetradecane	5.5	228	825	771	—	—	0.15
n–Octadecane	28	244	814	774	2.16	—	0.15
HDPE	126	180	960	900	2.88	2.51	0.36
Steric Acid	70	203	941	347	—	2.35	0.17 (ℓ)

2.2.4 Solar Ponds

Water absorbs solar radiation going through it causing its temperature to rise. The shorter the wave length of sunlight, the deeper it can penetrate the water column as shown in Table 5 [8]. Solar ponds are pools of water with a darkened bottom to maximize light absorption. They are designed to have increasing salinity with depth creating a density gradient that inhibits natural convection currents. The final outcome is a stratified pond with increasing temperature and salinity with depth, as shown in Figure 14 [7]. Solar ponds function as both solar collectors and thermal energy storage media.

Table 5. Spectral absorption of solar radiation in water [8]

Wavelength (μm)	*Layer Depth*				
	0	*1 cm*	*10 cm*	*1 m*	*10 m*
0.2–0.6	23.7	23.7	23.6	22.9	17.2
0.6–0.9	36.0	35.3	36.0	12.9	0.9
0.9–1.2	17.9	12.3	0.8	0.0	0.0
> 1.2	22.4	1.7	0.0	0.0	0.0
Total	100.0	73.0	54.9	35.8	18.1
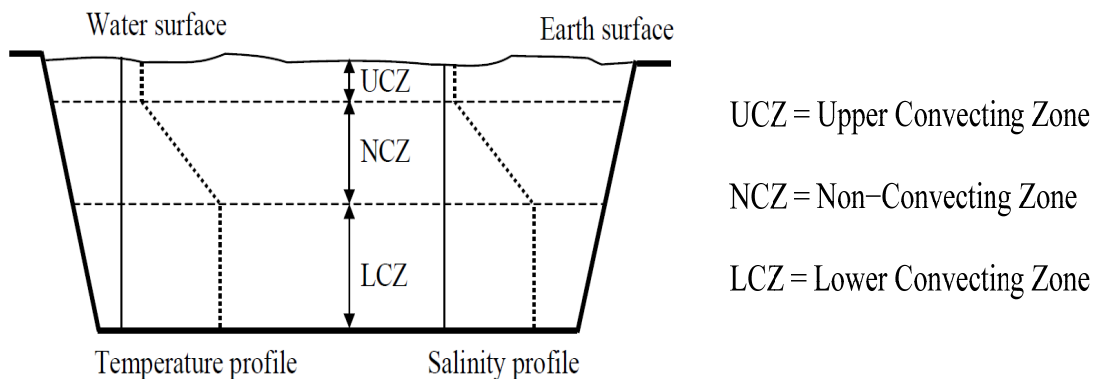
Figure 14. Vertical cross section of a solar pond

2.2.5 Photovoltaics

Photovoltaic cells are made from common semiconductor compounds and can directly convert solar radiation into useful electricity, as shown in Figure 15 [8]. Cells are arranged to form modules that are combined to form panels. Photovoltaic systems include an array of joined panels to produce the required electrical output, as shown in Figure 16 [8]. Photovoltaics can be employed independently or jointly with other sources to generate electricity needed to power physical desalination systems.
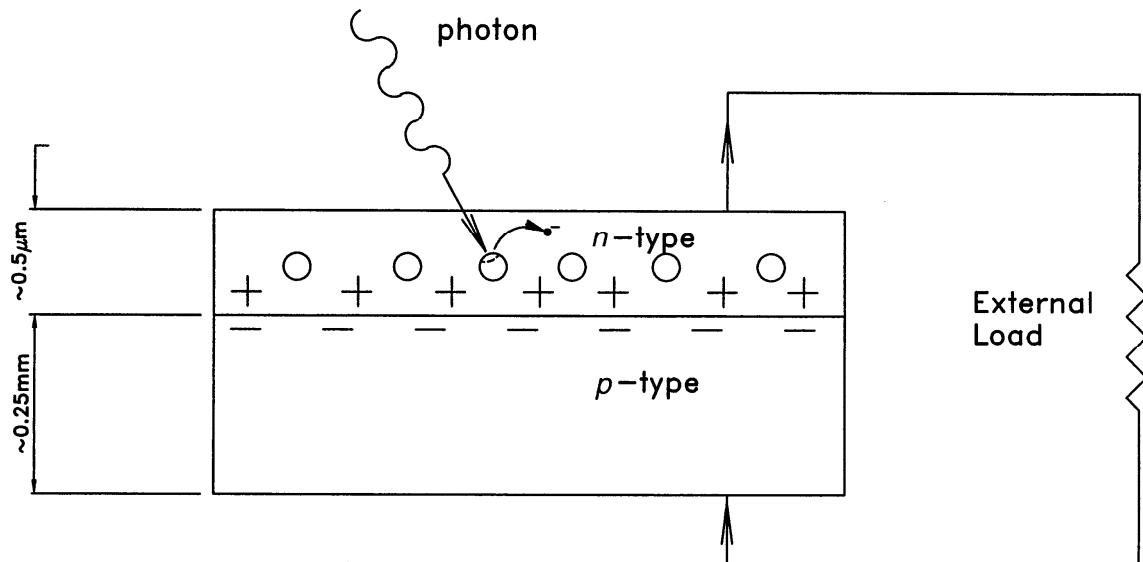
Figure 15. Photovoltaic cell schematics
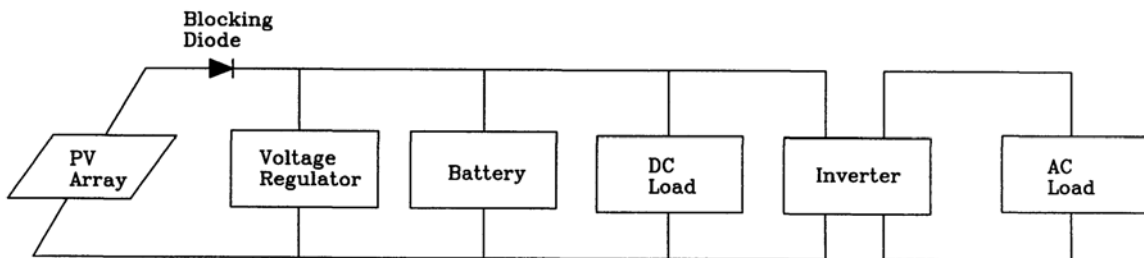
Figure 16. Photovoltaic system schematics

CHAPTER 3. RESEARCH BACKGROUND

3.1 Renewable Energy Desalination Systems

Water and energy are the most essential ingredients of a flourishing civilization. Fresh water and energy reserves are increasingly exhausted as was mentioned earlier in CHAPTER 1; hence, seawater desalination using renewable energy sources is a very appealing research area. In addition, desalination is an enormously energy exhaustive process making fossil fuel based conventional desalination methods extremely unpopular especially in light of the growing impact of environmental pollution and global warming.

The worldwide capacity of desalination using renewable energy amounts to less than 1 % of that of conventional desalination due to high capital and maintenance costs associated with using renewable energy sources [9]. Several renewable energy driven desalination plants were designed and constructed; however, most of them were geographically customized and built on pilot scale. A detailed record of renewable energy driven desalination plants was put together by Tzen and Morris [10].

Wind energy can be utilized to generate electricity via turbines to run physical and chemical desalination plants, while geothermal energy can be utilized to generate heat via underground heat exchangers to run thermal desalination plants. Solar energy is the most promising renewable energy source due to its ability to drive the more popular thermal desalination systems directly through solar collectors and to drive physical and chemical desalination systems indirectly through photovoltaic cells.

3.2 Passive Vacuum Solar Desalination

The passive vacuum desalination concept was initially developed and examined by Goswami and Kharabsheh [11]. Atmospheric pressure forces seawater from a ground level tank into an elevated vacuumed chamber through an injection pipe where water starts to evaporate due to solar energy supplied to the chamber via a closed loop heat exchanger. The concentrated brine is then withdrawn through a withdrawal pipe annulus to the injection pipe to recover heat, while vapor moves towards a condenser due to a vapor pressure gradient through a finned pipe. Vapor then condenses by losing its latent heat of condensation to the ambient and flows down to a fresh water tank due to gravity. The vacuum is maintained by the hydrostatic balance amongst all of the joined vessels. Figure 17 provides a simple illustration of the passive vacuum solar desalination process.
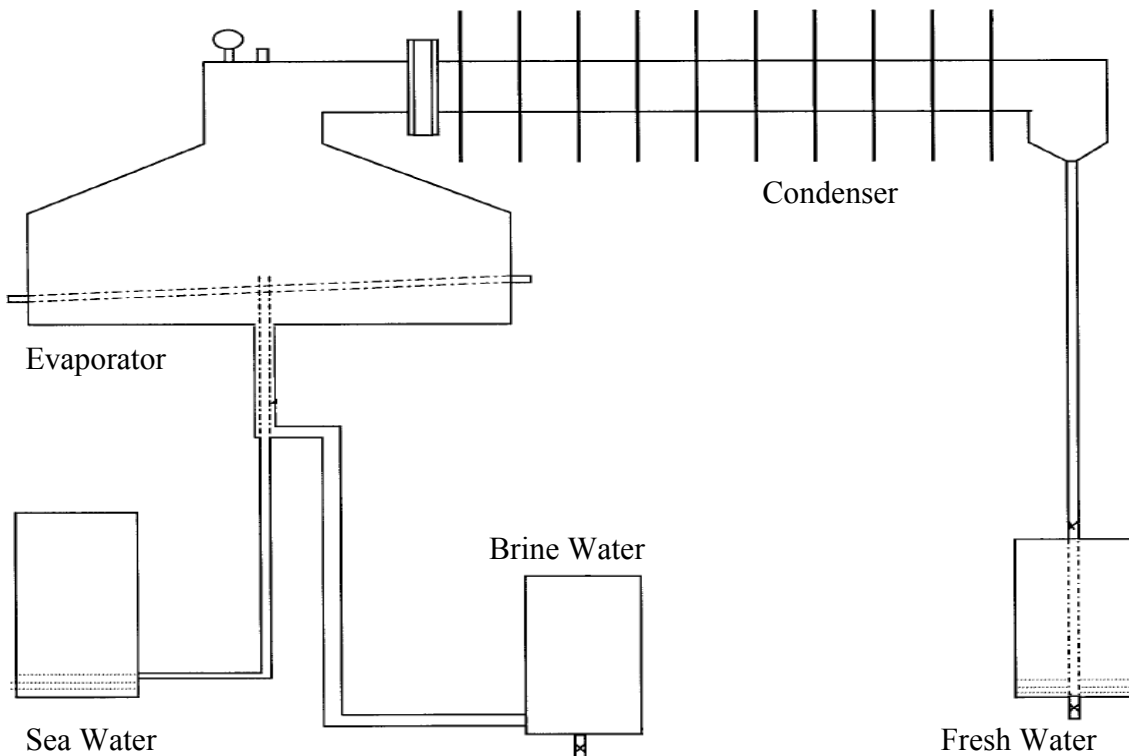
Figure 17. Passive vacuum solar desalination

3.3 Passive Vacuum Solar Flash Desalination

The prior passive vacuum solar process was modified to overcome the big size of the evaporator and its large level fluctuations. Seawater is pumped through a condenser to preheat it before it enters a solar heater where it flashes into the vacuumed evaporator through an expansion orifice to produce water vapor and concentrated brine. The flashed vapor then condenses by losing its latent heat of condensation to the entering seawater in the condenser. The condensate and the concentrated brine flow down to ground tanks due to gravity, while the vacuum is naturally maintained by the hydrostatic balance between the ground and the elevated vessels. Figure 18 provides a simple process flow diagram of the passive vacuum solar flash desalination process that was developed and examined theoretically by Goswami and Maroo [12].
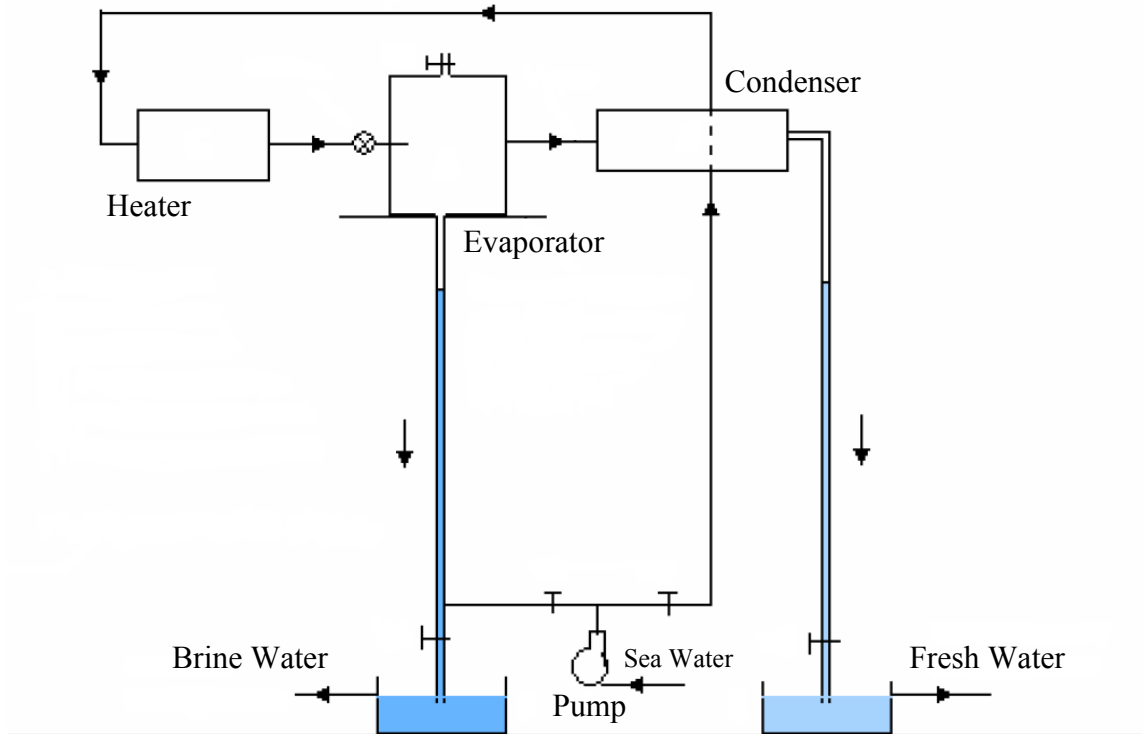
Figure 18. Passive vacuum solar flash desalination

3.4 Proposed Desalination System

The proposed desalination system consists of a saline water tank, a concentrated brine tank, and a fresh water tank placed on ground level plus an evaporator and a condenser located at least ten meters above ground, as shown in Figure 19. The evaporator–condenser assembly, or flash chamber, is initially filled with saline water that later drops into the ground tanks by gravity, creating a vacuum above the water surface in the unit without a vacuum pump. The vacuum is maintained by the hydrostatic pressure balance among all of the connected vessels. The ground tanks are open to the atmosphere, while the flash chamber is insulated and sealed to retain both heat and vacuum.

In a continuous process, cool saline water is pumped through the condenser to preheat it before it enters a solar heater and flashes into a vacuumed evaporator through an expansion orifice or a pressure–reducing valve producing water vapor and concentrated brine. The water vapor then condenses by losing its heat of condensation to the entering saline water in the condenser. The fresh water condensate and concentrated brine flow down to the fresh water and brine water tanks, respectively, due to gravity through linking pipes. Each of the fresh water and the brine water tanks has a discharge pipe located a few centimeters above the level of the inlet water pipes, keeping their levels constant to maintain the vacuum in the flash chamber hydrostatically as well as to retrieve the fresh water product and reject the concentrating brine.

Multi–stage flash desalination scheme of the proposed system can be achieved by flashing seawater in sequentially lower pressure flash chambers, as shown in Figure 20. Employing the multi–stage flash desalination scheme will result in more evaporation and better recovery of heat of condensation, resulting in more fresh water output.

24
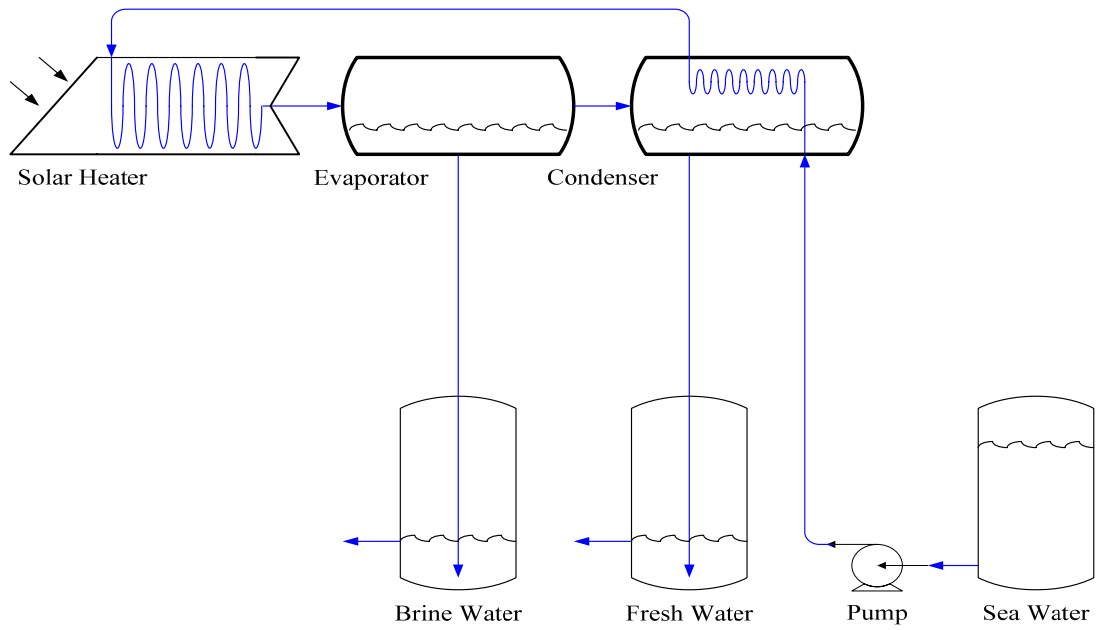
Figure 19. Single–stage solar flash desalination system
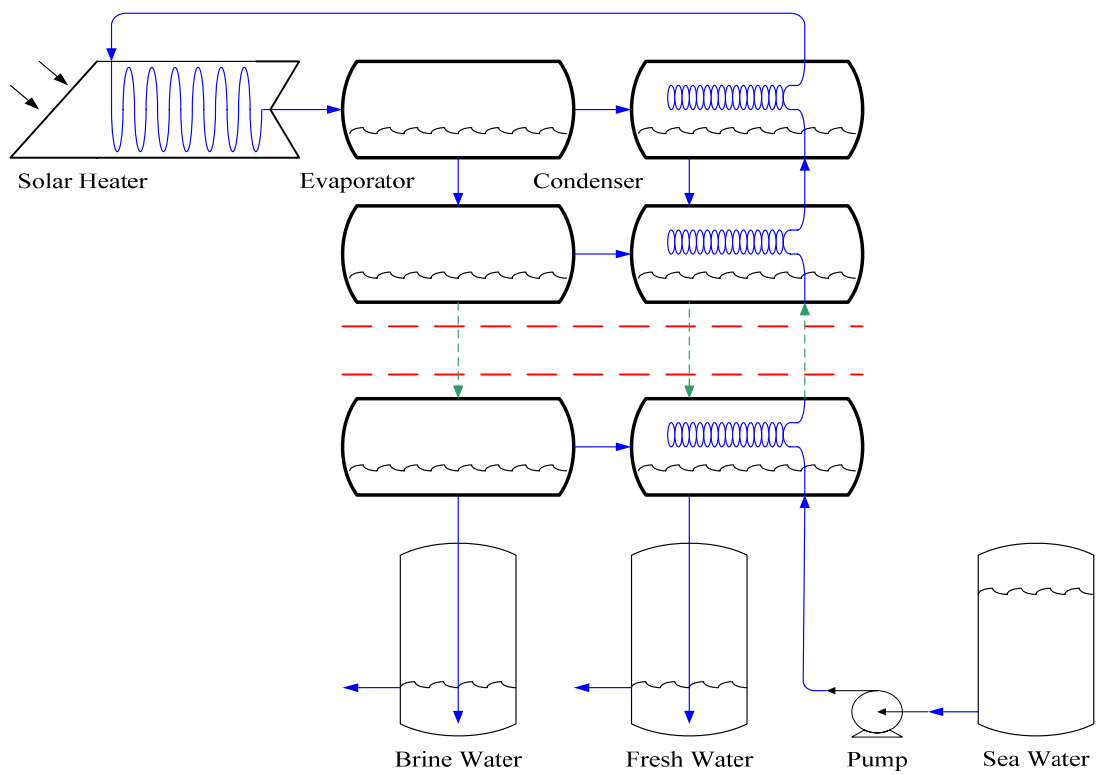
Figure 20. Multi–stage solar flash desalination system

CHAPTER 4. THEORETICAL ANALYSIS

4.1 Process Description

The proposed desalination system with its designated stream labels is outlined in Figure 21. The desalination process includes two consecutive steps: a start–up procedure and a continuous operation. The start–up procedure is a simple process invoked prior to running the continuous operation and will not be included in the model. The continuous operation is the essential part of the desalination process, and a model will be built to simulate it. The valve positions shown depict the system in continuous operation mode.

The start–up procedure begins by separately pumping the condenser with fresh water and the evaporator with seawater, while their top valves are open and their bottom ones are closed until they are completely filled with water and free of air. Valve positions of both vessels of the flash chamber are then switched to let water drop under gravity, leaving behind a vacuum that is created without a vacuum pump.

The continuous operation begins right after the initial start–up procedure and it consists of pumping seawater through the condenser, preheating it before flowing it through the channels of a solar heater to reach a desired flash temperature. The desired flash temperature is controlled by manipulating the residence time of seawater in the solar heater by varying its flow rate in relation to available solar insolation. Hot seawater then flashes into an insulated vacuumed evaporator through an expansion orifice or a pressure–reducing valve, producing water vapor and concentrated brine.

The produced water vapor flows to the condenser due to a vapor pressure gradient and condenses by losing its heat of condensation to seawater passing through the condenser while concentrated brine remains in the evaporator. The fresh water condensate and concentrated brine flow down to the fresh water and brine water ground tanks, respectively, due to gravity through linking pipes that stretch down till just above the bottom of the tanks. The fresh water and the brine water ground tanks have discharge pipes positioned a few centimeters higher than the lip of the linking pipes, keeping their levels constant to maintain the vacuum in the flash chamber by the hydrostatic balance with the levels in the flash chamber.

A comprehensive model will be developed to examine the dynamics of proposed continuous desalination operation. The model will employ fundamental laws to describe the process in addition to reliable empirical correlations to estimate physical properties of the involved species and operational parameters of the proposed system. The model will assume total steam condensation as well as quasi steady state operation, accounting for the build up of non–condensable gases in the flash chamber. The model will also account for the natural diffusion process of water vapor occurring because of a vapor pressure gradient present between the hot and cold sides of the flash chamber.

The model will include mass and energy balances around process equipment and geometrical formulas describing equipment layout and size. The Rachford–Rice method [13] will be employed to perform flash calculations, while Bernoulli's fluid equation will be used to perform hydrostatic balance relations. Thermodynamic equilibria and several physical property correlations will also be included in the model. In addition, an integrative equation of state will be used to express rising vacuum pressure.
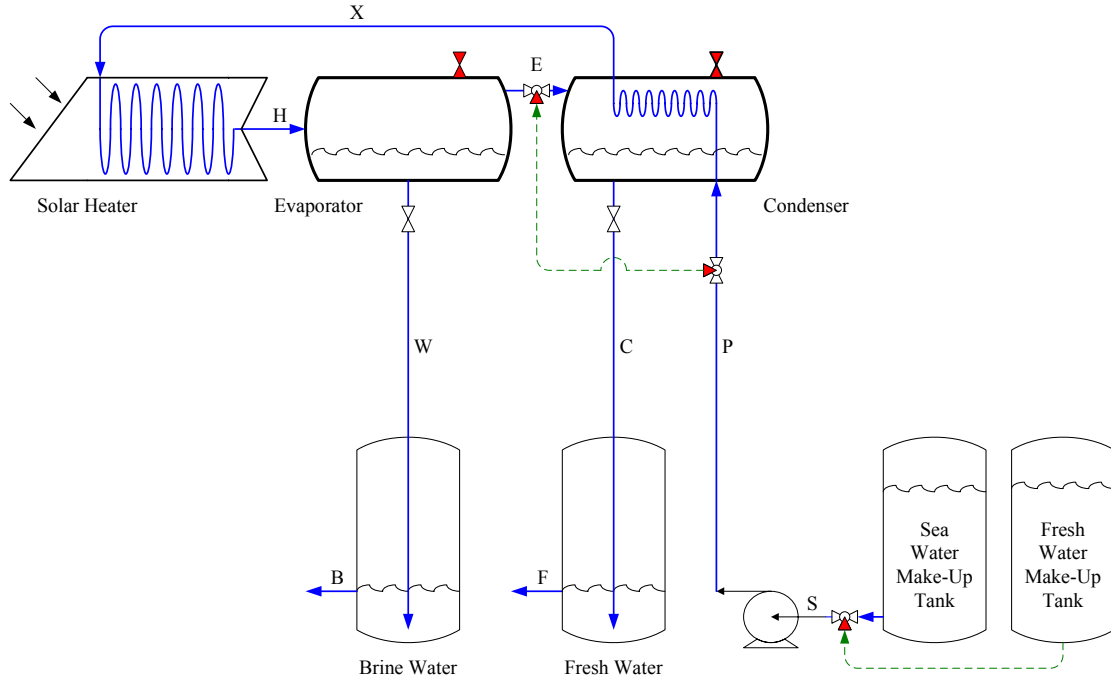
Figure 21. Process schematics

4.2 Model Development

Trace components in seawater may affect its kinetics but not its thermodynamic equilibrium; therefore, only major components will be considered in this theoretical analysis. The following sub–sections present all equations used in modeling the proposed system, while the next section sketches the solution algorithm.

The nomenclature and engineering units of all variables used in the model are detailed at the beginning of this dissertation in the LIST OF SYMBOLS section. In addition, stream symbols that appear on the process flow diagram of Figure 21 are used as subscripts for different stream property variables. Process equipment referred to in the model denote the pump, the condenser, the heater, and the evaporator. The complete code with its input and output values can be found in the APPENDICES section.

28

4.2.1 Mass and Energy Balance

Salt balances around process equipment are given by

$$\varphi_S \cdot M_S = \varphi_P \cdot M_P \tag{1}$$

$$\varphi_P \cdot M_P = \varphi_X \cdot M_X \tag{2}$$

$$\varphi_X \cdot M_X = \varphi_H \cdot M_H \tag{3}$$

$$\varphi_H \cdot M_H = \varphi_W \cdot M_W \tag{4}$$

Overall energy balances around process equipment are given by

$$Q_P - W_P + E_P^{in} - E_P^{out} = 0 \tag{5}$$

$$Q_C - W_C + E_C^{in} - E_C^{out} = E_C^a \tag{6}$$

$$Q_H - W_H + E_H^{in} - E_H^{out} = 0 \tag{7}$$

$$Q_E - W_E + E_E^{in} - E_E^{out} = E_E^d \tag{8}$$

Energy flow inputs to process equipment are given by

$$E_P^{in} = M_S \cdot H_S \tag{9}$$

$$E_C^{in} = M_P \cdot H_P + M_E \cdot \left(H_E + H_E^L\right) \tag{10}$$

$$E_H^{in} = M_X \cdot H_X \tag{11}$$

$$E_E^{in} = M_H \cdot H_H \tag{12}$$

Energy flow outputs from process equipment are given by

$$E_P^{out} = M_P \cdot H_P \tag{13}$$

$$E_C^{out} = M_X \cdot H_X + M_C \cdot H_C \tag{14}$$

$$E_H^{out} = M_H \cdot H_H \tag{15}$$

$$E_E^{out} = M_W \cdot H_W + M_E \cdot \left(H_E + H_E^L\right) \tag{16}$$

Energy accumulation in the condenser due to non–condensable gases is given by

$$E_C^a = M_C^a \cdot H_C^a \tag{17}$$

Energy transmitted by the diffusing water molecules from the concentrated brine phase to the fresh water vapor phase is accounted for in the above energy input and output expressions; therefore, an offset term is included in the energy balance of the evaporator to neutralize the effect of that transmitted energy on the flashing process. In other words, offsetting transmitted energy of diffusing water molecules effectively altered the boundary of the above energy balance from the evaporator to expansion orifice. Figure 22 illustrates the mass transfer operations of the proposed system, where flash and diffusion operations occur in the evaporator. The transmitted energy of the diffusing water molecules offset term in the evaporator is given by

$$E_E^d = M_E^d \cdot \left(H_W - H_E - H_E^L \right) \tag{18}$$
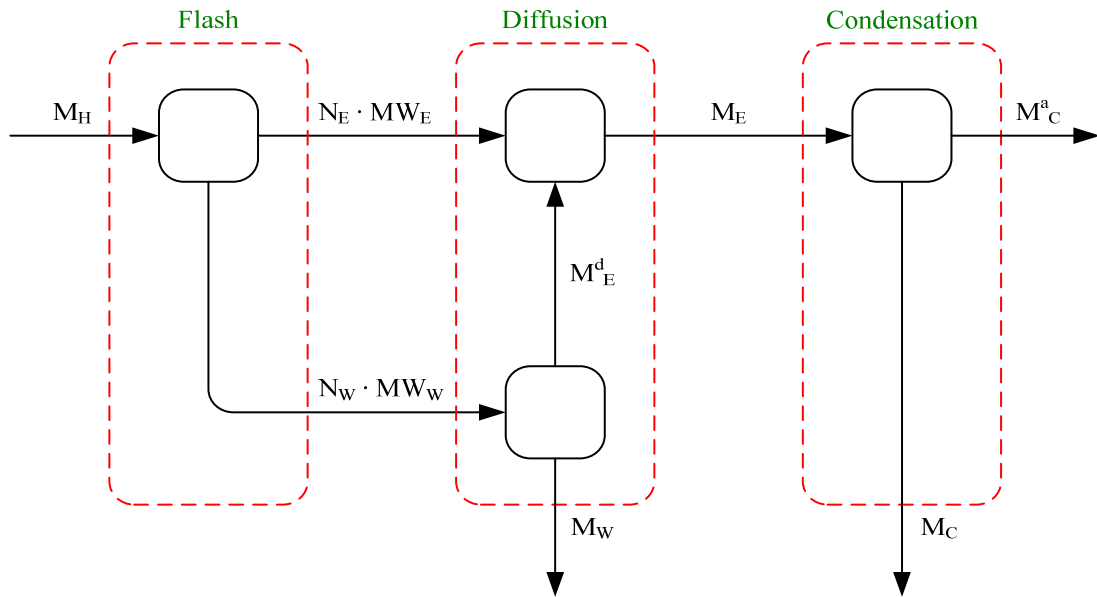
Figure 22. Mass transfer operations

Demisting is a standard unit operation in industry accomplished by devices called demisters that are fitted to process vessels to ensure a full removal of liquid droplets from vapor streams. No demister was attached to the experimental unit and no demisting is considered in the model; however, flashed vapor can be safely assumed free from entrained brine droplets yielding zero salinity expressed by

$$\varphi_E = \varphi_C = 0 \tag{19}$$

The experimental simulation will be thoroughly discussed in CHAPTER 5 and its output will be comprehensively disclosed in CHAPTER 7; nonetheless, a significant observation regarding the produced amount of fresh water vapor was made and needs to be mentioned here since it will be included in the model.

The maximum amount of fresh water that can be produced by flashing seawater can be approximated by the expression $\int [M_H \cdot (H_H - H_W) / (H_E + H^L_E - H_W)] dt$, which is obtained by conducting an energy balance around the expansion orifice assuming seawater to be a single component fluid and ignoring heat losses. Maximum amounts that can be produced were computed using experimental flow and temperature values, then they were compared to actual collected amounts.

Actual amounts of fresh water produced at lower flash temperatures were considerably less than predicted amounts by the single component flash calculation, indicating that a sizeable quantity of the flashed vapor condenses prematurely in the evaporator before making it to the condenser. In contrast, the actual amounts of fresh water produced at higher flash temperatures were much more than predicted amounts by the single component flash calculation, suggesting the presence of a diffusion process of vaporized water molecules from the evaporator to the condenser.

31

Bemporad [14] developed a correlation that estimates the diffusion rate of water vapor between two joined chambers under vacuum, where one chamber contains saline water and the other contains fresh water. The correlation was experimentally based with one empirical coefficient, and it identified the gradient $\Delta P_{H2O} / \sqrt{T}$ as the driving force for diffusion. The correlation was slightly modified to properly correspond to the current experimental results yielding the following expression

$$M_E^d = \sigma \cdot XA_E \cdot \left[\frac{(1 - 0.54 \cdot \varphi_W) \cdot P_{H_2O}^W}{\sqrt{T_W + 273.15}} - \frac{P_{H_2O}^C + \Omega}{\sqrt{T_C + 273.15}} \right] \tag{20}$$

Parameter σ serves as a diffusion coefficient, while parameter Ω serves as a diffusion barrier and both can be adjusted using experimental results. The two parameters can be thought of as conductance and resistance terms, and it is imperative to reiterate that their obtained values pertain to the geometry of the experimental set–up and should be readjusted whenever applied to different geometries using experimental records.

The vapor pressures corresponding to the brine and fresh water temperatures are needed to evaluate the above expression and can be calculated by [15]

$$P_{H_2O}^W = exp\left[PA - \left(\frac{PB}{T_W + PC} \right) \right] \tag{21}$$

$$P_{H_2O}^C = exp\left[PA - \left(\frac{PB}{T_C + PC} \right) \right] \tag{22}$$

Flash and accumulation computations will be carried out on molar basis; therefore, a mole balance is included in the model to represent both operations by

$$N_H = N_W + N_E \tag{23}$$

$$N_E = N_C + N_C^a \tag{24}$$

The flash operation is the heart of the desalination process and will be thoroughly discussed later. The condensation operation is considered a quasi–steady state operation where the formed non–condensable gases accumulate in the flash chamber, and all of the flashed water vapor condenses forming the fresh water product. This quasi–steady state operation is expressed by

$$N_C^a = \left(1 - y_{H_2O}\right) \cdot N_E \tag{25}$$

Note that the last equation can be replaced by $N_C = y_{H2O} \cdot N_E$ because total accumulation of non–condensable gases and total condensation of water vapor are interchangeable statements. Figure 23 represents a transformation of Figure 22 from mass to a molecular basis to correspond to the above mole balance and is accomplished by dividing the mass flow rates by the stream molecular weights presented next.
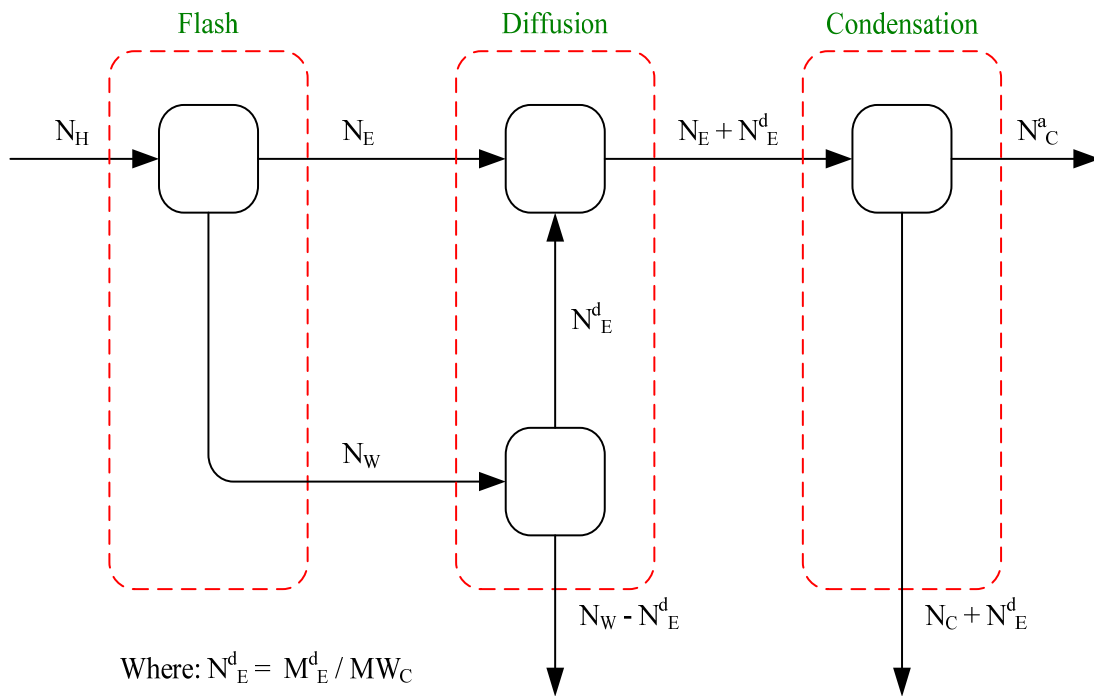
Figure 23. Molecular transfer operations

Mass flow rate and composition of process streams prior to flashing are considered constant, and their values will be input to the model

$$M_S = M_P = M_X = M_H \tag{26}$$

Both molar and mass flow rates are interchangeably used in this model to allow for flash and accumulation computations on a molar basis and for diffusion and production computations on a mass basis. They can be related using the average molecular weight of process streams that will be introduced later as follows

$$M_H = N_H \cdot MW_H \tag{27}$$

$$M_W = N_W \cdot MW_W - M_E^d \tag{28}$$

$$M_E = N_E \cdot MW_E + M_E^d \tag{29}$$

$$M_C = N_C \cdot MW_C + M_E^d \tag{30}$$

$$M_C^a = N_C^a \cdot MW_C^a \tag{31}$$

Seawater is a solution of many salts and contains a small amount of dissolved gases. To simplify calculations, seawater salt will be treated as one substance with nitrogen, oxygen, argon, and carbon dioxide making up the dissolved gases. The average molecular weights of seawater salt and process streams are used in relating molar and mass flow rates and can be estimated by considering their major components as [16]

$$\frac{1}{MW_{Salt}} = \left(\begin{array}{l} \dfrac{\omega_{Cl}}{MW_{Cl}} + \dfrac{\omega_{Na}}{MW_{Na}} + \dfrac{\omega_{SO_4}}{MW_{SO_4}} + \dfrac{\omega_{Mg}}{MW_{Mg}} + \dfrac{\omega_{Ca}}{MW_{Ca}} + \dfrac{\omega_K}{MW_K} \\[3mm] + \dfrac{\omega_{HCO_3}}{MW_{HCO_3}} + \dfrac{\omega_{Br}}{MW_{Br}} + \dfrac{\omega_{BO_3}}{MW_{BO_3}} + \dfrac{\omega_{Sr}}{MW_{Sr}} + \dfrac{\omega_F}{MW_F} \end{array} \right) \tag{32}$$

$$MW_H = \left(\begin{array}{l} z_{N_2} \cdot MW_{N_2} + z_{O_2} \cdot MW_{O_2} + z_{Ar} \cdot MW_{Ar} \\[2mm] + z_{CO_2} \cdot MW_{CO_2} + z_{Salt} \cdot MW_{Salt} + z_{H_2O} \cdot MW_{H_2O} \end{array} \right) \tag{33}$$

$$MW_W = \begin{pmatrix} x_{N_2} \cdot MW_{N_2} + x_{O_2} \cdot MW_{O_2} + x_{Ar} \cdot MW_{Ar} \\ + x_{CO_2} \cdot MW_{CO_2} + x_{Salt} \cdot MW_{Salt} + x_{H_2O} \cdot MW_{H_2O} \end{pmatrix} \tag{34}$$

$$MW_E = \begin{pmatrix} y_{N_2} \cdot MW_{N_2} + y_{O_2} \cdot MW_{O_2} + y_{Ar} \cdot MW_{Ar} \\ + y_{CO_2} \cdot MW_{CO_2} + y_{H_2O} \cdot MW_{H_2O} \end{pmatrix} \tag{35}$$

$$MW_C = MW_{H_2O} \tag{36}$$

$$MW_C^a = \frac{\left(y_{N_2} \cdot MW_{N_2} + y_{O_2} \cdot MW_{O_2} + y_{Ar} \cdot MW_{Ar} + y_{CO_2} \cdot MW_{CO_2} \right)}{\left(1 - y_{H_2O} \right)} \tag{37}$$

4.2.2 Equilibrium Distribution Coefficients

The distribution of non–condensable gases between the flashed vapor and concentrated brine in the flash chamber can be estimated by assuming equilibrium between the two phases. Salt is considered non–volatile and therefore is not present in the flashed vapor. Henry's constants for non–condensable gases and saturation pressure of water are needed to describe this assumed equilibrium.

Henry's constants for the non–condensable gases are given by [17]

$$HC_{N_2} = HC_{N_2}^o \cdot exp\left[-HF_{N_2} \cdot \left(\frac{1}{T_E + 273.15} - \frac{1}{298.15} \right) \right] \tag{38}$$

$$HC_{O_2} = HC_{O_2}^o \cdot exp\left[-HF_{O_2} \cdot \left(\frac{1}{T_E + 273.15} - \frac{1}{298.15} \right) \right] \tag{39}$$

$$HC_{Ar} = HC_{Ar}^o \cdot exp\left[-HF_{Ar} \cdot \left(\frac{1}{T_E + 273.15} - \frac{1}{298.15} \right) \right] \tag{40}$$

$$HC_{CO_2} = HC_{CO_2}^o \cdot exp\left[-HF_{CO_2} \cdot \left(\frac{1}{T_E + 273.15} - \frac{1}{298.15} \right) \right] \tag{41}$$

The saturated pressure of water is given by [15]

$$P_{H_2O} = exp\left[PA - \left(\frac{PB}{T_E + PC} \right) \right]$$ (42)

The equilibrium distribution coefficients are used in mass transfer computations to determine the distribution of chemicals between phases in equilibrium [18]. These are also known as the partition coefficients in the literature or more commonly as K–values. The mentioned vapor–liquid equilibrium distribution coefficient of species i is defined as $K_i = y_i / x_i = \gamma_i \cdot P_i^{sat} / P$.

The K–value of seawater salt is zero due to its non–volatility, while those of the non–condensable gases as well as water can be approximated using the above temperature–based correlations as follows

$$K_{N_2} = \frac{y_{N_2}}{x_{N_2}} = \frac{\dfrac{P_{N_2}}{P_V}}{x_{N_2}} = \frac{\dfrac{HC_{N_2} \cdot x_{N_2}}{P_V}}{x_{N_2}} = \frac{HC_{N_2}}{P_V}$$ (43)

$$K_{O_2} = \frac{y_{O_2}}{x_{O_2}} = \frac{\dfrac{P_{O_2}}{P_V}}{x_{O_2}} = \frac{\dfrac{HC_{O_2} \cdot x_{O_2}}{P_V}}{x_{O_2}} = \frac{HC_{O_2}}{P_V}$$ (44)

$$K_{Ar} = \frac{y_{Ar}}{x_{Ar}} = \frac{\dfrac{P_{Ar}}{P_V}}{x_{Ar}} = \frac{\dfrac{HC_{Ar} \cdot x_{Ar}}{P_V}}{x_{Ar}} = \frac{HC_{Ar}}{P_V}$$ (45)

$$K_{CO_2} = \frac{y_{CO_2}}{x_{CO_2}} = \frac{\dfrac{P_{CO_2}}{P_V}}{x_{CO_2}} = \frac{\dfrac{HC_{CO_2} \cdot x_{CO_2}}{P_V}}{x_{CO_2}} = \frac{HC_{CO_2}}{P_V}$$ (46)

$$K_{H_2O} = \frac{\gamma_{H_2O} \cdot P_{H_2O}}{P_V}$$ (47)

Vapor–liquid equilibrium distribution coefficients were obtained using the SUPERTRAPP™ program, an interactive computer code distributed by the National Institute of Standards and Technology that calculates thermodynamic properties of mixtures based on the Peng–Robinson equation of state. SUPERTRAPP™ was employed to perform isobaric phase equilibria flash calculations for water with an average content of non–condensable gas as reported in literature [16] at various temperatures to produce a dataset of K–values. Least squares regression was then used to fit the data to the above equilibrium equations by adjusting values of $HC°_i$, HF_i, PA, PB, and PC producing correlation coefficients very close to unity as will be seen later in CHAPTER 6.

The SUPERTRAPP™ code used in generating the vapor–liquid equilibrium distribution coefficient data and the Matlab™ codes used in regressing that data to adjust the vapor–liquid equilibrium parameters are in the APPENDICES section.

SUPERTRAPP™ simulations are fresh water based, and no salts were included in their flash calculations. To adjust phase equilibria computations of the current model for saline water, K–values are multiplied by a relativity parameter that can be defined as $α_i$ = *solubility in fresh water / solubility in seawater* for solutes and $α_{H2O}$ = *seawater saturated pressure / fresh water saturated pressure* for water. The relativity factor is a single constant obtained by averaging literature data given over the operating temperature range to simplify calculations [19].

Activity is a way for expressing the effective concentrations of species to account for their deviation from ideal behavior. Activity can be applied to any concentration scales such as molality, molarity, or fractional scales; however, molar fraction is the most common concentration scale used in flash calculation.

Activity accounts for deviations from ideal behavior by multiplying the concentration by an activity coefficient that can be experimentally determined or empirically computed using several available models. The value of an activity coefficient approaches unity as molecular interactions behave more ideally.

The activity coefficient of water is needed to calculate its K–value. Experimental data can be used to perform adiabatic flash calculations, generating activity coefficient data that are then used to find an activity coefficient correlation resembling

$$\gamma_{H_2O} = f\left(\frac{P_V}{P_{H_2O}}\right) \tag{48}$$

4.2.3 Adiabatic Flash

The flash operation of the proposed desalination process is an adiabatic expansion operation where the temperature of seawater drops upon entering the flash chamber due to the drawn enthalpy of vaporization by the flashing water vapor, attaining a saturation temperature used in the above equilibrium calculations. Flash computations are carried out on a molar basis, and the molar composition of the stream entering the flash chamber can be calculated from the average composition of seawater reported on mass basis [16]

$$z_{N_2} = \frac{\dfrac{\varphi_{N_2}}{MW_{N_2}}}{\dfrac{\varphi_{N_2}}{MW_{N_2}} + \dfrac{\varphi_{O_2}}{MW_{O_2}} + \dfrac{\varphi_{Ar}}{MW_{Ar}} + \dfrac{\varphi_{CO_2}}{MW_{CO_2}} + \dfrac{\varphi_{H}}{MW_{Salt}} + \dfrac{\varphi_{H_2O}}{MW_{H_2O}}} \tag{49}$$

$$z_{O_2} = \frac{\dfrac{\varphi_{O_2}}{MW_{O_2}}}{\dfrac{\varphi_{N_2}}{MW_{N_2}} + \dfrac{\varphi_{O_2}}{MW_{O_2}} + \dfrac{\varphi_{Ar}}{MW_{Ar}} + \dfrac{\varphi_{CO_2}}{MW_{CO_2}} + \dfrac{\varphi_{H}}{MW_{Salt}} + \dfrac{\varphi_{H_2O}}{MW_{H_2O}}} \tag{50}$$

$$z_{Ar} = \cfrac{\cfrac{\varphi_{Ar}}{MW_{Ar}}}{\cfrac{\varphi_{N_2}}{MW_{N_2}} + \cfrac{\varphi_{O_2}}{MW_{O_2}} + \cfrac{\varphi_{Ar}}{MW_{Ar}} + \cfrac{\varphi_{CO_2}}{MW_{CO_2}} + \cfrac{\varphi_{H}}{MW_{Salt}} + \cfrac{\varphi_{H_2O}}{MW_{H_2O}}} \tag{51}$$

$$z_{CO_2} = \cfrac{\cfrac{\varphi_{CO_2}}{MW_{CO_2}}}{\cfrac{\varphi_{N_2}}{MW_{N_2}} + \cfrac{\varphi_{O_2}}{MW_{O_2}} + \cfrac{\varphi_{Ar}}{MW_{Ar}} + \cfrac{\varphi_{CO_2}}{MW_{CO_2}} + \cfrac{\varphi_{H}}{MW_{Salt}} + \cfrac{\varphi_{H_2O}}{MW_{H_2O}}} \tag{52}$$

$$z_{Salt} = \cfrac{\cfrac{\varphi_{H}}{MW_{Salt}}}{\cfrac{\varphi_{N_2}}{MW_{N_2}} + \cfrac{\varphi_{O_2}}{MW_{O_2}} + \cfrac{\varphi_{Ar}}{MW_{Ar}} + \cfrac{\varphi_{CO_2}}{MW_{CO_2}} + \cfrac{\varphi_{H}}{MW_{Salt}} + \cfrac{\varphi_{H_2O}}{MW_{H_2O}}} \tag{53}$$

The molar composition of the concentrated brine is given by

$$x_{N_2} = \frac{z_{N_2} \cdot N_H}{N_W + N_E \cdot \alpha_{N_2} \cdot K_{N_2}} \tag{54}$$

$$x_{O_2} = \frac{z_{O_2} \cdot N_H}{N_W + N_E \cdot \alpha_{O_2} \cdot K_{O_2}} \tag{55}$$

$$x_{Ar} = \frac{z_{Ar} \cdot N_H}{N_W + N_E \cdot \alpha_{Ar} \cdot K_{Ar}} \tag{56}$$

$$x_{CO_2} = \frac{z_{CO_2} \cdot N_H}{N_W + N_E \cdot \alpha_{CO_2} \cdot K_{CO_2}} \tag{57}$$

$$x_{Salt} = \frac{z_{Salt} \cdot N_H}{N_W} \tag{58}$$

$$x_{H_2O} = \frac{z_{H_2O} \cdot N_H}{N_W + N_E \cdot \alpha_{H_2O} \cdot K_{H_2O}} \tag{59}$$

Similarly, the molar composition of the flashed vapor is given by

$$y_{N_2} = x_{N_2} \cdot \alpha_{N_2} \cdot K_{N_2} \tag{60}$$

$$y_{O_2} = x_{O_2} \cdot \alpha_{O_2} \cdot K_{O_2} \tag{61}$$

$$y_{Ar} = x_{Ar} \cdot \alpha_{Ar} \cdot K_{Ar} \tag{62}$$

$$y_{CO_2} = x_{CO_2} \cdot \alpha_{CO_2} \cdot K_{CO_2} \tag{63}$$

$$y_{H_2O} = x_{H_2O} \cdot \alpha_{H_2O} \cdot K_{H_2O} \tag{64}$$

Fraction summations are given by

$$\varphi_{N_2} + \varphi_{O_2} + \varphi_{Ar} + \varphi_{CO_2} + \varphi_{H} + \varphi_{H_2O} = 1 \tag{65}$$

$$z_{N_2} + z_{O_2} + z_{Ar} + z_{CO_2} + z_{Salt} + z_{H_2O} = 1 \tag{66}$$

$$x_{N_2} + x_{O_2} + x_{Ar} + x_{CO_2} + x_{Salt} + x_{H_2O} = 1 \tag{67}$$

$$y_{N_2} + y_{O_2} + y_{Ar} + y_{CO_2} + y_{H_2O} = 1 \tag{68}$$

4.2.4 Heat Transfer

Computing temperatures of streams exiting the flash chamber properly is essential in accurately evaluating performance of the proposed desalination system; therefore, heat transfer calculations are included in the model, complimenting the above energy balance to solve for those temperatures. Heat transfer calculations are included to estimate the amount of heat transferred from the condensing vapor to the entering seawater feed through the condenser tube as well as the heat loss from both compartments of the flash chamber through the walls of the condenser and evaporator.

The condenser is exposed to maximize heat loss, while the evaporator is insulated to minimize heat loss, and the entire flash chamber is vacuum sealed. The vapor pressure gradient between the two compartments of the flash chamber is the driving force of vapor transfer from the hot evaporator to the cold condenser to produce fresh water.

The condenser will be modeled as a shell and tube heat exchanger, both where the cold seawater is flowing inside a coiled tube placed in an exposed shell and where the flashed vapor is condensing on the outer surface of that coiled tube by losing its latent heat of condensation to the entering cold seawater. The evaporator will be modeled as an insulated vessel, where heated seawater is flashing producing fresh water vapor that moves to the condenser due to lower vapor pressure through a connecting duct.

Heat transfer is a complex process, particularly when phase change is involved. Heat transfer can come about in different modes; however, the current model will use the overall heat transfer approach to simplify computations.

The inside and outside fluid film coefficients can be estimated by the following correlations that were developed specifically for water and stagnant air [20] as well as evaporating and condensing steam [15]

$$h_{CT}^{i} = 3.0525 \cdot 10^{-4} \cdot \left(\frac{M_X}{D_{CT} \cdot \rho_X} \right)^{0.8} \cdot \left(\frac{1.35 + 0.02 \cdot T_X}{D_{CT}} \right) \tag{69}$$

$$h_{CT}^{o} = 0.725 \cdot \left(\frac{g \cdot H_E^L \cdot \rho_X^{2} \cdot k_X^{3}}{N_{CT} \cdot \mu_X \cdot (D_{CT} + \delta_{CT}) \cdot (T_E - T_X)} \right)^{0.25} \tag{70}$$

$$h_{C}^{i} = 1.13 \cdot \left(\frac{g \cdot H_E^L \cdot \rho_C^{2} \cdot k_C^{3}}{\mu_C \cdot L_C \cdot (T_E - T)} \right)^{0.25} \tag{71}$$

$$h_{C}^{o} = 0.0448 \cdot \left(\frac{T_E - T}{L_C} \right)^{0.25} \tag{72}$$

$$h_{E}^{i} = 1.13 \cdot \left(\frac{g \cdot H_E^L \cdot \rho_W^{2} \cdot k_W^{3}}{\mu_W \cdot L_E \cdot (T_E - T)} \right)^{0.25} \tag{73}$$

$$h_{E}^{o} = 0.0448 \cdot \left(\frac{T_E - T}{L_E} \right)^{0.25} \tag{74}$$

The overall heat transfer coefficient is a simplified parameter used in gauging overall convective and conductive resistance to heat transfer. Overall heat transfer coefficients are computed by the following correlations [20]

$$\frac{1}{U_{CT}} = \frac{1}{h_{CT}^o} + \frac{1}{h_{CT}^{od}} + \frac{D_{CT}+\delta_{CT}}{D_{CT} \cdot h_{CT}^i} + \frac{D_{CT}+\delta_{CT}}{D_{CT} \cdot h_{CT}^{id}} + \frac{D_{CT}+\delta_{CT}}{2 \cdot k_{CT}^w} \cdot Ln\left[\frac{D_{CT}+\delta_{CT}}{D_{CT}}\right] \qquad (75)$$

$$\frac{1}{U_C} = \frac{1}{h_C^o} + \frac{1}{h_C^{od}} + \frac{D_C+\delta_C}{D_C \cdot h_C^i} + \frac{D_C+\delta_C}{D_C \cdot h_C^{id}} + \frac{D_C+\delta_C}{2 \cdot k_C^w} \cdot Ln\left[\frac{D_C+\delta_C}{D_C}\right] \qquad (76)$$

$$\frac{1}{U_E} = \frac{1}{h_E^o} + \frac{1}{h_E^{od}} + \frac{D_E+\delta_E}{D_E \cdot h_E^i} + \frac{D_E+\delta_E}{D_E \cdot h_E^{id}} + \frac{D_E+\delta_E}{2 \cdot k_E^w} \cdot Ln\left[\frac{D_E+\delta_E}{D_E}\right] \qquad (77)$$

Heat transfer area is assumed to be equal to that of the inner surface of the heat transfer medium, with the end sections ignored; therefore, heat exchange surface areas are given by the following geometrical relationships

$$A_{CT} = \pi \cdot D_{CT} \cdot L_{CT} \qquad (78)$$

$$A_C = \pi \cdot D_C \cdot L_C \qquad (79)$$

$$A_E = \pi \cdot D_E \cdot L_E \qquad (80)$$

The log mean temperature difference is a logarithmic average of the temperature difference between the hot and cold streams of a heat exchanger. It represents the driving force for heat transfer in heat exchangers, since that heat transfer is directly proportional to its value. The log mean temperature difference expressions are given by

$$\Delta Tm_{CT} = \frac{T_X - T_P}{Ln\left[\dfrac{T_E - T_P}{T_E - T_X}\right]} \qquad (81)$$

$$\Delta Tm_C = \frac{T_C - T}{Ln\left[\dfrac{T_E - T}{T_E - T_C}\right]} \qquad (82)$$

$$\Delta Tm_E = \frac{T_W - T}{Ln\left[\dfrac{T_E - T}{T_E - T_W}\right]} \tag{83}$$

The counter–current departure parameters are dimensionless ratios used in correcting the log mean temperature difference expressions and are given by

$$S_{CT} = \frac{T_X - T_P}{T_E - T_P} \tag{84}$$

$$S_C = \frac{T_C - T}{T_E - T} \tag{85}$$

$$S_E = \frac{T_W - T}{T_E - T} \tag{86}$$

The heat transferred from the condensing vapor to the entering seawater, as well as the heat loss from the condenser and from the evaporator, are given by

$$M_X \cdot H_X - M_P \cdot H_P = 60 \cdot U_{CT} \cdot A_{CT} \cdot F_{CT} \cdot \Delta Tm_{CT} \tag{87}$$

$$-Q_C = 60 \cdot U_C \cdot A_C \cdot F_C \cdot \Delta Tm_C \tag{88}$$

$$-Q_E = 60 \cdot U_E \cdot A_E \cdot F_E \cdot \Delta Tm_E \tag{89}$$

The counter–current departure correction factors are dimensionless variables used in correcting log mean temperature difference expressions. The counter–current departure correction factors are widely available in literature as look–up charts for many types of heat exchangers and can be computed empirically as functions of counter–current departure parameters

$$F_{CT} = f(S_{CT}) \tag{90}$$

$$F_C = f(S_C) \tag{91}$$

$$F_E = f(S_E) \tag{92}$$

The vapor pressure of seawater is 1.84 % lower than that of pure water at the same temperature due to non–volatile salts, and therefore, the boiling point of seawater is slightly higher than that of fresh water. This phenomenon is known as the boiling point elevation or vapor pressure depression. Boiling point elevation is a function of salinity and does not depend on properties of solute or solvent [14].

The temperature of seawater drops upon entering the flash chamber to attain equilibrium; however, equilibrium is not always fully achieved. This phenomenon is known as the non–equilibrium allowance, and it depends on several factors such as flash temperature, flow rates, concentrated brine depth, and chamber geometry.

Correlations for boiling point elevation [21] and non–equilibrium allowance [22] can be incorporated into the model to account for flash efficiency as follows

$$T_W = T_E + BPE + NEA \tag{93}$$

4.2.5 Vacuum Volume

All vessels will be modeled as right circular cylinders with specified dimensions. The fresh water and the brine water tanks are equipped with discharge pipes located slightly above the level of the inlet water pipes, keeping their levels constant. Conversely, levels of the seawater tank, as well as condenser and evaporator, are constantly changing during operation; therefore, they need to be computed and included in the model. The level of the feed seawater tank is used in calculating the vertical discharge pressure head that will be used in determining the pumping requirements, while levels of the condenser and evaporator are used in calculating the vacuum volume that will be used in calculating the vacuum pressure.

The circular cross sectional areas of these vessels are needed to calculate their levels and are determined by

$$XA_S = \frac{\pi}{4} D_S^2 \tag{94}$$

$$XA_E = \frac{\pi}{4} D_E^2 \tag{95}$$

$$XA_C = \frac{\pi}{4} D_C^2 \tag{96}$$

The level of the seawater tank decreases with time because of the continuous pumping of seawater to the process, and it can be geometrically computed by

$$Z_S = Z_S^i - \frac{\int M_S dt}{\rho_S \cdot XA_S} \tag{97}$$

If the seawater flow rate remains constant during operation, the numerator of the second term of the above equation simplifies to $\int M_S\, dt = M_S \cdot t$.

The level in the condenser is hydrostatically balanced with the level in the fresh water tank. Since the level in the fresh water tank is kept constant, the vacuum pressure inside the flash chamber is the only variable controlling the level in the condenser. The level in the condenser decreases as vacuum pressure increases due to non–condensable gases building up in the flash chamber.

The initial and the dynamic levels in the condenser can be estimated using Bernoulli's fluid equation given by

$$Z_C^i = -\left(\frac{P - P_V^i - \Delta P_C}{\rho_C \cdot g} \right) \cdot 10^6 - PL_C + Z_F \tag{98}$$

$$Z_C = -\left(\frac{P - P_V - \Delta P_C}{\rho_C \cdot g} \right) \cdot 10^6 - PL_C + Z_F \tag{99}$$

Similarly, the level in the evaporator is hydrostatically balanced with the level in the brine water tank. Since the level in the brine water tank is kept constant, the vacuum pressure inside the flash chamber is the only variable controlling the level in the evaporator. The level in the evaporator decreases as vacuum pressure increases due to non–condensable gases building up in the flash chamber.

The initial and the dynamic levels in the evaporator can be estimated using Bernoulli's fluid equation given by

$$Z_E^i = -\left(\frac{P - P_V^i - \Delta P_W}{\rho_W \cdot g} \right) \cdot 10^6 - PL_W + Z_B \qquad (100)$$

$$Z_E = -\left(\frac{P - P_V - \Delta P_W}{\rho_W \cdot g} \right) \cdot 10^6 - PL_W + Z_B \qquad (101)$$

The initial and the dynamic volumes of the vacuum in the condenser depend on corresponding initial and dynamic levels of the condenser. They are geometrically computed by subtracting corresponding fresh water volume from total volume of the right circular horizontal cylinder condenser as follows

$$V_{CV}^i = L_C \cdot \left(\frac{\pi \cdot D_C^2}{8} + \frac{D_C^2}{4} \cdot Arc\,sin\left(1 - \frac{2 \cdot Z_C^i}{D_C} \right) + \left(\frac{D_C}{2} - Z_C^i \right) \cdot \left(Z_C^i \cdot \left(D_C - Z_C^i \right) \right)^{\frac{1}{2}} \right) \quad (102)$$

$$V_{CV} = L_C \cdot \left(\frac{\pi \cdot D_C^2}{8} + \frac{D_C^2}{4} \cdot Arc\,sin\left(1 - \frac{2 \cdot Z_C}{D_C} \right) + \left(\frac{D_C}{2} - Z_C \right) \cdot \left(Z_C \cdot \left(D_C - Z_C \right) \right)^{\frac{1}{2}} \right) \quad (103)$$

Initial and the dynamic volumes of the vacuum in the evaporator depend on corresponding initial and dynamic levels of the evaporator. They are geometrically computed by subtracting the corresponding brine water volume from total volume of the right circular horizontal cylinder evaporator as follows

$$V_{EV}^i = L_E \cdot \left(\frac{\pi \cdot D_E^2}{8} + \frac{D_E^2}{4} \cdot Arc\sin\left(1 - \frac{2 \cdot Z_E^i}{D_E}\right) + \left(\frac{D_E}{2} - Z_E^i\right) \cdot \left(Z_E^i \cdot (D_E - Z_E^i)\right)^{\frac{1}{2}} \right) \quad (104)$$

$$V_{EV} = L_E \cdot \left(\frac{\pi \cdot D_E^2}{8} + \frac{D_E^2}{4} \cdot Arc\sin\left(1 - \frac{2 \cdot Z_E}{D_E}\right) + \left(\frac{D_E}{2} - Z_E\right) \cdot \left(Z_E \cdot (D_E - Z_E)\right)^{\frac{1}{2}} \right) (105)$$

Vacuum volume is the total space occupied by vapor in the flash chamber and can be computed by adding the vapor space of both condenser and evaporator to the volume of the connecting duct and subtracting the volume of the coiled tube of the condenser. Therefore, the initial and dynamic vacuum volumes can be calculated by

$$V_V^i = V_{EV}^i + V_{CV}^i + \frac{\pi}{4} \cdot \left(PL_E \cdot PD_E^2 - L_{CT} \cdot D_{CT}^2 \right) \quad (106)$$

$$V_V = V_{EV} + V_{CV} + \frac{\pi}{4} \cdot \left(PL_E \cdot PD_E^2 - L_{CT} \cdot D_{CT}^2 \right) \quad (107)$$

4.2.6 Vacuum Pressure

Seawater flow rate and the flash temperature are the only controlled variables of the proposed continuous desalination operation, and their effects on the system will be analyzed later. Seawater flow rate determines the amount of non–condensable gases accumulated, while the flash temperature determines the equilibrium temperature reached inside the flash chamber in line with the above mass and energy balance.

The accumulated amount of non–condensable gases and the reached equilibrium temperature, as well as the calculated vacuum volume, determine vacuum pressure according to any equation of state. It is imperative to express the vacuum pressure properly to simulate the proposed continuous desalination operation accurately because of the profound impact of vacuum pressure on the outcome of the flash operation.

The ideal gas model describes fluid properties without considering molecular size or intermolecular attractions; therefore, its accuracy diminishes at higher pressures and lower temperatures. Low vacuum pressure marginalizes the effect of molecular size, while the fairly high flash temperature, manifested in higher thermal kinetic energy, weakens the relative importance of intermolecular attractions. Consequently, the ideal gas law becomes a suitable equation of state to express rising vacuum pressure inside the flash chamber due to build up of non–condensable gases in the flash chamber.

Initial vacuum pressure is an input value and should be very close to or equal to the saturated pressure of water at ambient conditions, while the initial vacuum volume can be determined by the above mentioned relations, knowing initial levels in the flash chamber. The gas phase primarily consists of water molecules at first, and their amount can then be estimated by

$$n_V^i = \frac{P_V^i \cdot V_V^i}{R \cdot (T + 273.15)} \qquad (108)$$

Non–condensable gas molecules progressively accumulate in the flash chamber, and their amount must be added to the initial amount computed above to express the dynamic amount of molecules in the gas phase as

$$n_V = n_V^i + \int N_C^a dt \qquad (109)$$

Initial and the dynamic saturated pressures of water are needed to express vacuum pressure in a little while. The dynamic saturated pressure of water is given above as a function of dynamic equilibrium temperature, while initial saturated pressure of water is a function of ambient temperature and can be calculated by [15]

$$P_{H_2O}^i = exp\left[PA - \left(\frac{PB}{T + PC} \right) \right] \qquad (110)$$

48

The vacuum pressure needs to be specified to proceed with the flash calculations ultimately leading to convergence of the whole model; therefore, the simulation is executed incrementally, where the computed vacuum pressure of one time increment becomes the input vacuum pressure to the next time increment. The known initial vacuum pressure value is input to the first time increment to initialize this progression. This scheme is known as the *Iterative and Incremental Development* in the art of software development. Consequently, the incremented vacuum pressure is expressed by

$$P_V\big|_t = \frac{\psi \cdot n_V \cdot R \cdot (T_E + 273.15)}{V_V} + \left[P_{H_2O} - P_{H_2O}^i\right] \tag{111}$$

$$P_V = P_V\big|_{t-\Delta t} \tag{112}$$

To illustrate the *Iterative and Incremental Development* concept as it pertains to the current model, consider the ensuing paradigm. The known initial vacuum pressure is fed to the computer code as dynamic vacuum pressure of the first increment resulting in a solution for the dynamic vacuum pressure of the second increment that is then fed to the computer code resulting in a solution for the vacuum pressure of the third increment, and so forth until the last increment is reached.

The dynamic quantity of molecules in the gas phase incorporates accumulated non–condensable gas molecules plus water molecules present at the initial ambient point; however, there are more water molecules in the gas phase not account for due to the temperature increase from ambient to equilibrium. Consequently, the second term on right hand side of the vacuum pressure expression, P_{H2O} - P^i_{H2O}, is added to correct the dynamic amount of water molecules in the gas phase by accounting for the increase in vapor pressure due to temperature rise from ambient to equilibrium.

The model assumes total accumulation of non–condensable gases in the flash chamber; however, water vapor dissolves a small quantity of non–condensable gases as it condenses. In addition, average values for seawater content of dissolved gases are input to the model, as the real seawater content of dissolved gases is indefinite and could be somewhat different from the average values. Moreover, the true vapor–liquid equilibrium for carbon dioxide involves more than just the afore mentioned K–values due to presence of several carbonates in seawater that are also in equilibrium with carbon dioxide.

Consequently, a correction factor for the dynamic amount of molecules in the gas phase is included in the vacuum pressure expression. Experimental data can be used to perform adiabatic flash calculations, generating correction factor data that are then used to find a correction factor correlation resembling

$$\psi = f\left(\frac{P_V}{P_{H_2O}}\right) \tag{113}$$

Other expressions of vacuum pressure can be worked out, but it is very important for the expressed vacuum pressure to match experimental values closely due to its strong impact on the outcome of the simulation as mentioned earlier.

Operating pressure inside the flash chamber has to be between the dew point and the bubble point to carry out a successful flash separation. Dew point and bubble point pressures are estimated by

$$\frac{P_{BP}}{P_V} = z_{N_2}\alpha_{N_2}K_{N_2} + z_{O_2}\alpha_{O_2}K_{O_2} + z_{Ar}\alpha_{Ar}K_{Ar} + z_{CO_2}\alpha_{CO_2}K_{CO_2} + z_{H_2O}\alpha_{H_2O}K_{H_2O} \tag{114}$$

$$\frac{P_V}{P_{DP}} = \frac{z_{N_2}}{\alpha_{N_2} \cdot K_{N_2}} + \frac{z_{O_2}}{\alpha_{O_2} \cdot K_{O_2}} + \frac{z_{Ar}}{\alpha_{Ar} \cdot K_{Ar}} + \frac{z_{CO_2}}{\alpha_{CO_2} \cdot K_{CO_2}} + \frac{z_{H_2O}}{\alpha_{H_2O} \cdot K_{H_2O}} \tag{115}$$

4.2.7 System Performance

Pressure drop is a design parameter used in accounting for pressure reduction due to friction. Total pressure drop of seawater flow from the seawater tank to flash chamber can be determined by summing up the pressure drops of each upstream pipe

$$\Delta P = \Delta P_S + \Delta P_P + \Delta P_X + \Delta P_H + \Delta P_{HT} + \Delta P_{CT} \tag{116}$$

If a throttling valve is used to control flow rate of seawater, the pump will run at full capacity, and work exerted on seawater by the pump is a direct function of the power of the pump, that is $W_P = - 44742 \cdot HP_P$. If a variable–frequency drive is used to control flow rate of seawater, the pump will run at modulated speeds, and work exerted on seawater by the pump is a function of the head pressure.

The proposed desalination system will consider a variable–frequency drive to control flow rate of seawater due to its superior energy efficiency over a throttling valve; therefore, work exerted on seawater by the pump can be estimated using Bernoulli's fluid equation as

$$W_P = -M_P \cdot \left[g \cdot (Z_S - Z_O) \cdot 10^{-7} + \frac{P_V - P - \Delta P}{10 \cdot \rho_P} \right] \tag{117}$$

An appropriate circulation pump can be selected from the catalog of any process equipment manufacture based on required flow rate and total head. Selecting the pump will set many parameters including its power and suction force. The procedure of selecting a pump or any required piece of equipment for the process is beyond the scope of this analysis; however, equipment sizing is a common straightforward practice. Formulae for sizing pumps, valves, vessels, pipes, expansion orifices, and many other process equipment are abundantly available in literature [23].

A solar heater is employed in the proposed desalination system to heat the preheated seawater coming out of the condenser further before flashing it in the evaporator. Solar heating can be accomplished in a variety of ways; however, the present model assumes the heater to be a single–glazed flat–plate solar collector directly heating seawater flowing through its absorbing tubes.

Solar insolation is geographically referenced and continually varying due to dynamic solar angles. In addition, solar insolation incident on the collector varies with plate geometry, sky clearness, ground reflectivity, and many other factors. Average values for a generic single–glazed flat–plate solar collector will be used to simplify comparison among the different simulation scenarios.

The solar insolation area of the collector needed to meet the required heating load can be found using the Hottel–Whillier–Bliss correlation [8]

$$A_{SC} = \frac{Q_H}{60 \cdot F_{SC} \cdot [\tau_{SC} \cdot \alpha_{SC} \cdot I - U_{SC} \cdot (T_X - T)]} \tag{118}$$

Solar heating is usually accomplished indirectly by an intermediary heat exchanger that transfers heat from a solar collector loop to a process loop. The proposed desalination system drops this intermediary heat exchanger by flowing seawater directly through the absorbing tubes of the solar collector; therefore, increasing the efficiency and reducing the cost of the solar heater. On the other hand, this direct heating scheme has its drawbacks by increasing the risk of corrosion and scale formation causing equipment damage and inhibiting heat transfer. Hermann–Koschikowski–Rommel [24] developed corrosion–free solar collectors for thermal desalination systems use composed of a series of coated glass tubes mounted inside a conventional flat-plate solar collector enclosure; therefore, flowing seawater directly through the collector is a viable alternative.

Condenser efficiency is defined as the percent of the ratio of the temperature gradient on the cold tube side to the temperature gradient on the hot shell side as

$$\eta_C = \frac{T_X - T_P}{T_E - T_C} \times 100\% \tag{119}$$

Heat recovery efficiency is defined as the percent of total enthalpy change that was essentially accomplished by reclaiming heat from the condensing vapor as

$$\eta_R = \frac{H_X - H_S}{H_H - H_S} \times 100\% \tag{120}$$

Thermal efficiency of the proposed desalination system is defined as the percent of the total thermal energy supplied that was actually used to vaporize water as

$$\eta_T = \frac{M_E \cdot \left(H_E + H_E^L\right)}{M_H \cdot H_H} \times 100\% \tag{121}$$

Prime energy consumption is a very important parameter in evaluating feasibility of any desalination system and is defined as the ratio of the amount of energy exhausted to the amount of fresh water produced. The total amount of energy exhausted is the heat supplied by the heater plus power supplied by the pump.

Prime energy consumption can be expressed as a constantly shifting parameter by $PEC = (Q_H + W_P) / M_C$ on instantaneous basis; however, it is typically desired to express prime energy consumption as a single value attained on a totalized basis by integrating the implicated dynamic process variables over the entire operating period. Total prime energy consumption of the proposed unit is given by

$$PEC = \frac{\int Q_H dt + \int W_P dt}{\int M_C dt} \tag{122}$$

4.2.8 Physical Properties

Laminar flow is a smooth flow pattern, where fluid layers are flowing in parallel concentric cylindrical layers without any inter–layer mixing in a manner determined by the viscosity of the fluid [25]. Turbulent flow is a rough flow pattern, where fluid particles are randomly fluctuating in transverse to the general flow direction in a manner determined by inertial forces of the fluid [25]. Figure 24 illustrates the streaming profile of both flow regimes.
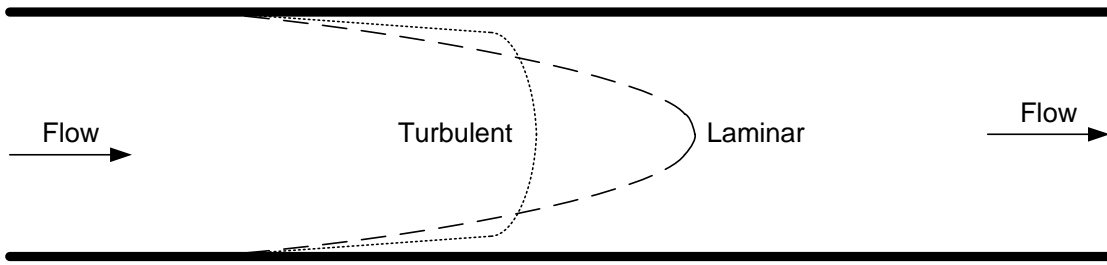
Figure 24. Flow regimes

Reynolds number is a dimensionless quantity that represents the ratio of inertial forces to viscous forces and is used to classify different flow regimes as either laminar or turbulent. Laminar flow behavior occurs at low Reynolds numbers, while turbulent flow behavior occurs at high Reynolds numbers. The critical Reynolds number of 2300 is generally accepted as the midpoint of the transition range between laminar and turbulent flows in cylindrical pipes.

Reynolds number of process streams is given by

$$Re_j = \frac{M_j}{15 \cdot \pi \cdot PD_j \cdot \mu_j} \tag{123}$$

The pressure of a flowing fluid inside a pipe inevitably drops due to gravity and wall drag. This pressure drop and loss can be approximated depending on the flow pattern by the Hagen–Poiseuille equation: $\Delta P_j = 6.79 \cdot 10^{-7} \cdot (\mu_j \cdot PL_j \cdot M_j) / (\rho_j \cdot PD_j^4)$ for laminar or by the Moody equation: $\Delta P_j = 9.01 \cdot 10^{-10} \cdot (f_j \cdot PL_j \cdot M_j^2) / (\rho_j \cdot PD_j^5)$ for turbulent flows [15], where f is the dimensionless Fanning Friction Factor available in literature as a function of both Reynolds number and pipe roughness. The current desalination process will be designed to include streams exhibiting laminar flow conditions to simplify experimental simulations later; hence, the model will employ the Hagen–Poiseuille equation to estimate average pressure drops of process streams as

$$\Delta P_j = \frac{6.79 \cdot 10^{-7} \cdot \mu_j \cdot PL_j \cdot M_j}{\rho_j \cdot PD_j^{\,4}} \tag{124}$$

Thermal conductivity is a property that gauges heat conduction ability of a given substance. Dependence of thermal conductivity on temperature relates to the freedom of movement molecules enjoy; therefore, thermal conductivity varies with temperature in fluids but remains fairly constant in solids. Thermal conductivities of process streams are calculated empirically by the Caldwell Relation [26]

$$k_j = \left(5711.16 + 17.1335 \cdot T_j - 0.0585 \cdot T_j^2 - 1656.2364 \cdot \varphi_j \right) \cdot 10^{-6} \tag{125}$$

Furthermore, thermal conductivities of flashing water vapor and accumulating non–condensable gases are not required but can be calculated empirically by [27]

$$k_E = \left[\begin{array}{l} 2.2744e\text{-}12 \cdot (1.8 \cdot T_j + 32)^3 - 5.8518e\text{-}10 \cdot (1.8 \cdot T_j + 32)^2 \\ + 3.8912e\text{-}7 \cdot (1.8 \cdot T_j + 32) + 1.6943e - 4 \end{array} \right] \tag{126}$$

$$k_C^a = \left[\begin{array}{l} 1.5207e - 13 \cdot (T_j + 273.15)^3 - 4.8574e\text{-}10 \cdot (T_j + 273.15)^2 \\ + 1.0184e - 6 \cdot (T_j + 273.15) - 3.9333e - 6 \end{array} \right] \tag{127}$$

The stream densities used in several correlations above will be calculated by an empirical relationship experimentally developed by the Rosenstiel School of Marine and Atmospheric Science at the University of Miami to calculate density of seawater as a function of temperature and salinity [28]. Densities of process streams are given by

$$\rho A_j = 0.82 + T_j \cdot \left(-4.09 \cdot 10^{-3} + T_j \cdot \left(7.64 \cdot 10^{-5} + T_j \cdot \left(-8.25 \cdot 10^{-7} + T_j \cdot 5.39 \cdot 10^{-9}\right)\right)\right) \quad (128)$$

$$\rho B_j = -5.72466 \cdot 10^{-3} + T_j \cdot \left(1.0227 \cdot 10^{-4} - 1.6546 \cdot 10^{-6} \cdot T_j\right) \quad (129)$$

$$\rho C_j = \left(6.79 \cdot 10^{-2} - \left(9.10 \cdot 10^{-3} - \left(10^{-4} - \left(1.12 \cdot 10^{-6} - 6.54 \cdot 10^{-9} T_j\right) \cdot T_j\right) \cdot T_j\right) \cdot T_j\right) \cdot T_j \quad (130)$$

$$\rho_j = \frac{999.84 + \rho C_j}{1000} + \varphi_j \cdot \left(\rho A_j + \rho B_j \cdot \left(1000 \cdot \varphi_j\right)^{\frac{1}{2}} + 0.48314 \cdot \varphi_j\right) \quad (131)$$

Stream viscosities used in several correlations above will be calculated by an empirical relationship that was experimentally developed to calculate the viscosity of seawater as a function of temperature and salinity [29]. Viscosities of process streams are given by

$$\mu A_j = 1.0675 \cdot 10^{-4} + 5.185 \cdot 10^{-5} \cdot T_j \quad (132)$$

$$\mu B_j = 2.591 \cdot 10^{-3} + 3.3 \cdot 10^{-5} \cdot T_j \quad (133)$$

$$\mu C_j = 553.5413 \cdot \rho_j \cdot \varphi_j \quad (134)$$

$$\mu D_j = 0.01002 \cdot 10^{\left[\frac{1.1709 \cdot (20 - T_j) - 1.827 \cdot 10^{-3} \cdot (T_j - 20)^2}{T_j + 89.93}\right]} \quad (135)$$

$$\mu_j = \left(1 + \mu A_j \cdot \mu C_j^{0.5} + \mu B_j \cdot \mu C_j\right) \cdot \mu D_j \quad (136)$$

stream enthalpies used in the energy balances above will be calculated by an empirical relationship that was experimentally developed to calculate heat capacity of seawater as a function of temperature and salinity [30] as follows

$$H_j = \begin{bmatrix} + \left(0.0530 - 1.6853 \cdot \varphi_j + 8.5367 \cdot \varphi_j^2 \right) \cdot 10^{-4} \cdot T_j^3 \\ - \left(0.0007 - 0.0310 \cdot \varphi_j + 0.1624 \cdot \varphi_j^2 \right) \cdot T_j^2 \\ + \left(4.2045 - 6.7823 \cdot \varphi_j + 14.7532 \cdot \varphi_j^2 \right) \cdot T_j - 0.04881 \end{bmatrix} \tag{137}$$

Seawater flashes in the evaporator producing water vapor that acquires its latent enthalpy of vaporization from the concentrated brine. Then, the produced water vapor condenses in the condenser by losing its latent enthalpy of condensation to the entering saline water. Latent enthalpy of vaporization and the latent enthalpy of condensation are numerically equal but have opposite signs and can be estimated by [27]

$$H_E^L = 2496.2101 - 1.9535 \cdot T_E - 0.0042 \cdot T_E^{\ 2} \tag{138}$$

Nitrogen, oxygen, argon, and carbon dioxide are the only non–condensable gases considered in the model, since they make up more than 99.9 % of the total dissolved gases in seawater [19]. The US National Institute of Standards and Technology provides the following correlation to calculate molar enthalpy of non–condensable gases [31]

$$\underline{H}_{NCG} = \begin{pmatrix} A_{NCG} \cdot (T_E + 273.15) + \dfrac{B_{NCG}}{2e3} \cdot (T_E + 273.15)^2 + \dfrac{C_{NCG}}{3e6} \cdot (T_E + 273.15)^3 \\ + \dfrac{D_{NCG}}{4e9} \cdot (T_E + 273.15)^4 - \dfrac{1e6 \cdot E_{NCG}}{(T_E + 273.15)} + 1e3 \cdot F_{NCG} \end{pmatrix} \tag{139}$$

Overall enthalpy of the accumulating non–condensable gases can be computed by adding molar enthalpies of each composing species weighted on a water–free basis, in relation to the assumption of total condensation of flashed water vapor. In addition, the average molecular weight of the accumulating gases referenced before was employed to convert its enthalpy units from molar to mass based. Thus, overall enthalpy of accumulating non–condensable gases is given by

$$H_C^a = \frac{y_{N_2} \cdot \underline{H}_{N_2} + y_{O_2} \cdot \underline{H}_{O_2} + y_{Ar} \cdot \underline{H}_{Ar} + y_{CO_2} \cdot \underline{H}_{CO_2}}{\left(1 - y_{H_2O} \right) \cdot MW_C^a} \tag{140}$$

57

4.3 Solution Algorithm

A computer code featuring the above equations, plus other correlations and parameters given later in CHAPTER 6 can be found in the APPENDICES section along with sample input and output values of process variables. Computer code execution is incremental due to time–based numerical integration used above to account for accumulation of non–condensable gases in the flash chamber, while convergence process is iterative due to interdependence of equations of the model. The increment size should be carefully selected to simplify convergence and reduce processing without jeopardizing the integrity of the simulation. A concise block diagram outlining the general scheme to solve the above model is shown in Figure 25.

Time is embedded in the model by flow rates of different streams; moreover, integration operations of the model are based on small time increments that evenly divide the entire run. Ambient temperature and pressure, as well as physical properties and geometrical dimensions of process pipes and vessels, are input to the model. Universal values such as gas constant and gravity acceleration, plus seawater composition and the molecular weights of the involved species, are also input to the model. Parameters for enthalpy and vapor–liquid equilibrium relations, as well as average values for a generic single–glazed flat–plate solar collector, are also supplied to the code.

Flash temperature is a controlled variable and will be supplied to code as a single set value. Initial vacuum pressure is a known quantity and will also be supplied to code to launch the simulation process. Initial vacuum pressure will be fed to the first increment, producing vacuum pressure for the second increment producing the vacuum pressure for the third increment and so forth.

58
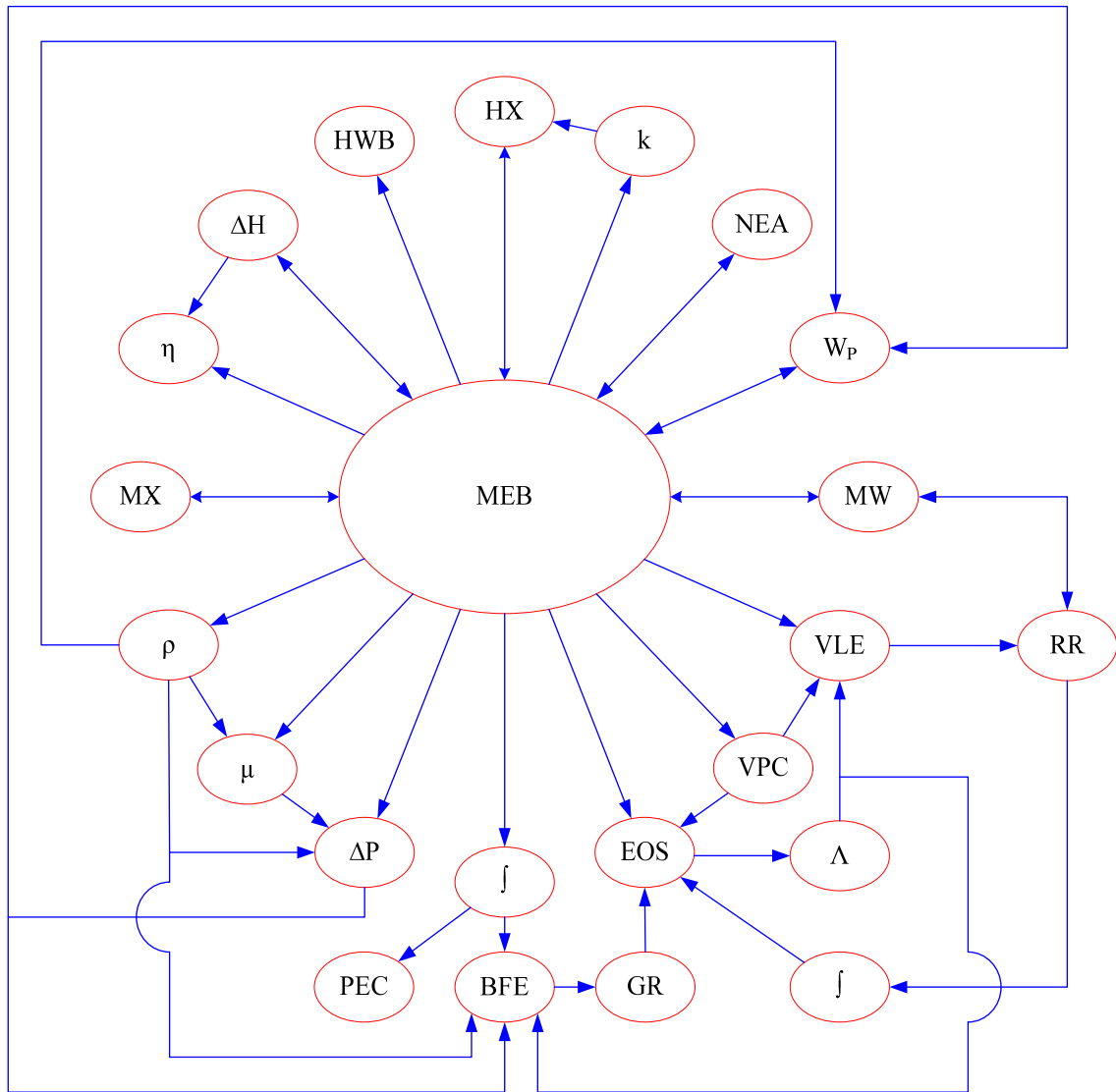
BFE	Bernoulli's Fluid Equation		RR	Rachford–Rice
EOS	Equation of State		VLE	Vapor–Liquid Equilibrium
GR	Geometrical Relations		VPC	Vapor Pressure Correlation
HWB	Hottel–Whillier–Bliss		W_P	Pump Work
HX	Heat Transfer		ΔH	Enthalpy
k	Thermal Conductivity		ΔP	Pressure Drop
MEB	Mass and Energy Balance		$\int$	Instantaneous Integration
MW	Molecular Weight		η	Efficiency
MX	Mass Transfer		Λ	Lag
NEA	Non–Equilibrium Allowance		μ	Viscosity
PEC	Prime Energy Consumption		ρ	Density

Figure 25. Developed model solution algorithm

The mass and energy balance simultaneously solves with mass and heat transfer relations, as well as enthalpy and non–equilibrium allowance correlations. Mass and energy balance indirectly solves with the pump work relation via density and pressure drop correlations and with molecular weight relations via Rachford–Rice calculations.

Mass and energy balance provides inputs for density, viscosity, and pressure drop correlations, producing outputs that are fed to the pump work relation and Bernoulli's fluid equation. In addition, mass and energy balance provides inputs for thermal conductivity correlations used in heat transfer calculations and for efficiency relations that use those inputs along with other inputs from the enthalpy correlations to evaluate system performance. The mass and energy balance also provides input values for the Hottel–Whillier–Bliss correlation to estimate solar collection area needed and for an integrator that totalizes system variables before forwarding them both to the prime energy consumption function and to Bernoulli's fluid equation.

Mass and energy balance and the Rachford–Rice calculations are linked via molecular weight relations and concurrently solve for equilibrium temperature that is fed to vapor–liquid equilibrium relations, a vapor pressure correlation, and an equation of state. The equation of state estimates system vacuum pressure before it is lagged and forwarded to vapor–liquid equilibrium relations, where K–values are generated and fed to Rachford–Rice calculations to calculate the rate of accumulation of non–condensable gases that is integrated and fed back to the equation of state to calculate the pressure of the next time increment. The lagged system pressure is also fed to Bernoulli's fluid equation, where tank levels are calculated and forwarded to geometrical relations to compute volume of the vacuum before forwarding it to the equation of state.

CHAPTER 5. EXPERIMENTAL ANALYSIS

5.1 Process Description

A small pilot unit has been built to simulate the proposed continuous desalination system described previously experimentally. Figure 26 outlines a general process and instrumentation diagram of the small pilot unit. Experimental simulations were performed inside a laboratory to simplify operation and maintenance. Due to this indoor process, solar heating was hard to implement due to lack of solar insolation, and passive vacuum was difficult to produce due to limited elevation.

Solar heating is widely used in several applications, including desalination systems as was mentioned in CHAPTER 2; therefore, replicating it with an electric heater is considered acceptable, since the concept of solar heating does not require further proof. In addition, vacuum was passively generated by Goswami and Kharabsheh [11] for their desalination unit as was mentioned in CHAPTER 3; therefore, producing it with a vacuum pump is considered acceptable, since the phenomenon of passive vacuum generation using gravity has been experimentally established.

Placing the flash chamber at a low elevation in the experimental unit removed hydraulic head of the proposed unit; thus, a circulation pump is no longer required to pass seawater through the unit. The pressure difference between the vacuumed flash chamber and open seawater feed tank becomes the driving force of seawater flow, which was manually controlled by manipulating valve positions.

61
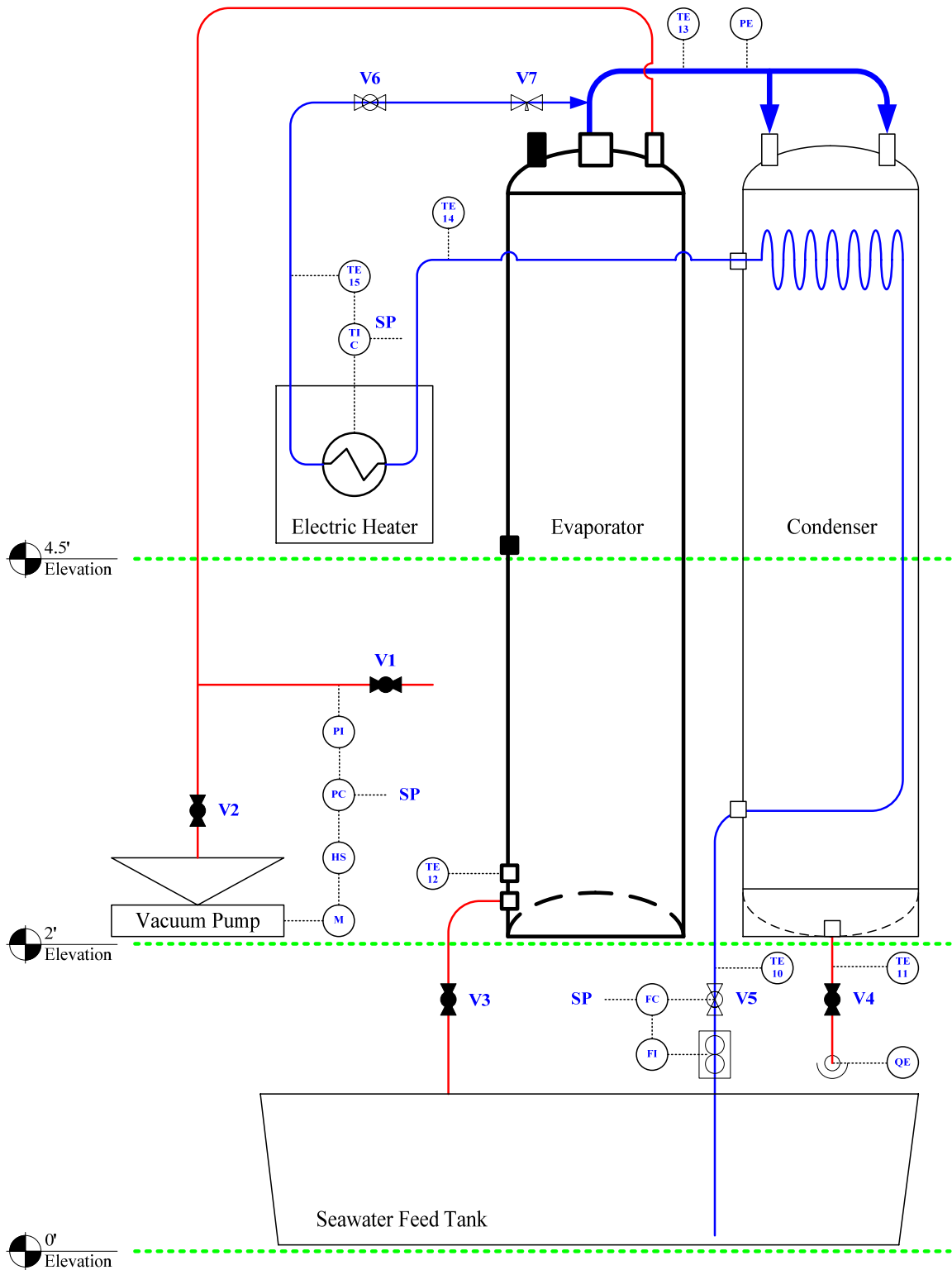
Figure 26. Process and instrumentation diagram of the experimental unit

5.2 Experimental Apparatus

The entire experimental unit is mounted on three–tier mobile skids built from slotted and unslotted struts with linking joints and brackets as shown in Figure 27. The three tiers are connected by four upright bars, the bottom two tiers include plywood for weight distribution, and the bottom tier is outfitted with four wheels for mobility.

The seawater feed tank is a 50–gallon open–top, horizontal polyethylene trough placed on the bottom tier of skids. The condenser is a 40–gallon painted–steel, upright cylinder, while the evaporator is a 40–gallon galvanized–steel, upright cylinder, and they are both placed on the middle tier of the skids directly above the seawater feed tank. Condenser, evaporator, and 2" Y–shaped CPVC pipe connecting them from the top make up the flash chamber. The condenser was cut open around its upper section to install a 4¾ m long ½" copper pipe coiled to provide the necessary condensing surface, then welded back to its original shape. In addition, a small hole was drilled at the bottom of the condenser to retrieve the condensed water. The evaporator and the 2" Y–shaped CPVC pipe are wrapped with sheets of insolating material to minimize heat loss. The condenser and evaporator have discharge pipes that drain into the seawater feed tank.

The heater is a 4.5 kW zinc–plated, copper electric heating element placed inside a copper shell, where seawater coming out of the condenser passes through it on its way to be flashed in the evaporator. A ½ HP vacuum pump is piped to the evaporator to create the initial vacuum, and a ½" polypropylene needle valve, V7 in Figure 26, is placed right before the evaporator to function as an expansion orifice for the incoming heated seawater to be flashed. The ½" CPVC pipe is used in connecting all of the above equipment as well as several ½" CPVC and copper pipe fittings.

Several instruments have been integrated into the experimental unit to manage system variables as shown in Figure 26. These are used in monitoring and controlling system vacuum, seawater flow, and flash temperature, as well as monitoring temperature of each process stream. Nomenclature used in the P&ID of Figure 26 is consistent with the International Society of Automation symbol standards.

Pressure indicator PI is a liquid–filled analog vacuum gauge, while pressure element PE is a high–precision vacuum transmitter. The PI was used to help establish the initial system vacuum and to monitor its gradual erosion. The PE was used to continually supply the value of the system vacuum to a data acquisition system.

Flow indicator FI is an acrylic in–line flowmeter, while quantitative element QE is a glass 500 ml graduated cylinder. The FI was used to help establish and monitor the seawater flow through the system. The quantitative element QE was used to collect and measure the amount of fresh water produced at the end of each experiment.

Temperature elements TE10, TE11, TE12, TE13, and TE14 are single–output, while temperature element TE15 is dual–output ⅛" diameter T–Type thermocouples. All used to supply the value of the temperature of each process stream continually to a data acquisition system. In addition, TE15 is used to supply the temperature controller with the value of its controlled variable.

Pressure controller PC and flow controller FC are imaginary pressure and flow manual controllers, while temperature indicating controller TIC is an LED–equipped digital PID automatic controller. Regulators V1 and V4 are ¼", while regulators V2, V3, V5, and V6 are ½" full port ball valves. Detailed descriptions of all of the above apparatus taken from their vendors are in the APPENDICES section.

Equipment

4.5' elevation tier

4 3.5'-bars
2 3'-bars
2 1.2' bars

Legend

──────── Plywood

━━━━1" slotted struts■

━━━━1" un-slotted struts■

━━━━1" slotted struts■

━━━━0.5" slotted struts■

⊖ 3" wheels

⊠ upright positions

2' elevation tier

2 3.5'-bars
4 3'-bars
3.5'X3' Plywood

0' elevation tier

2 5'-bars
4 3'-bars
5'X3' Plywood
4 wheels
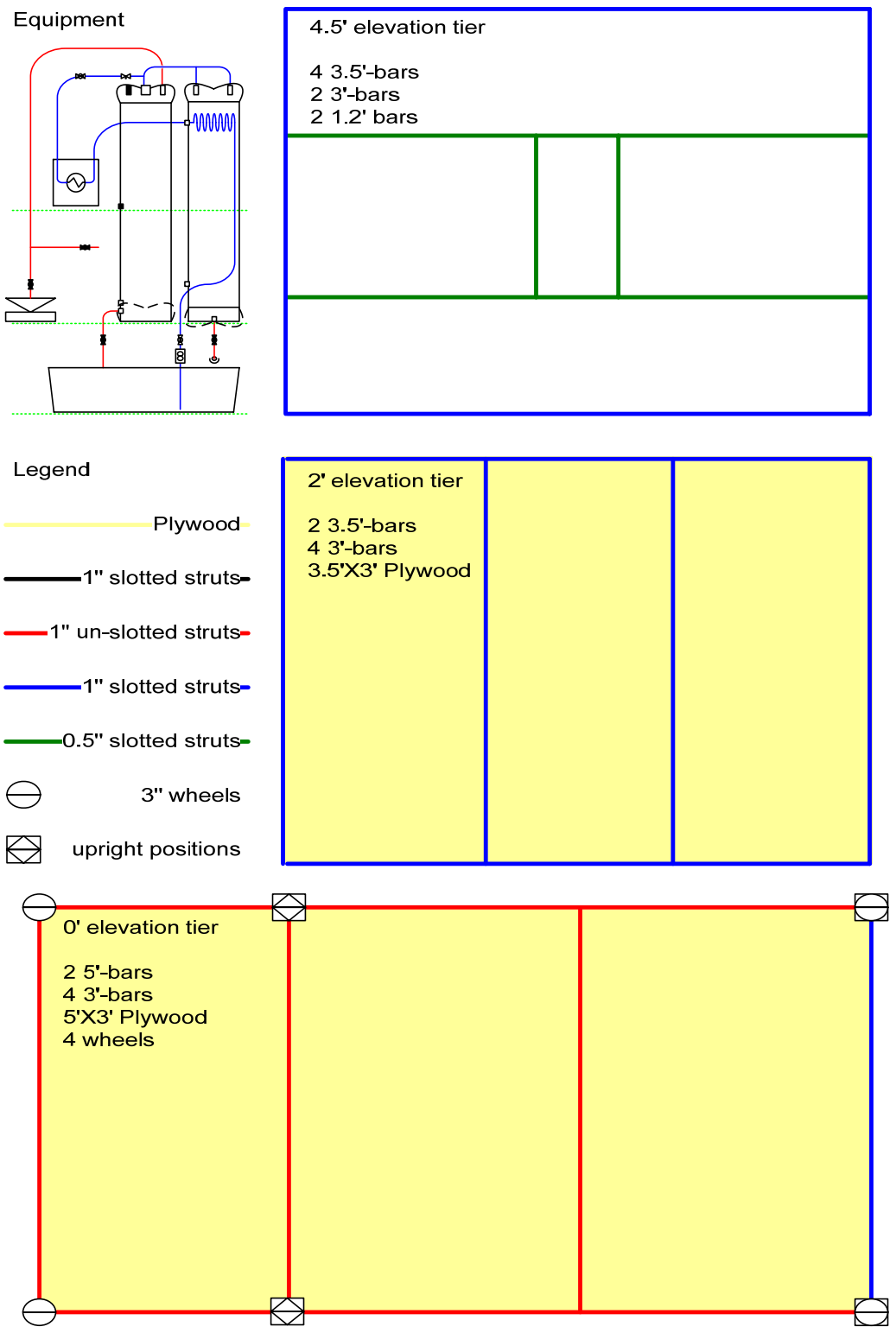
Figure 27. 3–tier mobile skids layout

65

5.3 Control Scheme

The three feedback control loops pertaining to system vacuum, seawater flow, and flash temperature shown in Figure 26 are replicated in Figure 28 in isolation to clarify their control techniques. System vacuum and seawater flow are manually adjusted, while flash temperature is automatically controlled.

The system vacuum feedback control loop is invoked prior to running the experiment to attain the desired initial vacuum. It consists of measuring the vacuum with pressure indicator PI while the vacuum pump is running. Once the desired vacuum set point SP is reached, hand switch HS is manually switched off to shut down motor M of the vacuum pump, which remains shut during the entire experiment.

The seawater flow feedback control loop is invoked at the beginning of the experiment to attain the desired seawater flow rate, which remains constant throughout the experiment. It consists of measuring flow with flow indicator FI, while manually manipulating the valve position of V5 until the desired flow rate set point SP is realized. The valve position is kept constant throughout the experiment.
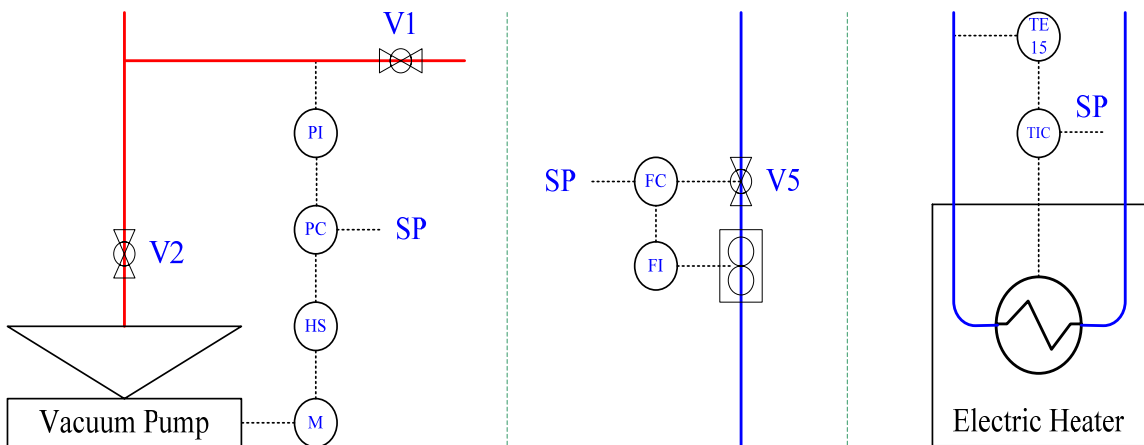
Figure 28. Feedback control loops of the experimental unit

The flash temperature feedback control loop is constantly active to stabilize flash temperature during the experiment. It consists of measuring temperature of seawater coming out of the heater with temperature element TE15, then supplying that measurement to temperature indicating controller TIC that automatically manipulates the current input into the heat element of the heater, effectively varying its heat output to the incoming seawater until the desired flash temperature set point SP is achieved.

A simplified block diagram of the flash temperature feedback control loop is given in Figure 29. The assigned arrows SP, E, CO, TO, and U are the frequency–domain Laplace transform functions of the set point, error, controller output, transmitter output, and disturbance signals, respectively.

Block TIC represents the transfer function of the digital PID automatic temperature controller given generically as

$$TIC(s) = K_C \cdot \left(1 + \frac{1}{\tau_I \cdot s} + \tau_D \cdot s \right) \tag{141}$$

Automatic temperature controller TIC is equipped with an automatic tuning ability that was used to tune its parameters during a dry run, yielding the following values

PB = 20 % TO / % CO

K_C = 100 / PB = 5 % CO / % TO

τ_I = 60 seconds

τ_D = 2 seconds

The cycle time or total period that controller output cycles on and off when the controlled variable is within the PB was set to 1 second. In addition, a derivative approach control of 2.5 × PB was used to remove derivative action at system start–up. The fail–safe mode of the controller was set to turn off SP upon input signal loss.

Block PL represents the transfer function of the process loop between the controlled and manipulated variables, which is usually represented by a first order model with dead time compensation as follows

$$PL(s) = \frac{K_{PL} \cdot EXP(-t_0 \cdot s)}{\tau_{PL} \cdot s + 1}$$ (142)

Block DL represents the transfer function of the disturbance loop between the controlled variable and disturbance, which is usually represented by a first order model with dead time compensation as follows

$$DL(s) = \frac{K_{DL} \cdot EXP(-t_0 \cdot s)}{\tau_{DL} \cdot s + 1}$$ (143)

Block PL and block DL are actually combinations of several transfer functions that were lumped into a single first order model to simplify representing the dynamic response of the process. Block PL merges a sequence of transfer functions characterizing thermocouple TE15, the heating process, and electric heater. Block DL merges a sequence of transfer functions characterizing thermocouple TE15 and flowing process. The automatic tuning ability of controller TIC is based on obtaining the parameters of the first order models representing block PL and block DL.
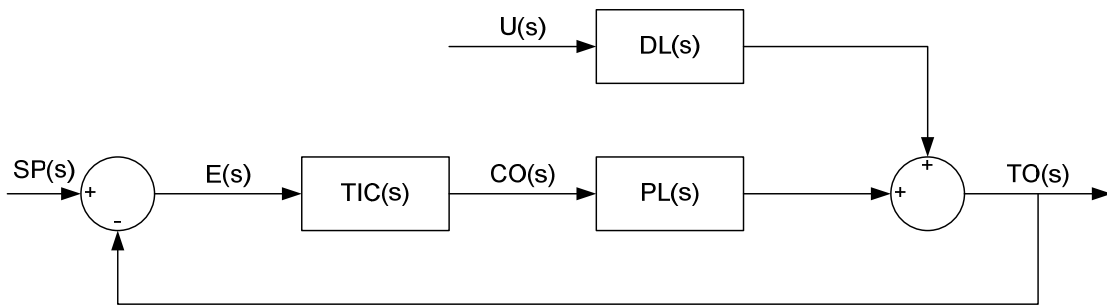
Figure 29. Block diagram of the flash temperature feedback control loop

5.4 Data Acquisition

A data acquisition system designed to sample and record process variables was assembled and attached to the experimental apparatus. Configuration of the data acquisition system is illustrated in Figure 30.

Pressure element PE outputs an analog current signal corresponding to system vacuum with a range from 4–20 mA to fieldbus module FBM1 through a 2–wire cable. Temperature elements TE10, TE11, TE12, TE13, TE14, and TE15 output analog voltage signals corresponding to system temperatures, each with a range from -0.001–0.01 mV to fieldbus module FBM2, through thermocouple extension wires.

Fieldbus module FBM1 is a multiplexing signal conditioner, where the analog current signal of pressure element PE is converted to a corresponding analog voltage signal with a range from 1–5 V. Fieldbus module FBM2 is a multiplexing signal conditioner, where the analog voltage signals of temperature elements TE10, TE11, TE12, TE13, TE14, and TE15 are converted to corresponding analog voltage signals with a range of 1–5 V. The conditioned analog output signals of fieldbus modules FBM1 and FBM2 are multiplexed via multiplexer MUX, which is a DC–37 ribbon connecting cable.

Analog to digital converter ADC is a 16–bit data acquisition system that converts continuous analog signals supplied by multiplexer MUX to discrete digital signals and forwards them to human–machine interface HMI through an enhanced parallel port LPT cable. Human–machine interface HMI is a notebook PC running a data acquisition software that converts acquired data from its conditioned voltage units to its corresponding physical attributes. The data acquisition software also displays and stores the acquired data for later analysis as shown in Figure 31.
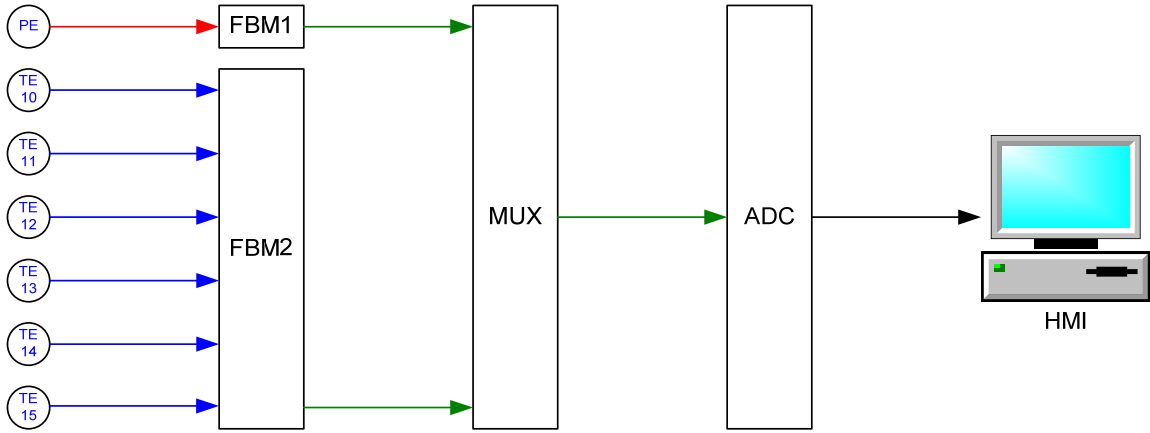
Figure 30. Data acquisition structure
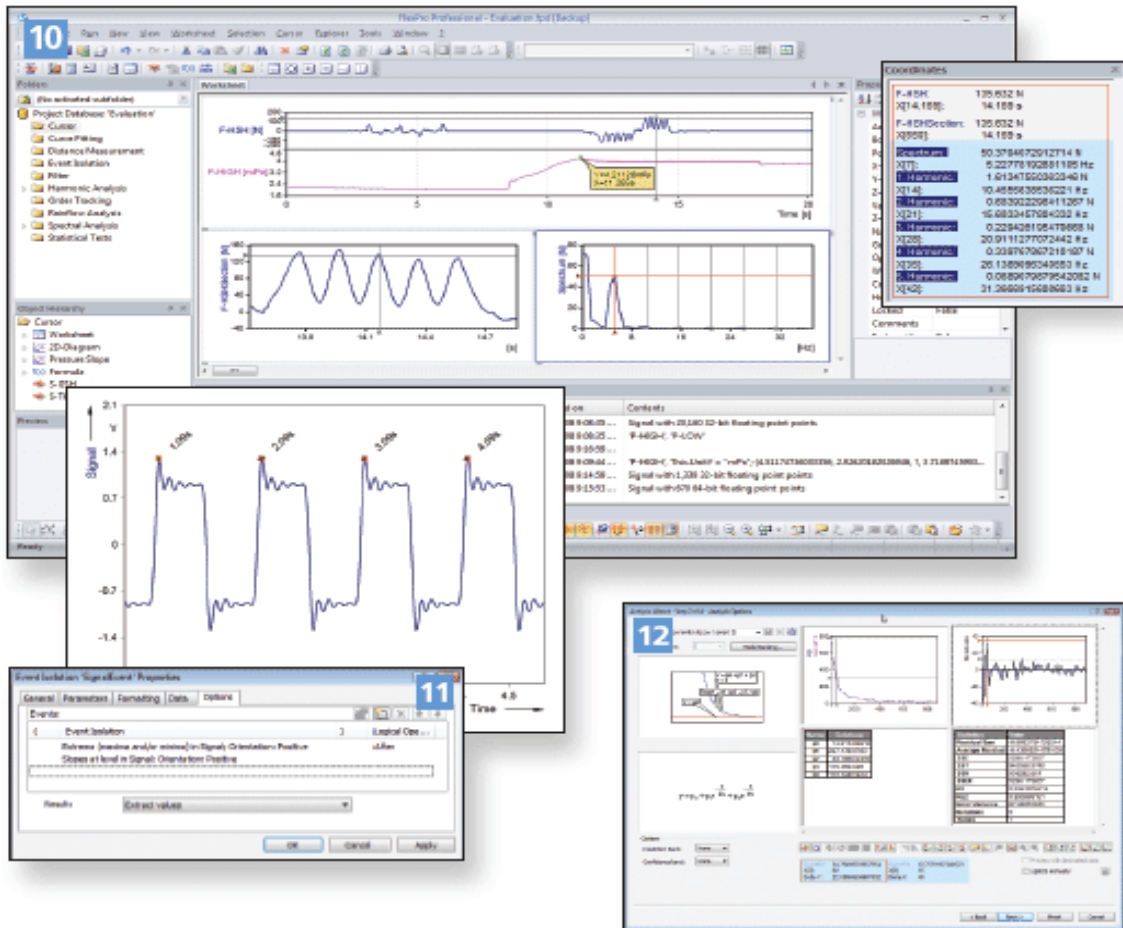
Figure 31. Data acquisition software

5.5 Operating Procedure

Operation of the experimental unit closely resembled that of the proposed desalination system described in CHAPTER 4. Initial vacuum was created by running the vacuum pump until a reasonable vacuum was reached. Running the vacuum pump further will trap moisture in its oil reservoir significantly inhibiting its performance.

Synthetic seawater was prepared by mixing 13 pounds of commercial–grade sea salt with 40 gallons of tap water. The seawater mix was stirred well before each experiment to ensure full solution of sea salt. The seawater trough has a large open surface that enhances evaporation; therefore, small amounts of fresh water were often added before running experiments to reach a 40–gallon level mark in the trough.

Temperature indicating controller TIC is not interlocked with seawater flow; thus, ensuring seawater flow through the electric heater is a very critical safety measure. Regulators V5 and V6, plus needle valve V7, are instruments that control seawater flow. The valve position of needle valve V7 was kept constant at about 90 % open for all runs, because narrowing valve position caused flow oscillations regardless of the valve positions of regulators V5 and V6. The valve position of regulator V6 was used to start and stop the experiment; therefore, it was toggled between fully open and fully close. Valve position of regulator V5 was used to manipulate the flow as was mentioned above.

Pressure element PE is calibrated by the manufacture, while Fieldbus module FBM2 contains a built–in cold junction compensation that automatically calibrates thermocouple outputs. In addition, data acquisition software wais set to execute one scan per second and to average every ten scans to reduce signal noise. The acquired data were saved to an assigned ASCII formatted file on the Human–machine interface HMI.

The experimental unit must be kept motionless during operation due to its high center of gravity, while its normal operating procedure is as follows

1.   Start data acquisition system

2.   Open regulator V2 fully

3.   Start vacuum pump until desired vacuum is reached

4.   Close regulator V2 fully

5.   Stop vacuum pump

6.   Slowly open regulator V6 fully

7.   Set seawater flow rate through regulator V5 and flow indicator FI

8.   Activate temperature indicating controller TIC

9.   Trigger data recording function of data acquisition software

10.   Run unit until the specified period of the experiment is reached

11.   Stop data recording function of data acquisition software

12.   Disable temperature indicating controller TIC

13.   Quickly close regulator V6 fully

14.   Stop data acquisition system

15.   Open regulator V1 to terminate the vacuum

16.   Open regulator V3 to drain brine into the seawater trough

17.   Open regulator V4 to drain fresh water into quantitative element QE

18.   Record amount produced then drain into the seawater trough

19.   Fully close regulator V1

20.   Fully close regulator V3

21.   Fully close regulator V4

5.6 Experimental Design

Experiments were conducted at analogous conditions to simplify design evaluation but with different values of the controlling variables to enhance process analysis and modeling. All experiments were run for a period of three hours starting with an initial system vacuum of 0.14 bars. Experiments were carried out at two different seawater flow rate ranges and at four different flash temperatures of 50, 60, 70, and 80 degrees centigrade. In addition, each experiment was duplicated three times to estimate its variation. Table 6 illustrates the experimental matrix, while Figure 32 gives an overall view of the experimental unit.

Table 6. Experimental matrix

Number	Start Time	Stop Time	Initial PI (bar)	FI (LPM)	TIC SP (°C)	QE (ml)
1						
2					50	
3						
4				lower flow		
5					60	
6						
7						
8				around ~ 0.50	70	
9						
10						
11					80	
12			0.14			
13						
14					50	
15						
16				higher flow		
17					60	
18						
19						
20				around ~ 0.70	70	
21						
22						
23					80	
24						

Figure 32. Overall view of the experimental unit

CHAPTER 6. PARAMETRIC ANALYSIS

6.1 Analyses Synchronization

Theoretical and experimental analyses must be synchronized to compare their outputs properly. The model developed in CHAPTER 4 holds for the proposed desalination system outlined in Figure 21; however, it needs to be modified to represent the experimental unit outlined in Figure 26 to validate its predictions.

The flash chamber of the experimental unit is not elevated for passive vacuum generation, and levels of the flash chamber are not hydrostatically balanced as was mentioned in CHAPTER 5. Vacuum is created before running the unit by a vacuum pump; furthermore, the flash chamber is closed during operation to maintain that vacuum, since it can not be maintained hydrostatically. Consequently, Bernoulli's fluid equation can not be used to estimate initial and the dynamic levels in the evaporator and condenser. Initial levels are equal to zero as vessels are drained before operation while dynamic levels are functions of totalized, or integrated, inlet flows. Therefore, Equation 98 through Equation 101 are substituted with

$$Z_C^i = 0 \qquad\qquad\qquad\qquad \text{(Alternate 98)}$$

$$Z_C = Z_C^i - \frac{\int M_C dt}{\rho_C \cdot XA_C} \qquad\qquad\qquad\qquad \text{(Alternate 99)}$$

$$Z_E^i = 0 \qquad\qquad\qquad\qquad \text{(Alternate 100)}$$

$$Z_E = Z_E^i - \frac{\int M_W dt}{\rho_W \cdot XA_E} \qquad\qquad\qquad\qquad \text{(Alternate 101)}$$

The condenser and evaporator are modeled as horizontally–mounted right circular cylinders as can be seen in Figure 21; however, the condenser and evaporator of the experimental unit are vertically–mounted right circular cylinders as can be seen in Figure 26. Consequently, the geometry of the vacuum volume needs to adapt; therefore, Equation 102 through Equation 105 are substituted with

$$V_{CV}^{i} = XA_C \cdot \left(L_C - Z_C^{i} \right) \qquad\qquad \text{(Alternate 102)}$$

$$V_{CV} = XA_C \cdot \left(L_C - Z_C \right) \qquad\qquad \text{(Alternate 103)}$$

$$V_{EV}^{i} = XA_E \cdot \left(L_E - Z_E^{i} \right) \qquad\qquad \text{(Alternate 104)}$$

$$V_{EV} = XA_E \cdot \left(L_E - Z_E \right) \qquad\qquad \text{(Alternate 105)}$$

The experimental unit does not include a feed pump as was mentioned in CHAPTER 5; therefore, Equation 117 is substituted with

$$W_P = 0 \qquad\qquad \text{(Alternate 117)}$$

6.2 Parameter Expressions

The model developed in CHAPTER 4 along with the above alternate equations were coded and executed using experimental temperature, pressure, and flow rate values as inputs generating pseudo–experimental data of model parameters. This data mining process is used to uncover patterns in model parameters so they can be properly expressed in the model via correlations obtained using non–linear regression.

The counter–current departure correction factor for the condenser tube is used to correct its log mean temperature difference to solve accurately for the temperature of preheated seawater before it enters the heater, which is essential for estimating prime energy consumption and efficiency of the condenser and heat recovery.

A correlation for the counter–current departure correction factor for the condenser tube is obtained by regressing the mined data as shown in Figure 33 yielding

$$F_{CT} = 0.0293 + 0.1655 \cdot S_{CT} + 2.9102 \cdot S_{CT}^2 - 6.1629 \cdot S_{CT}^3 + 4.2518 \cdot S_{CT}^4 \qquad \text{(Alternate 90)}$$

The counter–current departure correction factor for the condenser is used to correct its log mean temperature difference to solve for the temperature of the condensed fresh water accurately; however, experimental data show that the temperature of the condensed fresh water remained rather constant with a value about two degrees above ambient regardless of how high the equilibrium temperature was. This outcome is most likely due to a good heat rejection by the condenser, in addition to the fact that the amount of cool seawater flowing through the condenser tube vastly exceeds that of the condensing water vapor outside the condenser tube.

Consequently, a correlation for the counter–current departure correction factor for the condenser will be replaced by

$$T_C = T + 2 \qquad \text{(Alternate 91)}$$

The counter–current departure correction factor for the evaporator is used in correcting its log mean temperature difference to estimate its heat loss accurately. Temperatures of the flashed vapor and concentrated brine diverge due to boiling point elevation and non–equilibrium allowance as mentioned in CHAPTER 4 as well as a small amount of heat loss from the insulated evaporator.

To simplify calculations, heat loss from the evaporator is ignored, and a correlation for the non–equilibrium allowance is obtained by regressing the experimental data as shown in Figure 34 yielding

$$Q_E = 0 \qquad \text{(Alternate 92)}$$

$$\xi = 1.6836 \cdot \zeta^2 - 3.3898 \cdot \zeta + 2.7785 - 0.1399 \cdot exp\left(-5.9154 \cdot \zeta^{-29.3208}\right)$$

$$Where \quad \xi = \frac{T_W + 273.15}{T_E + 273.15} \quad \zeta = \frac{T_H + 273.15}{25 + 273.15} \qquad \text{(Alternate 93)}$$

The activity coefficient of water is used to correct its molar fractions to solve for its K–value accurately. Theoretical expressions for activity coefficients of species in electrolyte solutions, such as seawater, are available in literature but very challenging to implement due to the large number of interactions present among all ions and molecules. Those interactions are characterized by parameters that in most cases must be experimentally determined.

To simplify calculations, a correlation for the activity coefficient of water is obtained by regressing the mined data as shown in Figure 35 yielding

$$\gamma_{H_2O} = 0.0020 + 1.0385 \cdot \frac{P_V}{P_{H_2O}} \qquad \text{(Alternate 48)}$$

The gas phase molecular content correction factor is used in correcting the equation of state to solve for the vacuum pressure accurately as was mentioned earlier in CHAPTER 4. It accounts for both gases dissolving in the condensing water vapor and any possible discrepancy in the input seawater content of dissolved gases or the calculated vapor–liquid equilibrium for carbon dioxide.

To simplify calculations, a correlation for gas phase molecular content correction factor is obtained by regressing the mined data as shown in Figure 36 yielding

$$\psi = 1 - 2.2861 \cdot exp\left(-\frac{P_V}{P_{H_2O}}\right) \qquad \text{(Alternate 113)}$$

The Matlab™ codes used for regressing all of the above mined data are found in the APPENDICES section.
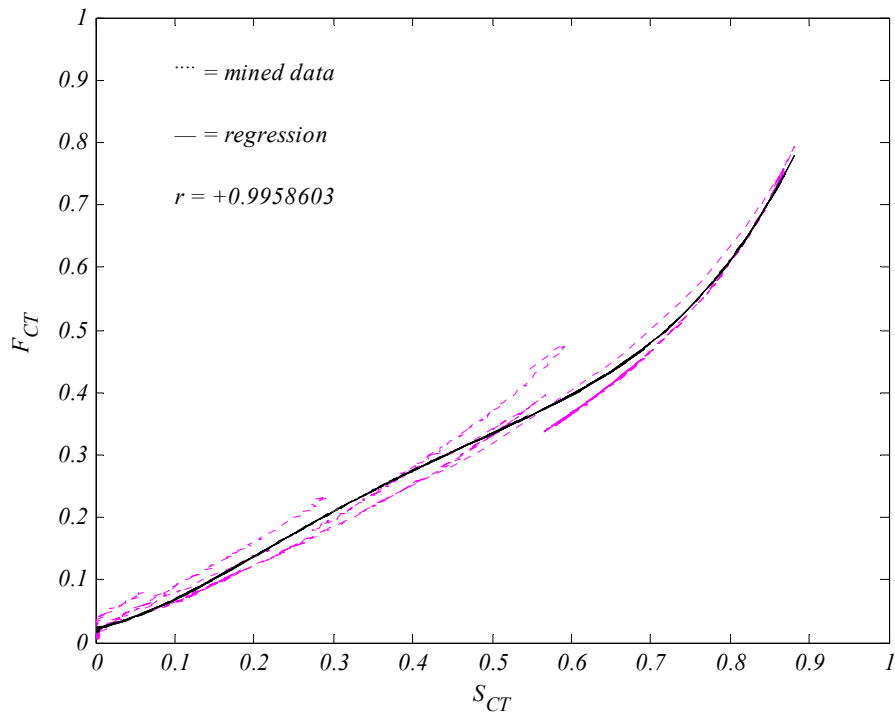
Figure 33. Counter–current departure correction factor of condenser tube
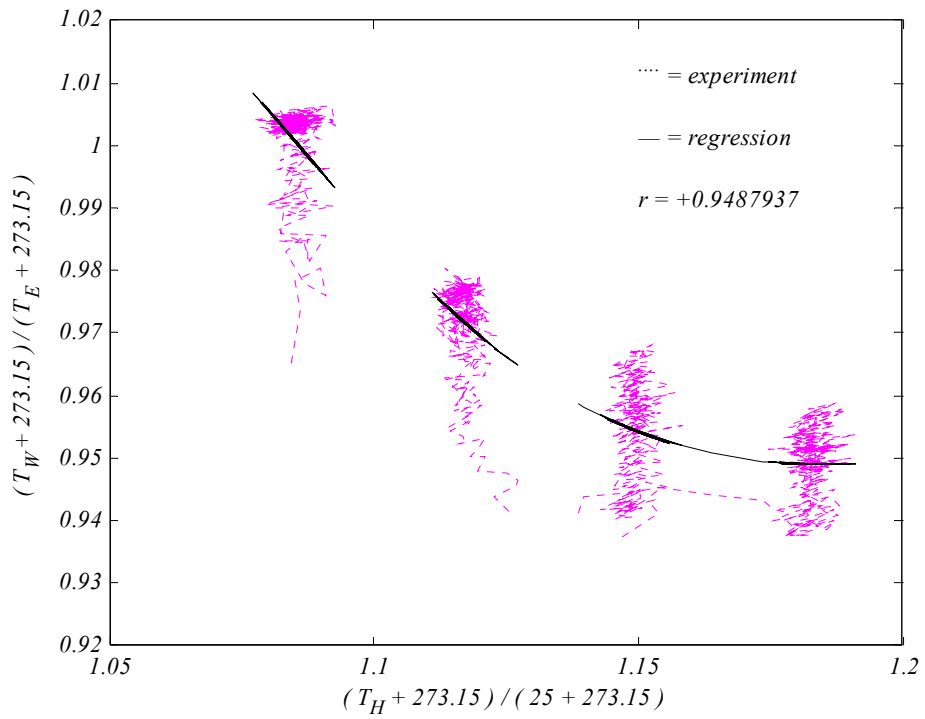
Figure 34. Non–equilibrium allowance representation
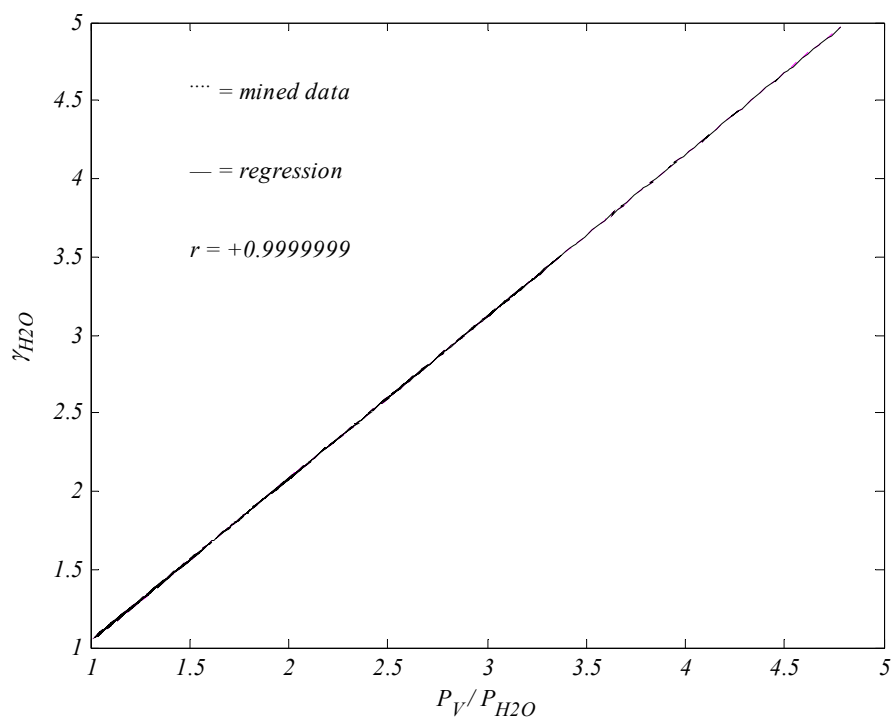
Figure 35. Activity coefficient of water
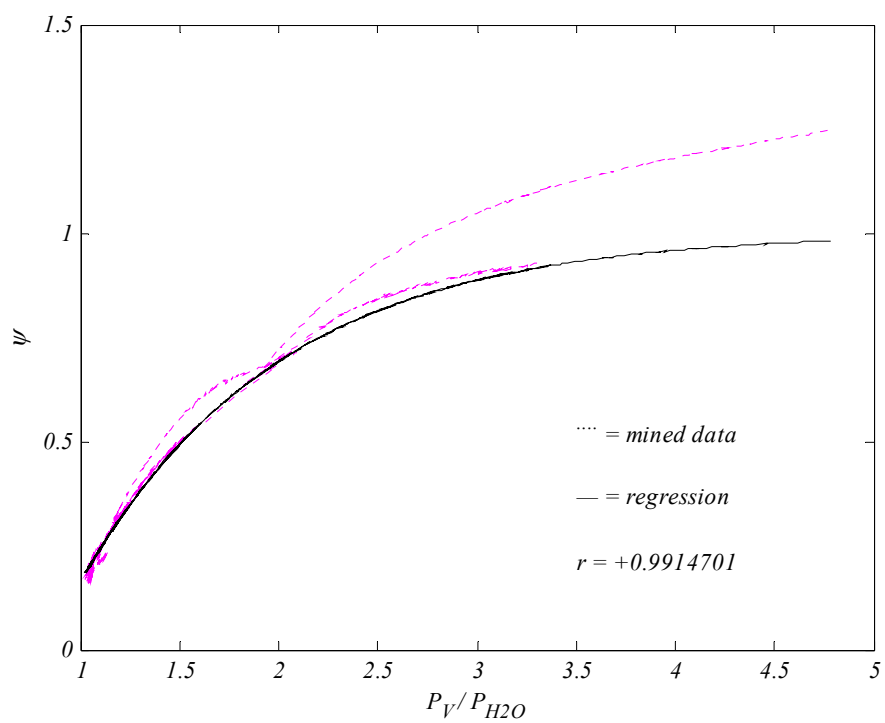
Figure 36. Gas phase molecular content correction factor

6.3 Parameter Inputs

Seawater is a solution of many salts and contains a small amount of dissolved gases as mentioned earlier in CHAPTER 4. Input parameters used for sea salt are given in Table 7, while input parameters used for seawater are given in Table 8. The molecular weights given in both tables are obtained from NIST [31], while mass fractions given in both tables are obtained from an oceanography manual [16]. In addition, the relativity factors given in Table 8 are found by averaging temperature–stamped data [19], while enthalpy parameters given in Table 8 are obtained from NIST [31].

As mentioned in CHAPTER 4, the SUPERTRAPP™ code was employed to perform isobaric phase equilibria flash calculations for water with an average content of non–condensable gas as reported in literature [16] at various temperatures to produce a dataset of K–values. SUPERTRAPP™ flash calculations were executed at a constant pressure of 1 bar; therefore, the produced K–values are equivalent to Henry's constant for non–condensable gases and vapor pressure for water. The reported values of $HC°_i$ and HF_i [17] plus PA, PB, and PC [15] were used as initial guesses in Matlab™ least squares regression codes to adjust their values to best fit the produced K–value dataset to Henry's constant and vapor pressure correlations.

The SUPERTRAPP™ code used for generating the K–value dataset and Matlab™ codes used for regressing them are in the APPENDICES section. The performed regressions yielded excellent results with correlation coefficients very close to unity as can be seen in Figure 37 through Figure 41. Better estimates of K–values denote better representation of the vapor–liquid equilibrium, ultimately resulting in more reliable flash calculations.

81

Table 7. Sea salt parameters [16] [31]

	MW	ω		MW	ω		MW	ω
Cl	35.45	0.55030	Ca	40.08	0.01180	BO_3	58.81	0.00080
Na	22.99	0.30590	K	39.10	0.01110	Sr	87.62	0.00040
SO_4	96.06	0.07680	HCO_3	61.02	0.00410	F	19.00	0.00003
Mg	24.31	0.03680	Br	79.90	0.00190			

Table 8. Seawater parameters [16] [31]

	MW	φ	α	A	B	C	D	E	F	HC°	HF	PA	PB	PC
N_2	28.01	1.26E-05	1.21	26.0920	8.2188	-1.9761	0.1593	0.0444	-7.9892	8067573	-3546			
O_2	32.00	7.70E-06	1.22	29.6590	6.1373	-1.1865	0.0958	-0.2197	-9.8614	358815	-2209			
Ar	39.94	4.00E-07	1.23	20.7860	2.83E-07	-1.46E-07	1.09E-08	-3.66E-08	-6.1974	384073	-2308			
CO_2	44.01	2.20E-07	1.17	24.9974	55.1870	-33.6914	7.9484	-0.1366	-10.0851	10915	-445			
Salt		3.50E-02												
H_2O	18.01		0.9816	30.0920	6.8325	6.7934	-2.5345	0.0821	-9.0546			13	4391	245
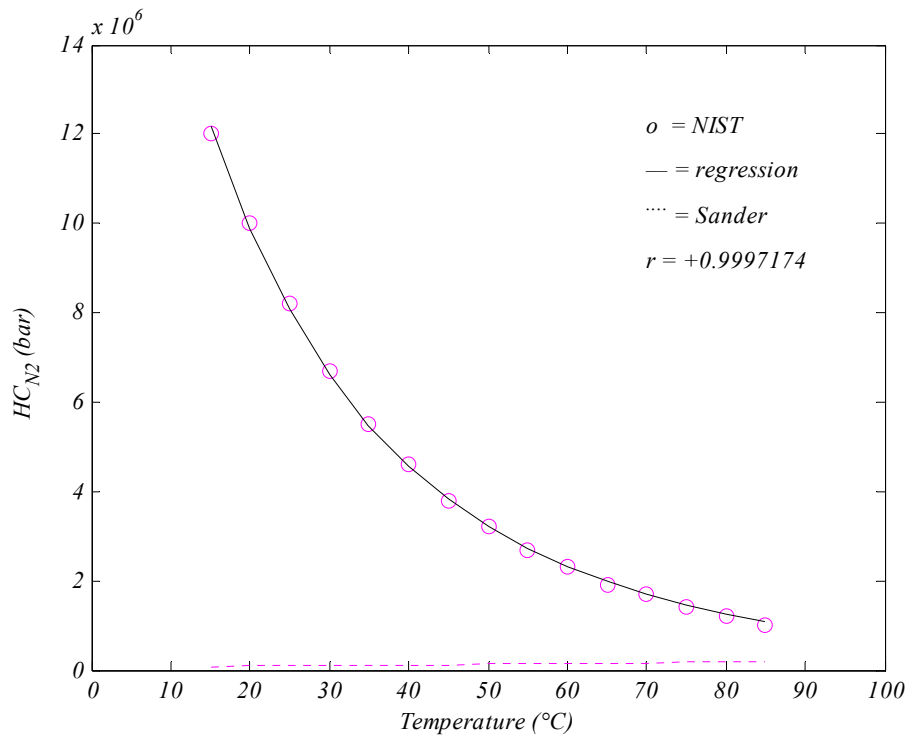
Figure 37. Henry's constant of nitrogen
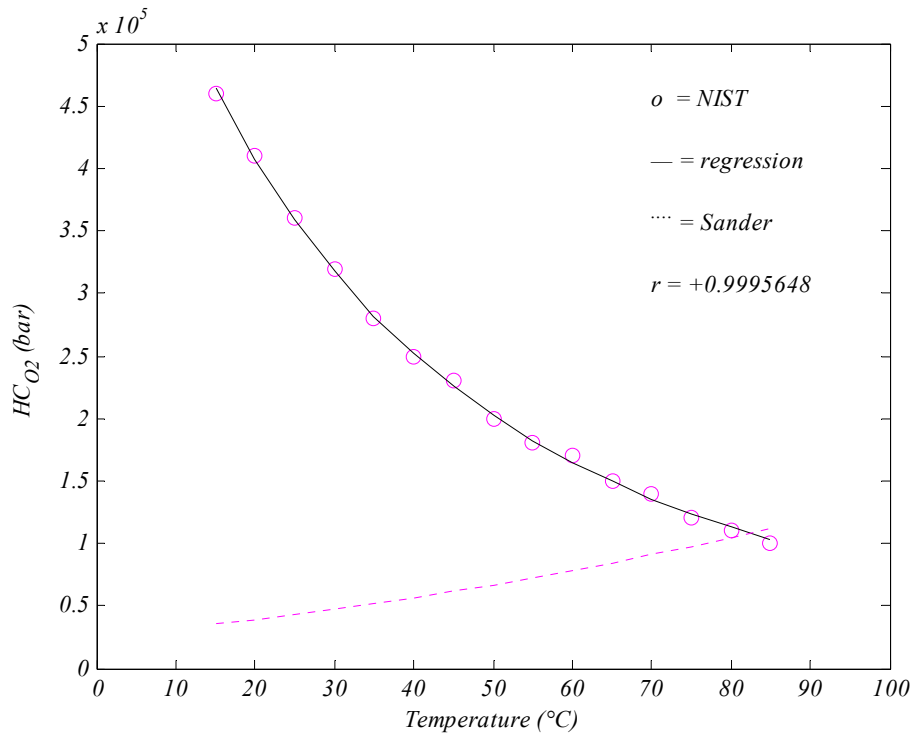
Figure 38. Henry's constant of oxygen
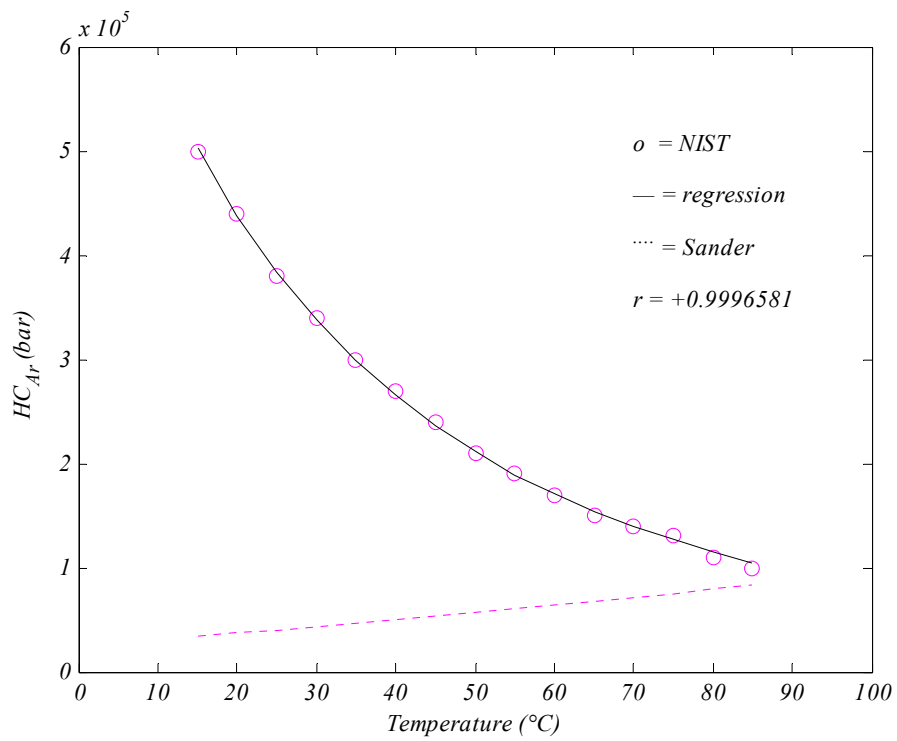
Figure 39. Henry's constant of argon
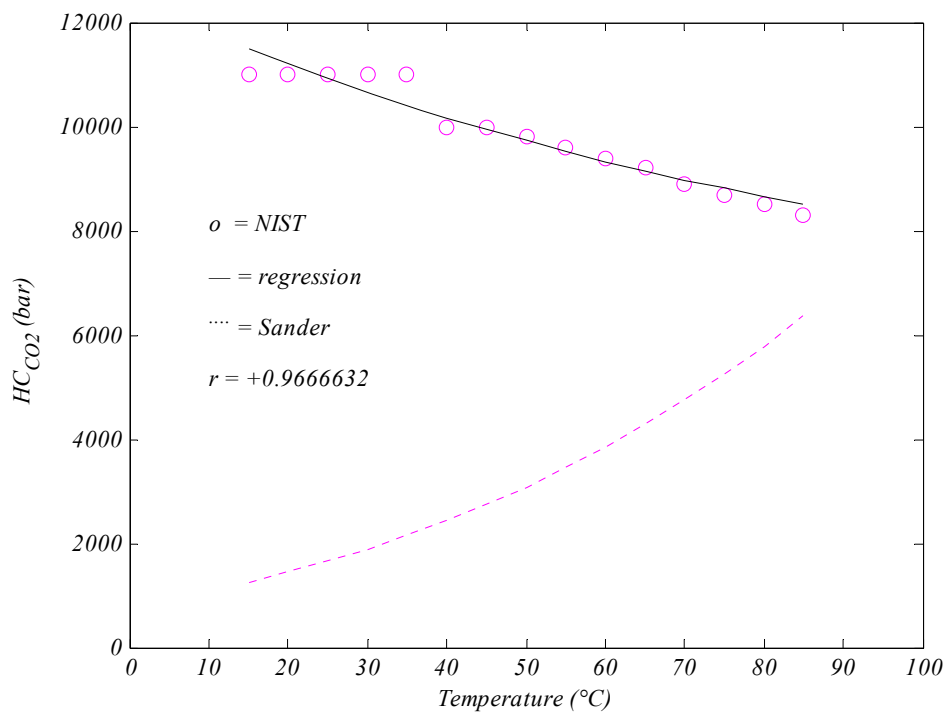
Figure 40. Henry's constant of carbon dioxide
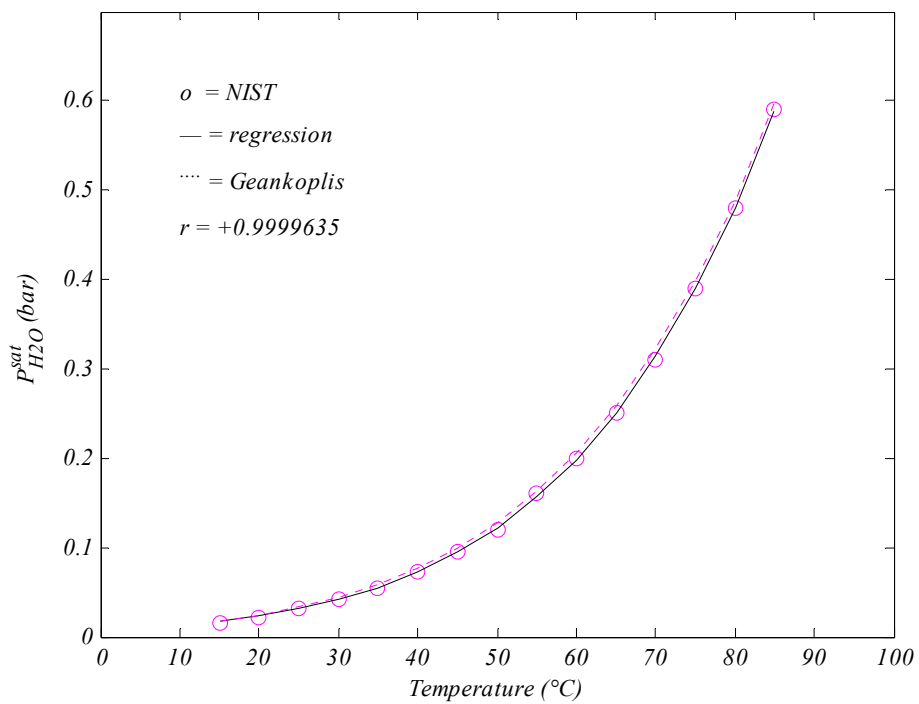
Figure 41. Vapor pressure of water

6.4 Equipment Specifications

The seawater feed as well as brine and fresh water tanks are modeled as horizontal polyethylene troughs; moreover, the condenser and evaporator are modeled as painted–steel and galvanized–steel upright cylinders, respectively. The connecting pipes are modeled as CPVC with copper tubing used inside the condenser and heater. The condenser tube is a protracted copper tube vertically coiled inside the condenser in four loops, that is $N_{CT} = 4$. Copper is not suited for seawater due to its corrosivity and should not be used in desalination systems; however, for theoretical and short–term experimental simulations, it is considered acceptable. Dimensions and the heat transfer parameters of the experimental unit are given in Table 9 and Table 10, and these values will be input to the model as well. In addition, the model neglects any heat input by any pump as well as any work output by the heater, condenser, or evaporator, that is $Q_P = W_C = W_H = W_E = 0$.

Table 9. Equipment dimensions

Vessel	D	L	Pipe	D	L	Pipe	D	L
Seawater	90	30	S	1.27	95	E	5.08	180
Brine Water	90	30	P	1.27	25	C	0.32	35
Fresh Water	90	30	X	1.27	60	CT	1.27	475
Evaporator	35	160	H	1.27	75	HT	1.27	13
Condenser	35	160	W	1.27	30			

Table 10. Heat transfer equipment parameters

	h^{id}	h^{od}	δ	k^w
Condenser Tube	0.20	0.50	0.125	3.810
Condenser	0.50	0.75	0.250	0.450
Evaporator	0.50	0.75	0.250	0.001

The model also uses typical absorptance and transmittance values plus average heat transfer and removal factors pertaining to a single–glazed flat–plate solar collector, in addition to a standard value for the intensity of solar insolation, to estimate the solar collection area needed to meet the computed heater load adequately. Explicitly declaring: $I = 600$ W/m^2, $F_{SC} = 0.82$, $U_{SC} = 0.92$ W/m^2–°C, $\alpha_{SC} = 0.92$, $\tau_{SC} = 0.90$.

6.5 Simulation Specifications

Model simulations will be carried out at conditions corresponding to those of the experimental simulations so they can be compared. Simulated operations will run for a period of three hours and will be modeled using one minute increments with the same initial seawater tank level and vacuum pressure. Simulations were carried out at two different seawater flow rate ranges and at four different flash temperatures.

Mass flow rate of a fluid across an orifice is given by $M = \rho \cdot CV \cdot \sqrt{(\Delta P / SG)}$. The flow rate was manually adjusted during experiments using a ball valve. The valve position was kept constant for each flow rate range; however, flow rate slightly varied within each range due to varying fluid densities caused by different fluid temperatures and varying differential pressures across the valve caused by the different vacuum pressures. In addition, flow rates were progressively decreasing during each experiment due to declining differential pressure caused by the increasing vacuum pressure. An average flow rate value was computed for each experiment and input to the corresponding model simulation as a constant value to simplify calculations. The average flow rate value was obtained by dividing the estimated amount of seawater transferred from the seawater feed tank by the duration of the experiment.

The diffusion rate correlation given in CHAPTER 4 includes two adjustable parameters. Parameter σ serves as a diffusion coefficient and can be thought of as a conductance term, while parameter Ω serves as a diffusion barrier and can be thought of as a resistance term. Both parameters were adjusted using the same code mentioned earlier for generating pseudo–experimental data of model parameters by arbitrarily assigning a value for parameter σ while tuning parameter Ω to match the output amount of fresh water produced by the code to the actual amount of fresh water produced. It is important to point out once more that those obtained diffusion rate correlation parameter values pertain to the geometry of the current experimental set–up and should be readjusted whenever applied to different geometries using new experimental records.

The above mentioned experimental and adjusted simulation settings are given in Table 11 and will be input to the model. The experimental simulations were conducted in a laboratory; consequently, ambient conditions are considered accordingly, $T = 20\ °C$ and $P = 1.01325\ bar$. Finally, temperature in the seawater feed tank is assumed equal to ambient, $T_S = T$, while common literature values were used for the universal gas constant and the gravity acceleration, $R = 83.14472\ bar–cm^3/mol–°C$ and $g = 980.0665\ cm/s^2$.

Table 11. Simulation settings

Simulation	Z^i_S	P^i_V	M_S	T_H	σ	Ω
1	24	0.14	496	50	2	0.118
2	24	0.14	474	60	2	0.150
3	24	0.14	453	70	2	0.120
4	24	0.14	388	80	2	0.019
5	24	0.14	711	50	2	0.135
6	24	0.14	690	60	2	0.197
7	24	0.14	668	70	2	0.229
8	24	0.14	582	80	2	0.103

CHAPTER 7. DISCUSSION OF RESULTS

7.1 Discussion Guide

Model and experimental results will be compared and discussed throughout this chapter. Model results are obtained by executing a code comprised of the equations given in CHAPTER 4 as well as the alternate equations and the parameter values given in CHAPTER 6. Experimental results correspond to two sets of experiments, where one set was conducted at lower seawater flow rates, and the other set was conducted at higher seawater flow rates. In addition, each set of experiments includes four variations of flash temperature, where each variation was duplicated three times to validate its outcome. So, each table value and figure curve given in this dissertation designated as an experimental result is in fact the averaged outcome of three matching experiments. The experimental matrix and conditions were provided earlier in Table 6 and Table 11. Experimental results will sometimes correspond to pseudo–experimental data generated by a code comprised of the equations and the alternate equations mentioned above, but with the mass and energy balance relations replaced by experimental temperature and pressure as well as flow rate values. Each figure will use a solid line to represent model data and a dotted line fitted with a translucent error band to represent experimental data. A detailed error analysis can be found in the APPENDICES section. The figures will also indicate if the experimental data correspond to real experimental data or to pseudo–experimental data by dubbing the data as either "experiment" or "mined", respectively, in their legend.

The controlled variables of the current desalination system are seawater flow rate and flash temperature. Their effects on the desalination process will be analyzed through graphical representations of several system variables that illustrate their dynamics during each simulation. Twelve time–varying system variables will be examined by a set of twelve figures provided for each one. Every set includes four figures, each corresponding to a single flash temperature at lower seawater flow rates, as well as four figures, each corresponding to a single flash temperature at higher seawater flow rates. Furthermore, each figure will sketch two profiles, where one corresponds to model simulation, and the other corresponds to experimental simulation, both at analogous conditions. Each set also includes four figures, where the four different flash temperature profiles of each seawater flow rate range are joined on one figure for both model and experimental simulations.

The legend of each figure includes the correlation coefficient that measures the linear dependence between the modeled and experimental datasets. The correlation coefficient is also known as the Pearson product moment correlation coefficient and is computed by dividing the covariance of two variables by the product of their standard deviations, yielding a value between *-1* and *+1*. The computation process of the correlation coefficient is rather cumbersome; however, it is available as a built–in function in many software packages. A correlation coefficient of *0* indicates the total lack of correlation, while a correlation coefficient of *-1* indicates a perfect negative linear correlation and a correlation coefficient of *+1* indicates a perfect positive linear correlation. A correlation coefficient less than *-0.8* or greater than *0.8* typically indicates a strong correlation, while a correlation coefficient between *-0.5* and *+0.5* typically indicates a weak correlation.

7.2 Vacuum Erosion

System vacuum pressure accounts for the water vapor in addition to the accumulating non–condensable gases as was mentioned in CHAPTER 4. System vacuum gradually eroded for both seawater flow rates; moreover, it eroded a little faster at higher seawater flow rates. Vacuum pressure increased with flash temperatures for both seawater flow rates, since vapor pressure is directly proportional to flashing temperature.

The initial rapid increase of vacuum pressure was caused by the early rapid increase of water vapor pressure caused by the early rapid increase of temperature inside the flash chamber. Vacuum pressure continued to increase afterwards but at a much lower rate due to slow accumulation of non–condensable gases. The rate of increase of vacuum pressure, $\partial P_V / \partial t$, was decelerating for higher flash temperatures but was accelerating for lower flash temperatures for both seawater flow rates. This is especially obvious for higher flow experiments flashing at 50 °C indicating that higher flow rates entail a higher rate of accumulation of non–condensable gases. Decreasing pressure at a given temperature increases vapor–liquid equilibrium coefficient value resulting in more overall evaporation. Consequently, flashing seawater at lower flow rates slowed the rate accumulation of non–condensable gases, which decelerated vacuum erosion rate, resulting in more evaporation and more fresh water production.

Model prediction of vacuum pressure resembled the experimental results but was generally lower, and the discrepancy increased with temperature. This is probably due to the constant seawater flow rate assumed by the model, while it was progressively decreasing during experiments due to the declining differential pressure caused by the eroding vacuum. Vacuum pressure profiles are shown in Figure 42 through Figure 53.
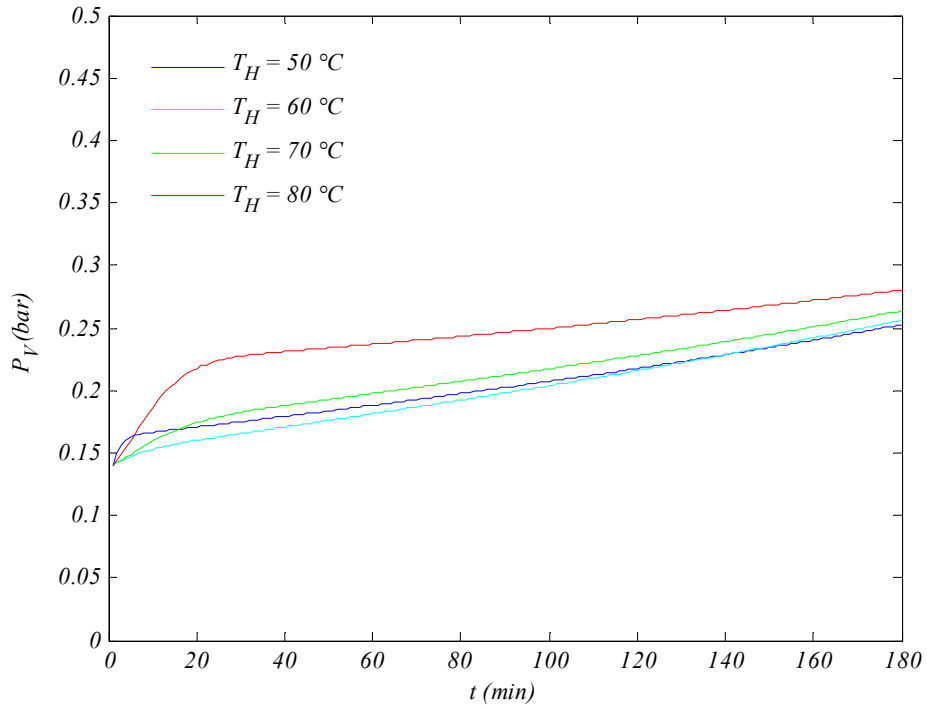
Figure 42. Modeled vacuum pressure profiles at lower flow
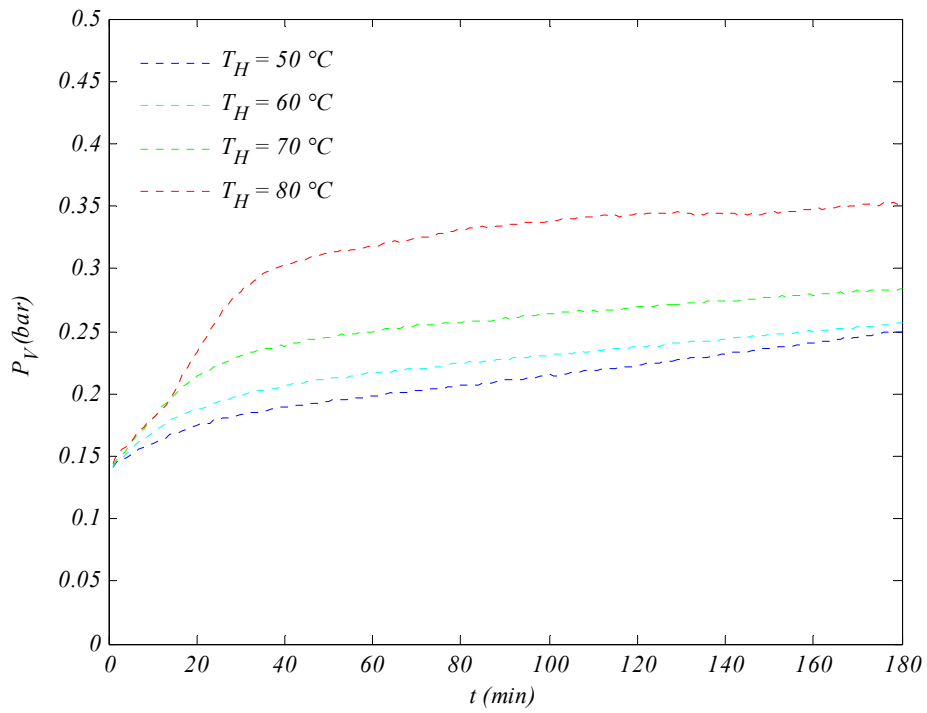
Figure 43. Experimental vacuum pressure profiles at lower flow
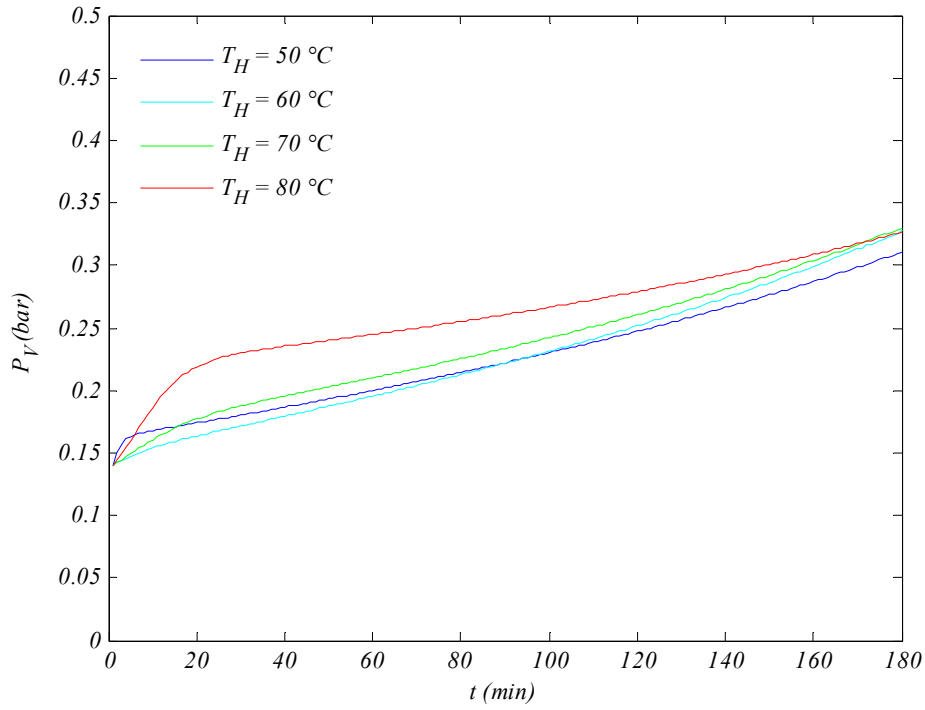
Figure 44. Modeled vacuum pressure profiles at higher flow
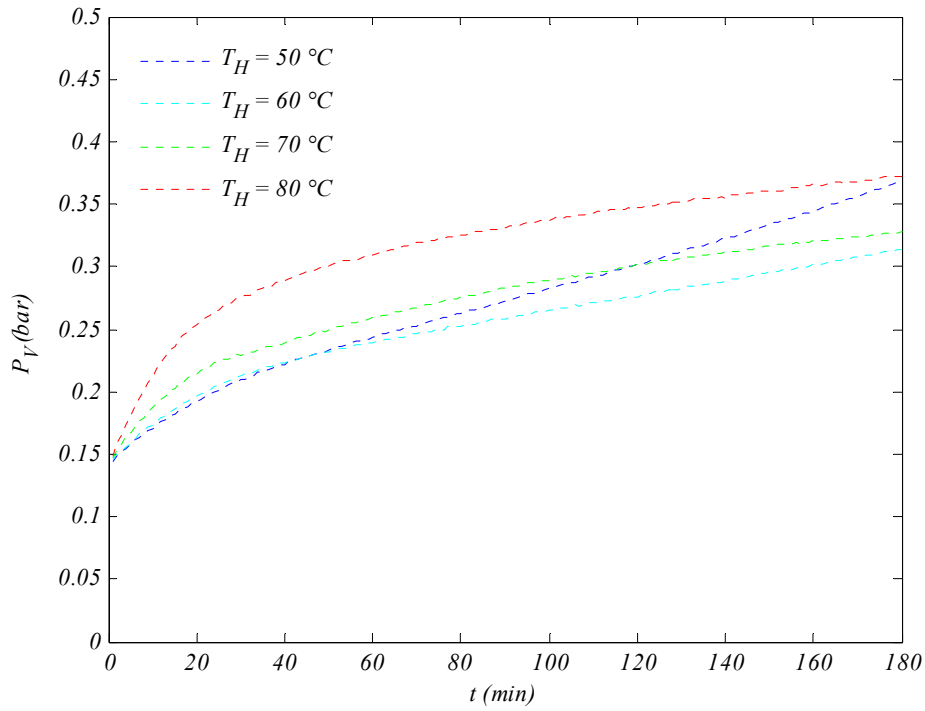
Figure 45. Experimental vacuum pressure profiles at higher flow
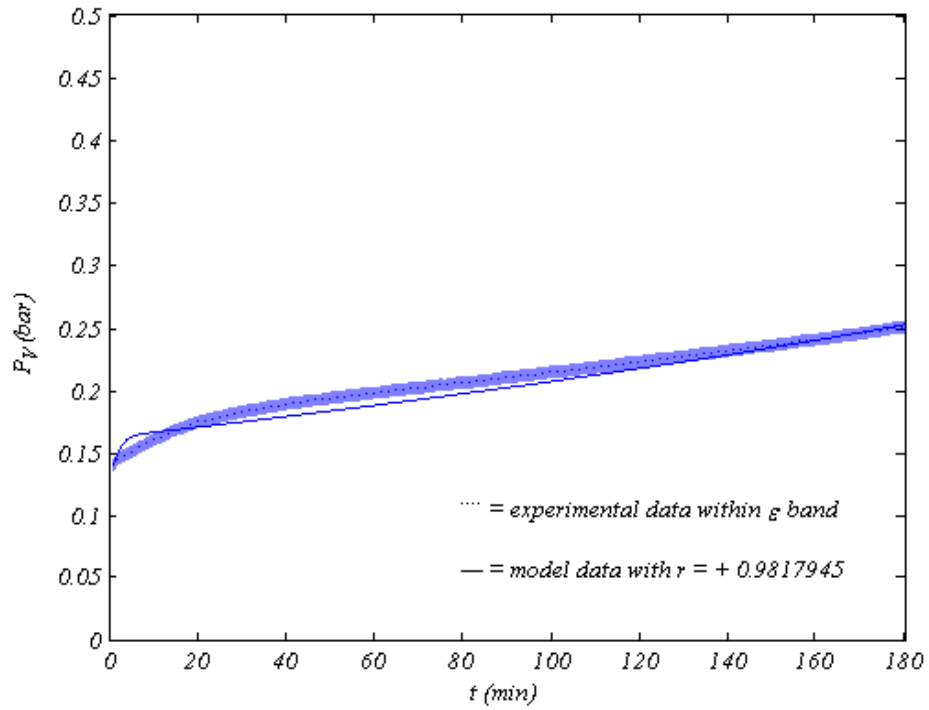
Figure 46. Vacuum pressure at 50°C flash and lower flow
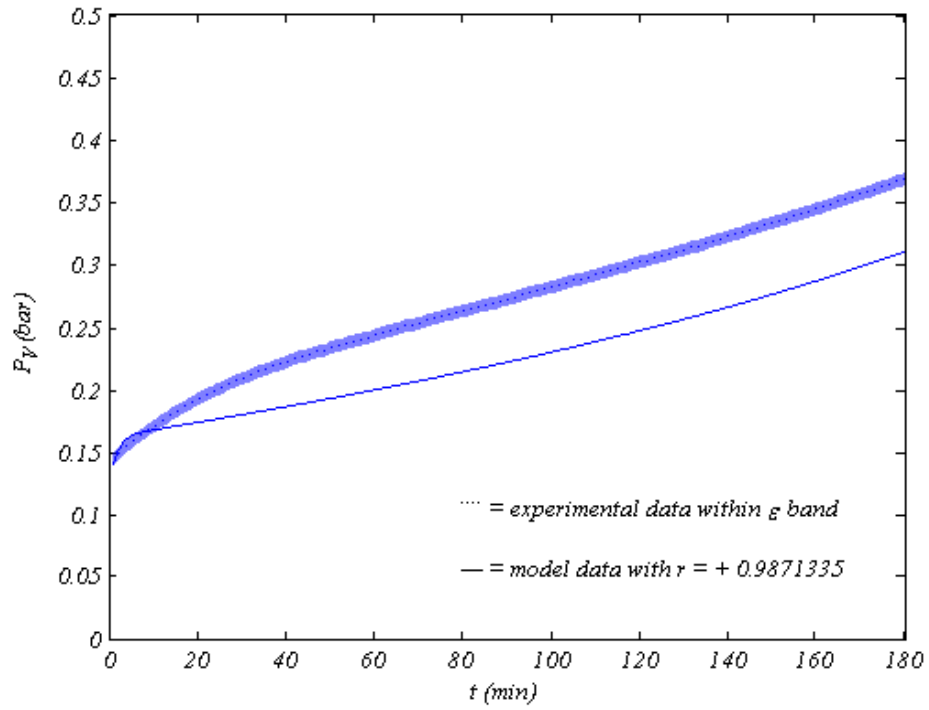
Figure 47. Vacuum pressure at 50°C flash and higher flow

93
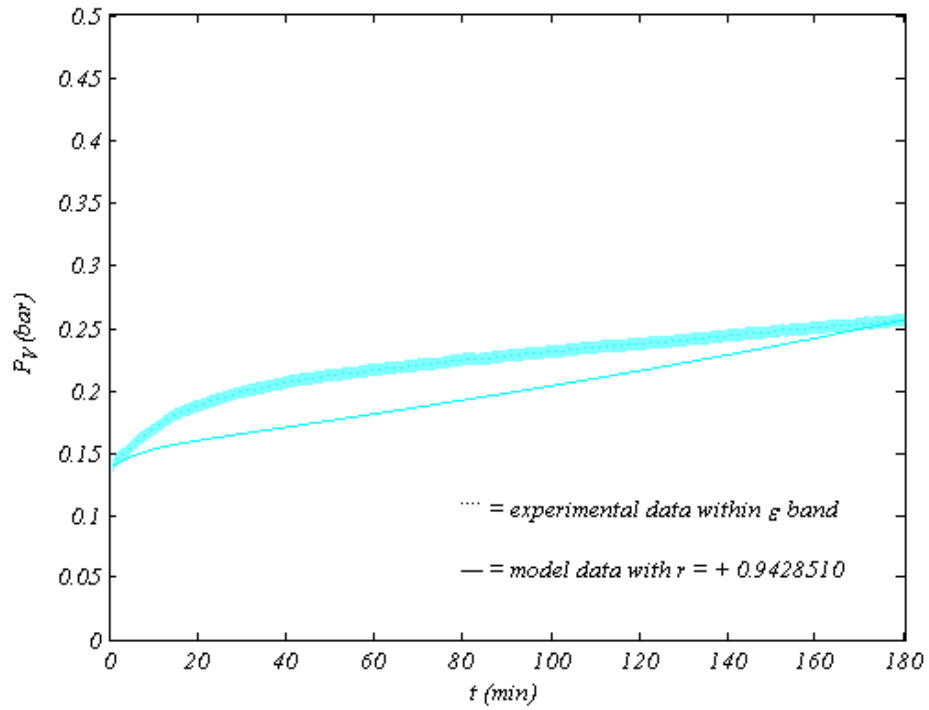
Figure 48. Vacuum pressure at 60°C flash and lower flow
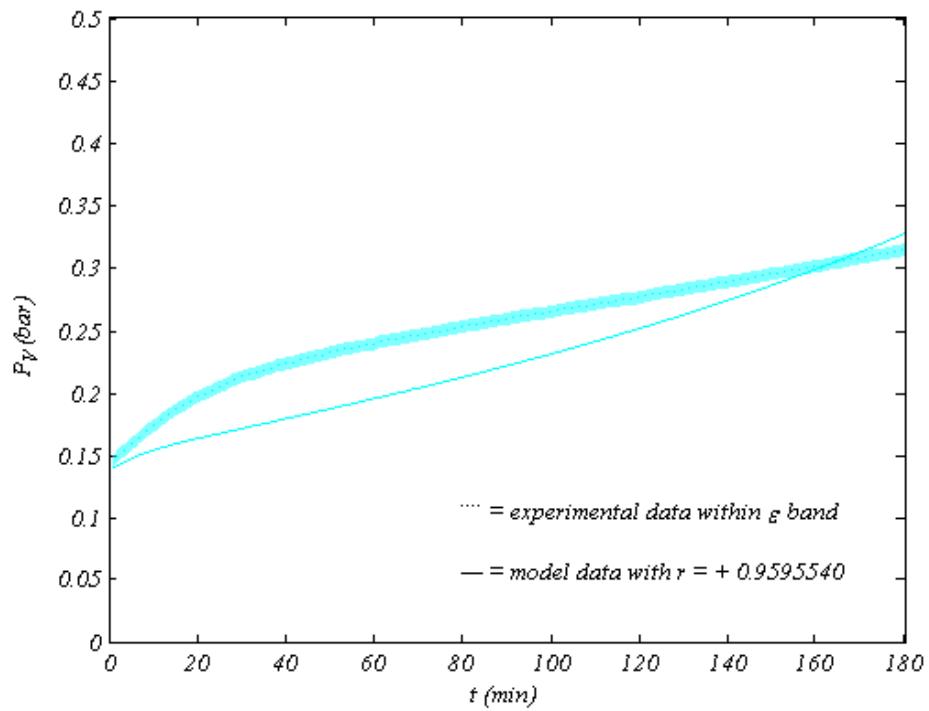
Figure 49. Vacuum pressure at 60°C flash and higher flow
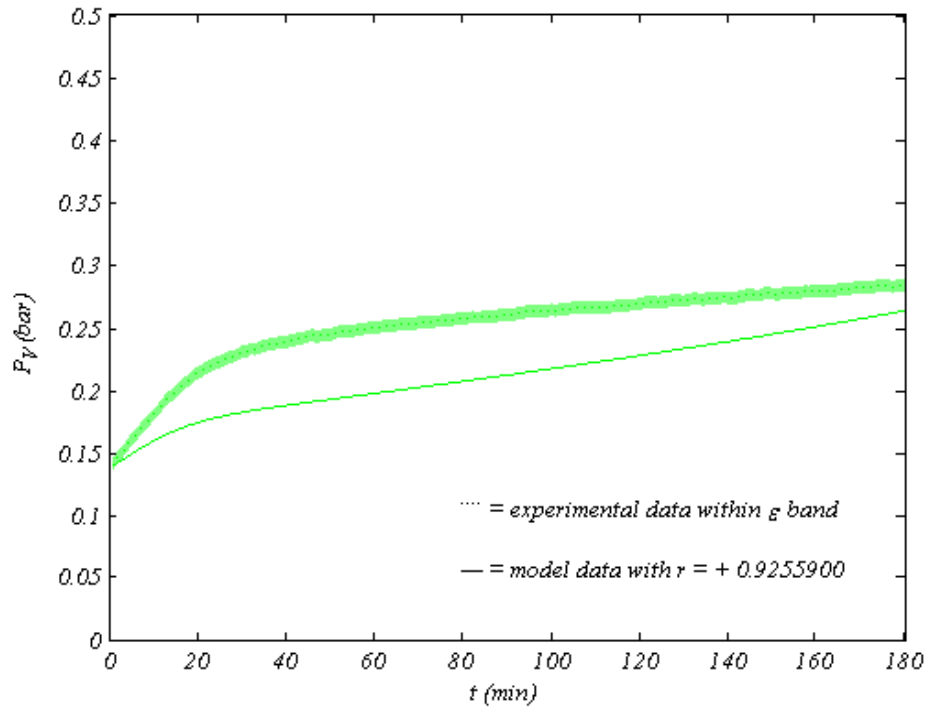
Figure 50. Vacuum pressure at 70°C flash and lower flow
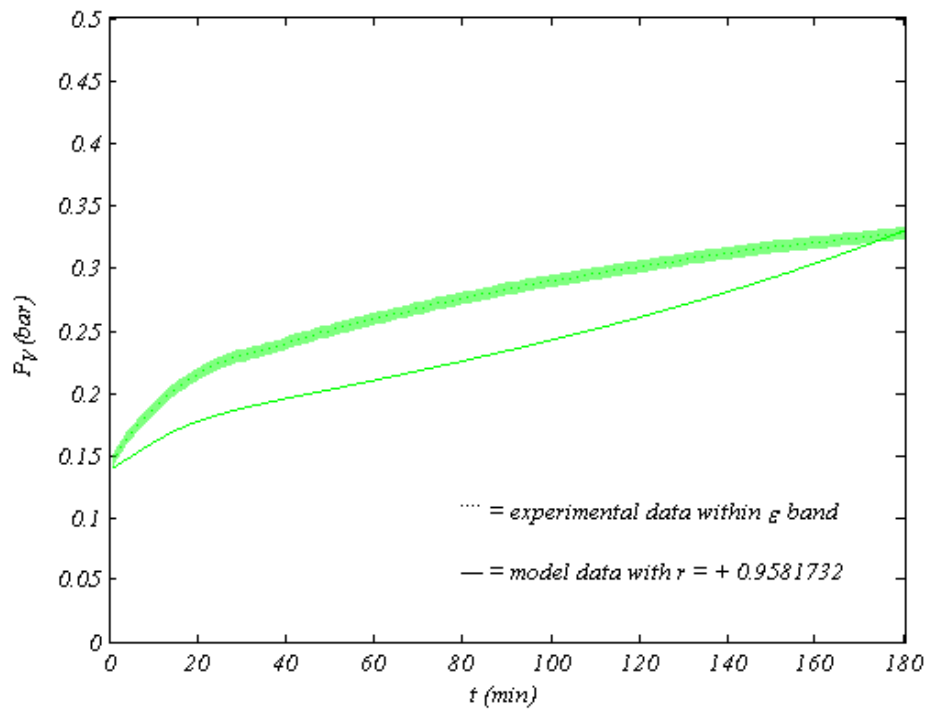
Figure 51. Vacuum pressure at 70°C flash and higher flow
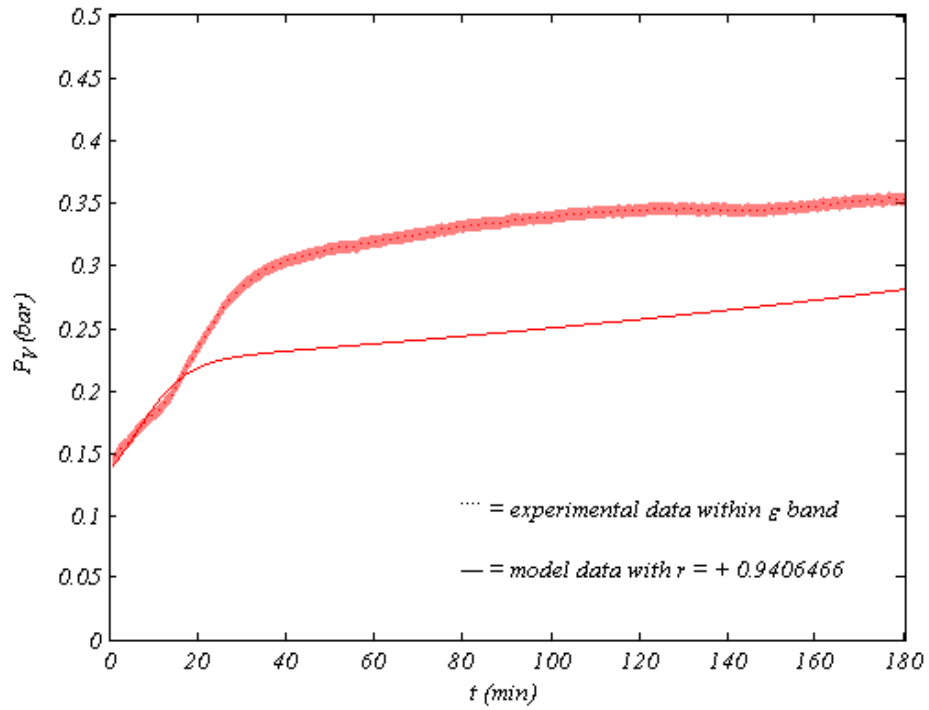
Figure 52. Vacuum pressure at 80°C flash and lower flow
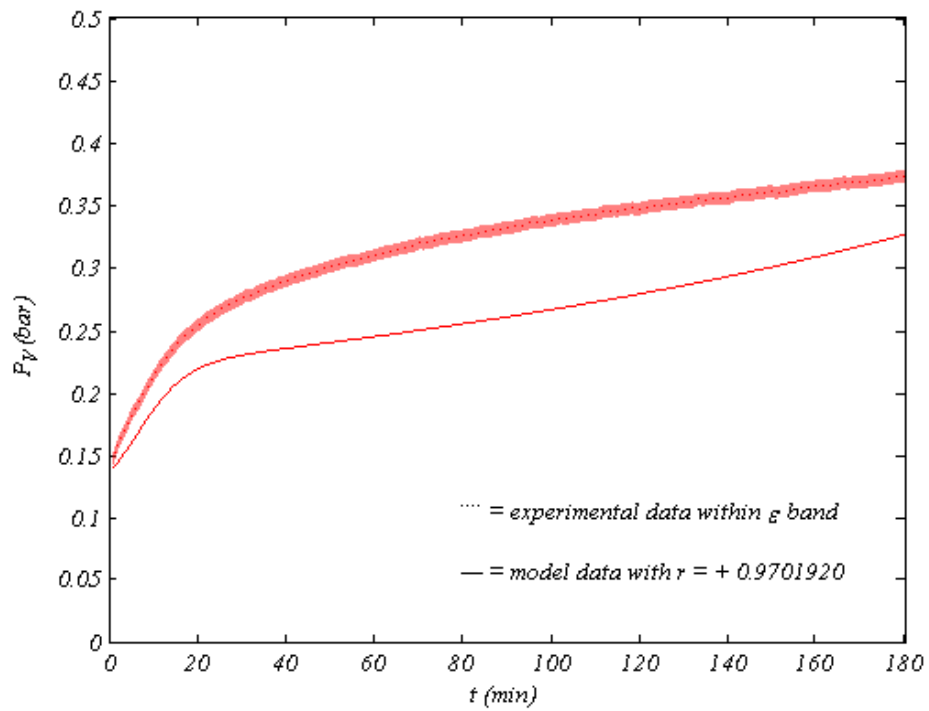
Figure 53. Vacuum pressure at 80°C flash and higher flow

96

7.3 Equilibrium Attainment

The temperature of seawater drops from a set flash temperature to an equilibrium temperature corresponding to the system vacuum pressure as it enters the evaporator. Equilibrium temperature quickly increased, then mostly leveled for both seawater flow rates; moreover, it was higher to some extent at higher seawater flow rates. In addition, equilibrium temperatures increased with elevated flash temperatures for both seawater flow rates in compliance with the energy balance around the evaporator.

The equilibrium temperature was close to ambient at first; however, it rapidly increased as hot seawater was introduced to the evaporator, reaching a plateau comparable to the flash temperature for both seawater flow rates. Flash operation of the proposed desalination process is an adiabatic expansion, where temperature of seawater drops upon entering the flash chamber due to the drawn enthalpy of vaporization, forming fresh water vapor at an equilibrium status corresponding to the vacuum pressure.

The model utilizes the *Iterative and Incremental Development* scheme as mentioned in CHAPTER 4, where the computed vacuum pressure of a previous time increment becomes the input vacuum pressure to the executing time increment, solving for the equilibrium temperature and vacuum pressure of the next time increment. The entire model execution progression is initiated by the known initial vacuum pressure.

The model prediction of equilibrium temperature resembled the experimental results but was slightly lower, and the discrepancy increased with temperature. This observation understandably matches that of vacuum pressure seen earlier, since the attained equilibrium temperature depends on the system vacuum pressure. Equilibrium temperature profiles are shown in Figure 54 through Figure 65.
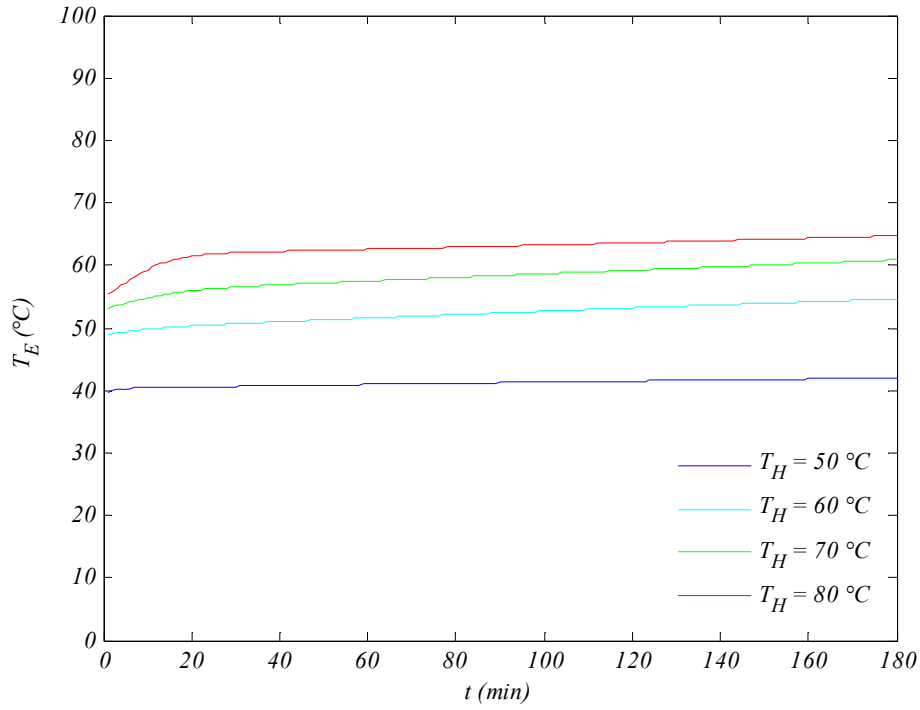
Figure 54. Modeled equilibrium temperature profiles at lower flow
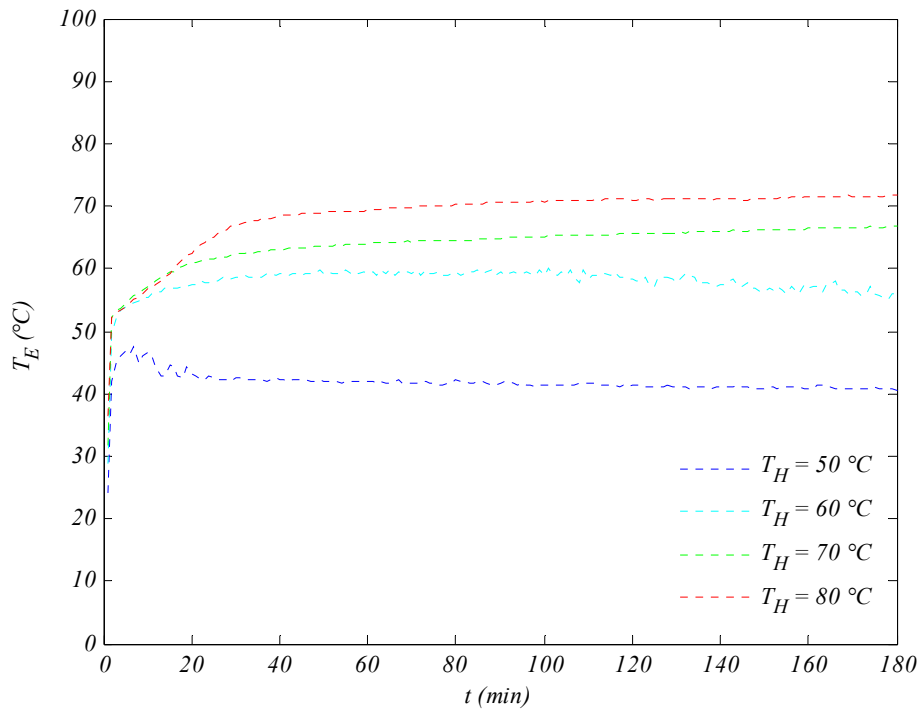
Figure 55. Experimental equilibrium temperature profiles at lower flow
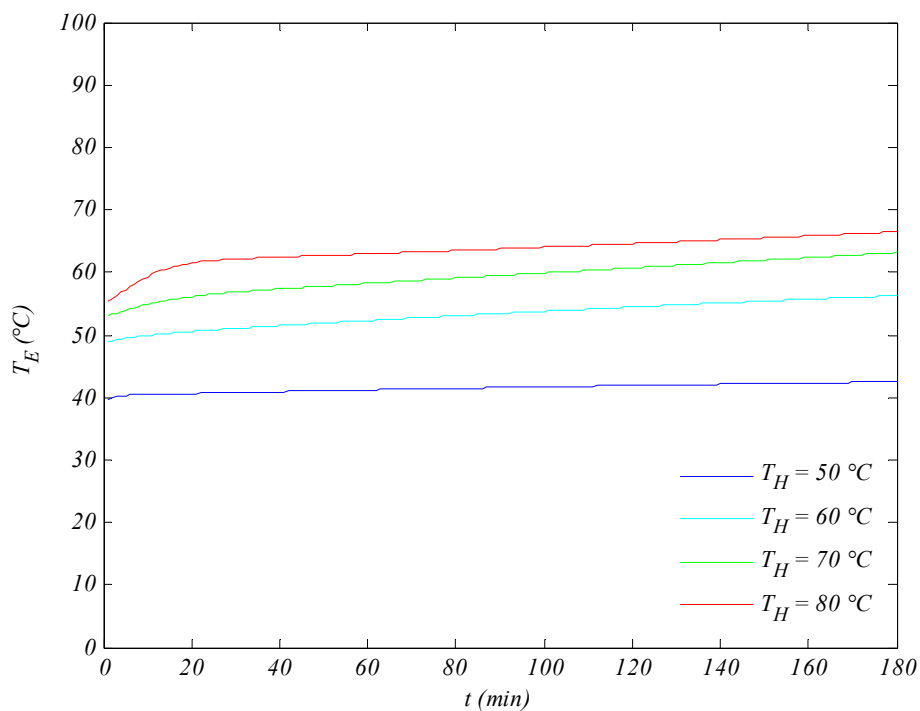
Figure 56. Modeled equilibrium temperature profiles at higher flow
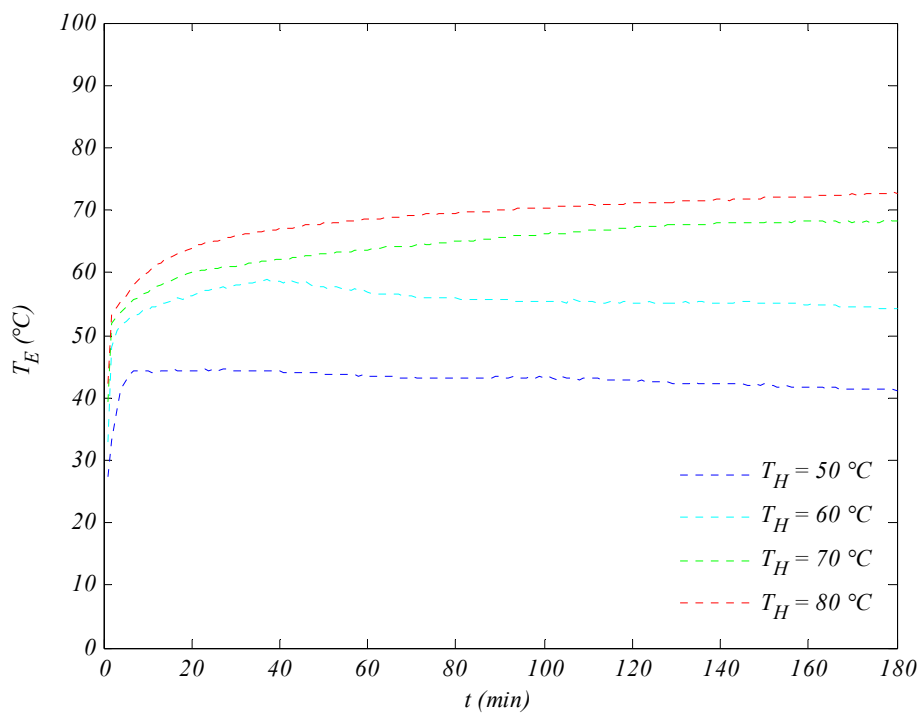
Figure 57. Experimental equilibrium temperature profiles at higher flow
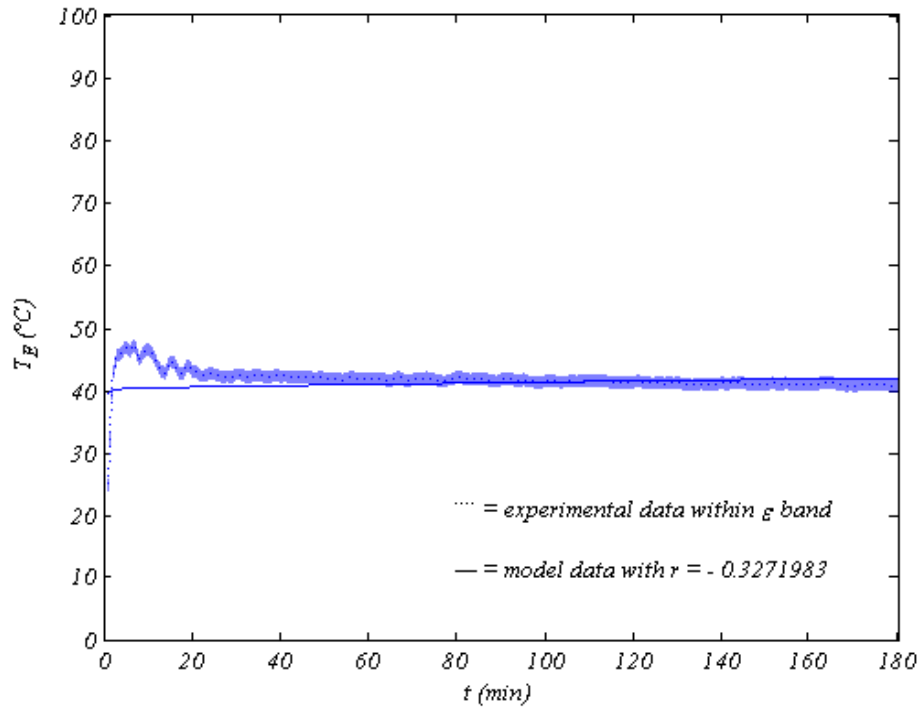
Figure 58. Equilibrium temperature at 50°C flash and lower flow
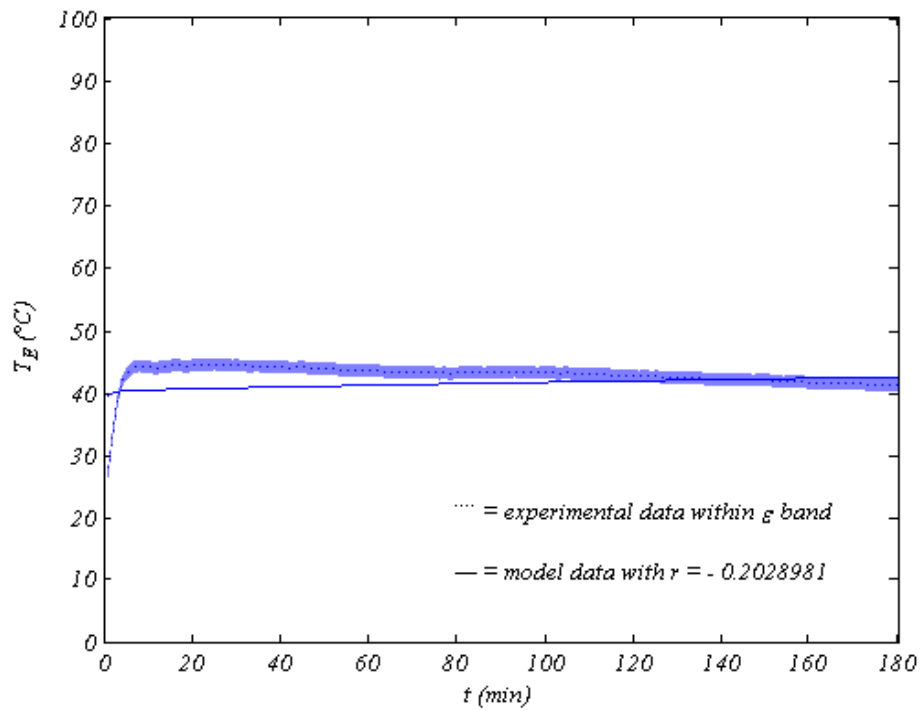
Figure 59. Equilibrium temperature at 50°C flash and higher flow

100
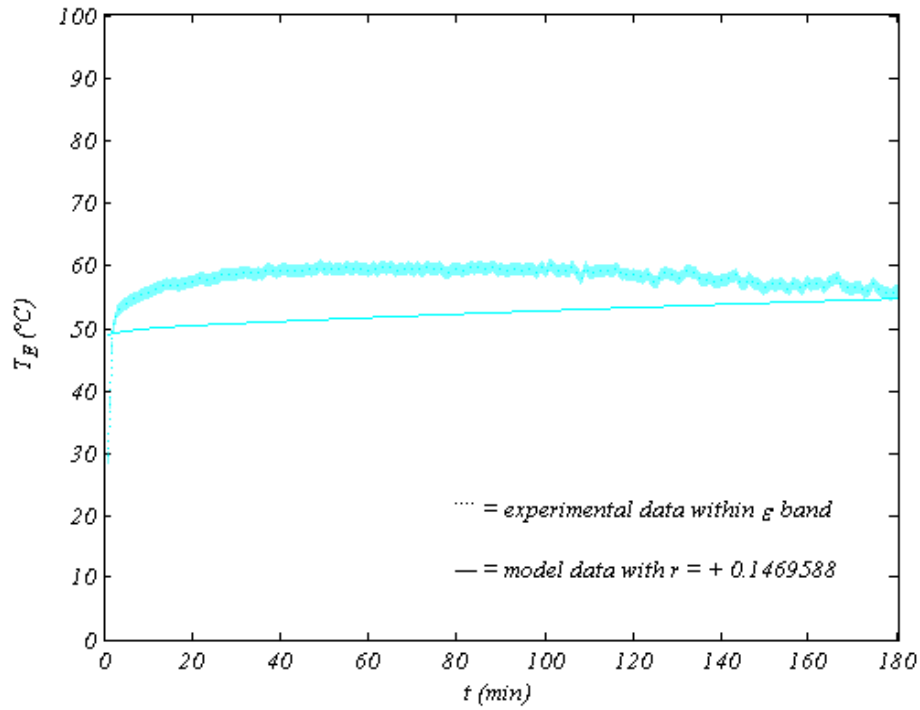
Figure 60. Equilibrium temperature at 60°C flash and lower flow
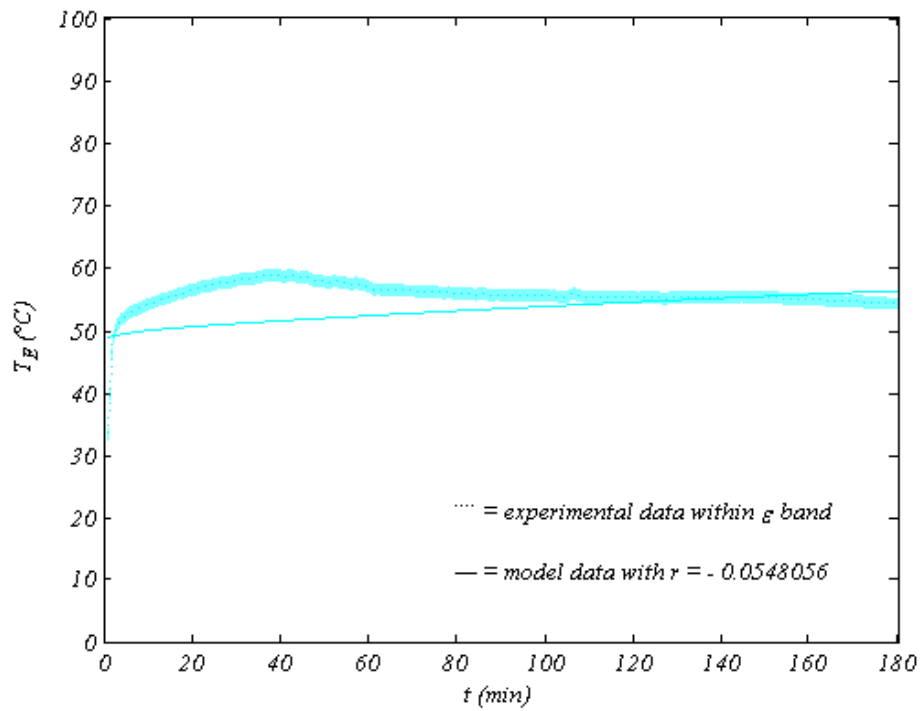
Figure 61. Equilibrium temperature at 60°C flash and higher flow
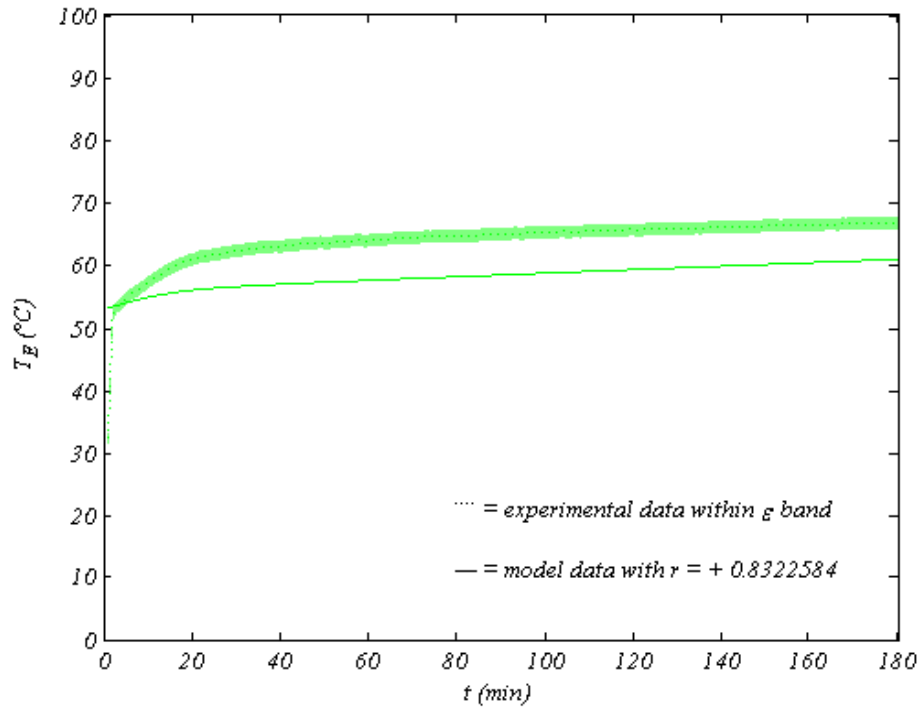
Figure 62. Equilibrium temperature at 70°C flash and lower flow
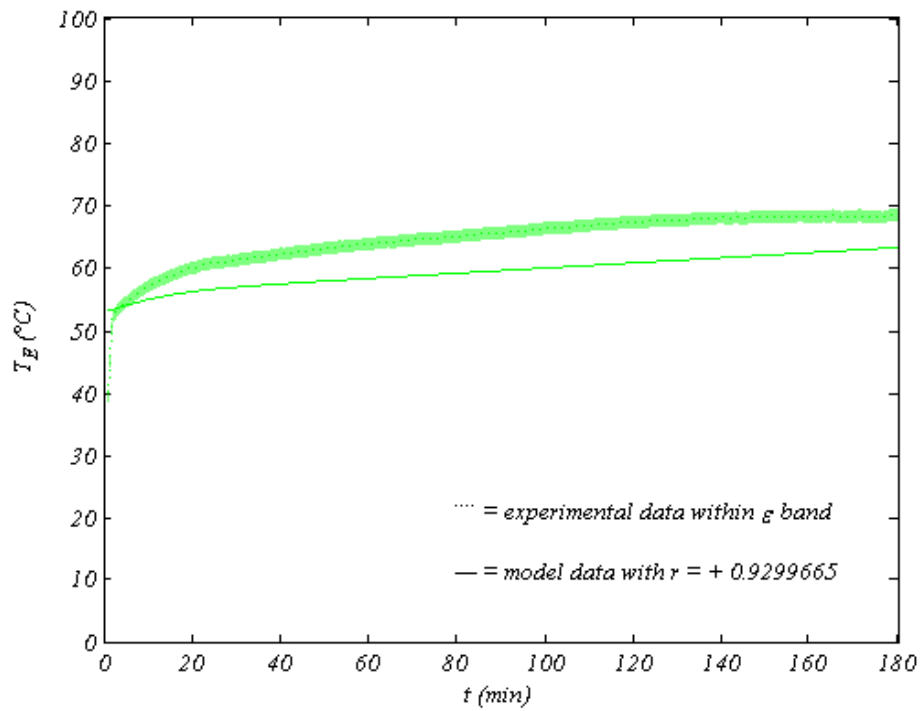
Figure 63. Equilibrium temperature at 70°C flash and higher flow

102
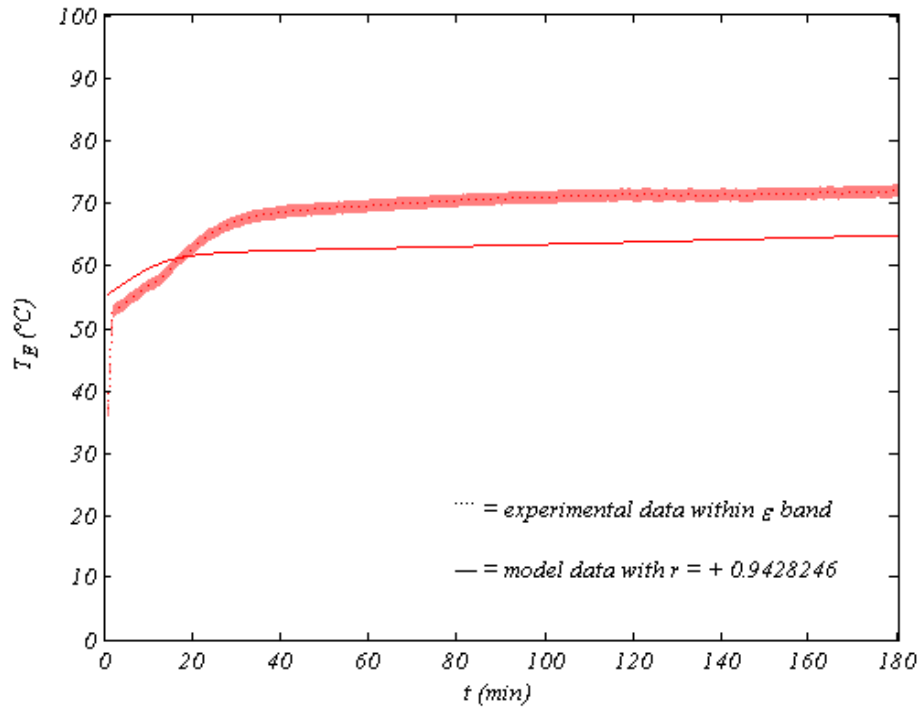
Figure 64. Equilibrium temperature at 80°C flash and lower flow
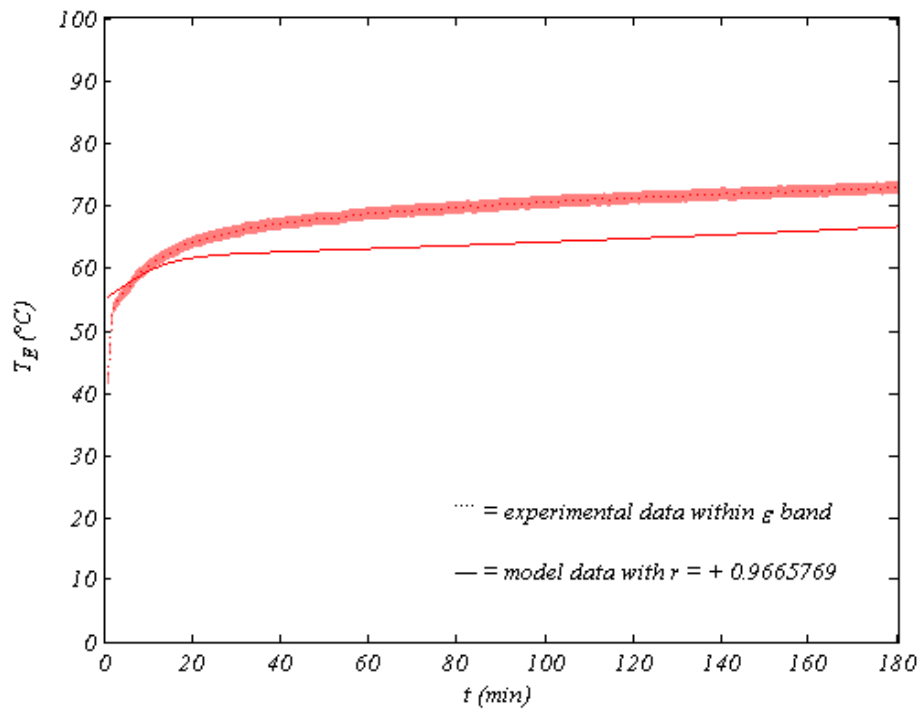
Figure 65. Equilibrium temperature at 80°C flash and higher flow

103

7.4 Equilibrium Departure

Concentrated brine temperature is usually a bit lower than equilibrium temperature due to boiling point elevation and non–equilibrium allowance plus a small amount of heat loss from the insulated evaporator as mentioned in CHAPTER 4. Concentrated brine temperature quickly increased then leveled for both seawater flow rates; moreover, it was slightly higher at lower seawater flow rates. In addition, concentrated brine temperatures increased with elevated flash temperatures for both seawater flow rates in compliance with the energy balance around the evaporator.

The concentrated brine temperature was close to ambient at first; however, it rapidly increased as hot seawater was introduced to the evaporator, reaching a plateau parallel to equilibrium temperature for both seawater flow rates. The concentrated brine temperature remained lower than the equilibrium temperature except for the lowest flash temperature for both seawater flow rates, where concentrated brine temperature started lower but ended higher than equilibrium temperature. This can be attributed to some heat loss from the flashed water vapor along with diminishing vaporization rates as vacuum pressure rises at a relative low equilibrium temperature since the flashed vapor obtains its heat of vaporization from the concentrated brine.

The model prediction of concentrated brine temperature resembled the experimental results but was slightly higher, with the discrepancy rising with increasing flash temperatures. This can be attributed to the neglected small amount of heat loss from the insulated hot evaporator to the cool ambiance combined with the imprecision of the non–equilibrium allowance correlation used in the model. Concentrated brine temperature profiles are shown in Figure 66 through Figure 77.

104
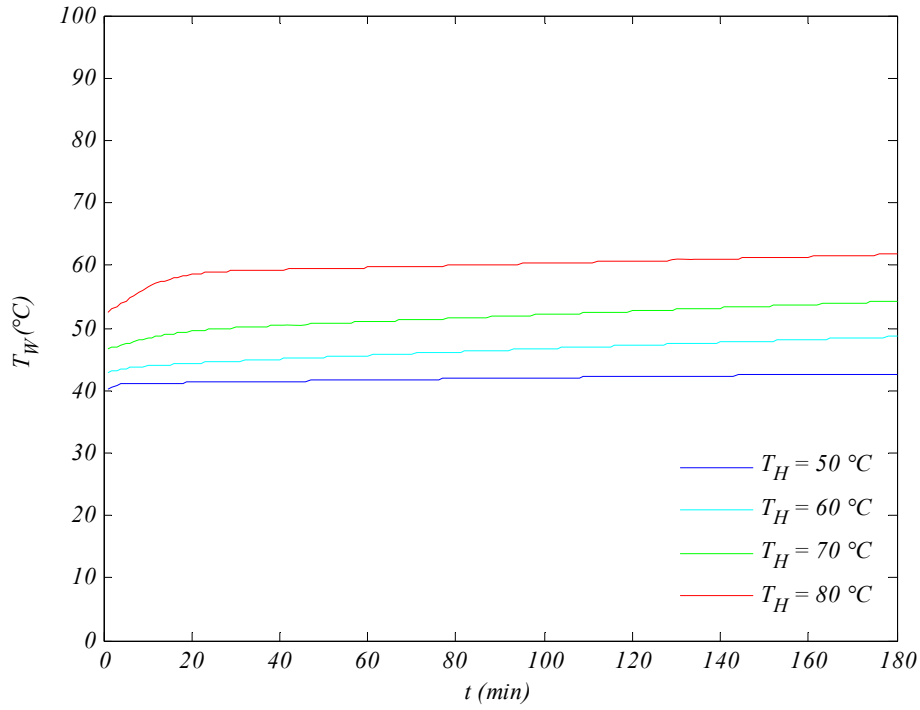
Figure 66. Modeled concentrated brine temperature profiles at lower flow
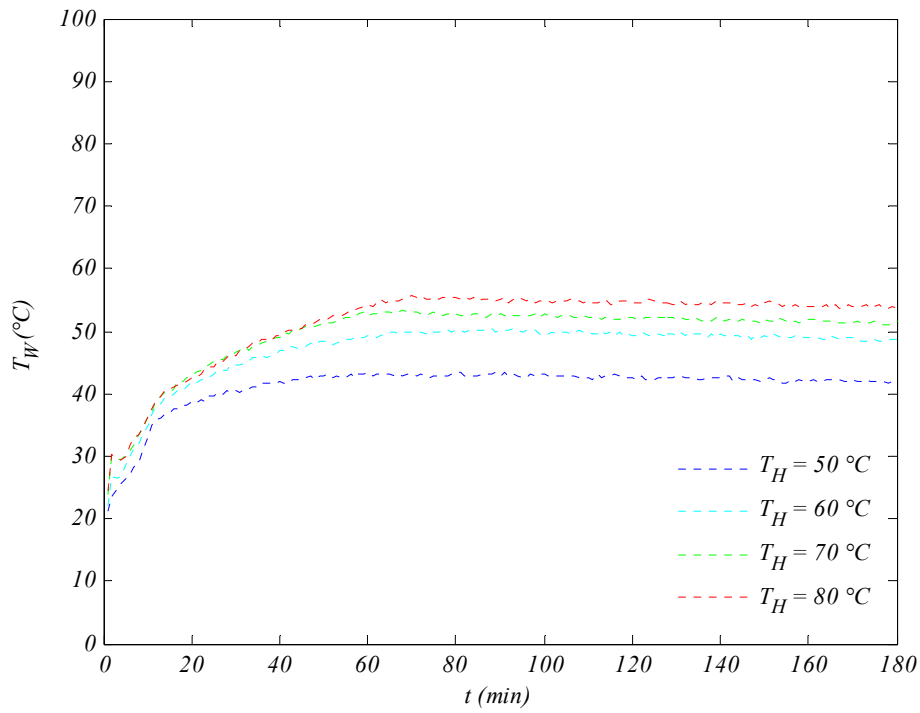
Figure 67. Experimental concentrated brine temperature profiles at lower flow

105
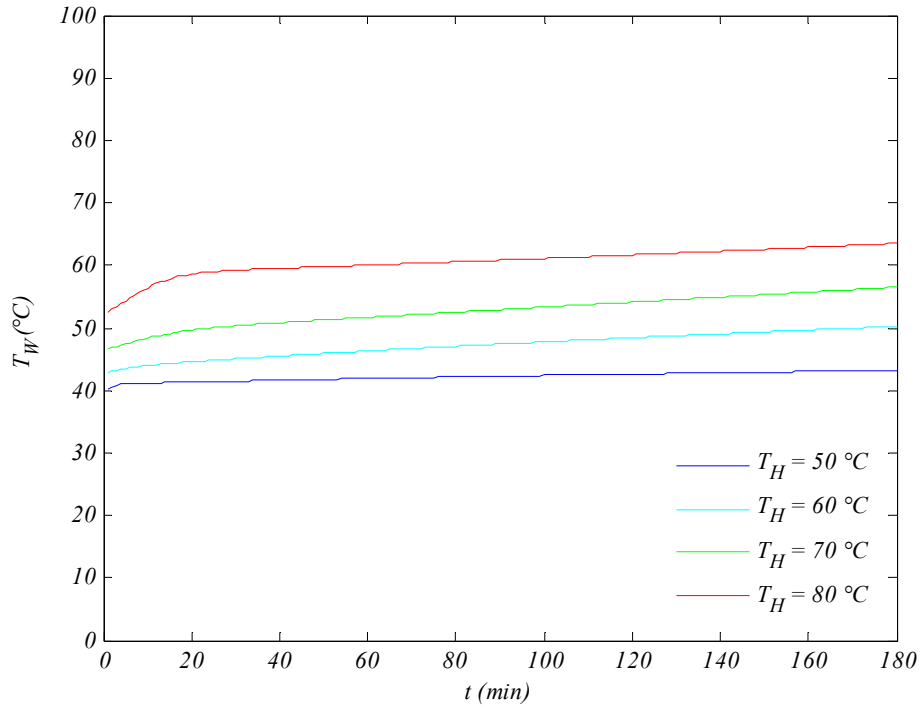
Figure 68. Modeled concentrated brine temperature profiles at higher flow
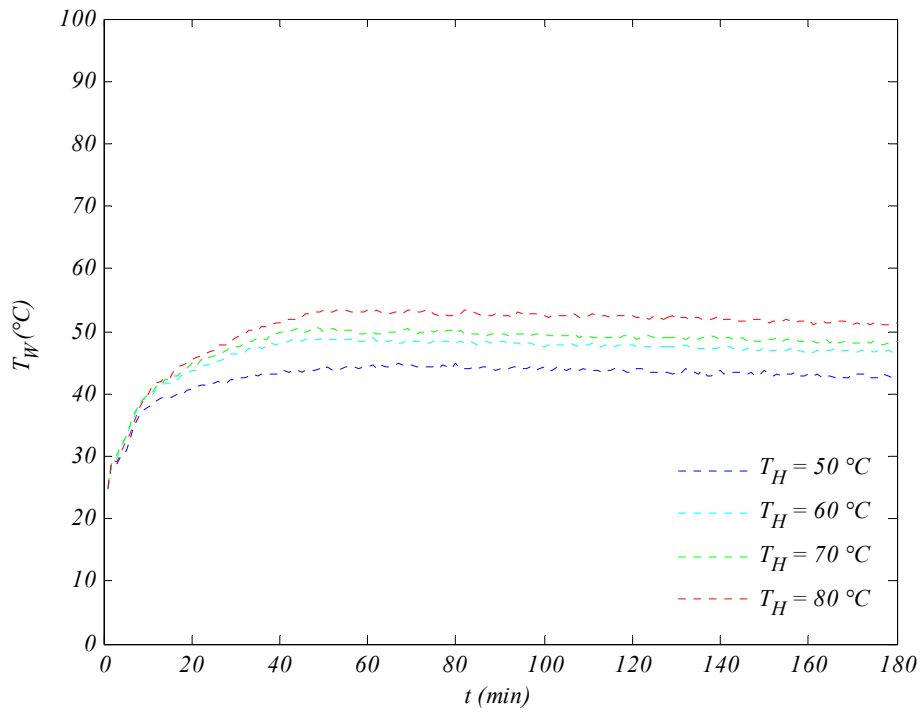
Figure 69. Experimental concentrated brine temperature profiles at higher flow
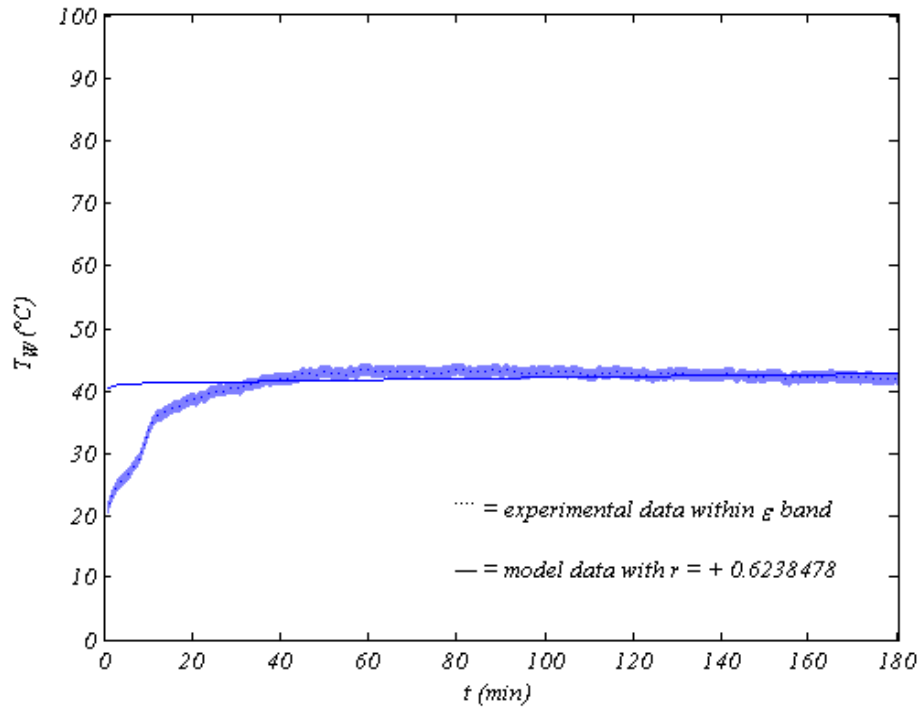
Figure 70. Concentrated brine temperature at 50°C flash and lower flow
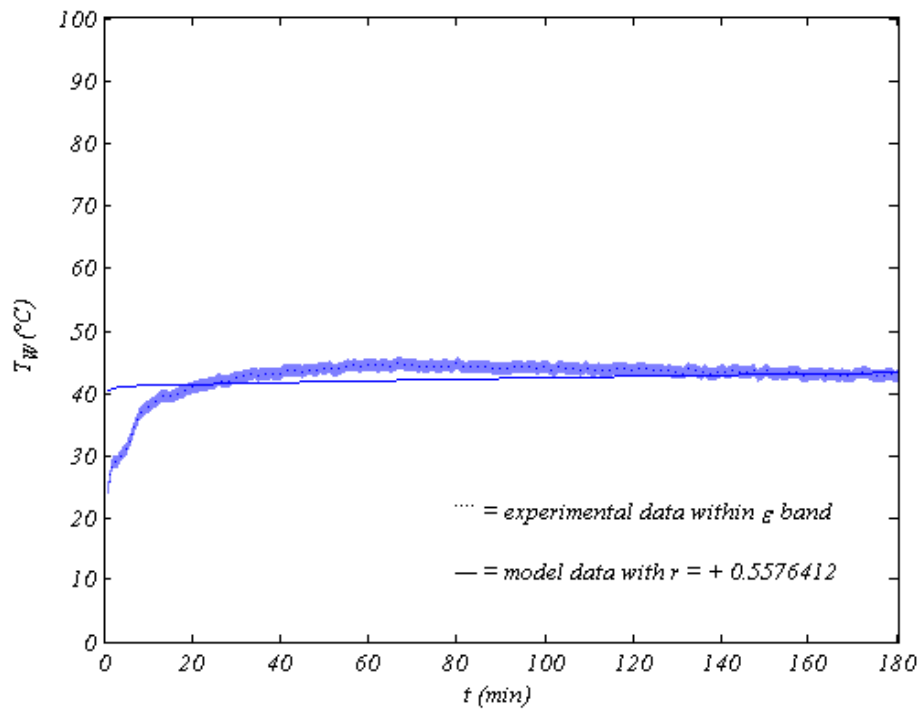
Figure 71. Concentrated brine temperature at 50°C flash and higher flow
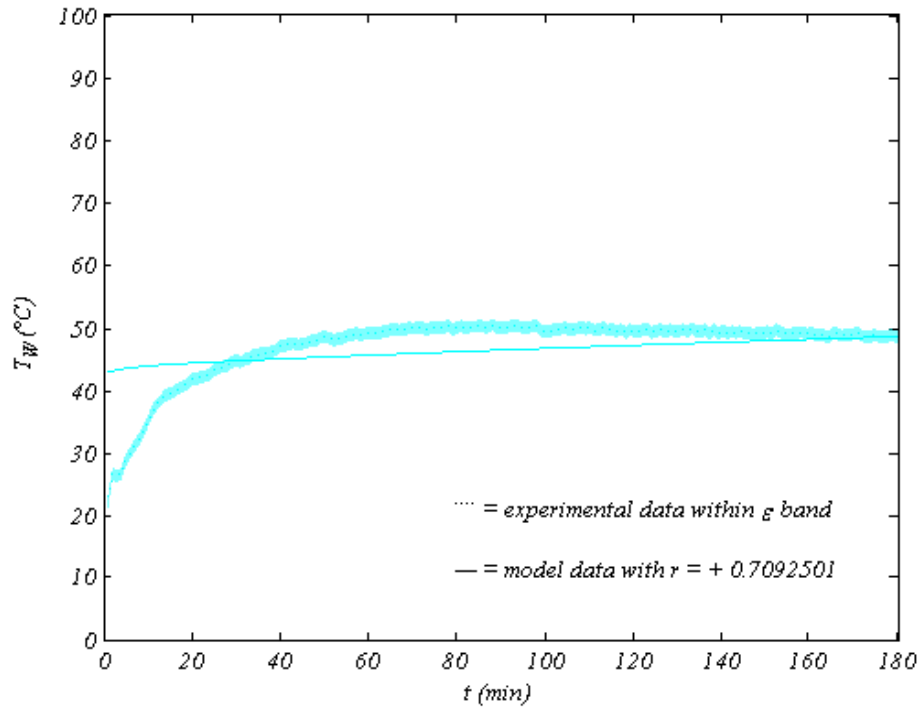
Figure 72. Concentrated brine temperature at 60°C flash and lower flow
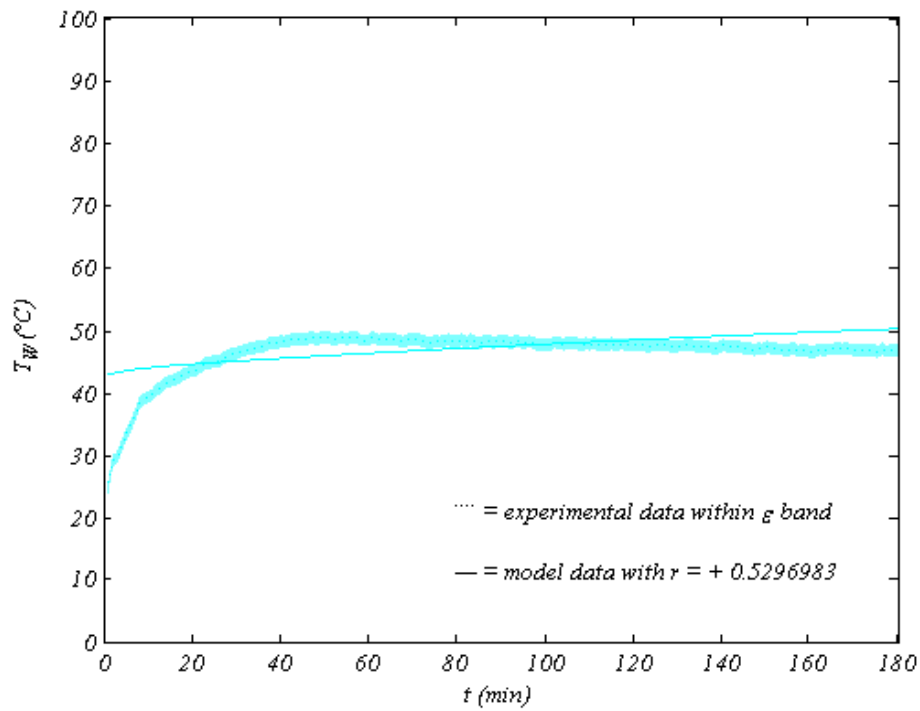
Figure 73. Concentrated brine temperature at 60°C flash and higher flow
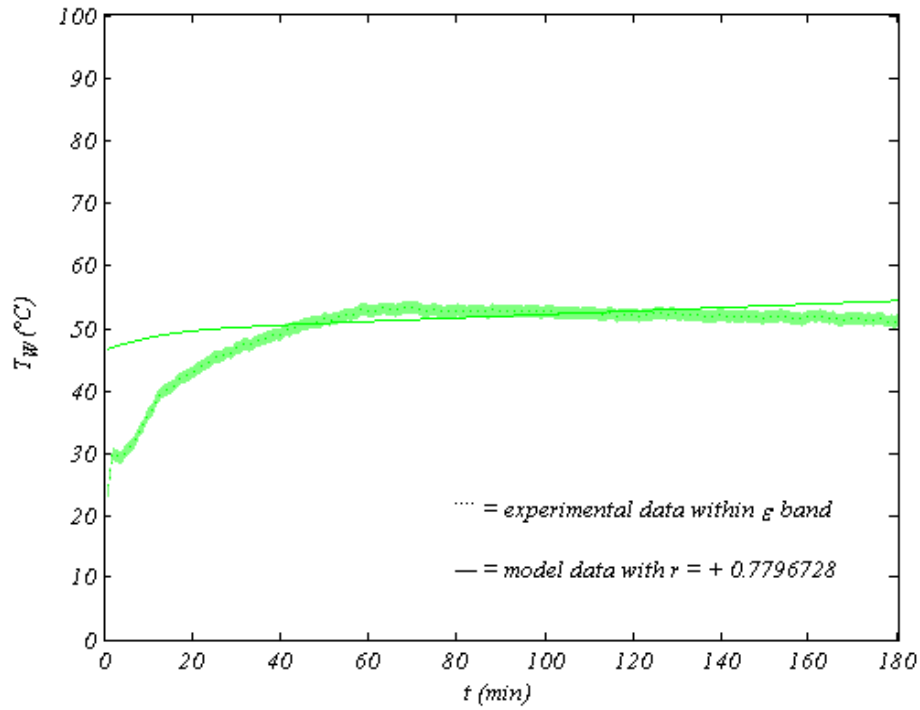
Figure 74. Concentrated brine temperature at 70°C flash and lower flow
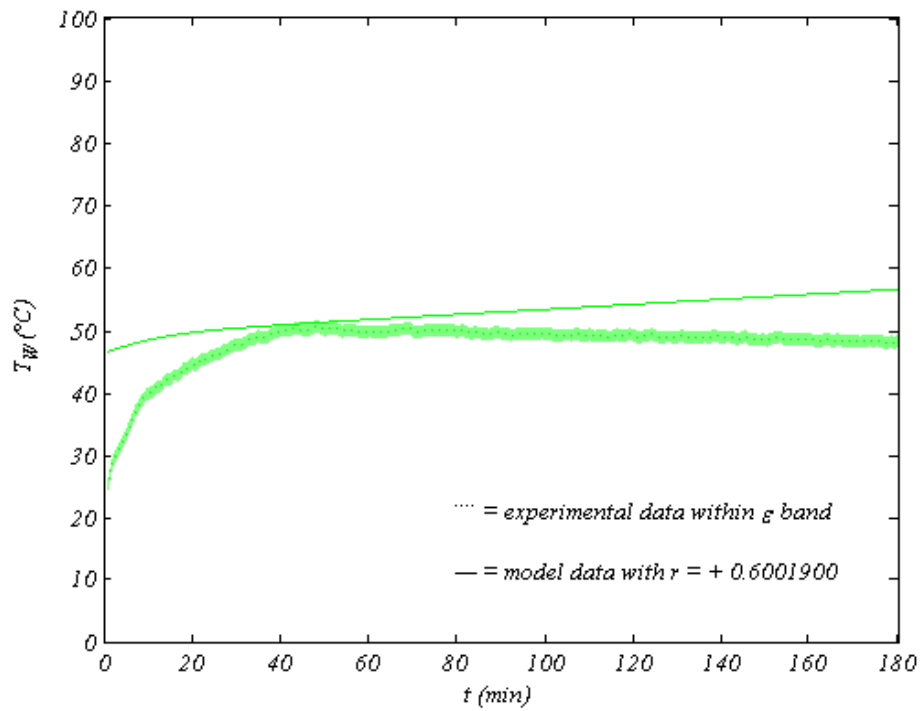
Figure 75. Concentrated brine temperature at 70°C flash and higher flow
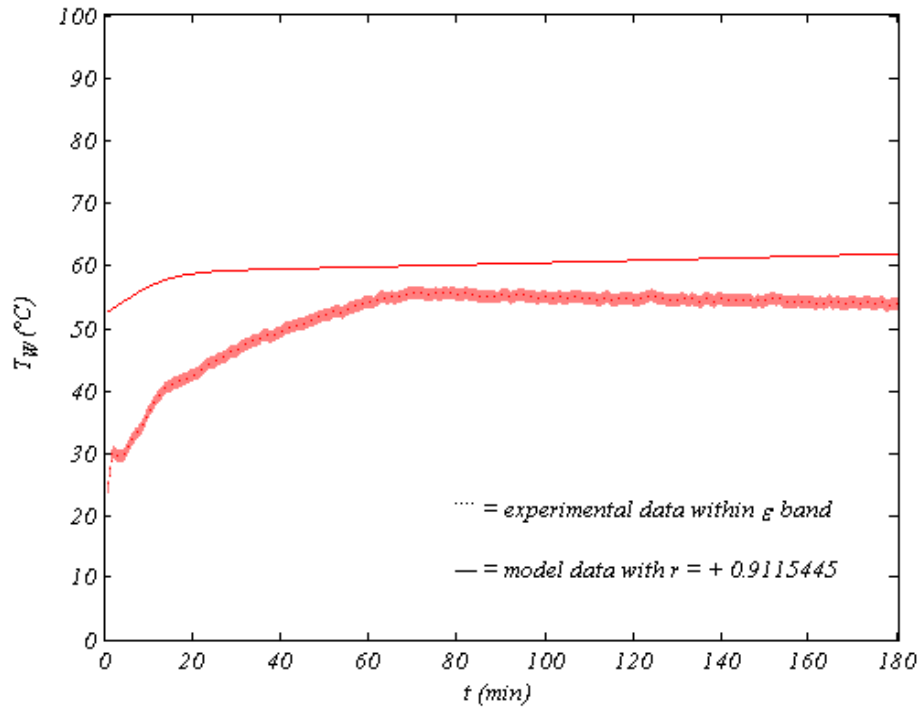
Figure 76. Concentrated brine temperature at 80°C flash and lower flow
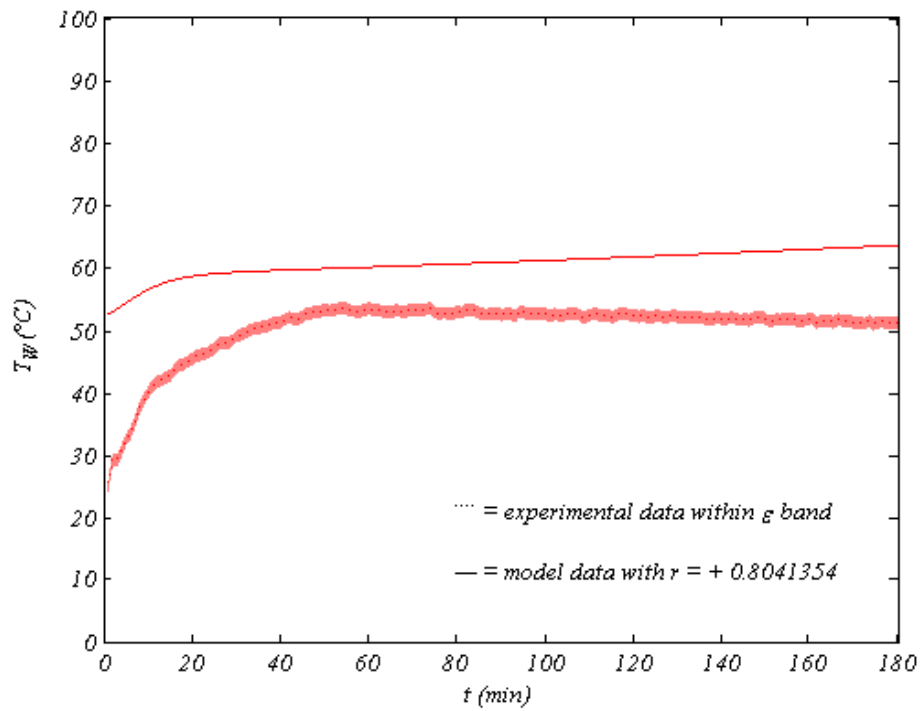
Figure 77. Concentrated brine temperature at 80°C flash and higher flow

7.5 Heat Reclamation

Cold incoming seawater is preheated in the condenser by hot water vapor condensing on the surface of the condenser tube before it enters the heater as mentioned in CHAPTER 4. The preheat temperature rapidly increased to reach a maximum early, before it slowly declined for both seawater flow rates; moreover, the preheat temperature attained at lower seawater flow rates, was higher. It increased with flash temperatures for both seawater flow rates since the amount and temperature of the condensing water vapor are directly proportional to flashing temperature.

Hot water vapor condenses by losing its latent heat of condensation to the entering seawater in the condenser; hence, preheat temperature indirectly denotes the rate of water vaporization and condensation. The preheat temperature rapidly increased due to high initial rate of vaporization caused by rapidly increasing equilibrium temperature at lower vacuum pressures, then it slowly declined due to the decreasing rate of vaporization caused by the stabilizing equilibrium temperature at rising vacuum pressures for both seawater flow rates as was shown previously. The preheat temperature profiles for both seawater flow rates are similar; however, they were higher for lower flow rates due to more condensation caused by more vaporization as will be seen later.

Model prediction of preheat temperature loosely resembled the experimental results due to the inability of the condenser tube heat transfer module to capture the rate of condensation. Modeling a heat transfer operation with a phase change is extremely complex, especially in the presence of non–condensable gases. The precision of the model in predicting the preheat temperature affects the quality of its evaluation of system performance. Preheat temperature profiles are shown in Figure 78 through Figure 89.

111
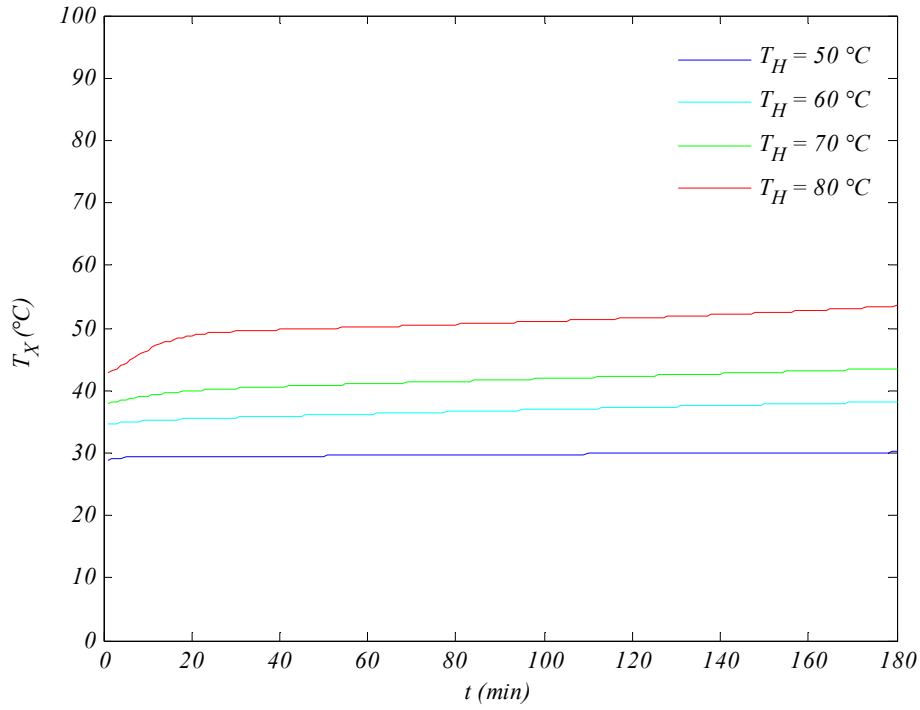
Figure 78. Modeled preheat temperature profiles at lower flow
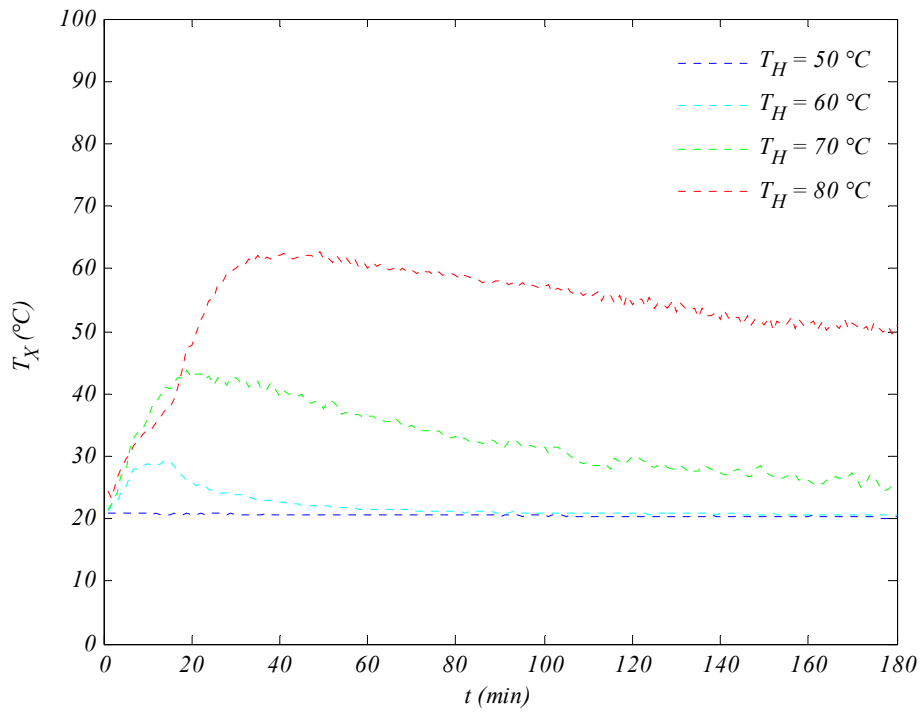
Figure 79. Experimental preheat temperature profiles at lower flow
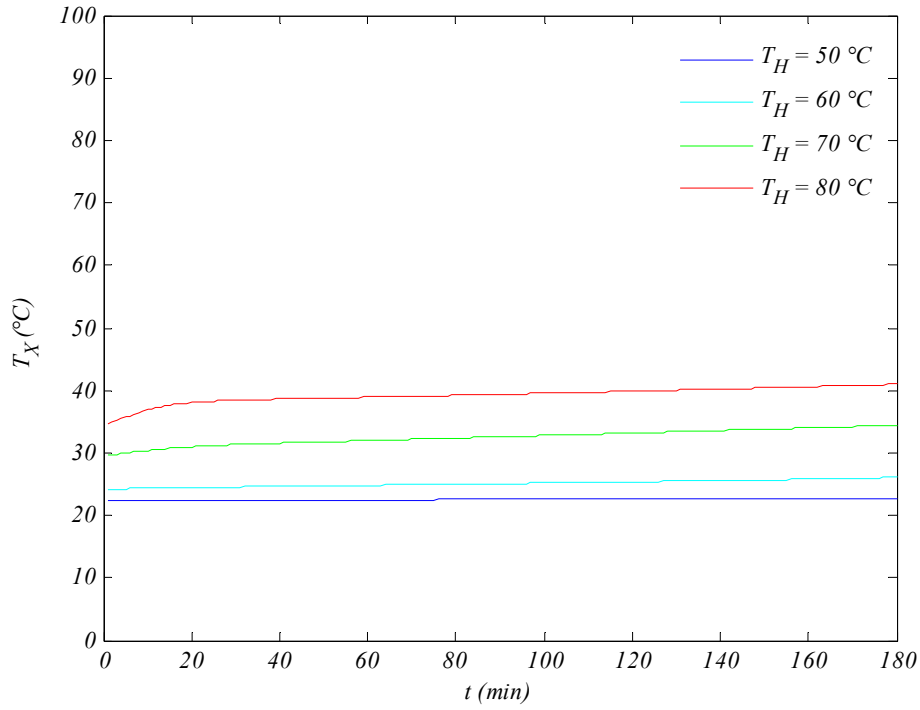
Figure 80. Modeled preheat temperature profiles at higher flow
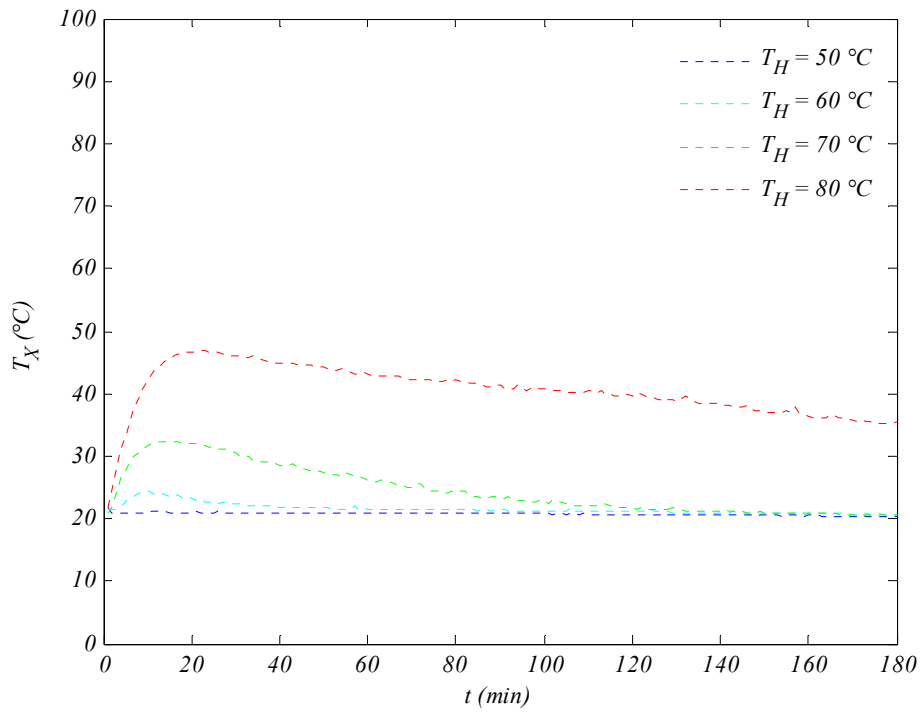
Figure 81. Experimental preheat temperature profiles at higher flow

113
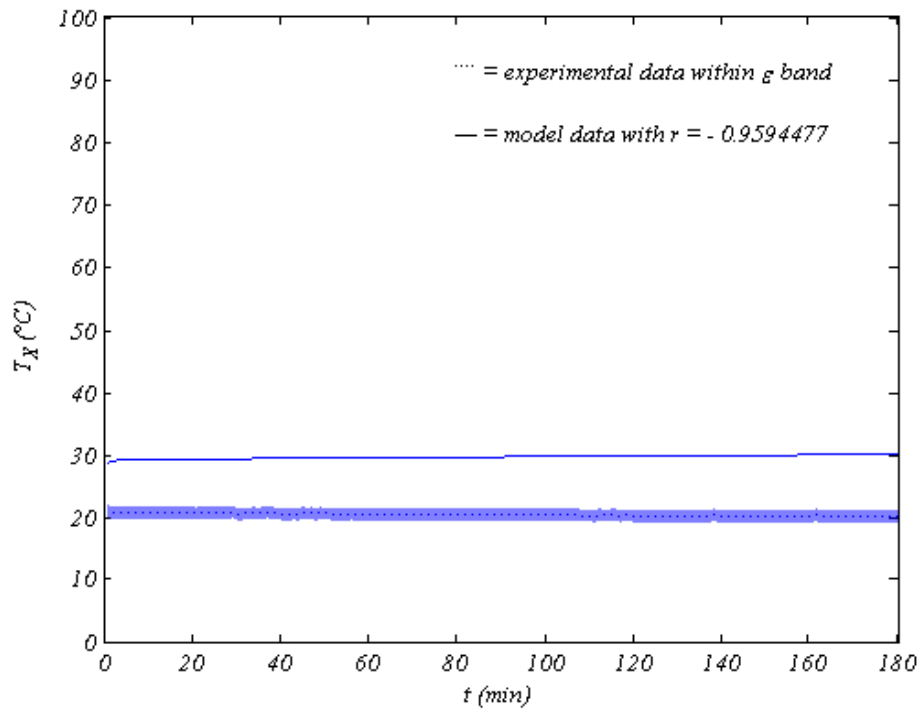
Figure 82. Preheat temperature at 50°C flash and lower flow
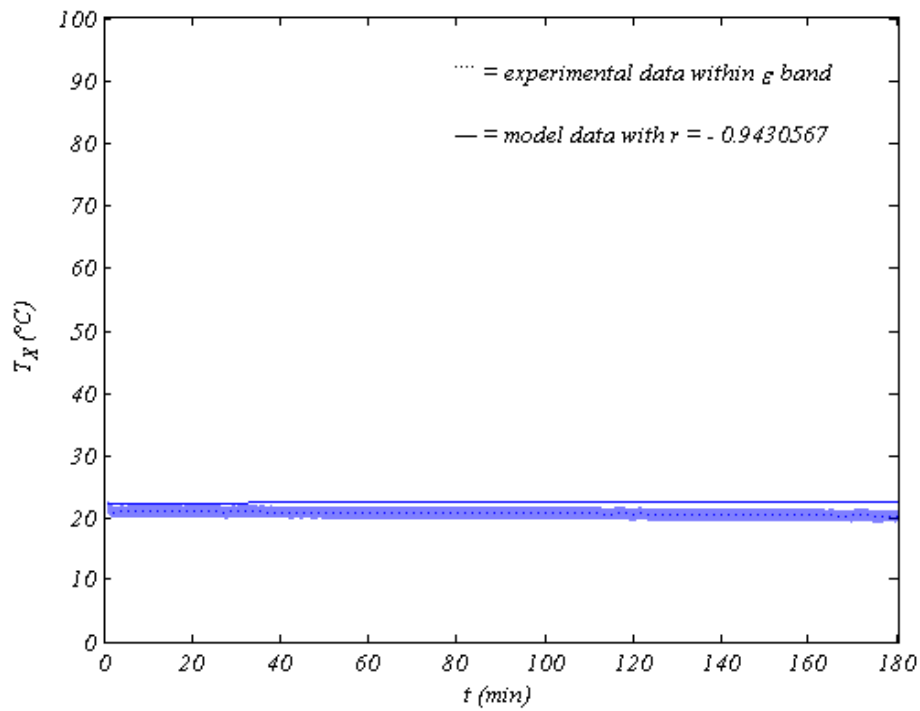
Figure 83. Preheat temperature at 50°C flash and higher flow

114
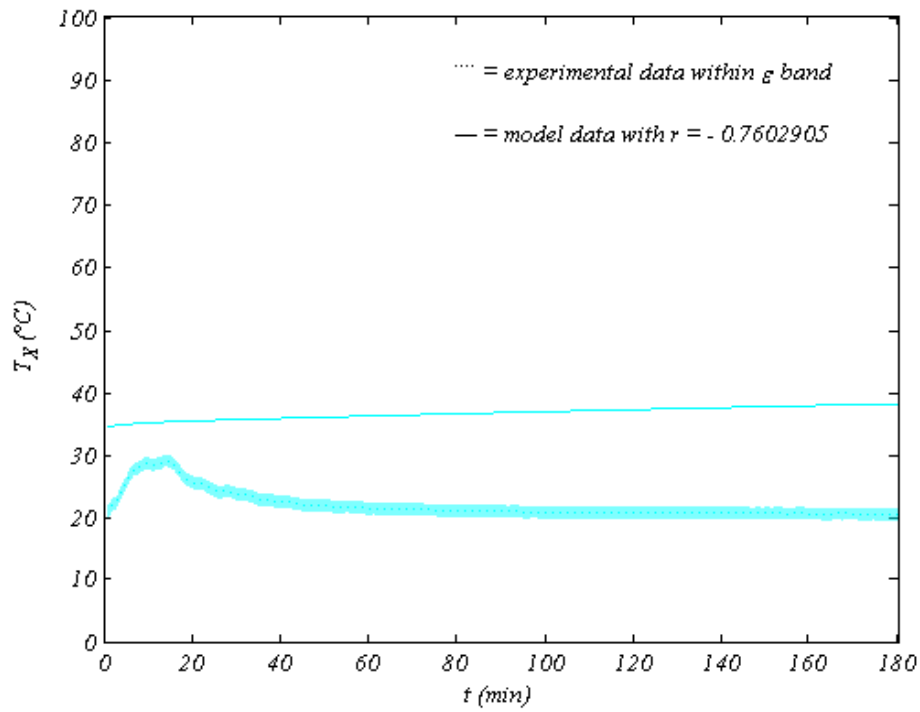
Figure 84. Preheat temperature at 60°C flash and lower flow
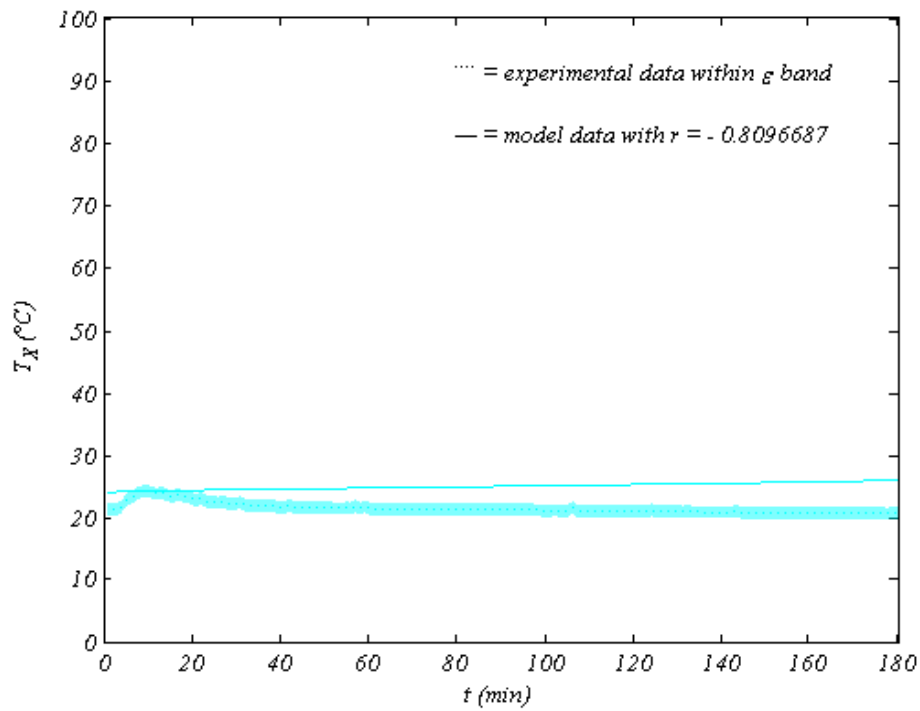
Figure 85. Preheat temperature at 60°C flash and higher flow
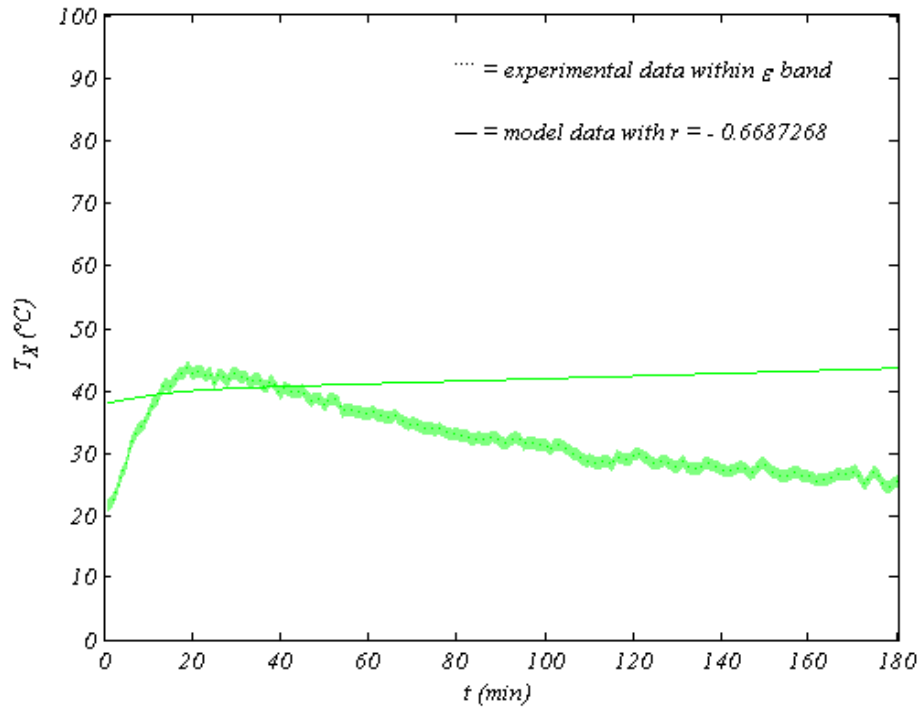
Figure 86. Preheat temperature at 70°C flash and lower flow
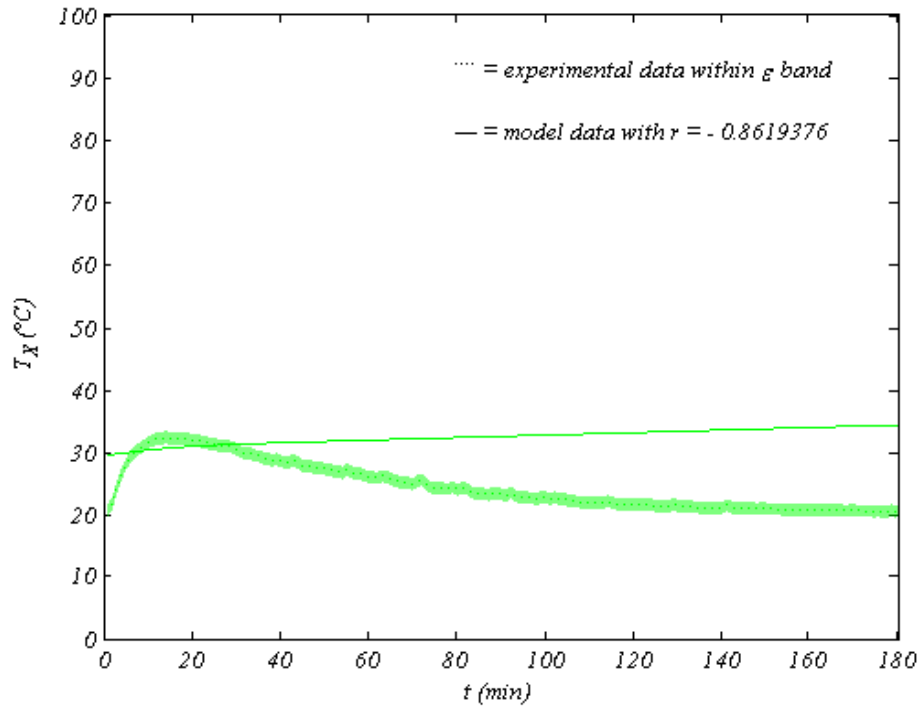
Figure 87. Preheat temperature at 70°C flash and higher flow

116
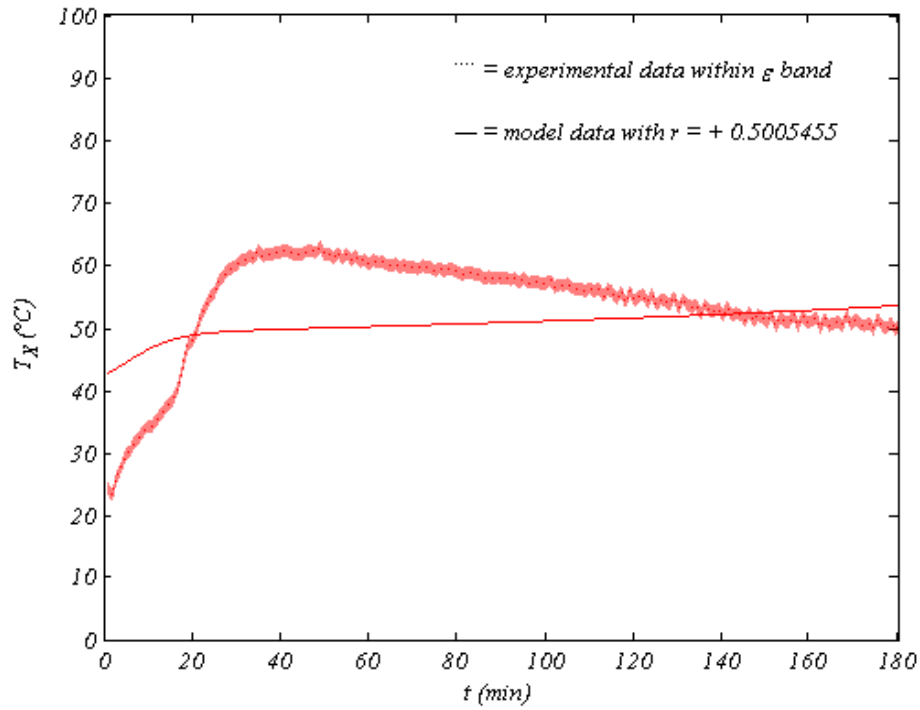
Figure 88. Preheat temperature at 80°C flash and lower flow
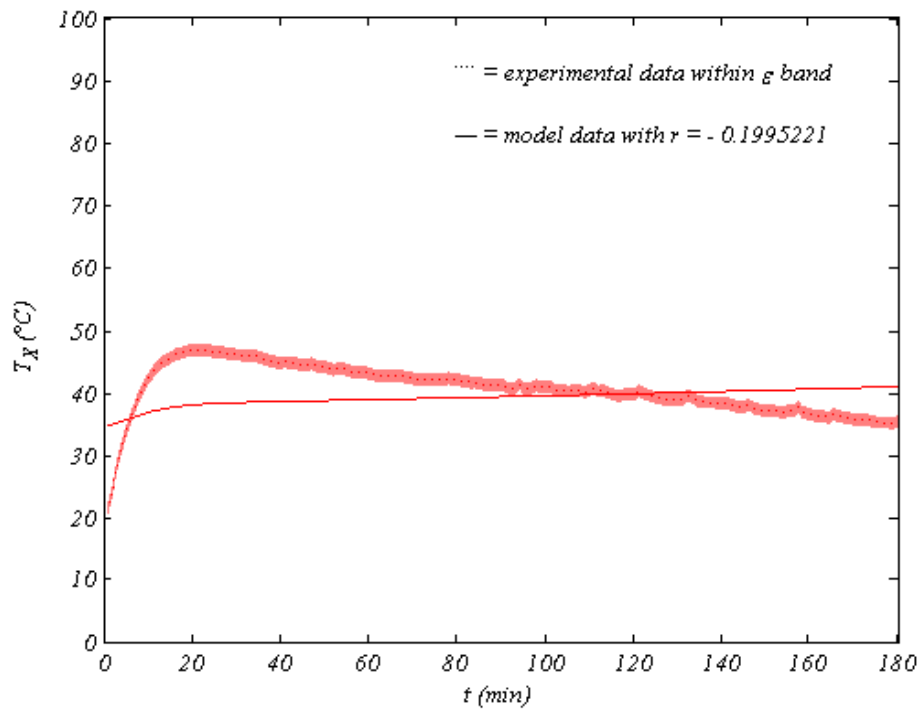
Figure 89. Preheat temperature at 80°C flash and higher flow

117

7.6 Heater Size

Preheated seawater coming out of the condenser is further heated by the solar heater to a set flash temperature as mentioned in CHAPTER 4. The heater load was fairly constant at lower flash temperatures but spiked, then rapidly decreased, reaching a minimum before it steadily increased at higher flash temperatures for both seawater flow rates. Moreover, heater loads at lower seawater flow rates were lower. The heater load increased with flash temperatures, reaching a maximum between 60 and 70 °C, after which it decreased for both seawater flow rates due to improved heat recovery caused by increased condensation experienced at higher flashing temperature as was mentioned.

The heater load makes up nearly all energy input to the desalination system due to the relatively small pumping work; hence, curtailing it enhances the feasibility of the process. The heater load logically increased with flash temperature at first but started to decrease later at higher flash temperature due to improved heat recovery caused by increased condensation for both seawater flow rates. Increased vaporization and the subsequent condensation improve heat recovery manifested in higher preheat temperatures that reduce the temperature gradient around the heater, ultimately reducing the heater load in line with the energy balance. The heater load profiles for both seawater flow rates are similar; however, they were lower for lower flow rates, since there was less volume to heat as well as the superior heat recovery as was seen earlier.

Model prediction of heater load loosely resembled the pseudo–experimental results due to the inexact preheat temperature calculation seen earlier. The precision of the model in predicting the heater load affects the quality of its evaluation of system performance. Heater load profiles are shown in Figure 90 through Figure 101.
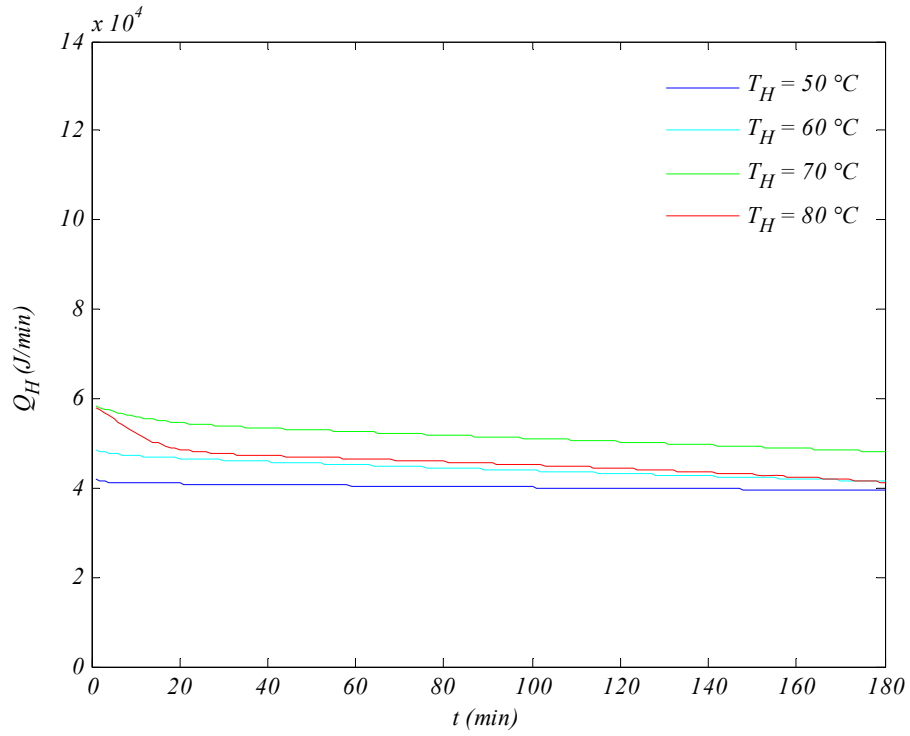
Figure 90. Modeled heat load profiles at lower flow
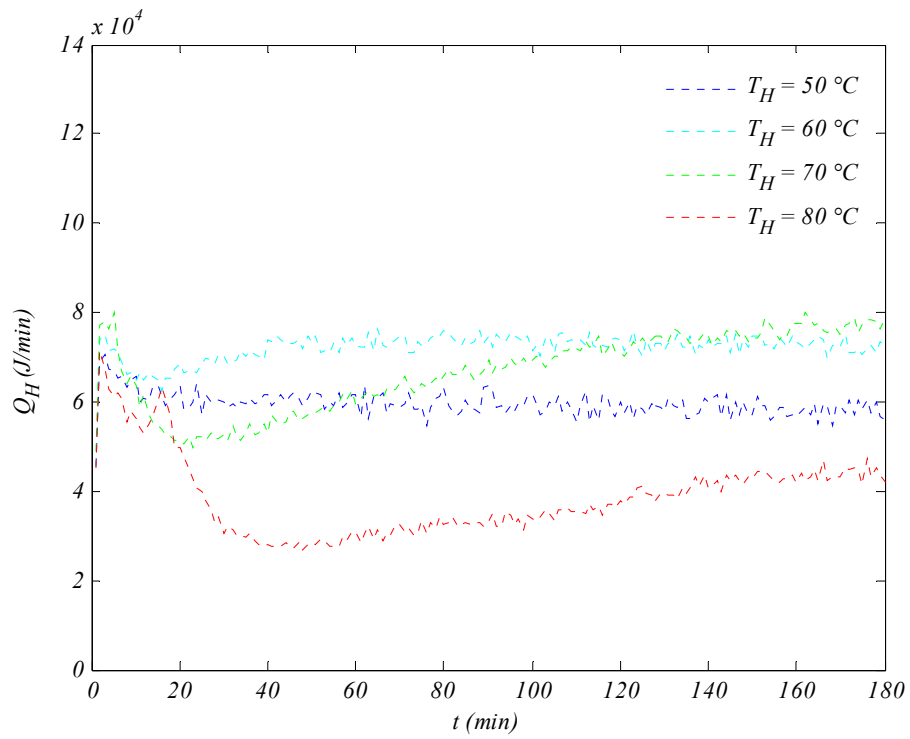
Figure 91. Mined heat load profiles at lower flow

119
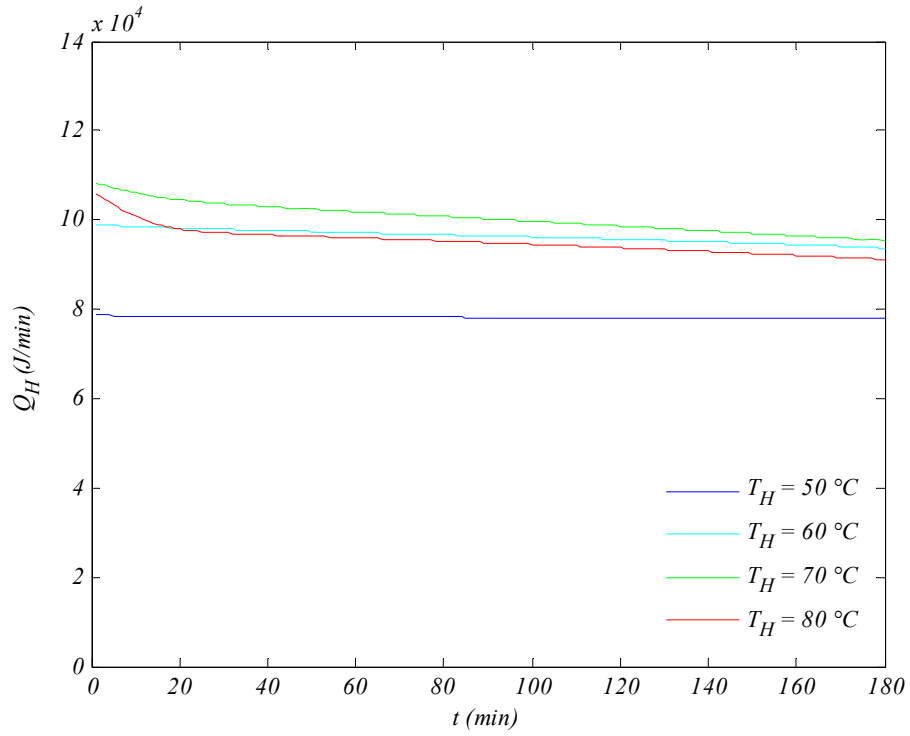
Figure 92. Modeled heat load profiles at higher flow
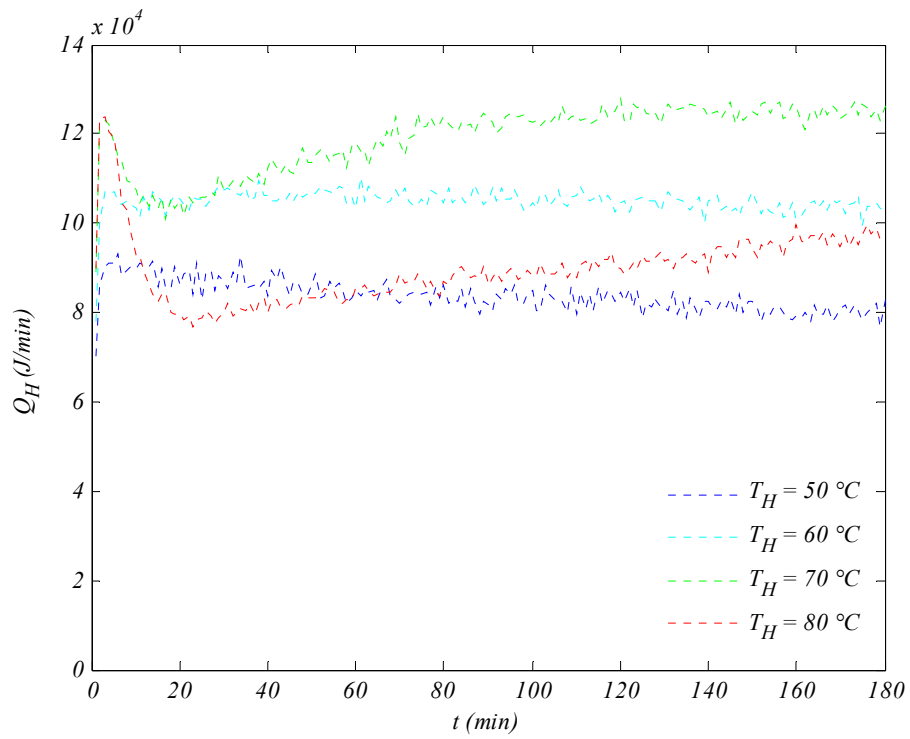
Figure 93. Mined heat load profiles at higher flow

120
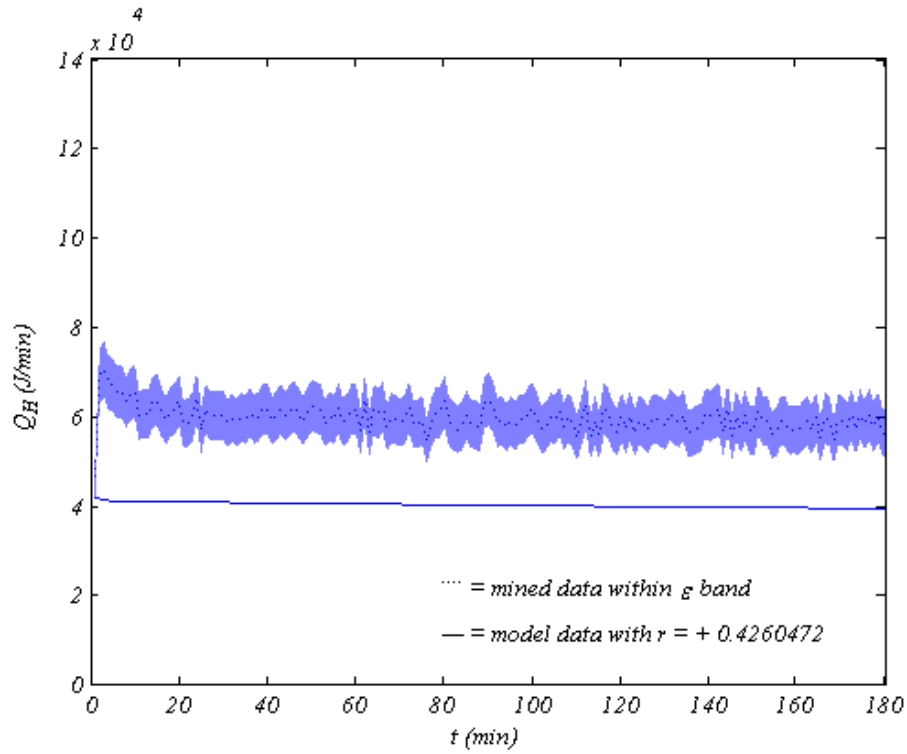
Figure 94. Heat load at 50°C flash and lower flow
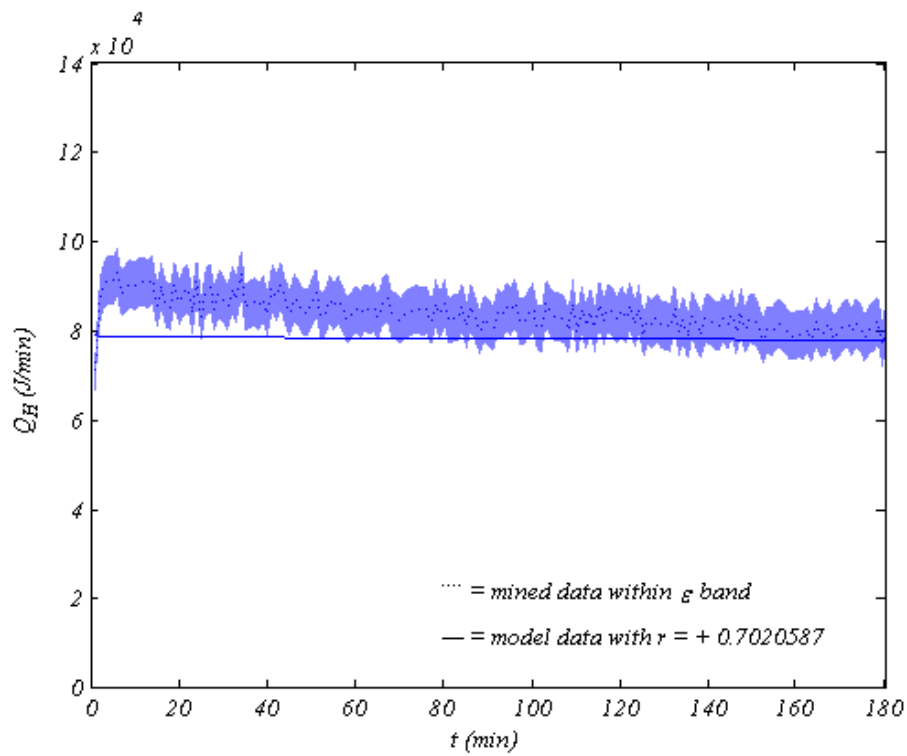
Figure 95. Heat load at 50°C flash and higher flow

121
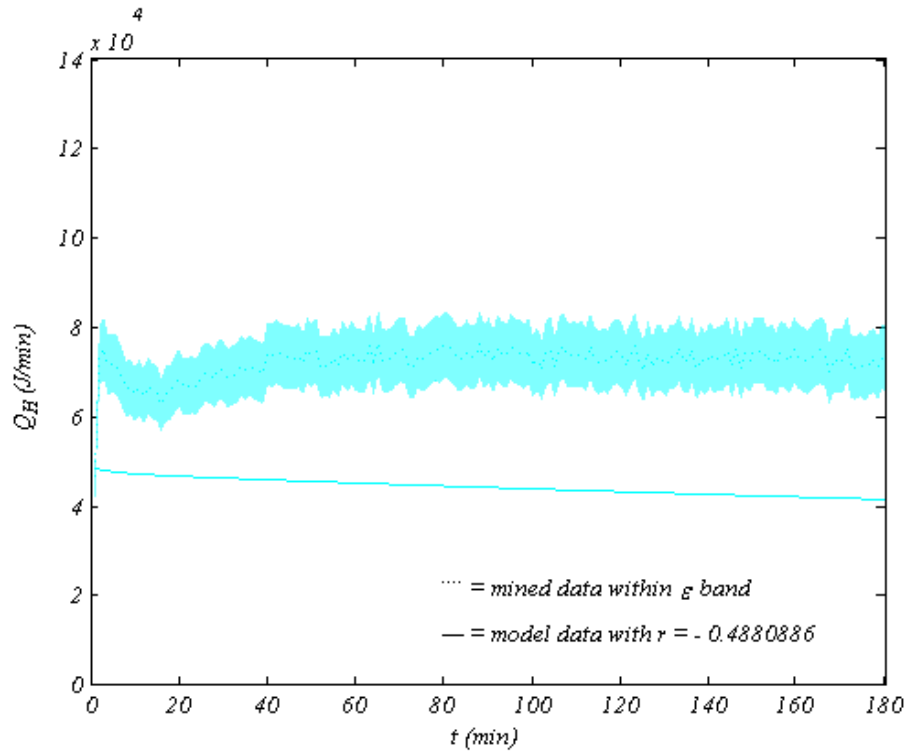
Figure 96. Heat load at 60°C flash and lower flow
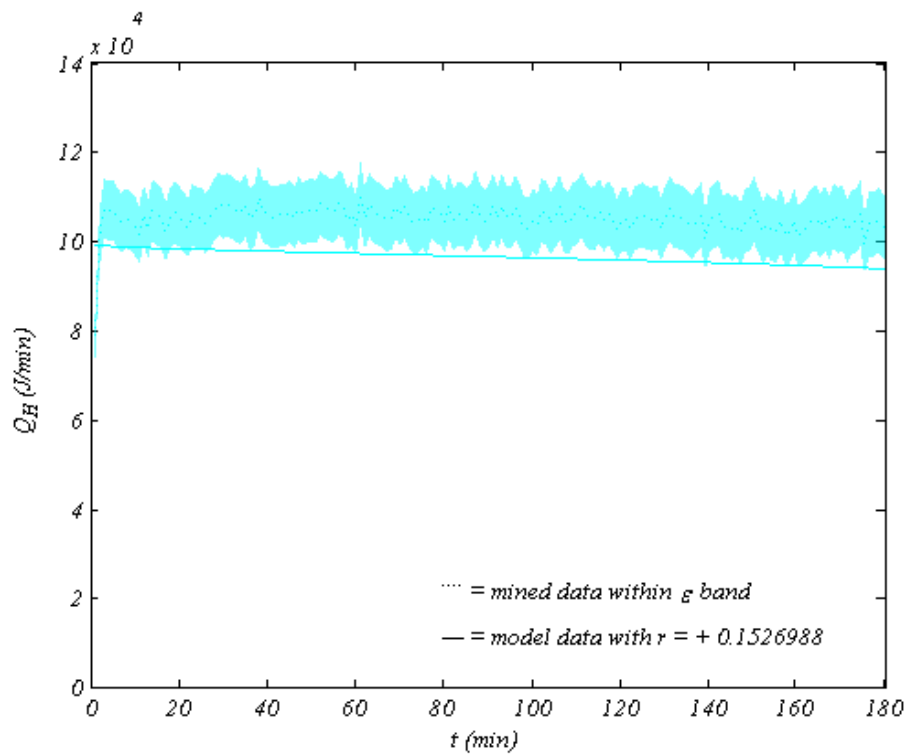
Figure 97. Heat load at 60°C flash and higher flow

122
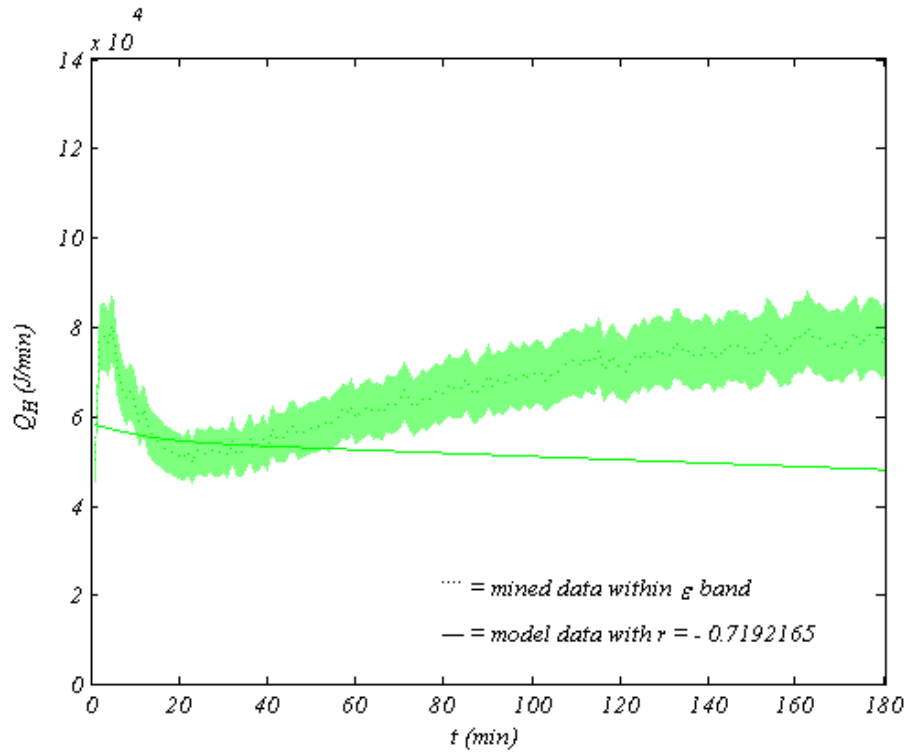
Figure 98. Heat load at 70°C flash and lower flow
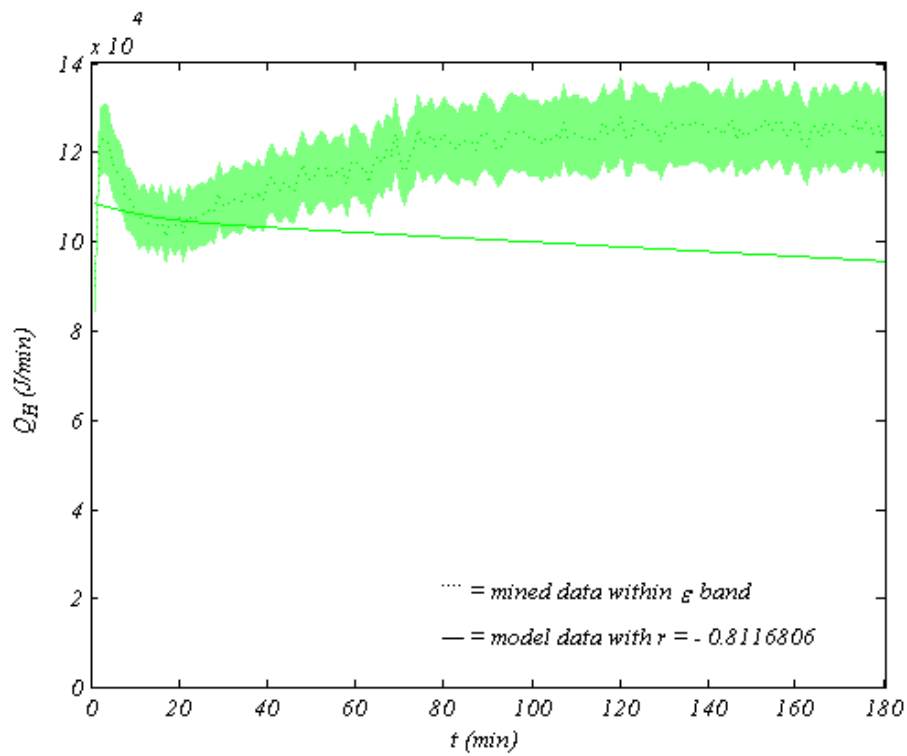
Figure 99. Heat load at 70°C flash and higher flow

123
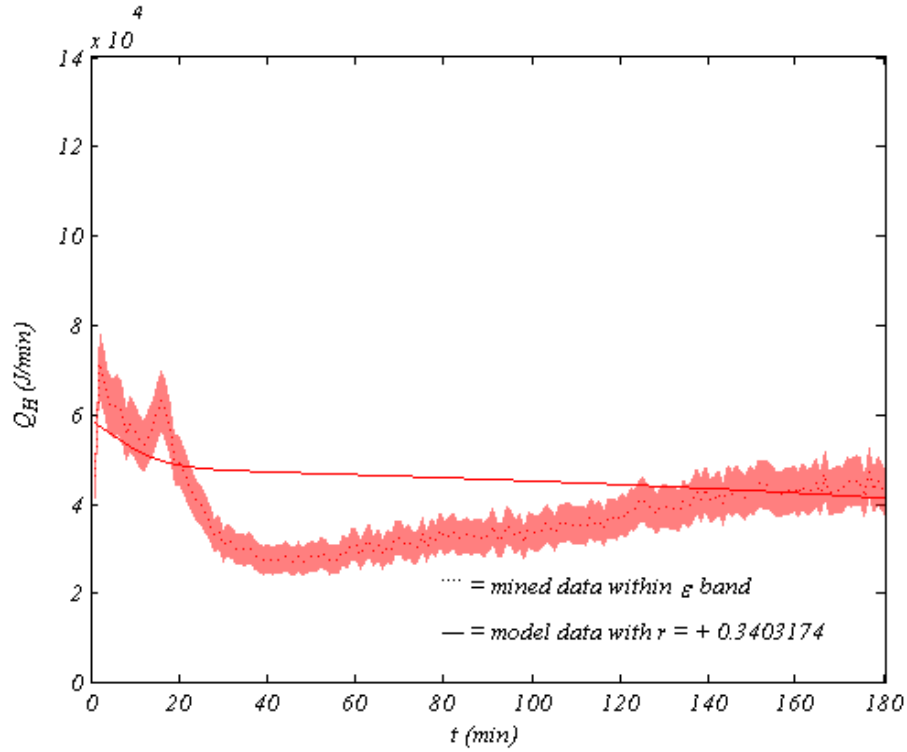
Figure 100. Heat load at 80°C flash and lower flow
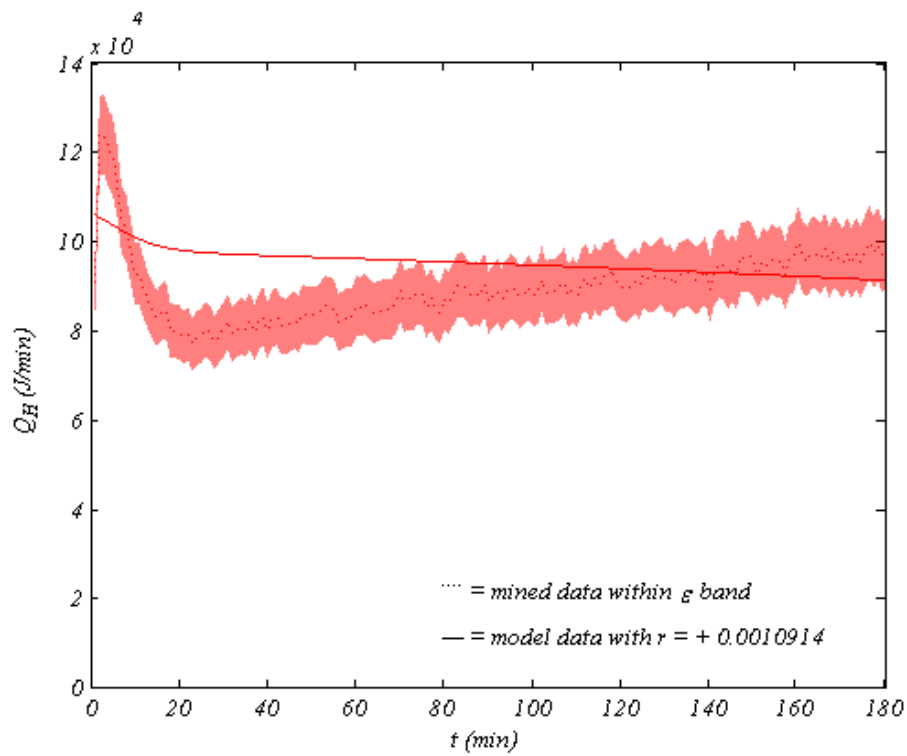
Figure 101. Heat load at 80°C flash and higher flow

124

7.7 Collector Size

The heater is modeled as a single–glazed flat–plate solar collector directly heating seawater flowing through its absorbing tubes; moreover, it is sized by the solar collection area needed to meet the heater load computed by a correlation given in CHAPTER 4 [8]. The required solar collection area is directly proportional to the heater load, resulting in matching profiles of both variables. The required solar collection area was fairly constant at lower flash temperatures, but spiked, then rapidly decreased, reaching a minimum before it steadily increased at higher flash temperatures for both seawater flow rates; moreover, the required solar collection areas at lower seawater flow rates were lower. Required solar collection area increased with flash temperatures, reaching a maximum between 60 and 70 °C, after which it decreased for both seawater flow rates due to improved heat recovery caused by increased condensation at higher flashing temperature.

The required solar collection area increased with flash temperature at first but started to decrease later at higher flash temperature, matching the above detailed profile of heater load for both seawater flow rates. The required solar collection area profiles for both seawater flow rates were similar; however, they were lower for lower flow rates due to reduced heater load, since there was less volume to heat as was seen earlier.

Model prediction of required solar collection area did not closely resemble the pseudo–experimental results because of poorly estimated heater load values caused by inexact preheat temperature calculation as was mentioned earlier. Reliability of model estimates of the required solar collection area depends on the accuracy of heater load computations, which relies on precision of preheat temperature computations. Required solar collection area profiles are shown in Figure 102 through Figure 113.

125
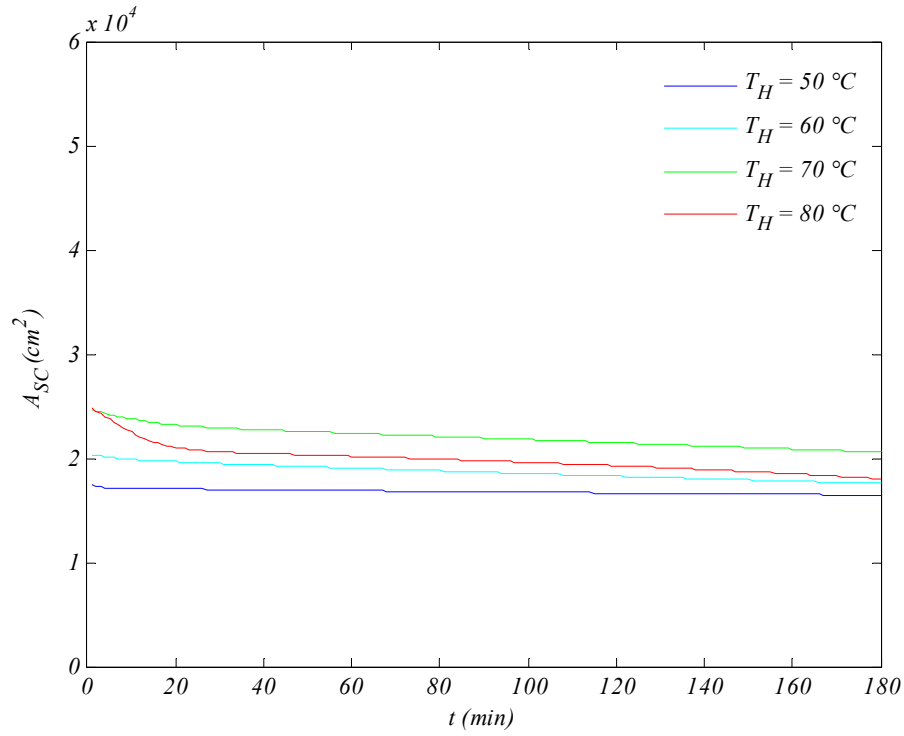
Figure 102. Modeled required solar collection area profiles at lower flow
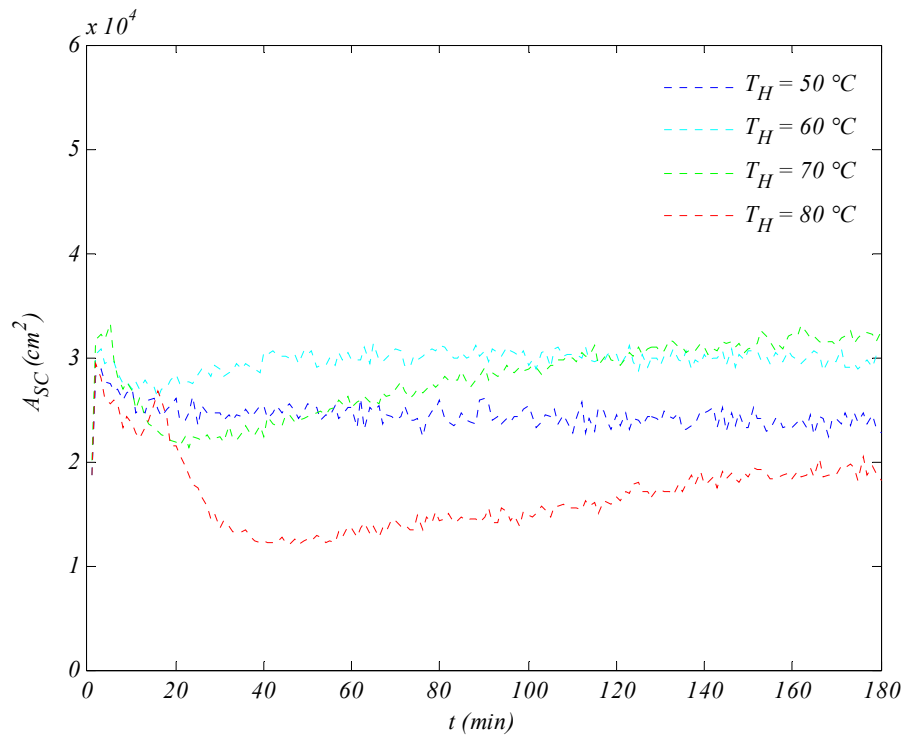
Figure 103. Mined required solar collection area profiles at lower flow
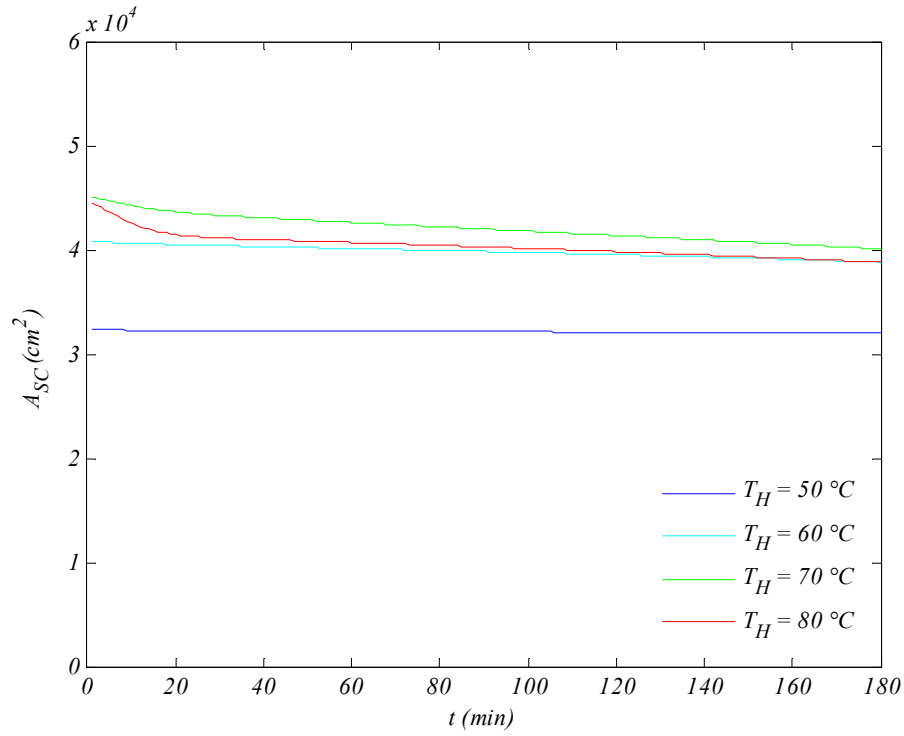
Figure 104. Modeled required solar collection area profiles at higher flow
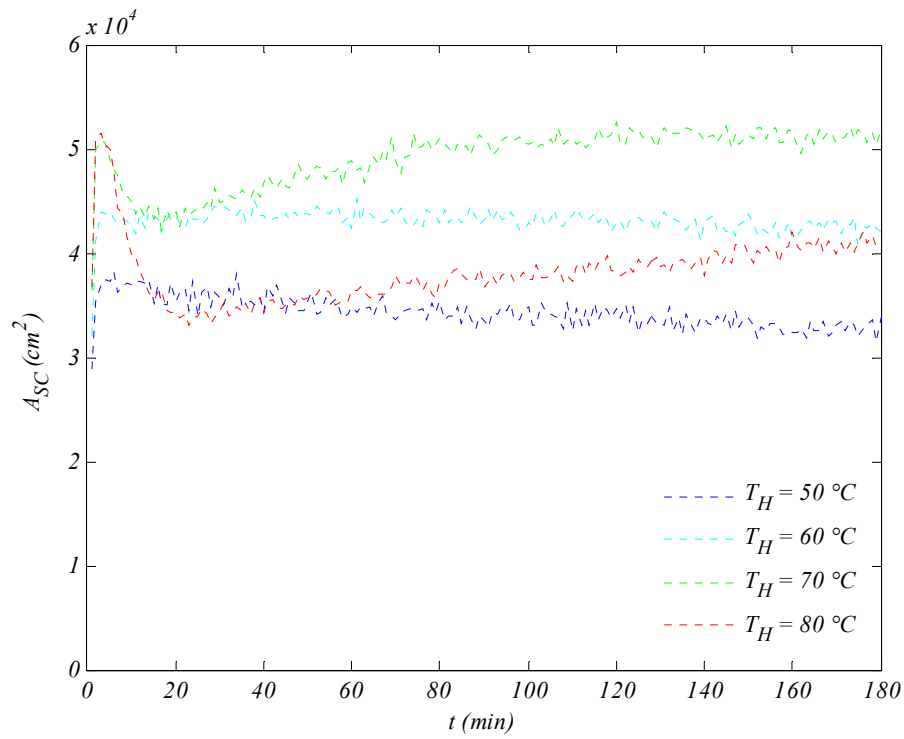
Figure 105. Mined required solar collection area profiles at higher flow

127
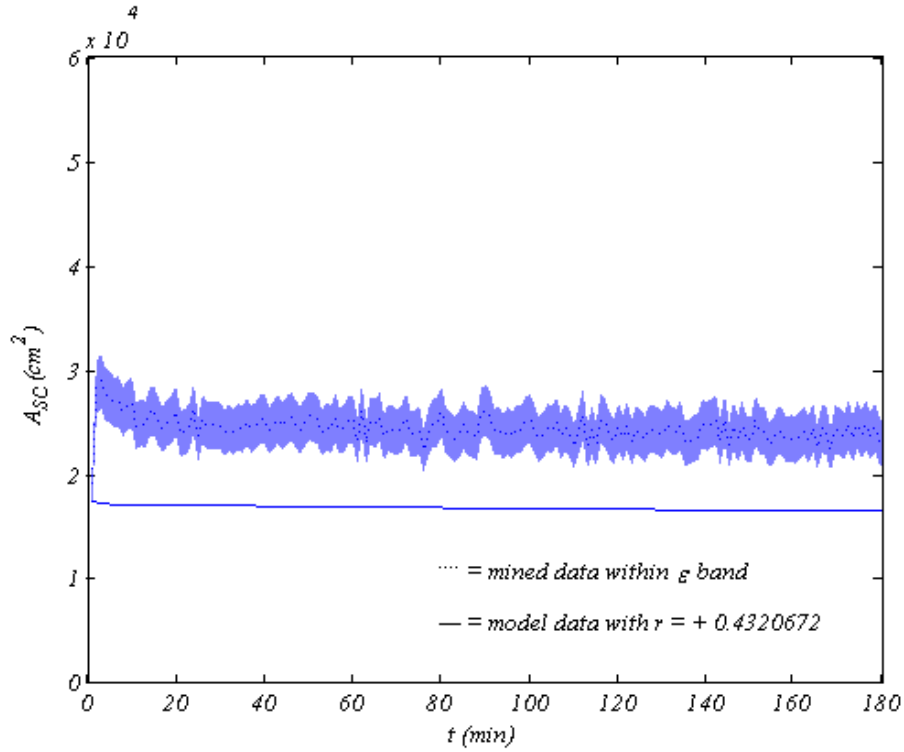
Figure 106. Required solar collection area at 50°C flash and lower flow
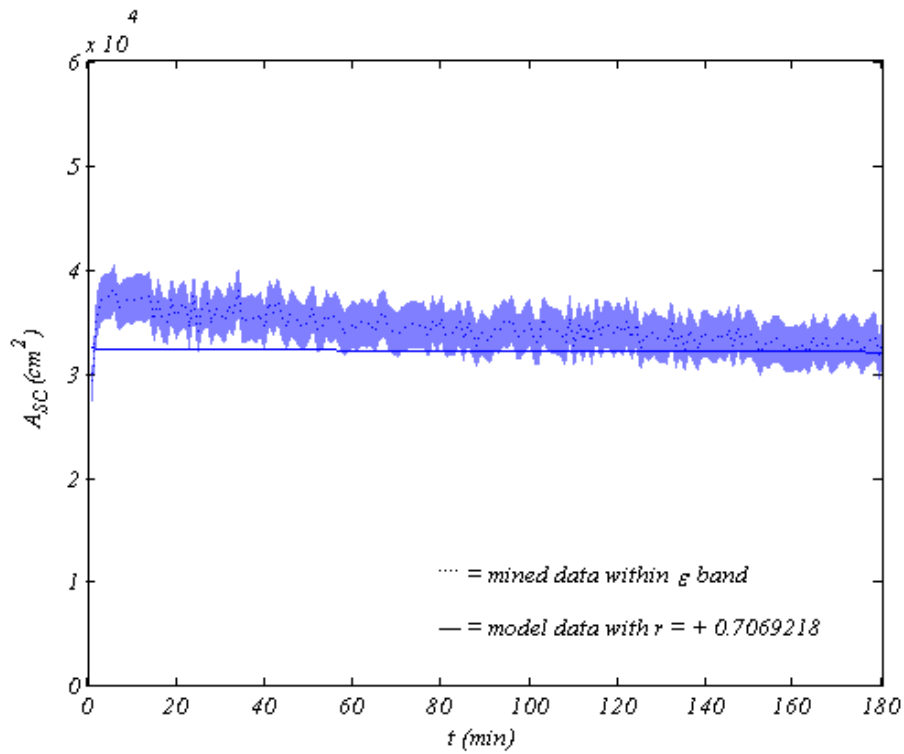
Figure 107. Required solar collection area at 50°C flash and higher flow

128
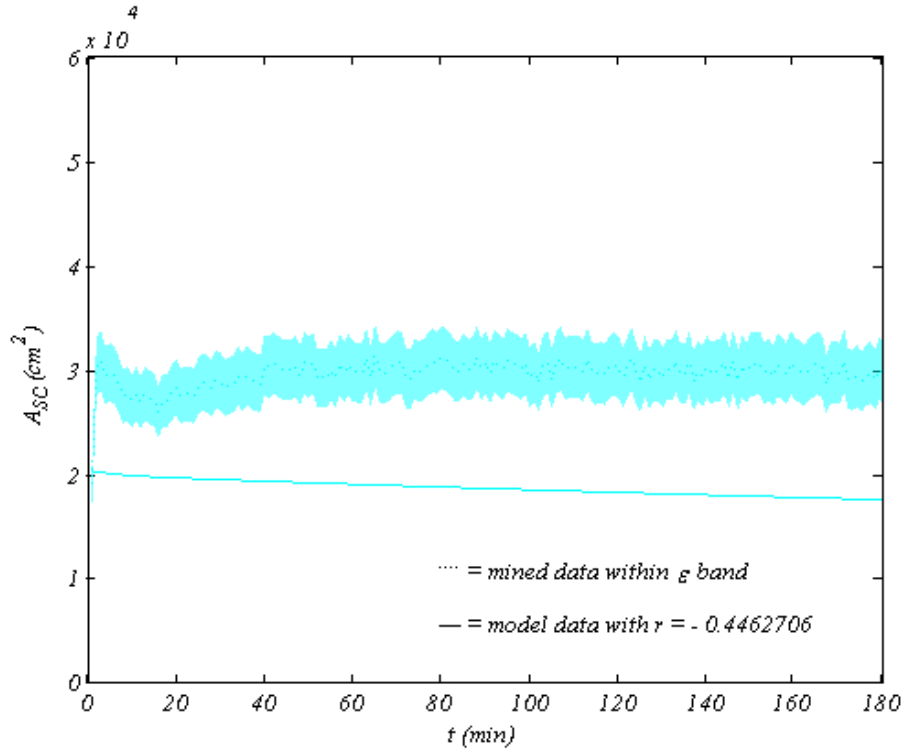
Figure 108. Required solar collection area at 60°C flash and lower flow
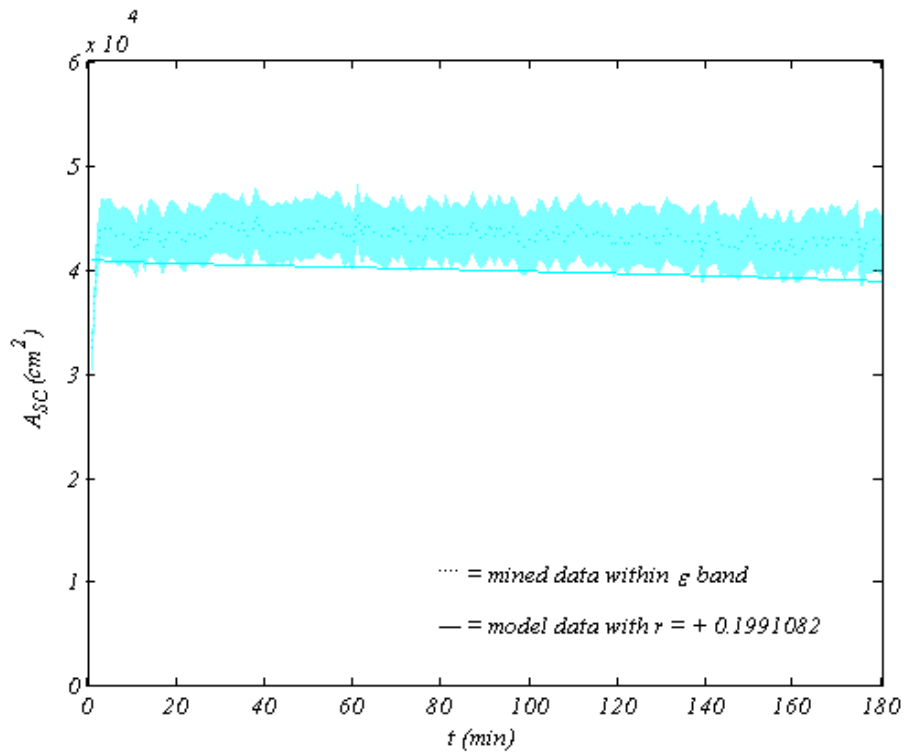
Figure 109. Required solar collection area at 60°C flash and higher flow

129
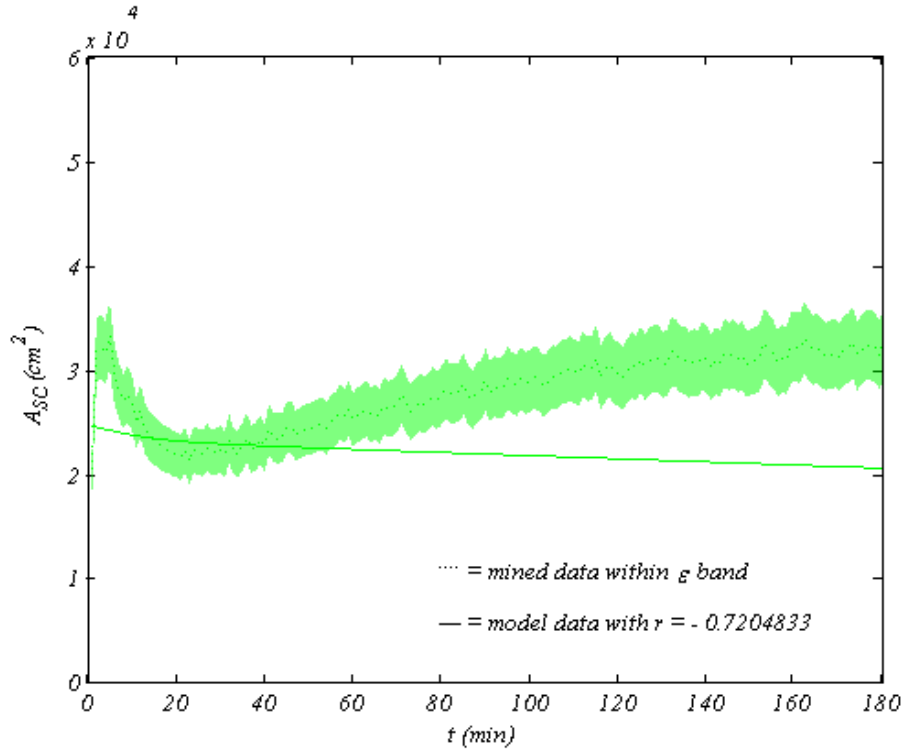
Figure 110. Required solar collection area at 70°C flash and lower flow
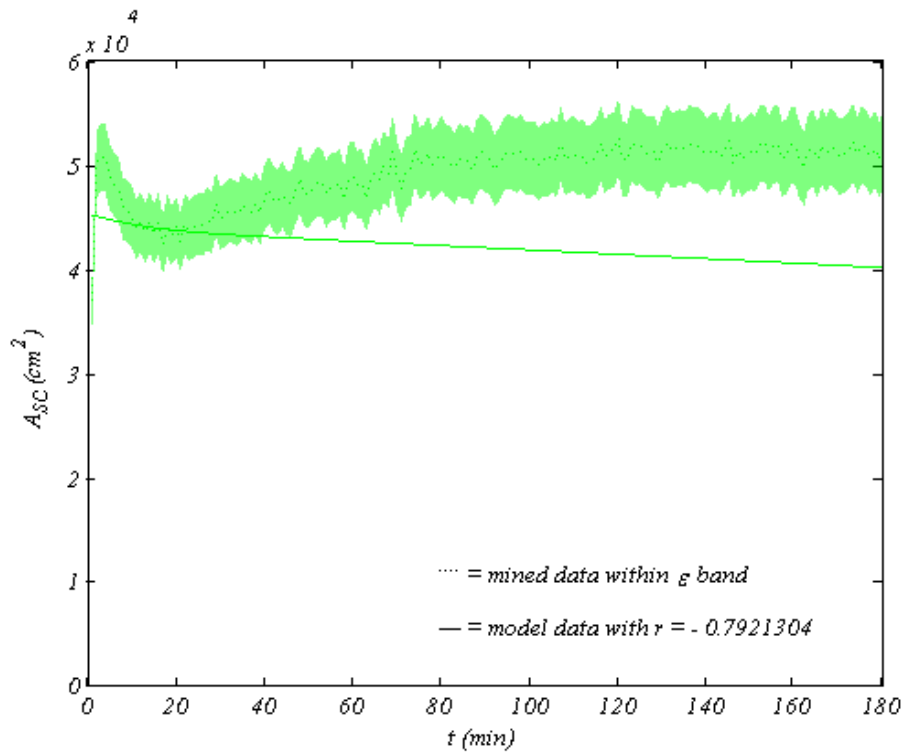
Figure 111. Required solar collection area at 70°C flash and higher flow

130
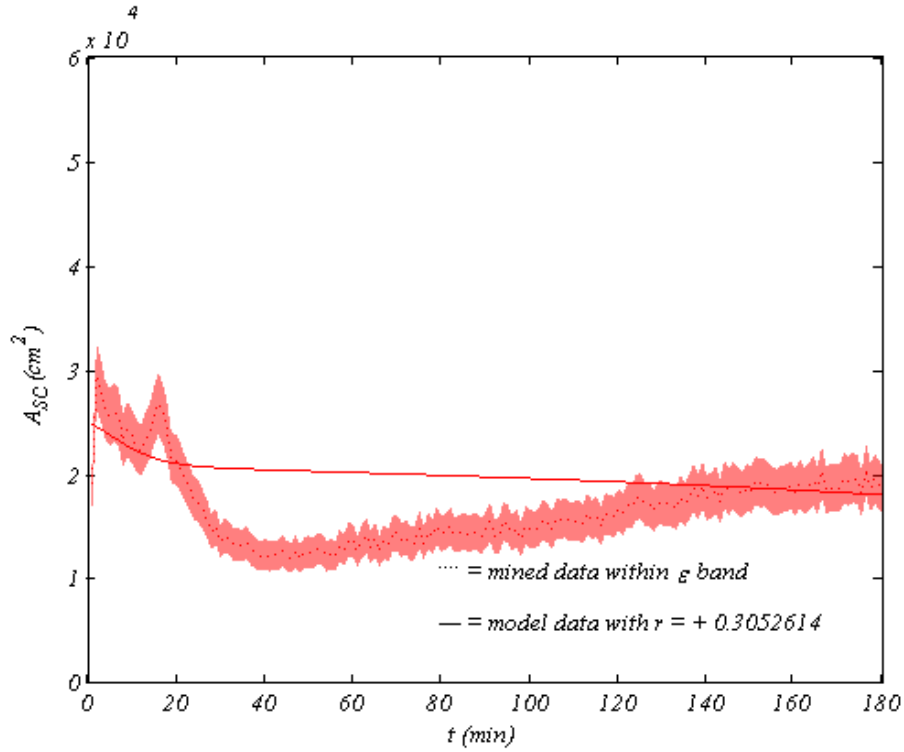
Figure 112. Required solar collection area at 80°C flash and lower flow
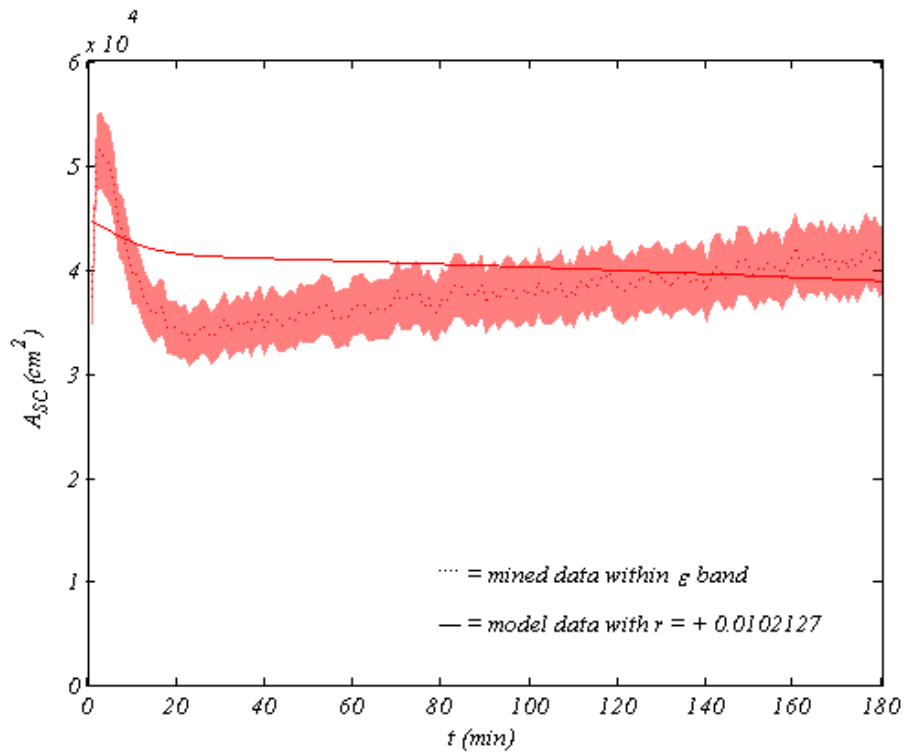
Figure 113. Required solar collection area at 80°C flash and higher flow

131

7.8 System Throughput

The fresh water produced is due to condensation of flashed and diffused water vapor moving from the evaporator to condenser as was mentioned in CHAPTER 4. Fresh water production rate was highest at first, then slowly declined for both seawater flow rates; moreover, it was generally higher for lower seawater flow rates. The difference between fresh water production rates of both seawater flow rates is more significant at medium flash temperatures and seems to diminish at both low and high flash temperatures. Fresh water production rate increased with flash temperatures for both seawater flow rates, since the amounts of flashing and diffusing water vapor are directly proportional to flashing temperature and the temperature–induced vapor pressure gradient between the evaporator and condenser, respectively.

Fresh water production rate was high at first due to the high initial rate of vaporization caused by the rapidly increasing equilibrium temperature at lower vacuum pressures, then it slowly declined due to the decreasing rate of vaporization caused by the stabilizing equilibrium temperature at rising vacuum pressures, almost reaching a plateau comparable to the flash temperature for both seawater flow rates. Fresh water production rate profiles for both seawater flow rates are similar; however, they were higher for lower flow rates due to more condensation caused by more vaporization.

Model prediction of fresh water production rate appropriately resembled the pseudo–experimental results due to adequate prediction of system vacuum and equilibrium temperature. Furthermore, adjusted parameters played a significant role in shifting the profile of fresh water production rate to match pseudo–experimental results. Fresh water production rate profiles are shown in Figure 114 through Figure 125.
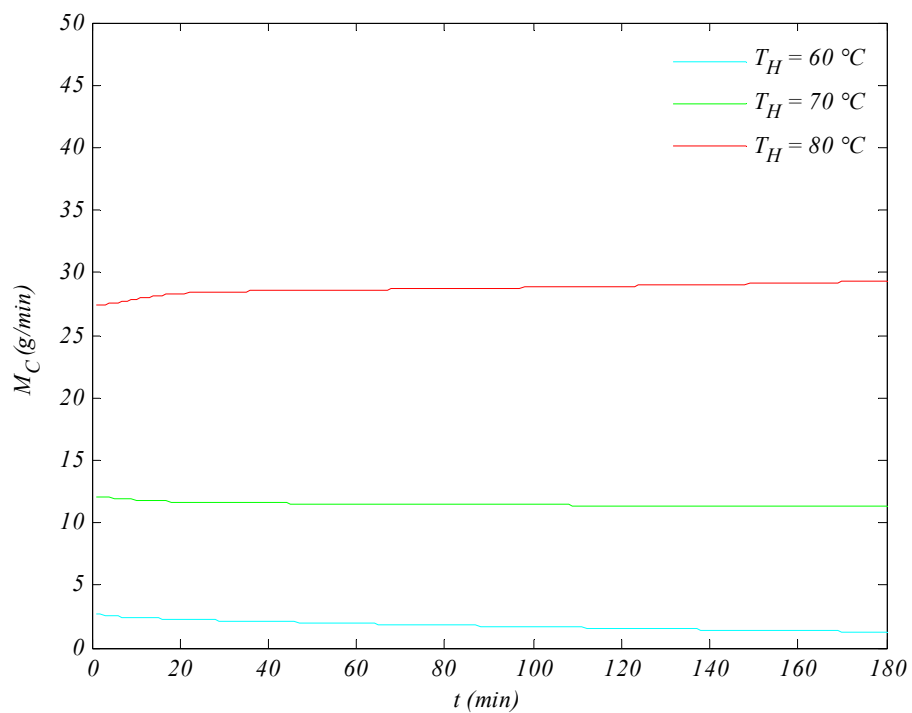
Figure 114. Modeled fresh water production rate profiles at lower flow
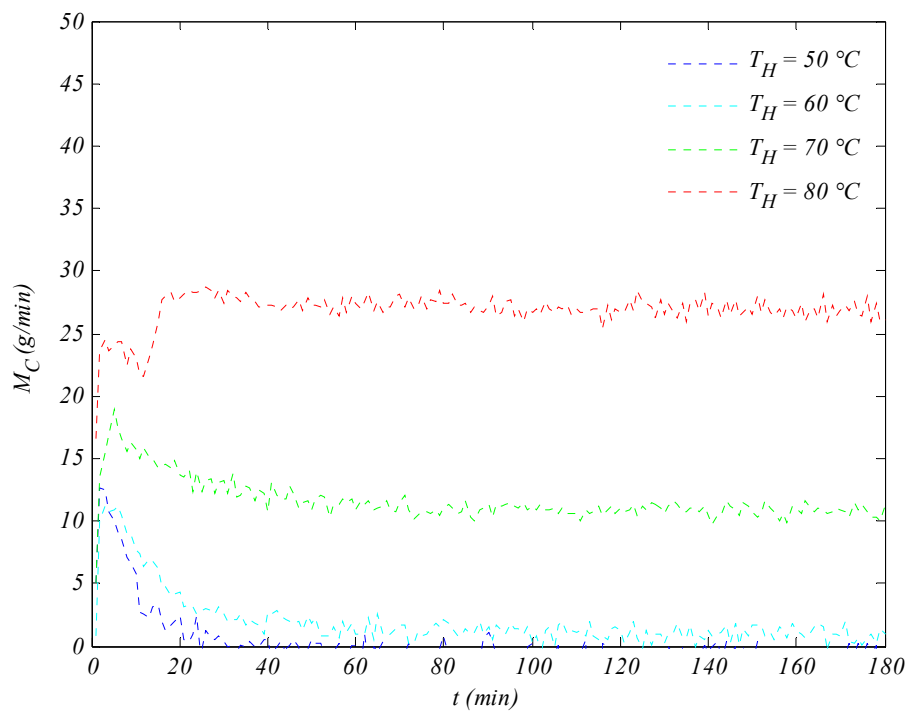
Figure 115. Mined fresh water production rate profiles at lower flow

133
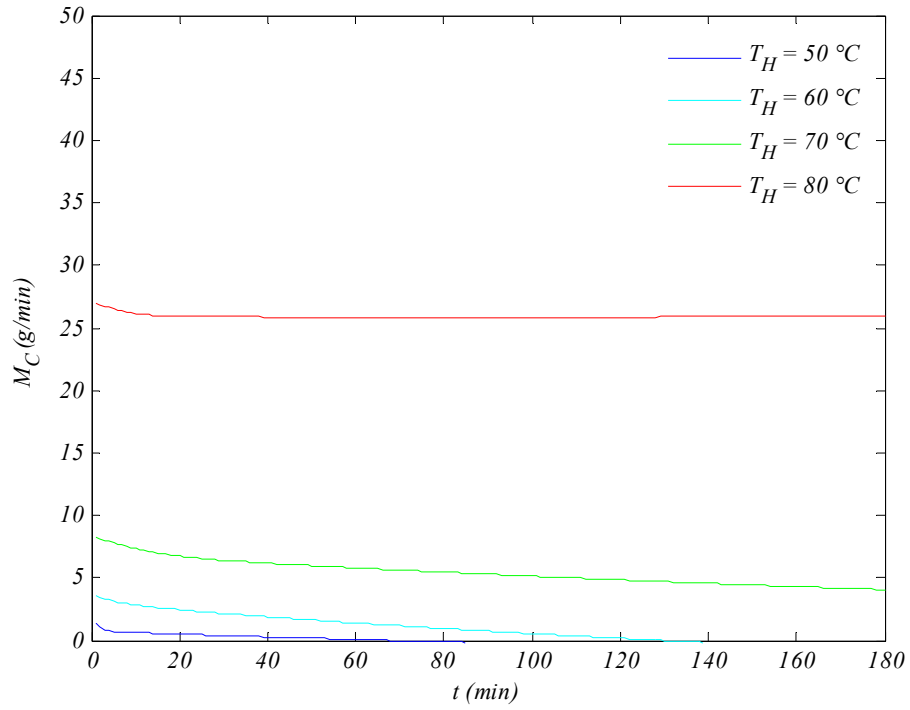
Figure 116. Modeled fresh water production rate profiles at higher flow
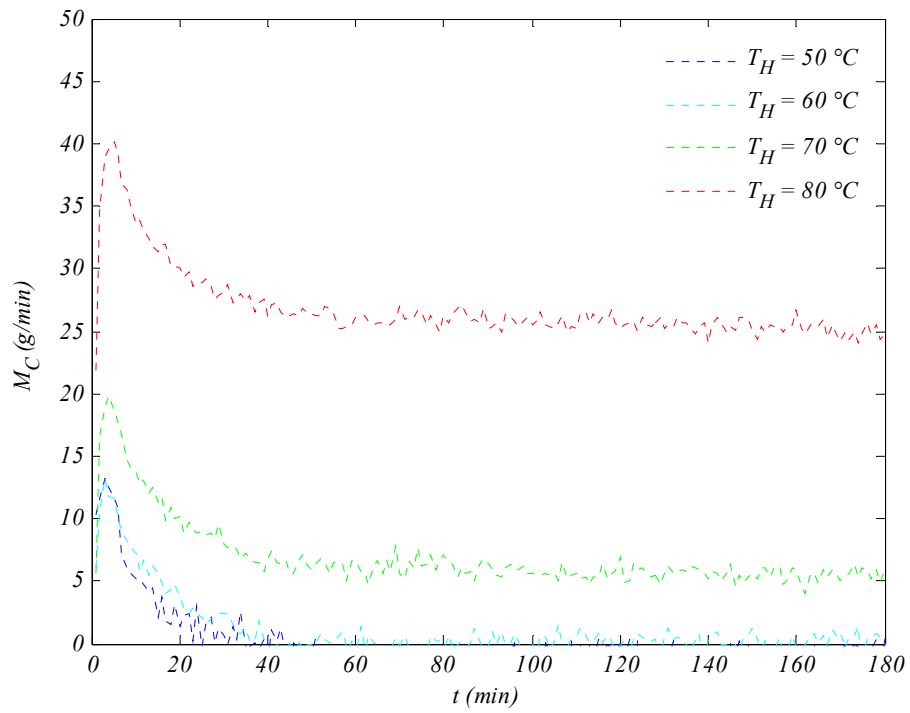
Figure 117. Mined fresh water production rate profiles at higher flow

134
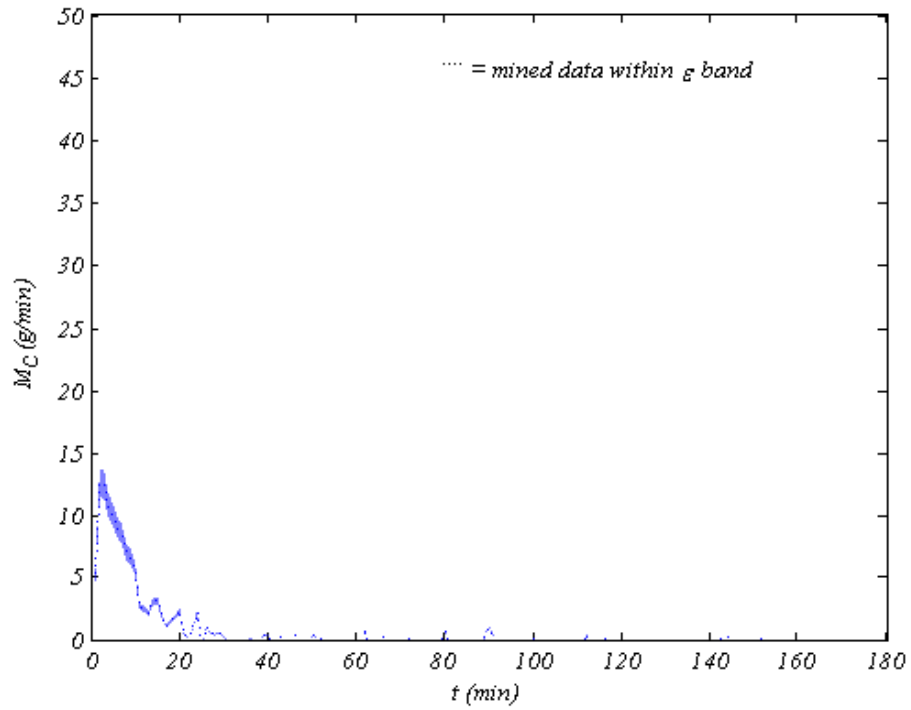
Figure 118. Fresh water production rate at 50°C flash and lower flow
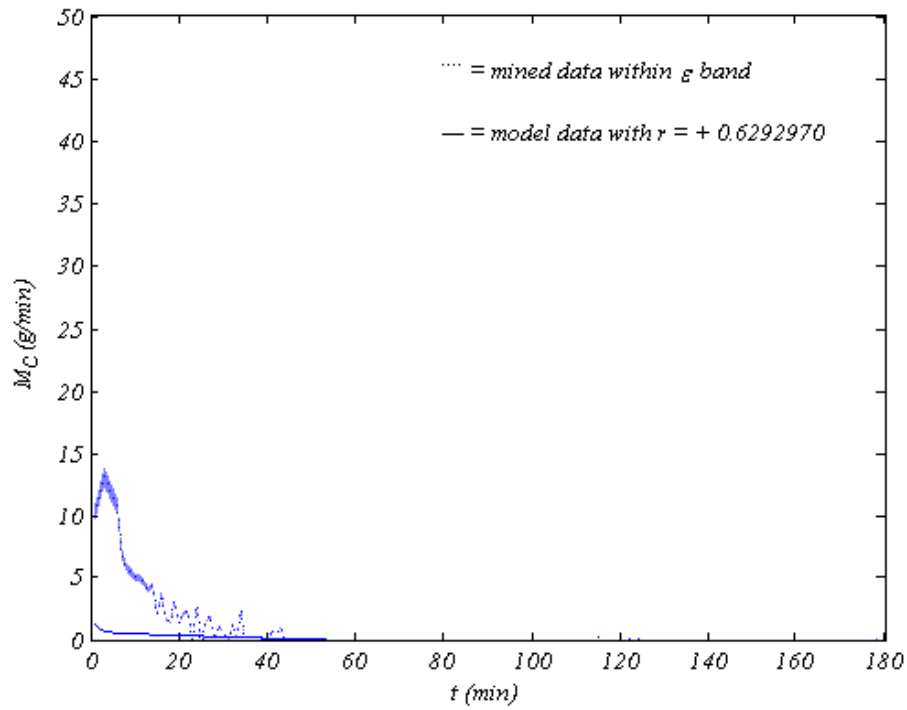
Figure 119. Fresh water production rate at 50°C flash and higher flow
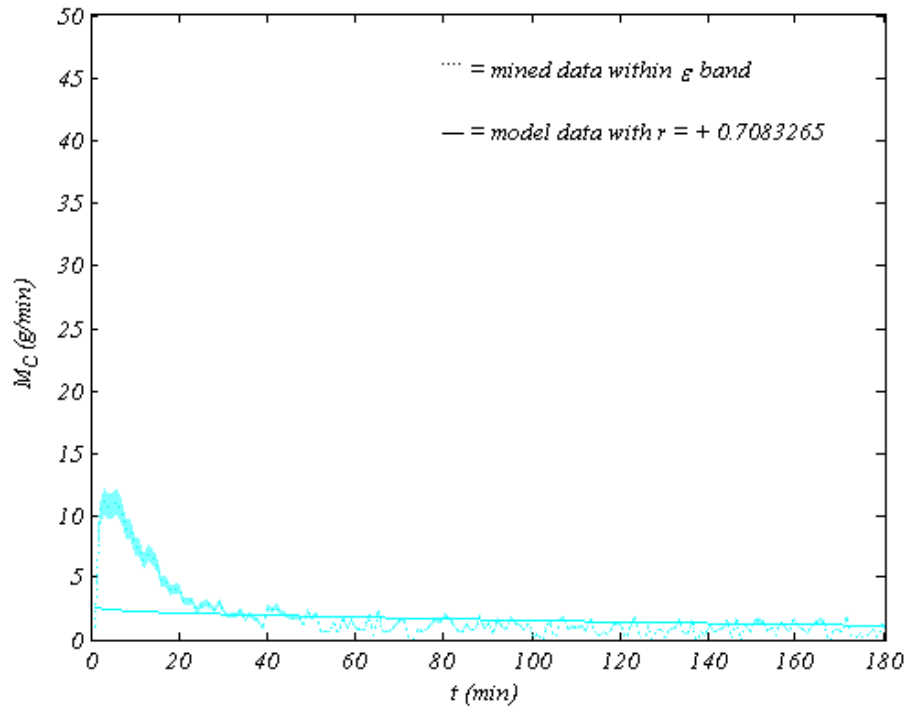
Figure 120. Fresh water production rate at 60°C flash and lower flow
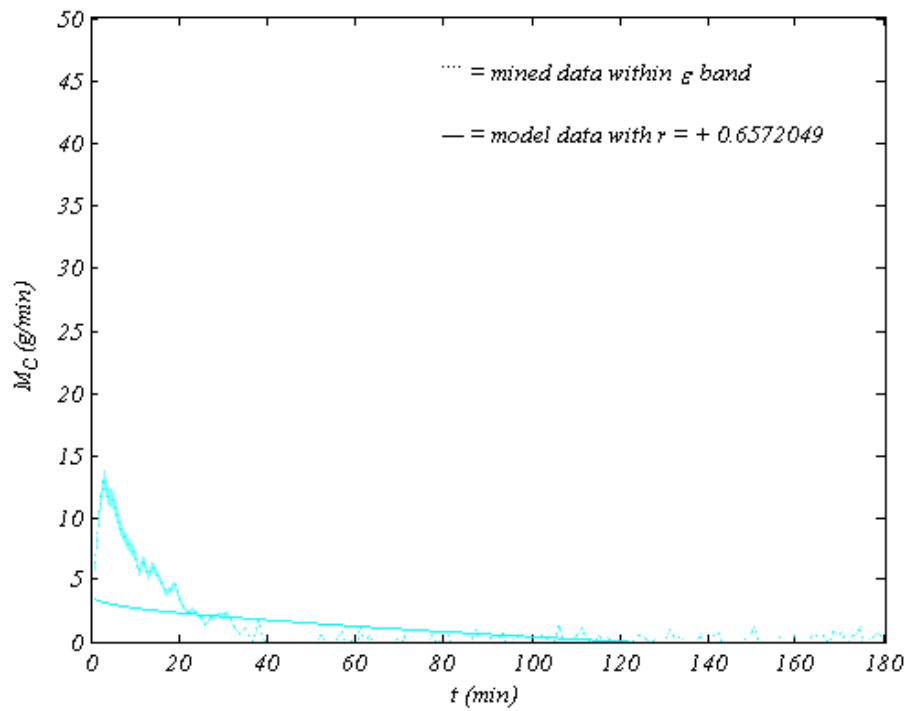
Figure 121. Fresh water production rate at 60°C flash and higher flow

136
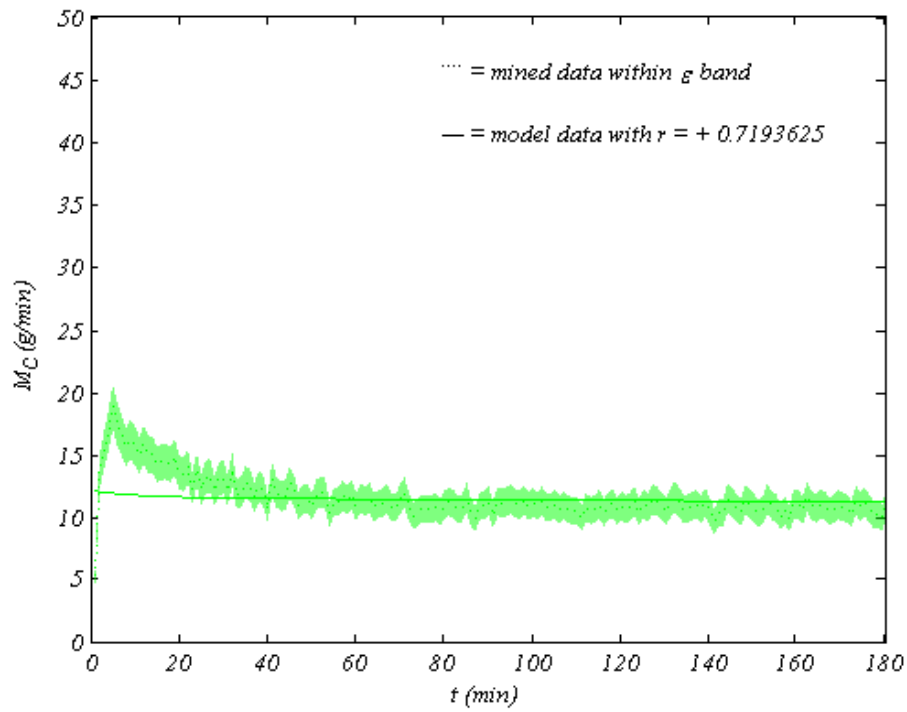
Figure 122. Fresh water production rate at 70°C flash and lower flow
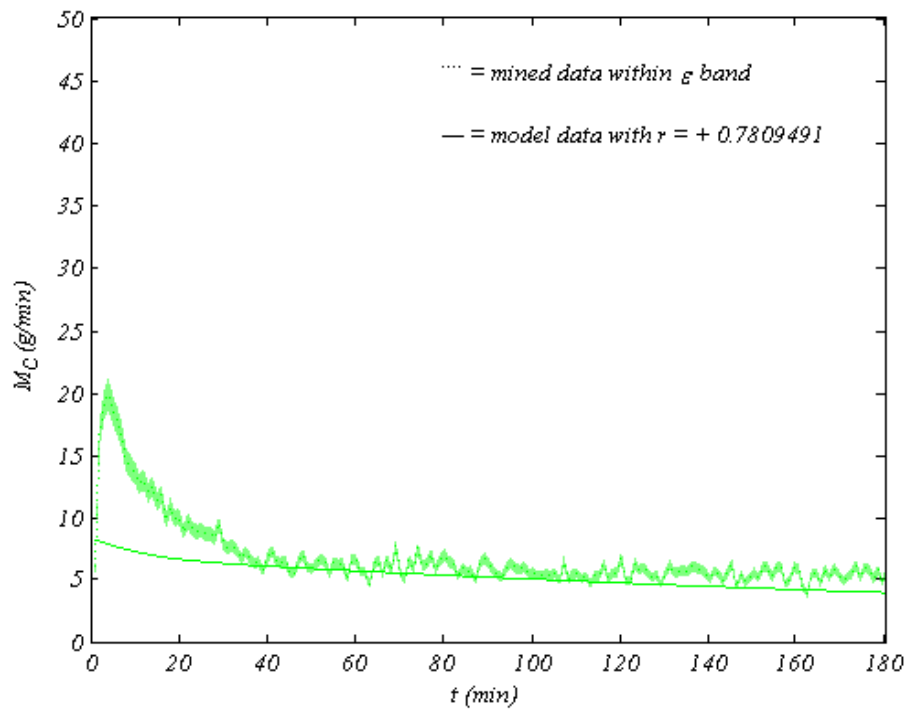
Figure 123. Fresh water production rate at 70°C flash and higher flow

137
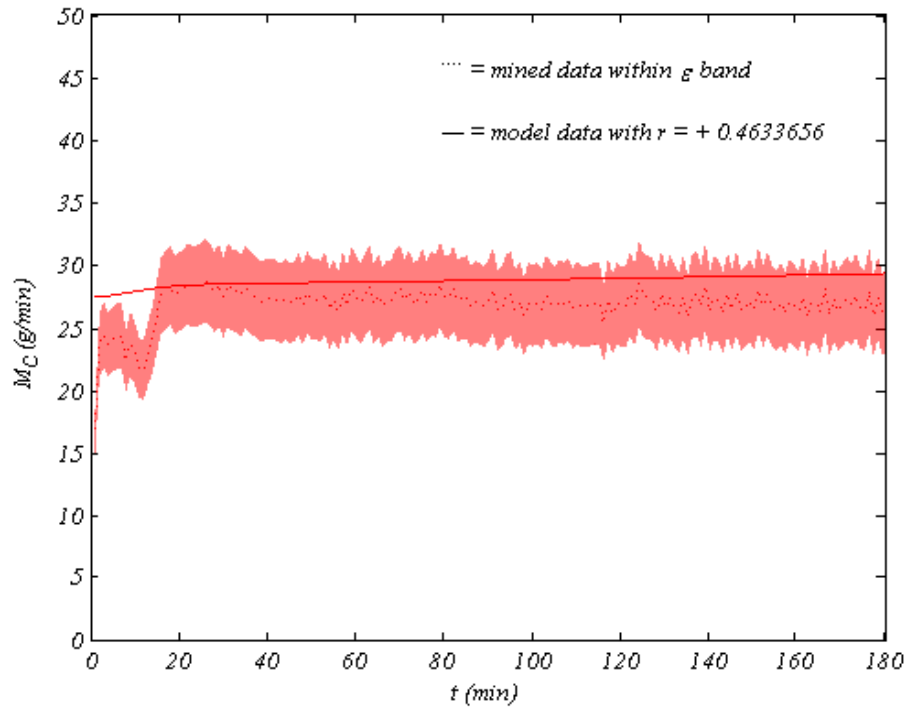
Figure 124. Fresh water production rate at 80°C flash and lower flow
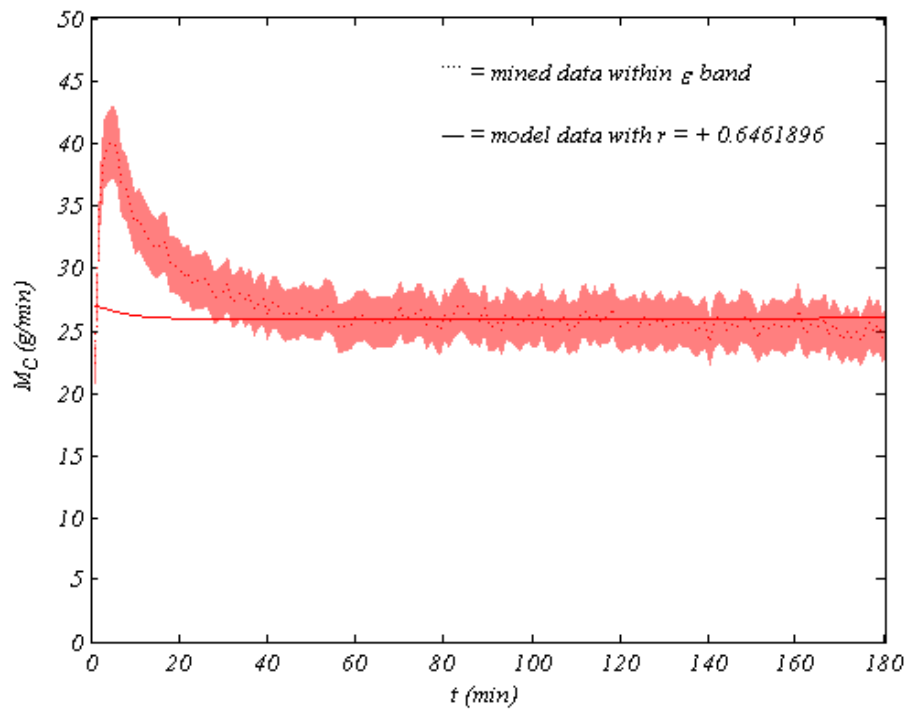
Figure 125. Fresh water production rate at 80°C flash and higher flow

138

7.9 System Capacity

The total amount of fresh water produced is calculated by numerically integrating the dynamic fresh water production rate over the entire operating period as was revealed in CHAPTER 4. Fresh water production amount was rising for both seawater flow rates; moreover, it was generally higher for lower seawater flow rates. The difference between fresh water production amounts of both seawater flow rates is more obvious at medium flash temperatures and diminishes at both low and high flash temperatures corresponding to the fresh water production rate results. The fresh water production amount increased with flash temperatures for both seawater flow rates in line with the fresh water production rate results due to enhanced evaporation rates at higher flash temperatures according to thermodynamic phase equilibria resulting in more fresh water production.

The profile of fresh water production amount is not exactly linear, as it was rising at a higher rate at first due to the high initial fresh water production rate, as seen earlier for both seawater flow rates. Fresh water production amount profiles for both seawater flow rates are similar; however, they were higher for lower seawater flow rates due to higher fresh water production rates, as seen earlier.

Model prediction of fresh water production amount properly resembled the pseudo–experimental results due to accurate portrayal of fresh water production rate as a result of adequate prediction of system vacuum and equilibrium temperature mentioned earlier; furthermore, adjusted parameters played a significant role in shifting the fresh water production rate profile to match pseudo–experimental results, resulting in good estimates of fresh water production amount. Fresh water production amount profiles are shown in Figure 126 through Figure 137.
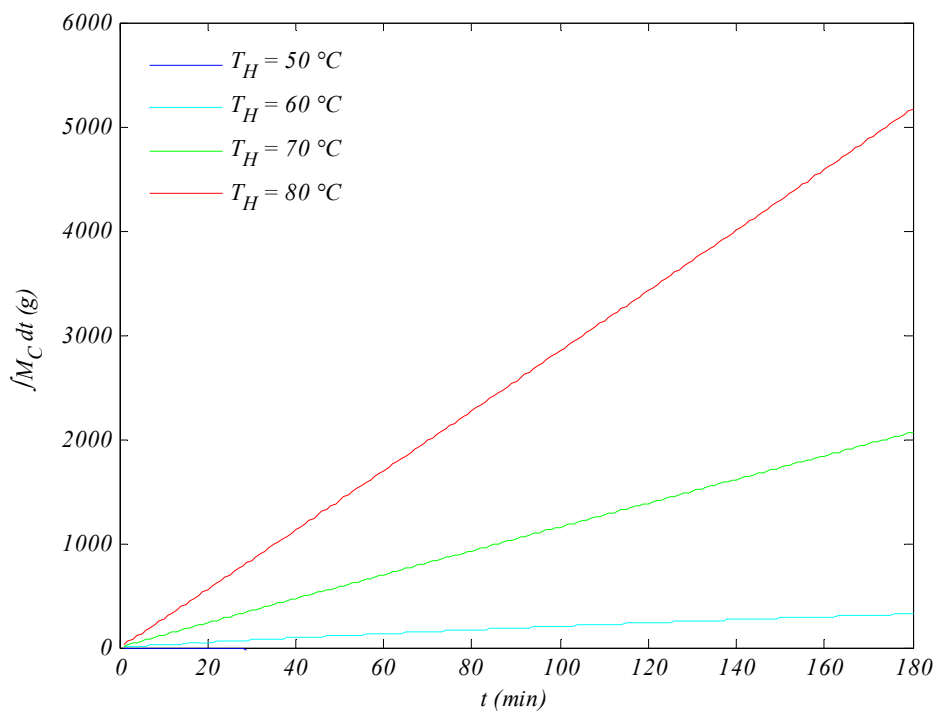
Figure 126. Modeled fresh water production amount profiles at lower flow
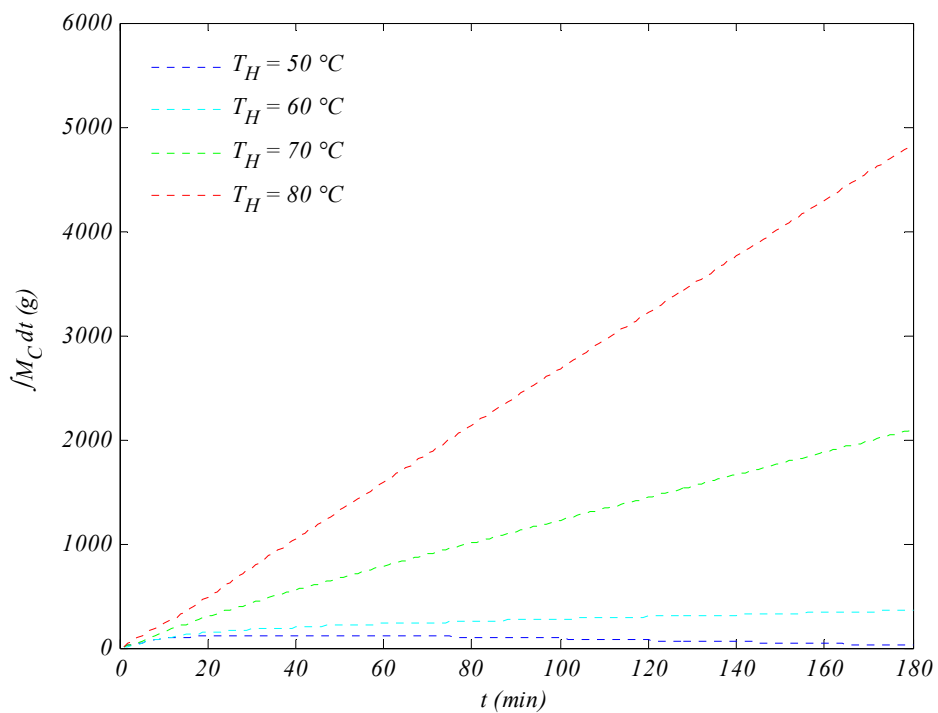
Figure 127. Mined fresh water production amount profiles at lower flow
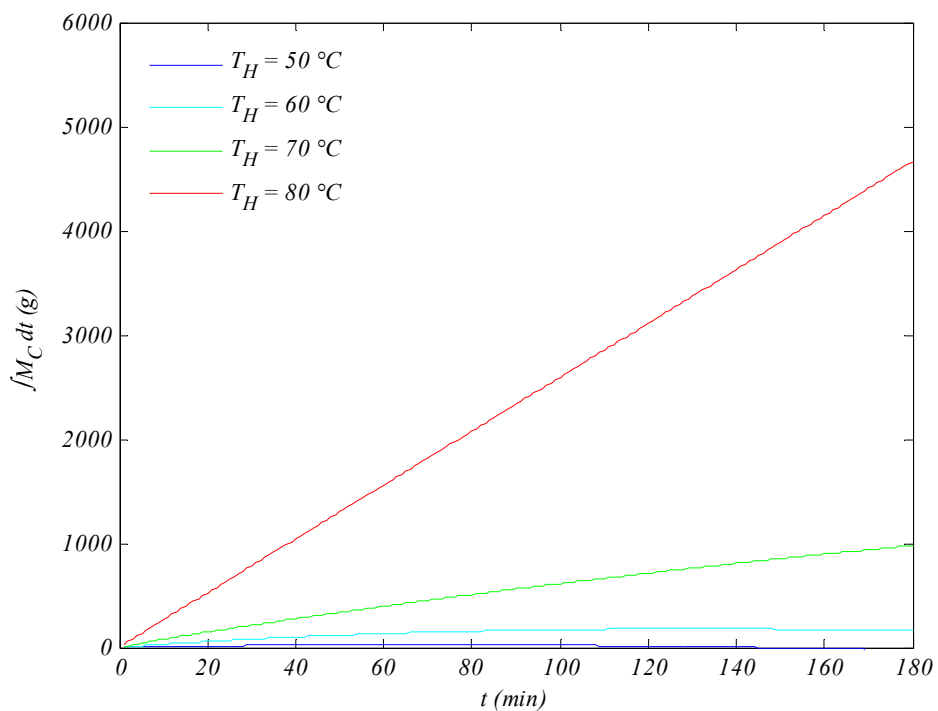
Figure 128. Modeled fresh water production amount profiles at higher flow
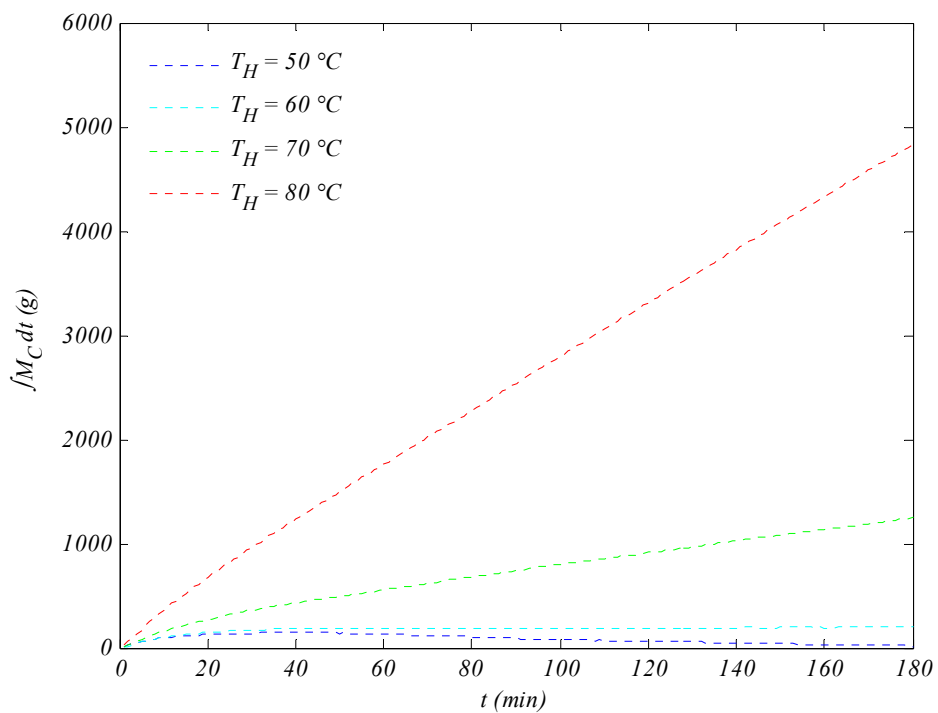
Figure 129. Mined fresh water production amount profiles at higher flow
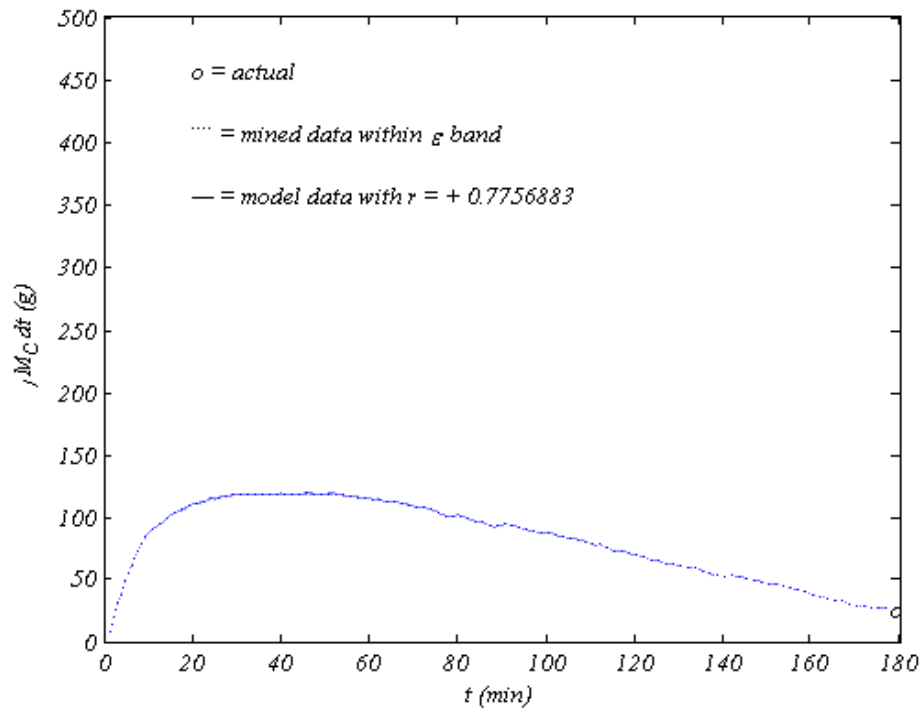
Figure 130. Fresh water production amount at 50°C flash and lower flow
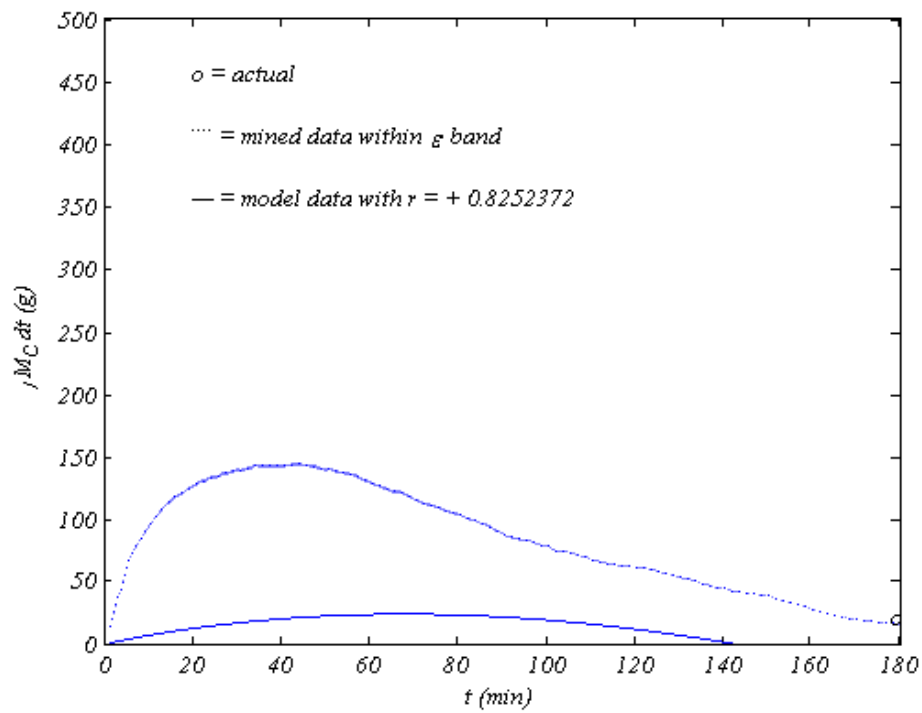
Figure 131. Fresh water production amount at 50°C flash and higher flow

142
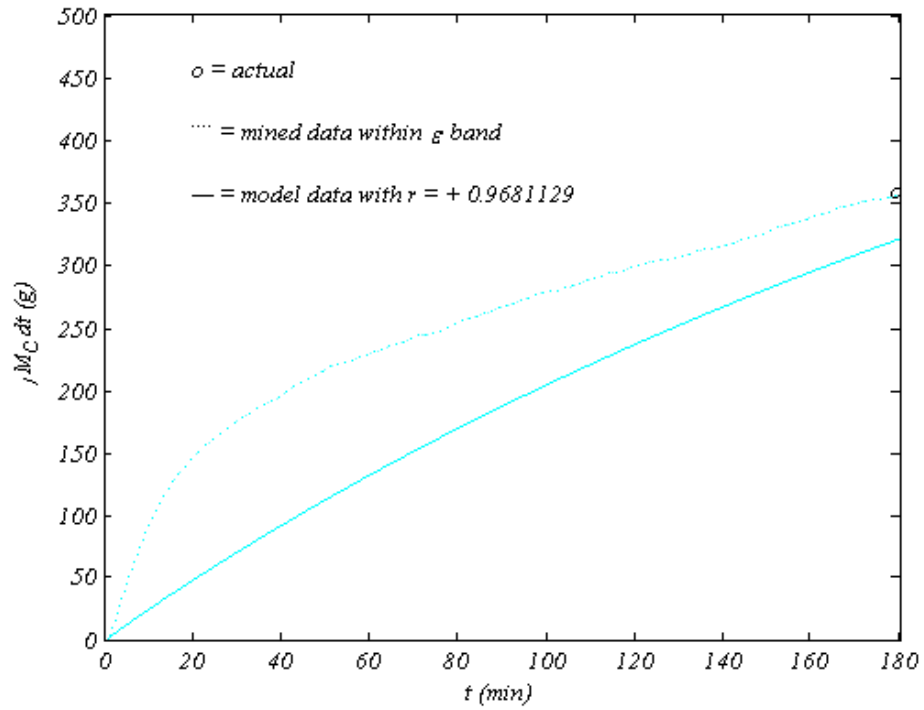
Figure 132. Fresh water production amount at 60°C flash and lower flow
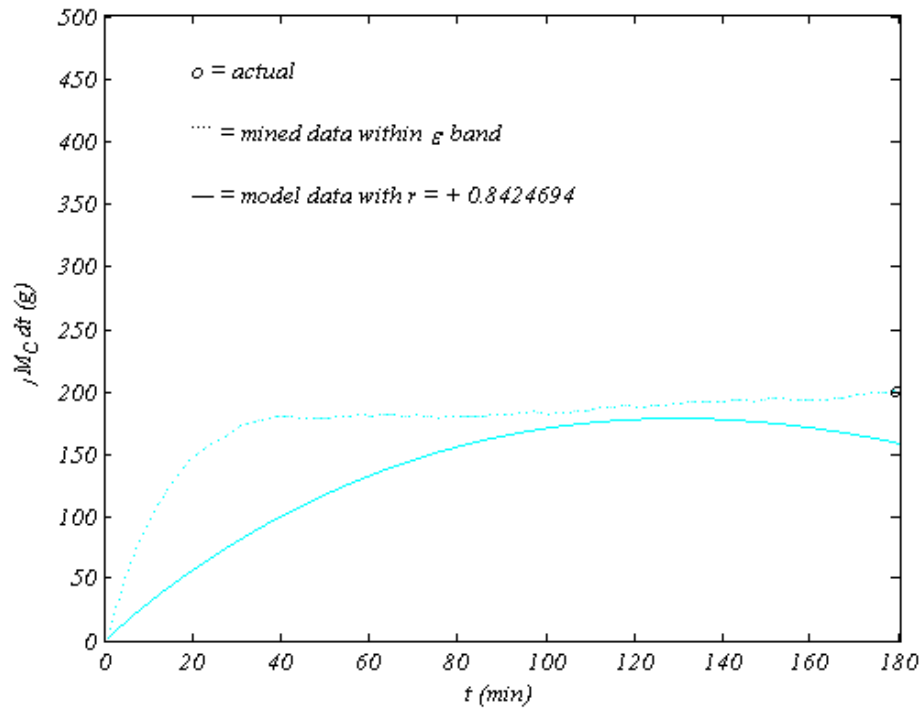
Figure 133. Fresh water production amount at 60°C flash and higher flow

143
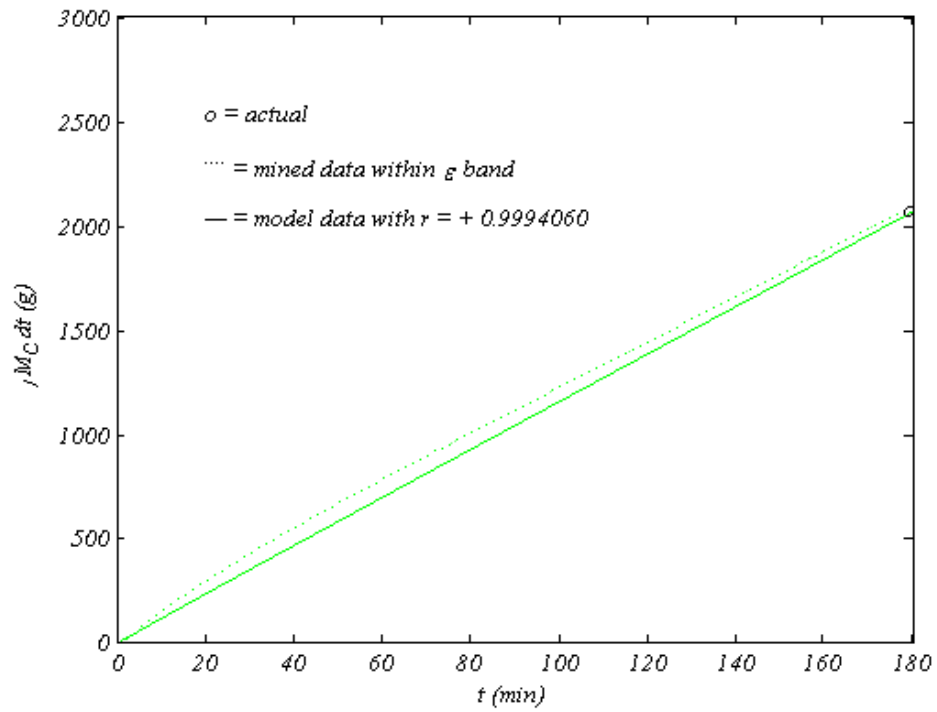
Figure 134. Fresh water production amount at 70°C flash and lower flow
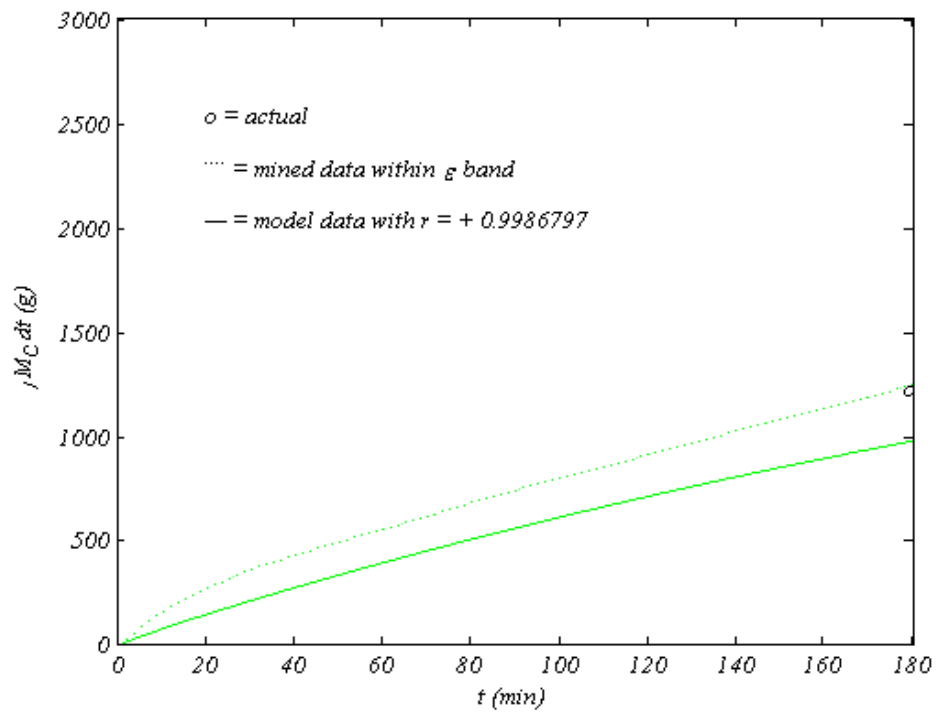
Figure 135. Fresh water production amount at 70°C flash and higher flow

144
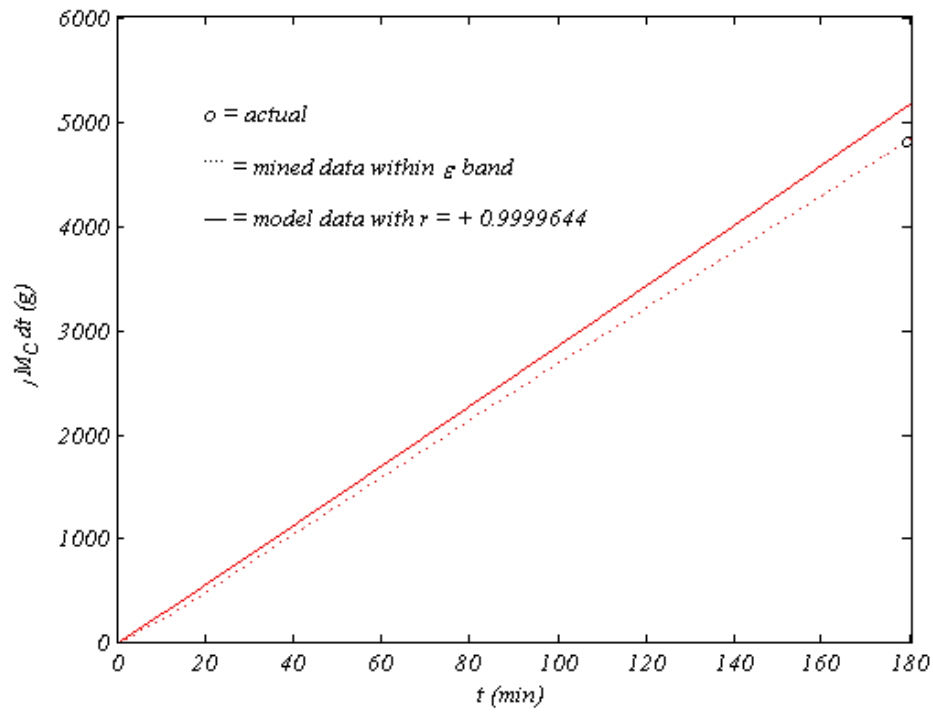
Figure 136. Fresh water production amount at 80°C flash and lower flow
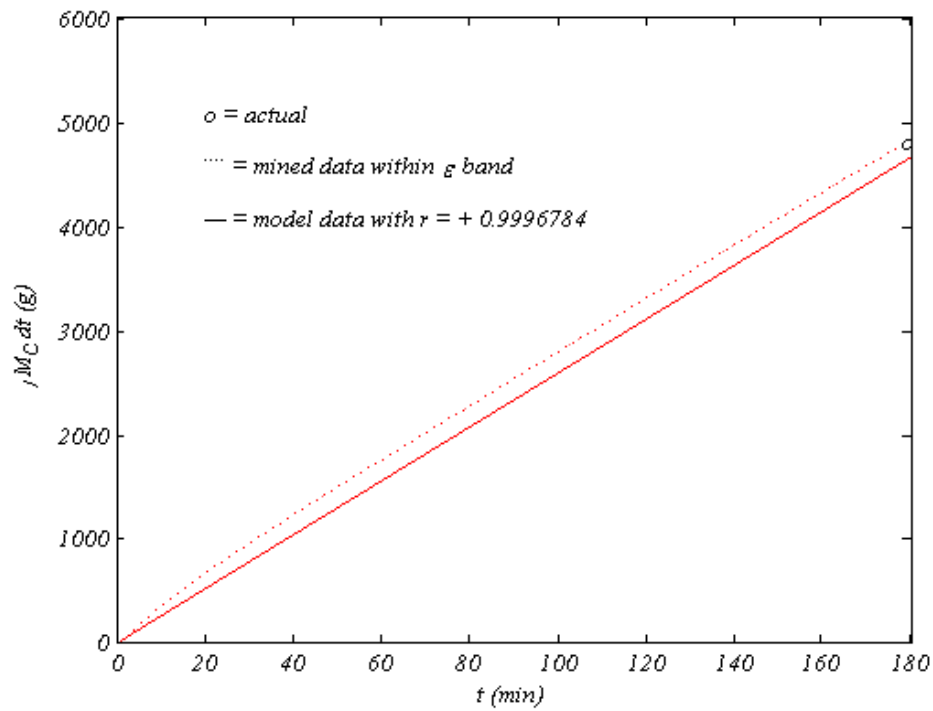
Figure 137. Fresh water production amount at 80°C flash and higher flow

145

7.10 Process Feasibility

Feasibility of the proposed desalination system can be evaluated using its resulting prime energy consumption, defined as the ratio of the total amount of energy exhausted to total amount of fresh water produced, as mentioned in CHAPTER 4. Energy consumed is attributed to heat provided by the heater plus work supplied by the pump. The pumping work of the proposed desalination system was insignificant relative to the heater load whether the flow rate of seawater was controlled with a throttling valve or a variable–frequency drive; hence, the presented prime energy consumption computations ignore the pumping work, that is $PEC \approx \int Q_H \, dt \, / \int M_C \, dt$. No economic analysis was performed in this venture, but the optimization process of the proposed desalination system lies within minimizing the prime energy consumption via maximizing production and minimizing heater load.

Prime energy consumption steadily increased for both seawater flow rates; however, it was higher at higher seawater flow rates due to higher heater loads. It declined rapidly with flash temperature due to the increasing fresh water production and decreasing heater load due to the improved heat recovery caused by the increased condensation associated with higher flash temperatures. In addition; the difference between prime energy consumption experienced at both seawater flow rates was more significant at low flash temperatures and diminished at higher flash temperatures.

Model prediction of prime energy consumption deteriorated with decreasing flash temperatures but improved with increasing flash temperatures due to contrasting effects of poor heater load prediction and good production amount prediction. Prime energy consumption profiles are shown in Figure 138 through Figure 149.
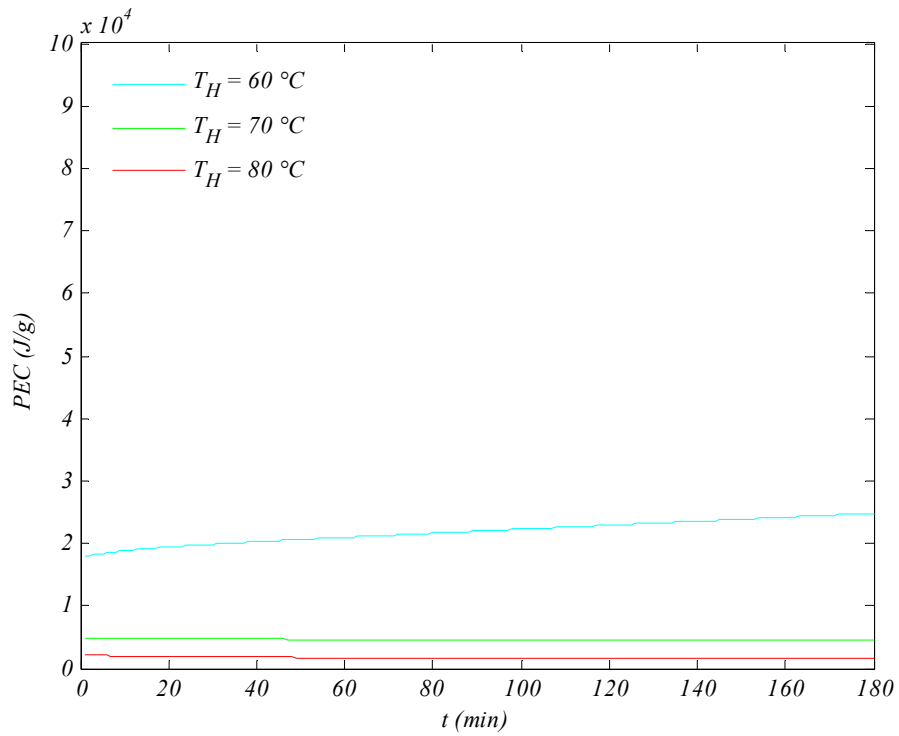
Figure 138. Modeled prime energy consumption profiles at lower flow
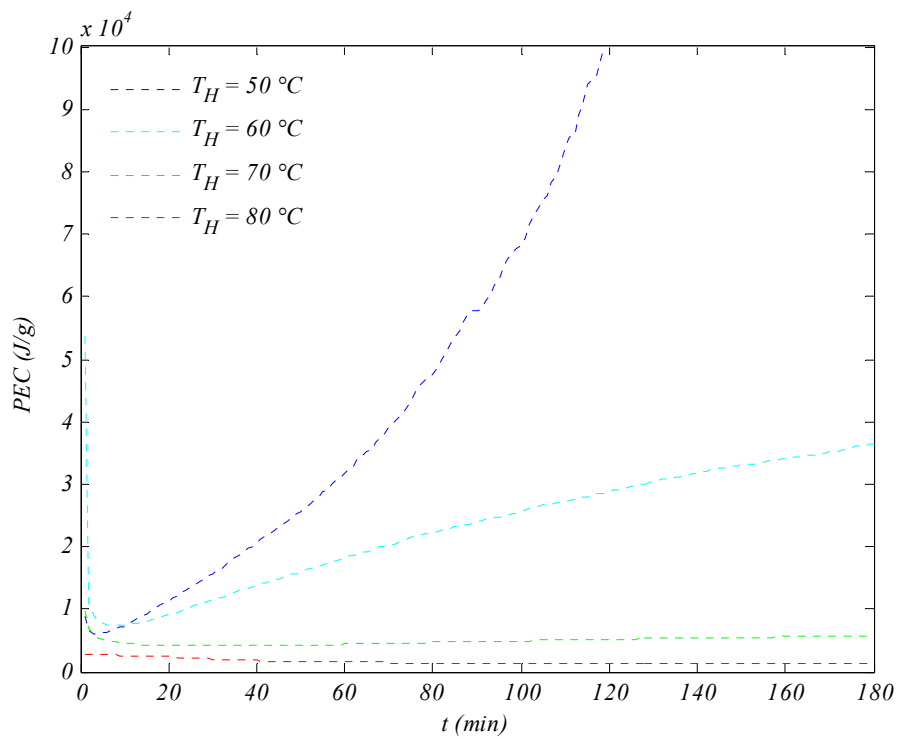
Figure 139. Mined prime energy consumption profiles at lower flow

147
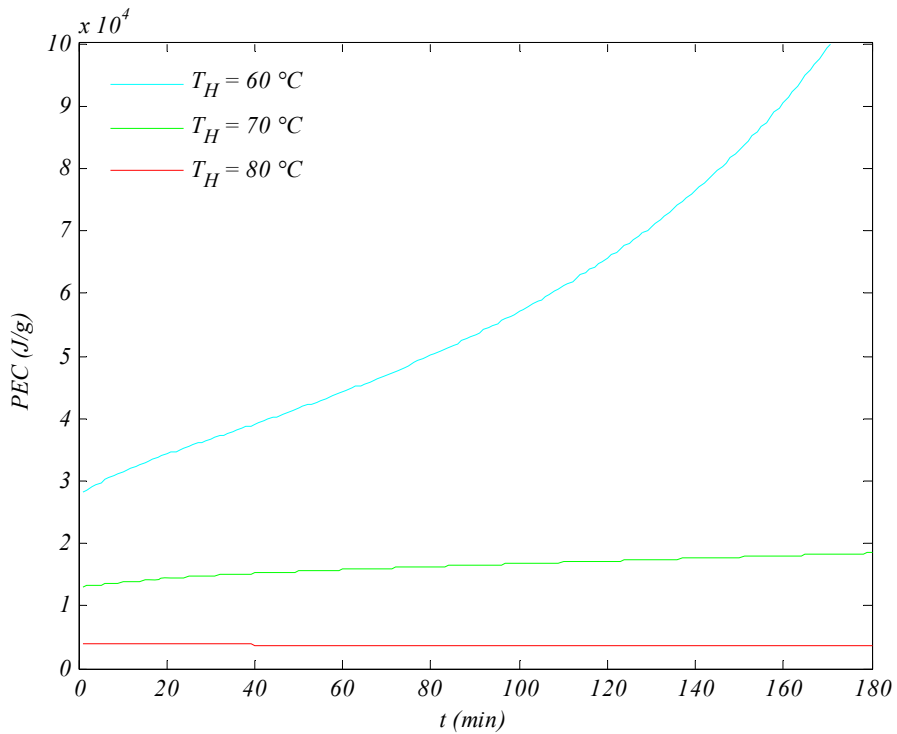
Figure 140. Modeled prime energy consumption profiles at higher flow
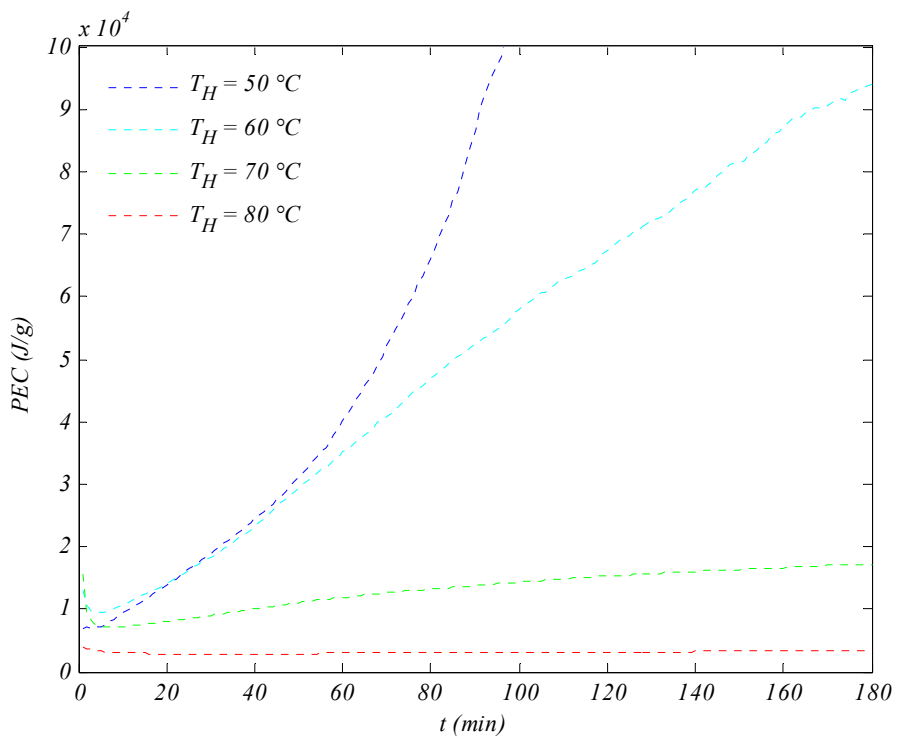
Figure 141. Mined prime energy consumption profiles at higher flow

148
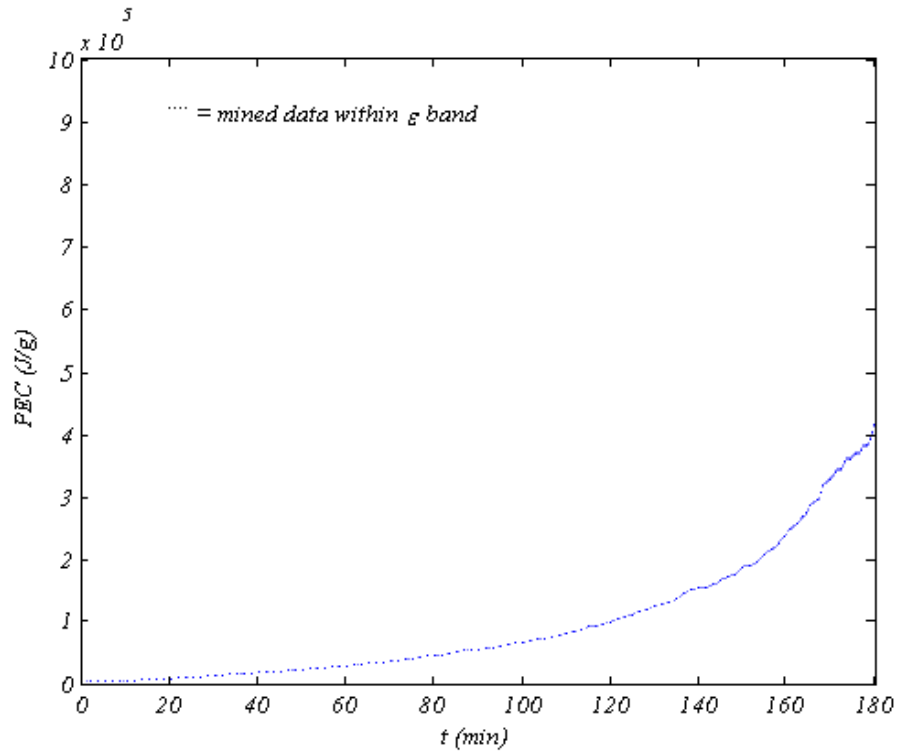
Figure 142. Prime energy consumption at 50°C flash and lower flow
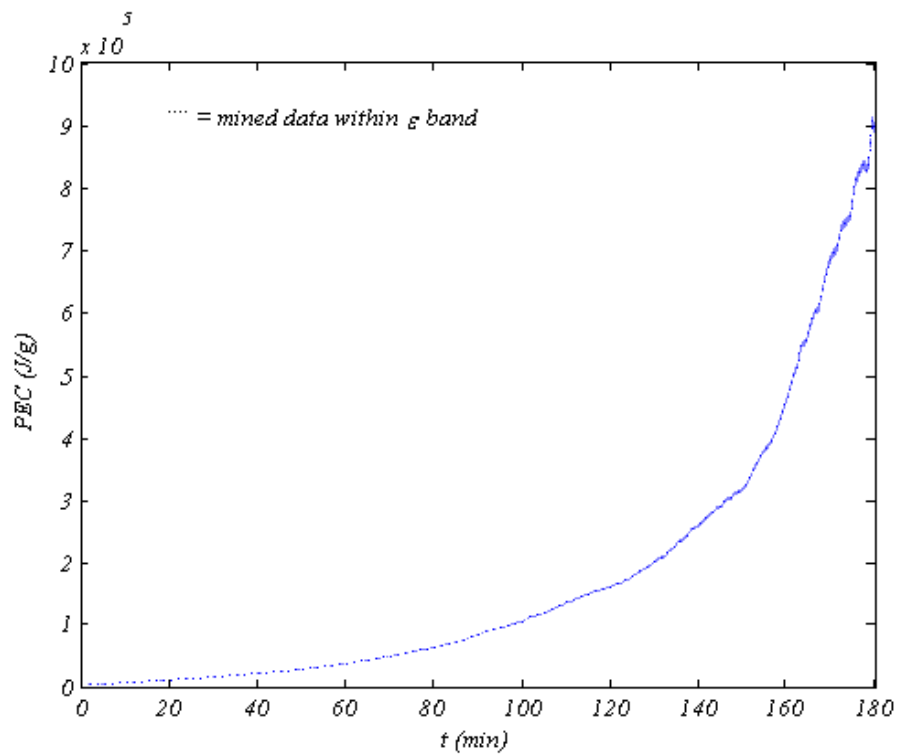
Figure 143. Prime energy consumption at 50°C flash and higher flow
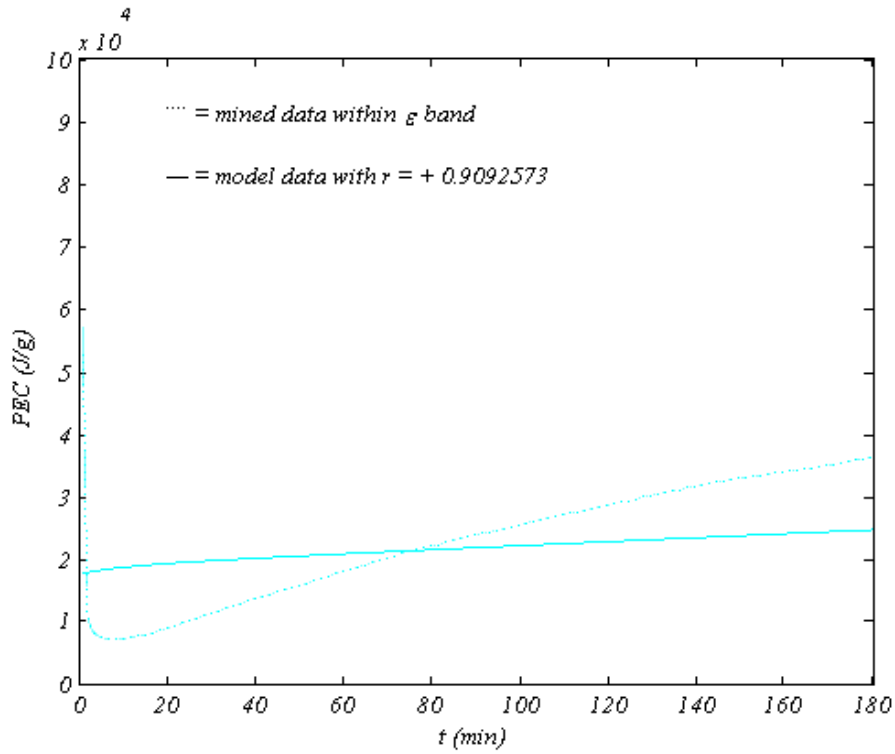
Figure 144. Prime energy consumption at 60°C flash and lower flow
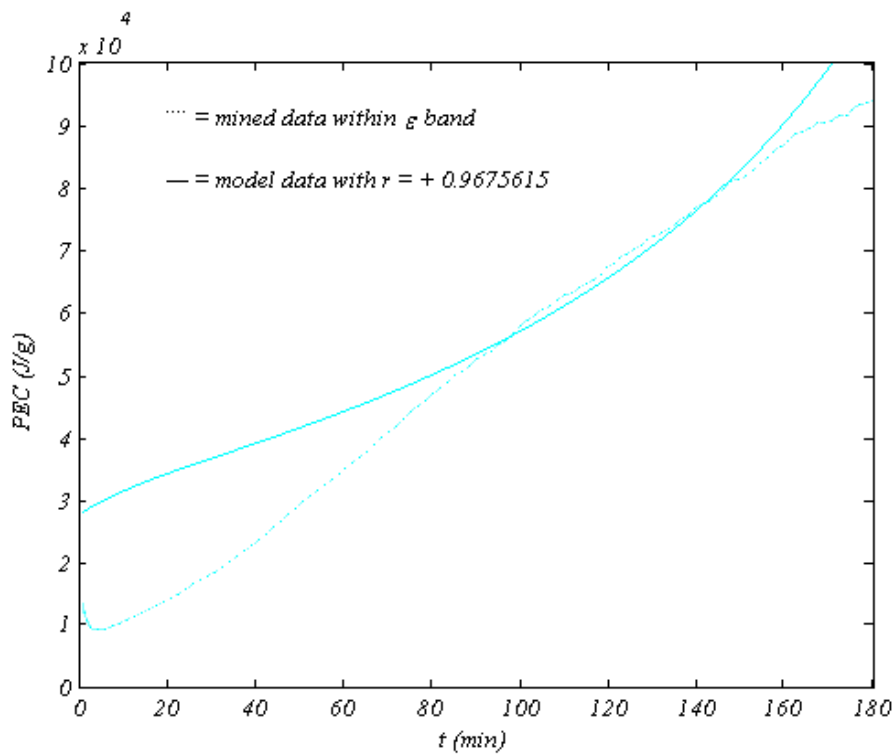
Figure 145. Prime energy consumption at 60°C flash and higher flow

150
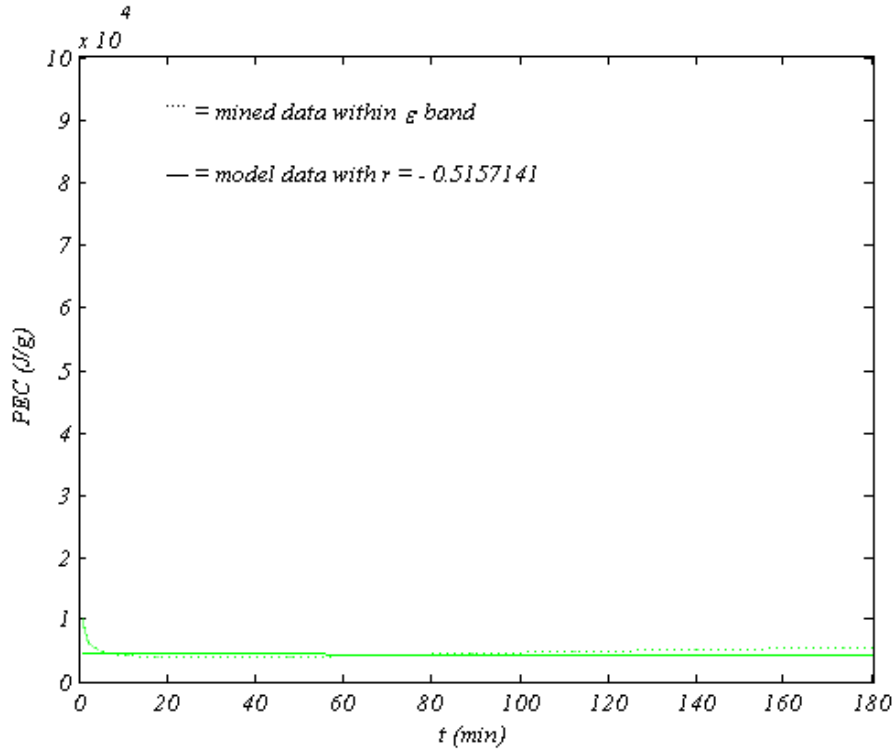
Figure 146. Prime energy consumption at 70°C flash and lower flow
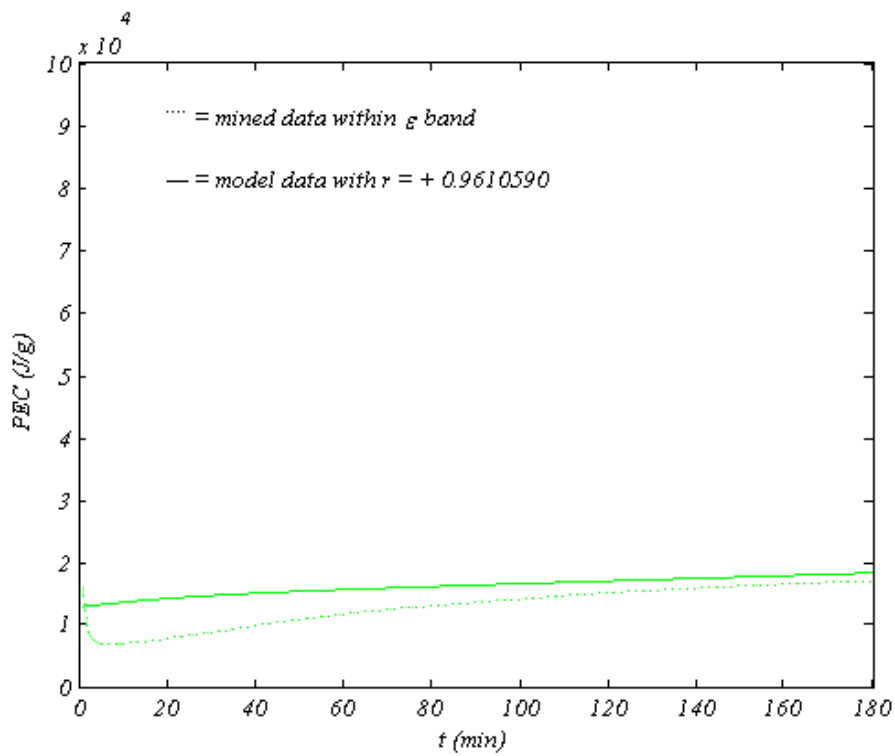
Figure 147. Prime energy consumption at 70°C flash and higher flow

151
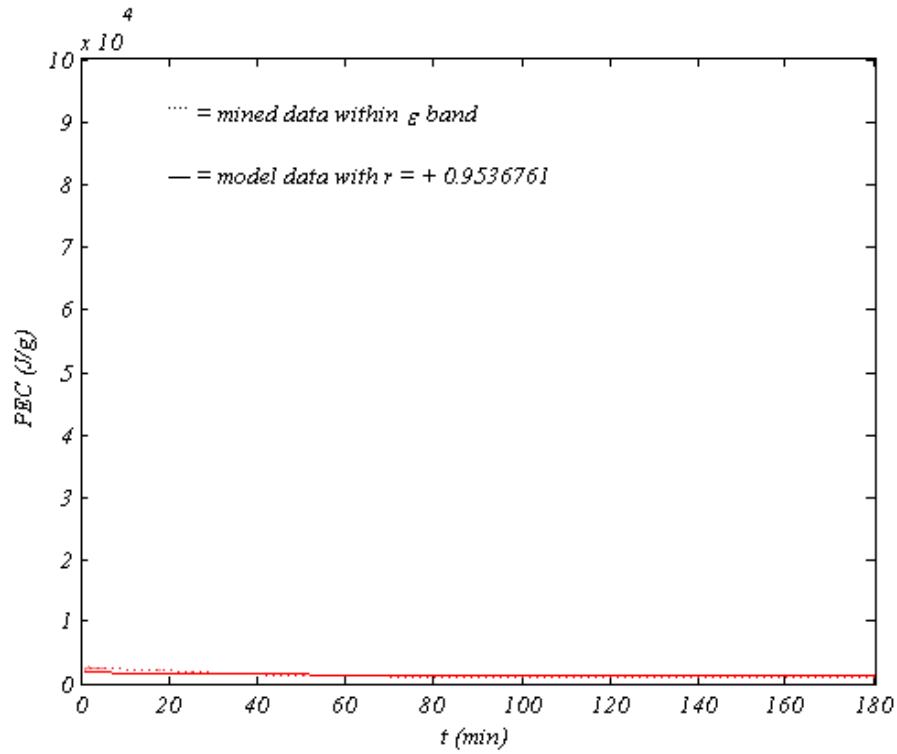
Figure 148. Prime energy consumption at 80°C flash and lower flow
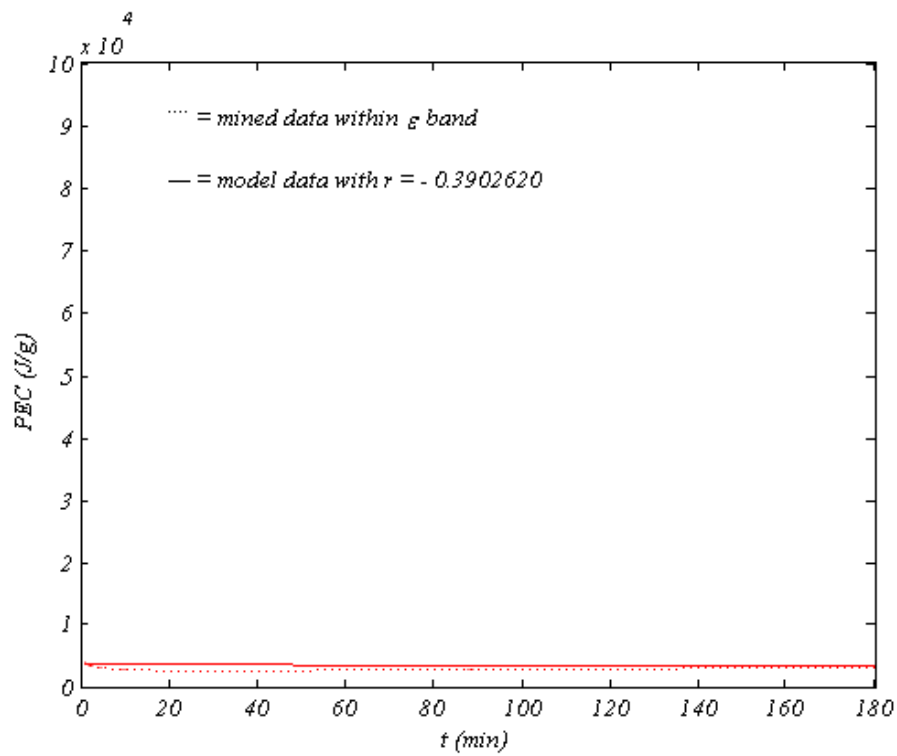
Figure 149. Prime energy consumption at 80°C flash and higher flow

7.11 Condensing Efficiency

Condenser efficiency describes its heat transfer effectiveness and is defined as the ratio of the temperature gradient on the cold tube side to the temperature gradient on the hot shell side written as a percentage, that is $\eta_C = [\ (\ T_X - T_P \ ) \ / \ (\ T_E - T_C \ ) \ ] \cdot 100 \ \%$, as was mentioned in CHAPTER 4. Condenser efficiency rapidly increased to reach a maximum early before it slowly declined for both seawater flow rates; however, condenser efficiency attained at lower seawater flow rates was higher. The condenser efficiency increased with flash temperatures for both seawater flow rates, since the preheat temperature is directly proportional to the flashing temperature.

The condenser efficiency indirectly conveys the percent of available heat that was utilized for preheating seawater. It rapidly increased because of the rapidly rising preheat temperature due to the high initial rate of vaporization caused by rapidly increasing equilibrium temperature at lower vacuum pressures, then it slowly declined because of the decreasing preheat temperature due to the decreasing rate of vaporization caused by stabilizing equilibrium temperature at rising vacuum pressures for both seawater flow rates. The condenser efficiency profiles for both seawater flow rates are similar; however, they are higher for lower flow rates because of the higher preheat temperature experienced at lower seawater flow rates due to more condensation caused by more vaporization as seen before.

Model prediction of condenser efficiency loosely resembled experimental results because of the loose depiction of the preheat temperature due to the inability of the condenser tube heat transfer module of the model to capture the rate of condensation. Condenser efficiency profiles are shown in Figure 150 through Figure 161.
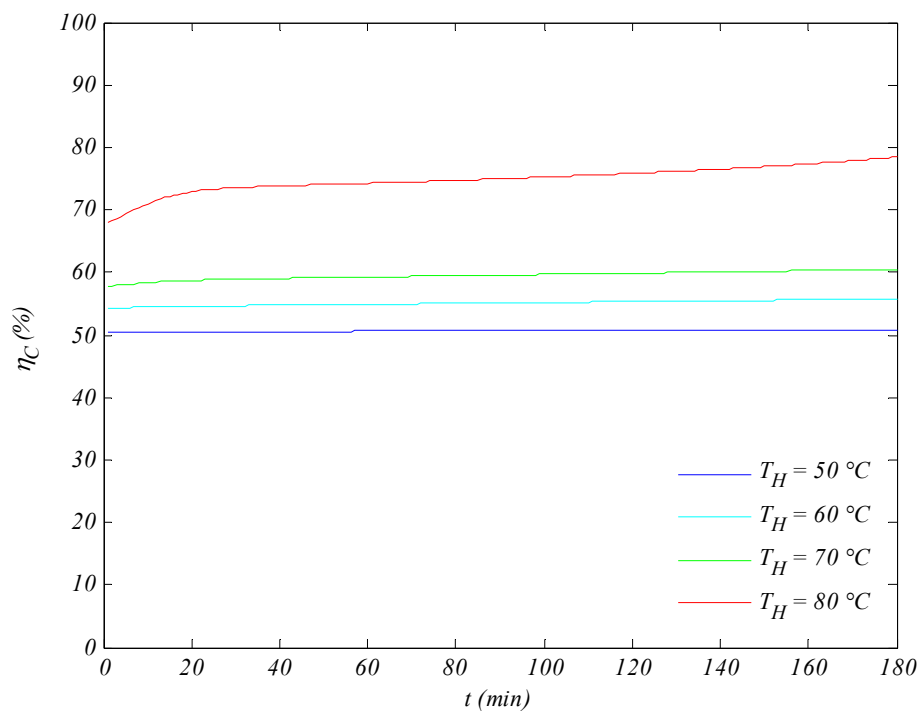
Figure 150. Modeled condenser efficiency profiles at lower flow
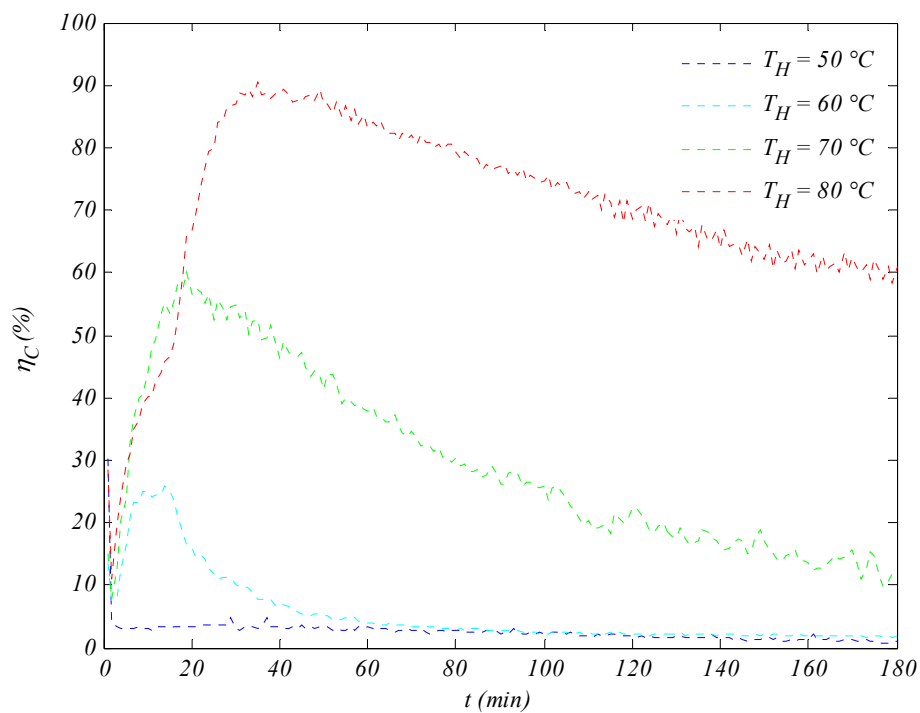
Figure 151. Experimental condenser efficiency profiles at lower flow

154
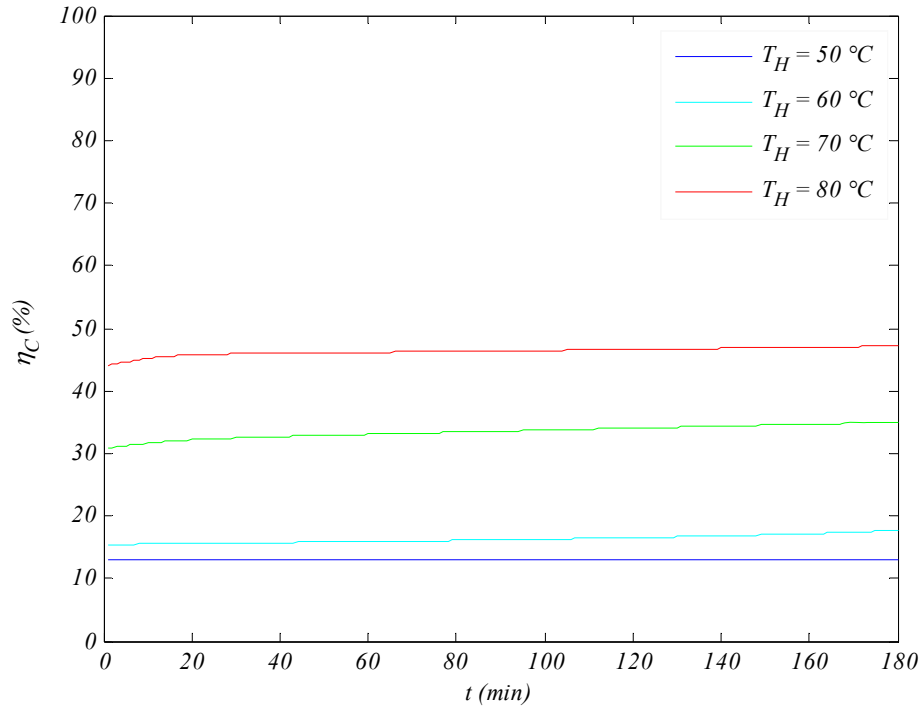
Figure 152. Modeled condenser efficiency profiles at higher flow
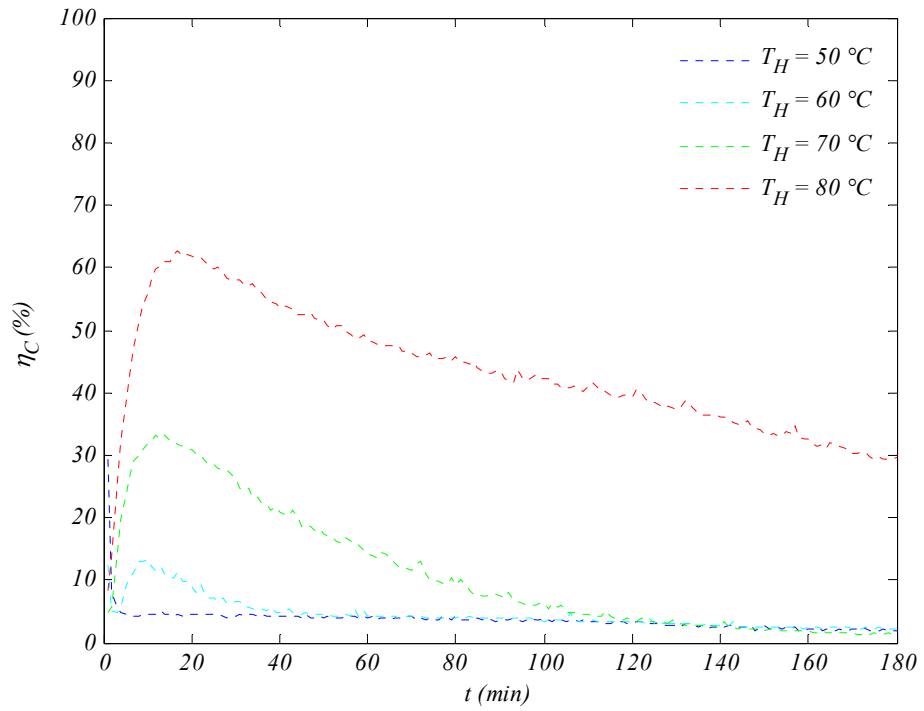
Figure 153. Experimental condenser efficiency profiles at higher flow
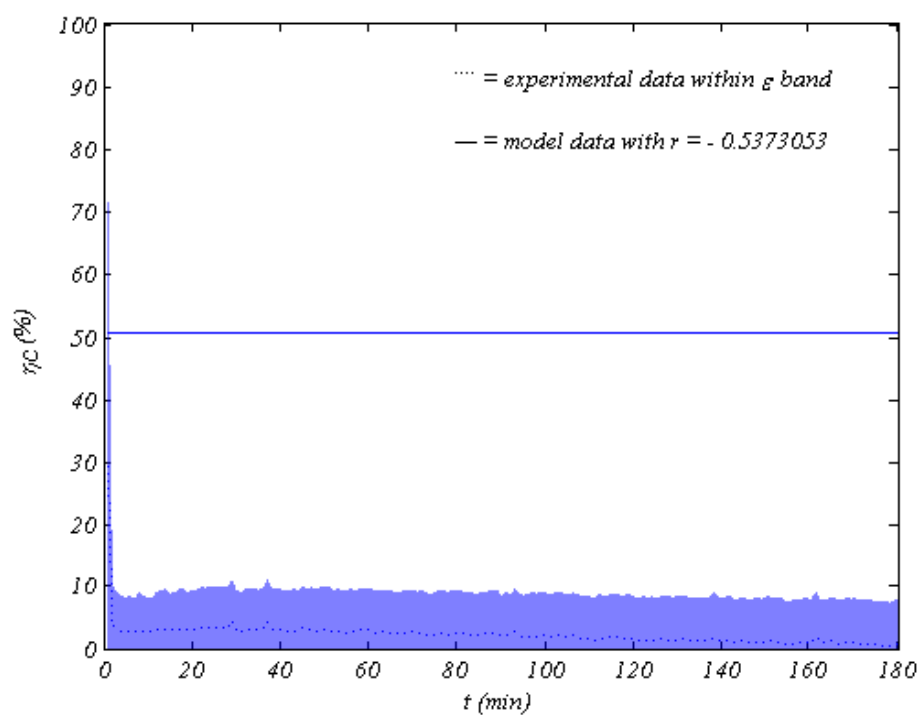
Figure 154. Condenser efficiency at 50°C flash and lower flow
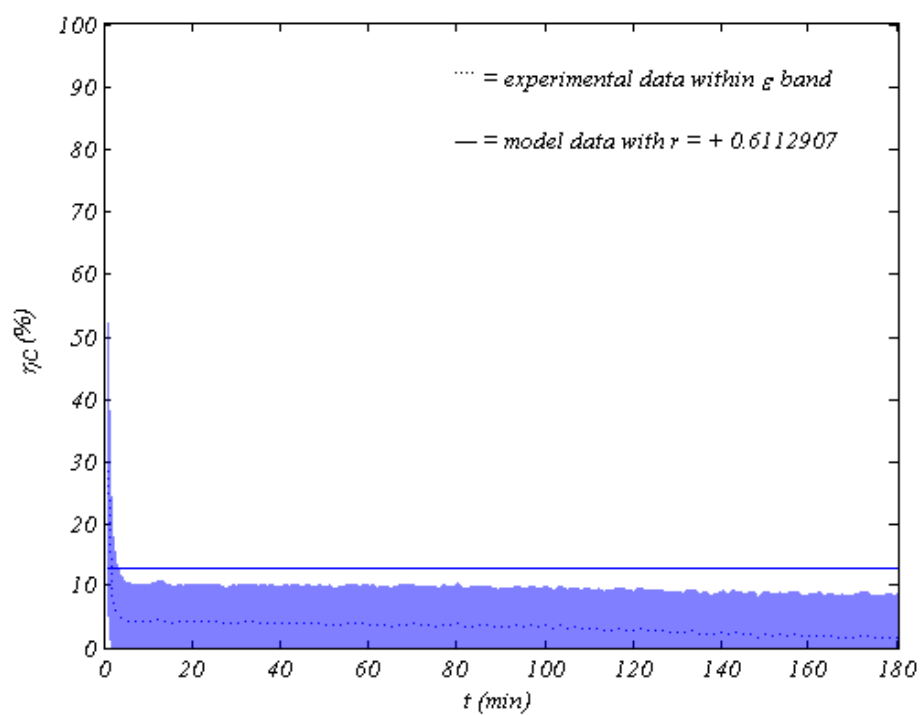
Figure 155. Condenser efficiency at 50°C flash and higher flow

156
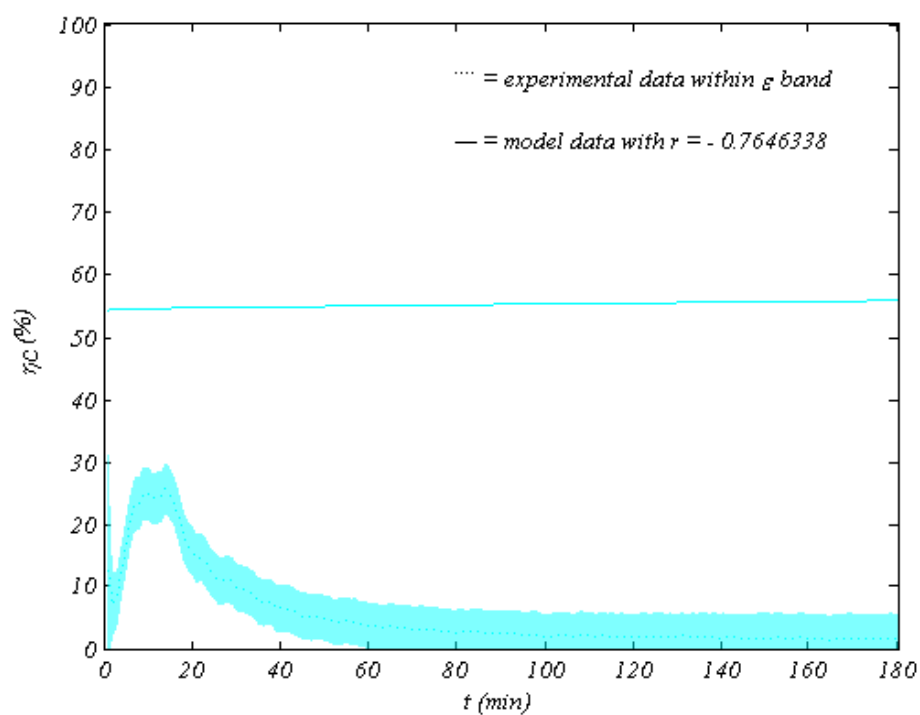
Figure 156. Condenser efficiency at 60°C flash and lower flow
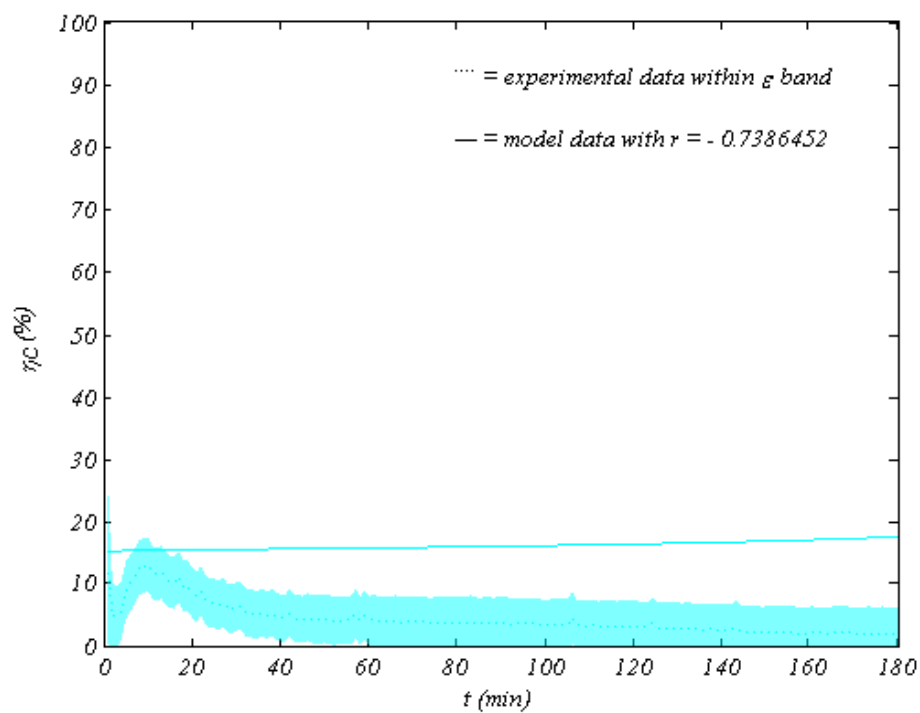
Figure 157. Condenser efficiency at 60°C flash and higher flow

157
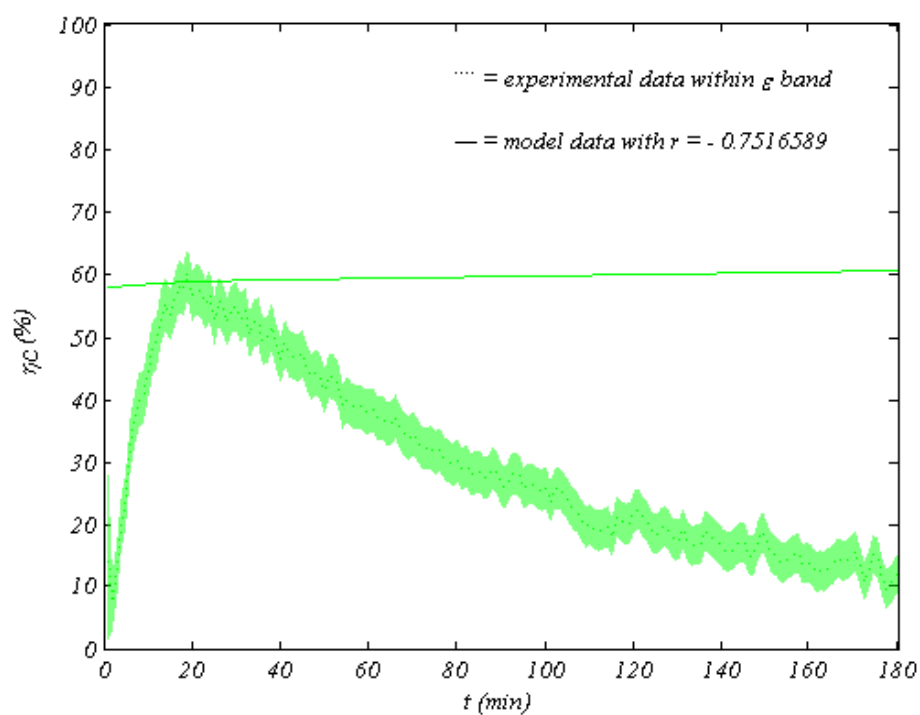
Figure 158. Condenser efficiency at 70°C flash and lower flow
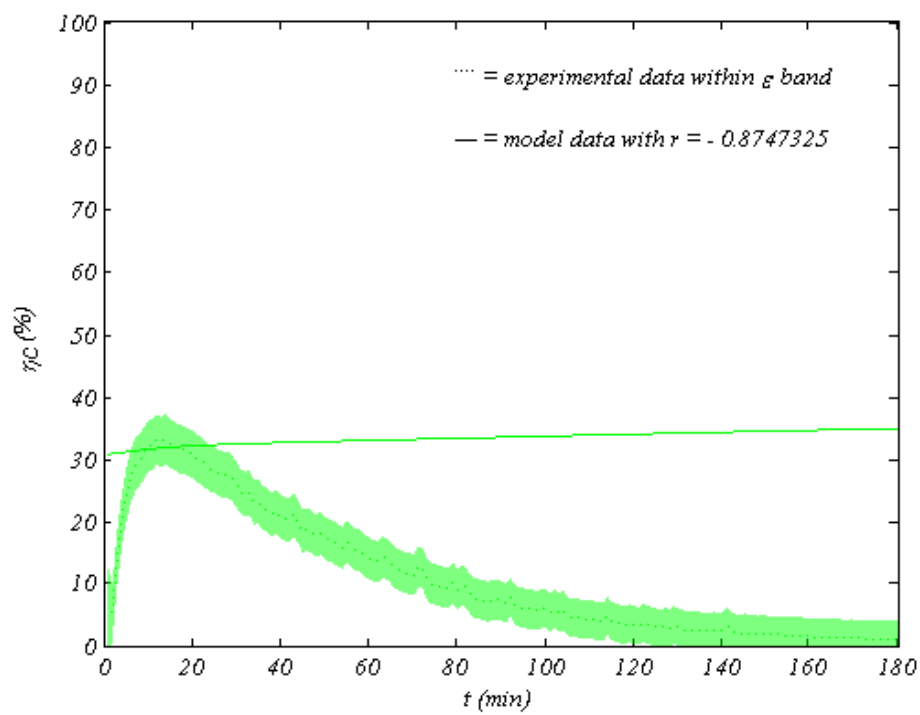
Figure 159. Condenser efficiency at 70°C flash and higher flow
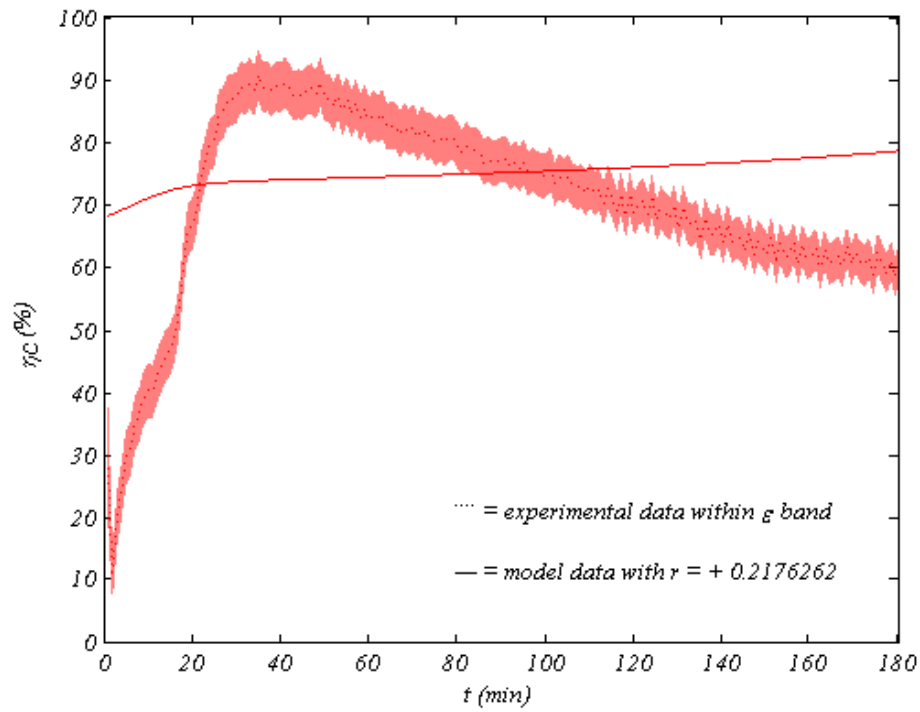
Figure 160. Condenser efficiency at 80°C flash and lower flow
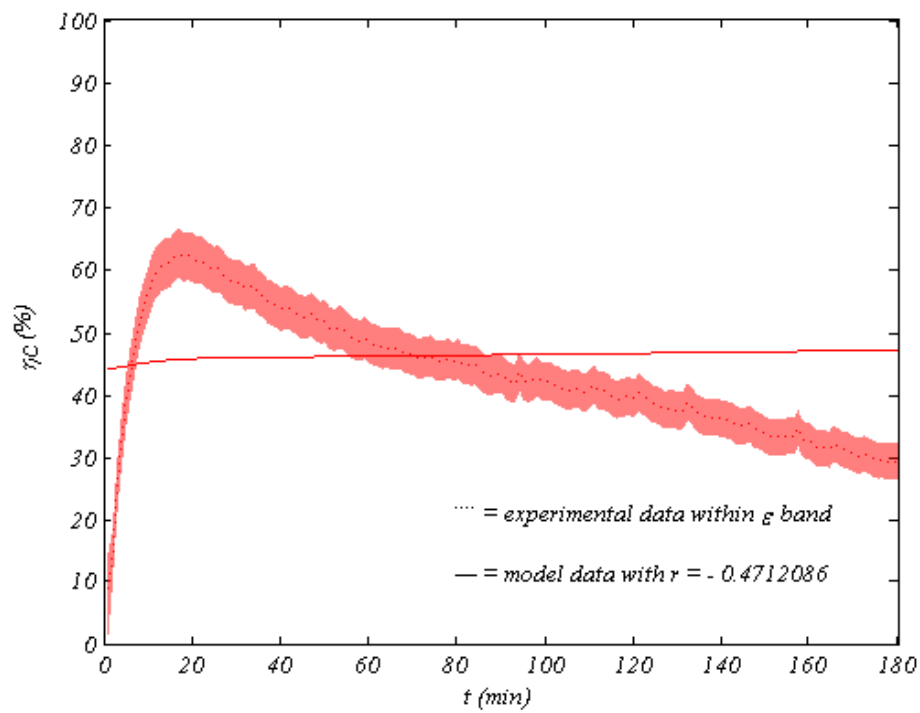
Figure 161. Condenser efficiency at 80°C flash and higher flow

159

7.12 Recovery Efficiency

Recovery efficiency is defined as the ratio of seawater enthalpy change due to condensing water vapor to the overall enthalpy change required to attain the set flash temperature written as a percentage, that is $\eta_R = [(H_X - H_S) / (H_H - H_S)] \cdot 100\ \%$, as was mentioned in CHAPTER 4. In other words, it is the percent of total enthalpy change that was essentially accomplished by reclaiming heat from condensing vapor. Recovery efficiency rapidly increased to reach a maximum early before it slowly declined for both seawater flow rates; however, recovery efficiency was higher at lower seawater flow rates. It increased with flash temperatures for both seawater flow rates, since preheat enthalpy is directly proportional to preheat temperature that is directly proportional to flashing temperature as seen earlier.

Recovery efficiency directly expresses the percent of required heat that is reclaimed from condensing vapor. Recovery efficiency rapidly increased because of rapidly rising preheat enthalpy due to rapidly rising preheat temperature, then it slowly declined because of decreasing preheat enthalpy due to decreasing preheat temperature. Recovery efficiency profiles for both seawater flow rates are similar; however, they were higher for lower flow rates because of higher preheat enthalpy due to higher preheat temperature experienced at lower seawater flow rates due to more condensation caused by more vaporization.

Model prediction of recovery efficiency loosely resembled experimental results because of loose depiction of preheat temperature due to inability of the condenser tube heat transfer module of the model to capture the rate of condensation. Recovery efficiency profiles are shown in Figure 162 through Figure 173.
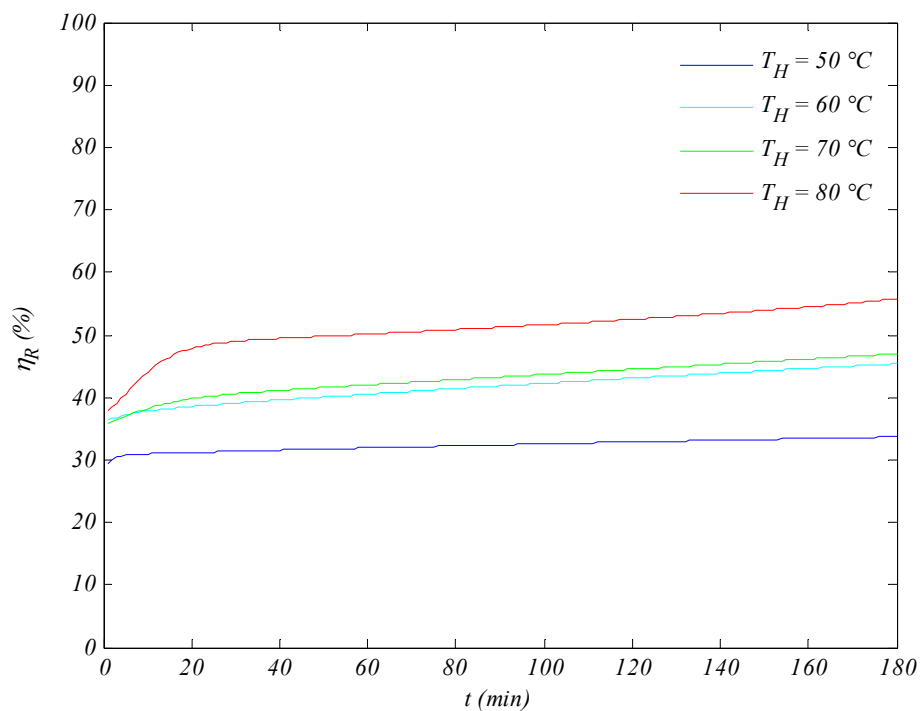
Figure 162. Modeled recovery efficiency profiles at lower flow
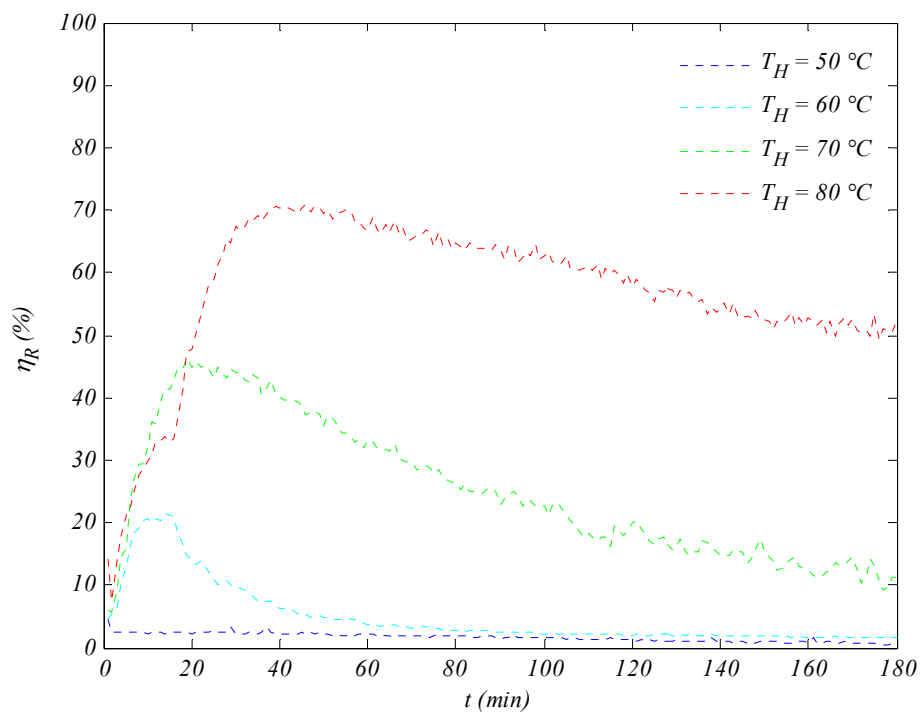
Figure 163. Experimental recovery efficiency profiles at lower flow
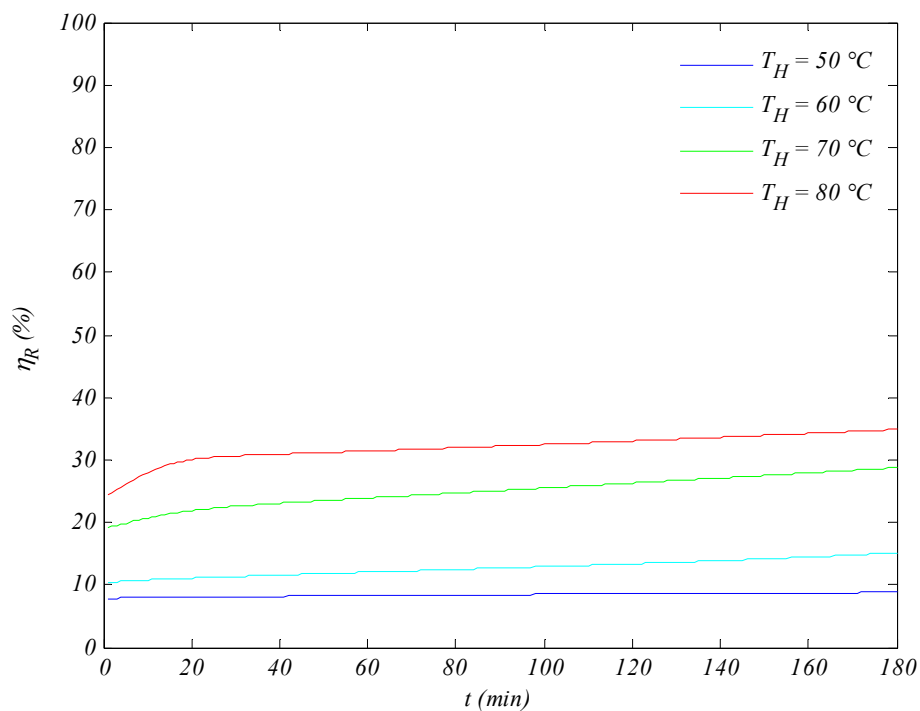
Figure 164. Modeled recovery efficiency profiles at higher flow
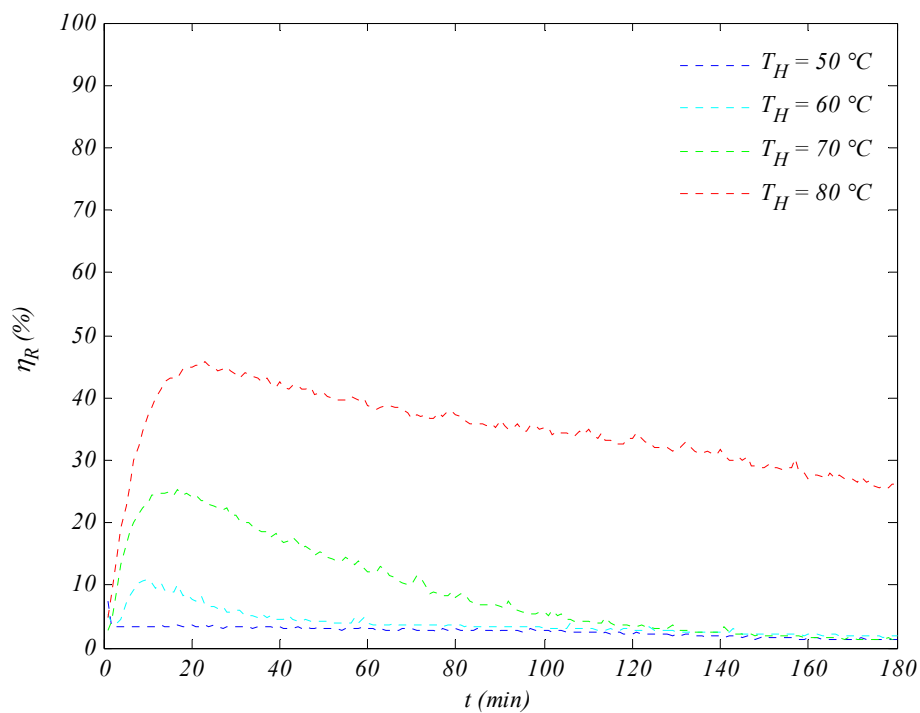
Figure 165. Experimental recovery efficiency profiles at higher flow
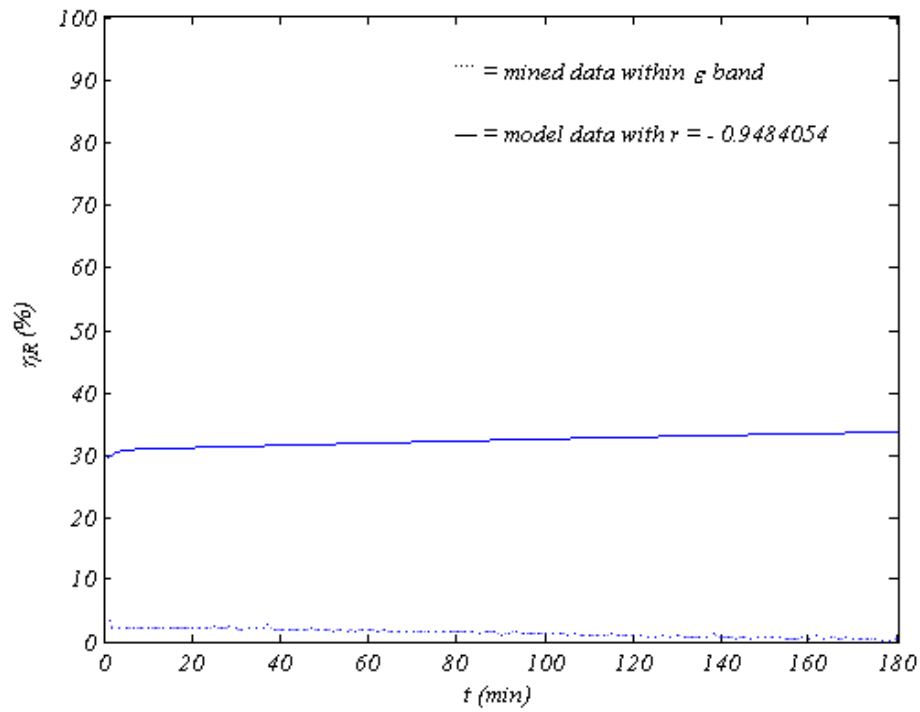
Figure 166. Recovery efficiency at 50°C flash and lower flow
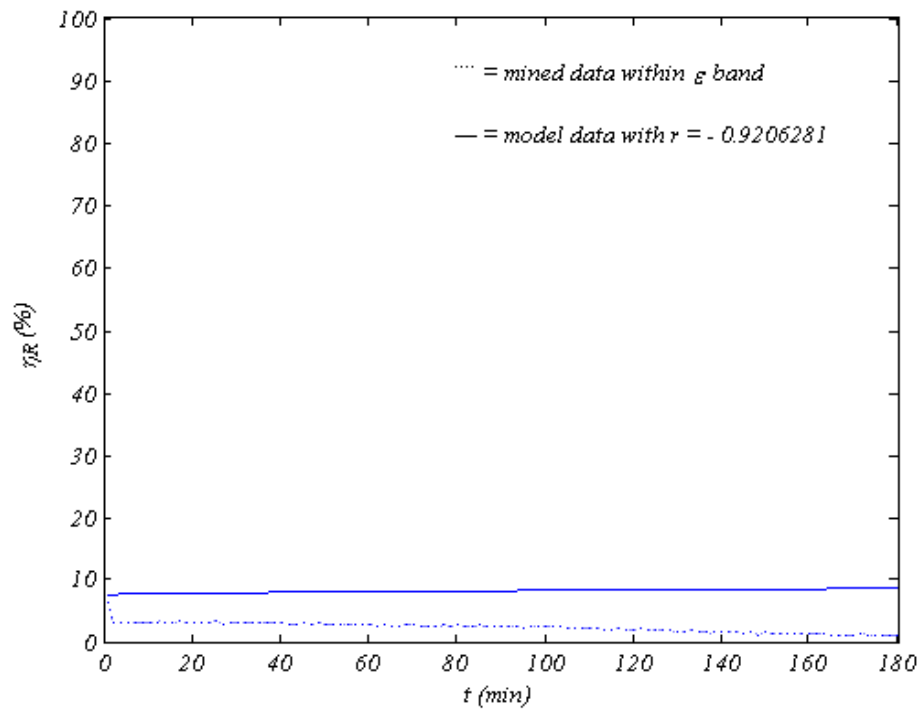
Figure 167. Recovery efficiency at 50°C flash and higher flow

163
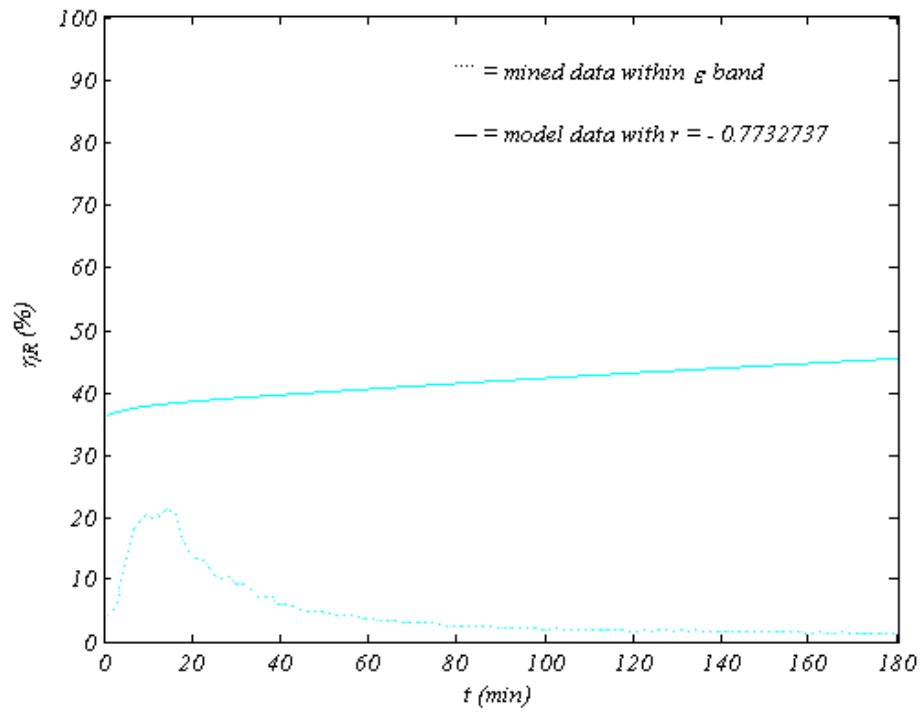
Figure 168. Recovery efficiency at 60°C flash and lower flow
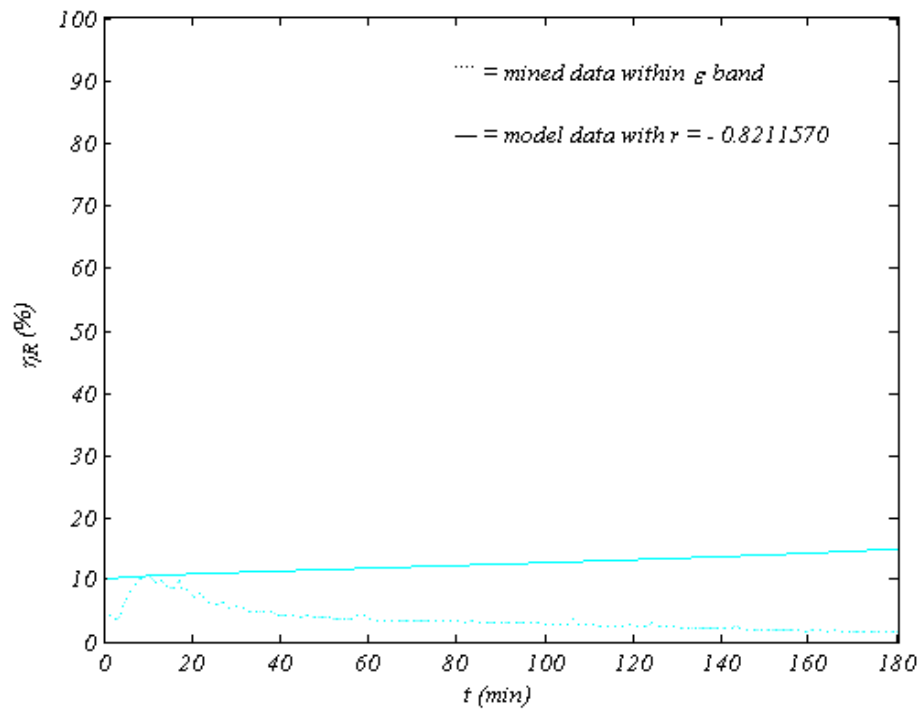
Figure 169. Recovery efficiency at 60°C flash and higher flow

164
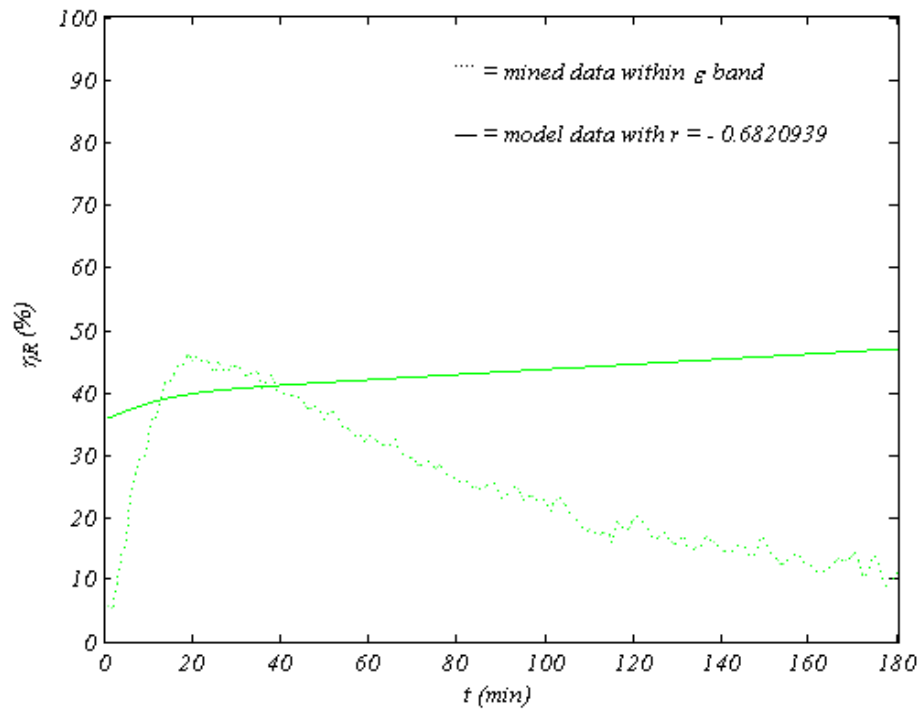
Figure 170. Recovery efficiency at 70°C flash and lower flow
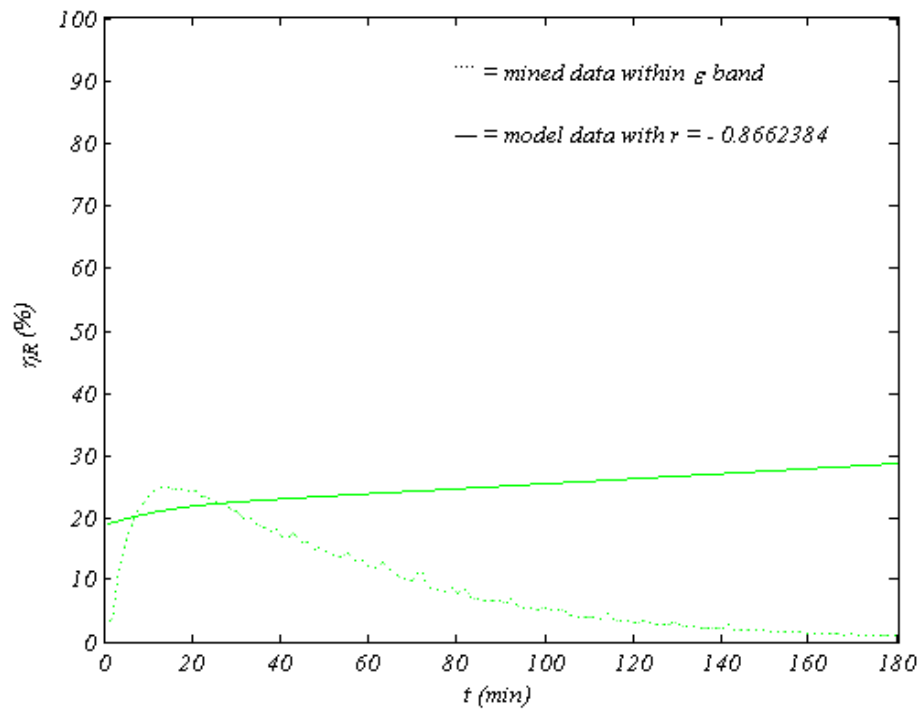
Figure 171. Recovery efficiency at 70°C flash and higher flow

165
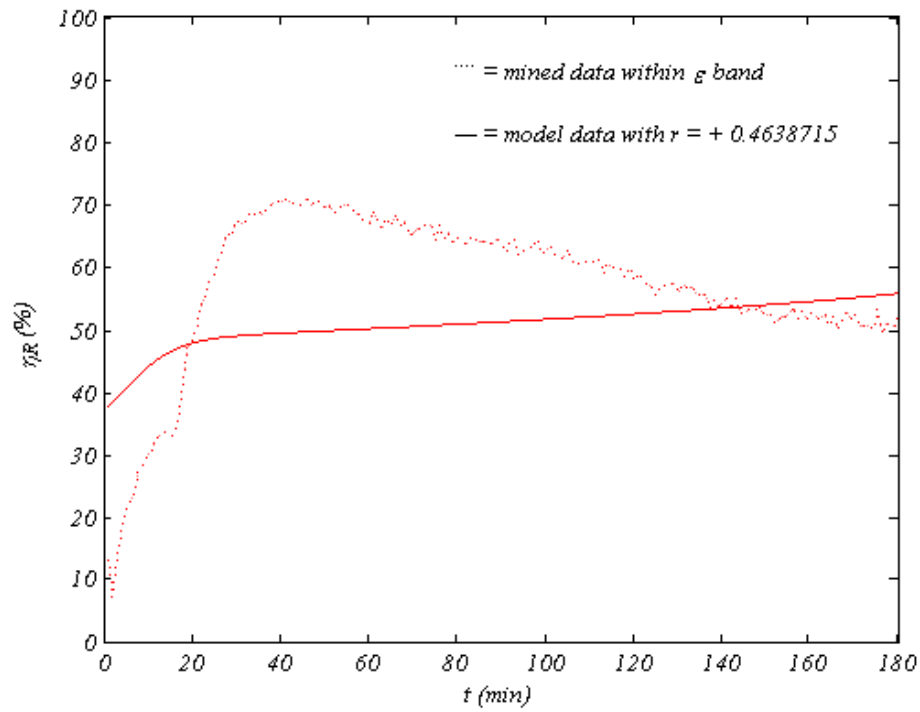
Figure 172. Recovery efficiency at 80°C flash and lower flow
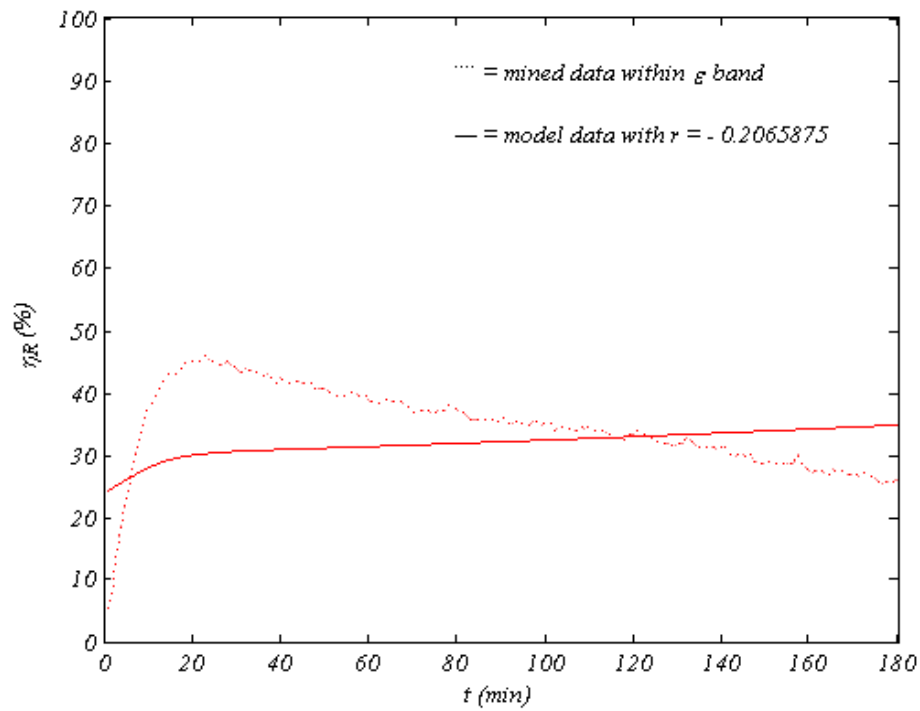
Figure 173. Recovery efficiency at 80°C flash and higher flow

166

7.13 Thermal Efficiency

Thermal efficiency of the desalination process is a performance measure defined as the ratio of heat used in vaporizing water to overall heat added to bulk seawater written as a percentage, that is $\eta_T = [\, M_E \cdot (\, H_E + H^L_E \,) \,/\, (\, M_H \cdot H_H \,) \,] \cdot 100\ \%$, as was mentioned in CHAPTER 4. In other words, it is the percent of total thermal energy supplied that was actually used to vaporize water. Thermal efficiency rapidly increased to reach a maximum early before it slowly declined, then stabilized for both seawater flow rates; however, thermal efficiency was higher at lower seawater flow rates. The thermal efficiency increased with flash temperatures for both seawater flow rates, since the amounts and the temperatures of the water vapor are directly proportional to the flashing temperature as seen earlier.

Thermal efficiency rapidly increased because of rapidly increasing water vapor enthalpy due to its rising amount and temperature, and then it slowly declined, reaching a plateau because of slowly stabilizing water vapor enthalpy due to gradually declining vaporization rates, but gradually rising temperatures, of the water vapor for both seawater flow rates. Thermal efficiency profiles for both seawater flow rates are similar; however, they were higher for lower flow rates due to higher vaporization rates.

Model prediction of thermal efficiency of the proposed desalination process properly resembled pseudo–experimental results due to accurate portrayal of water vaporization rates; furthermore, adjusted parameters and correlations played a significant role in shifting vaporization rate profiles to match pseudo–experimental results, resulting in excellent thermal efficiency estimates for the proposed desalination process. Thermal efficiency profiles are shown in Figure 174 through Figure 185.
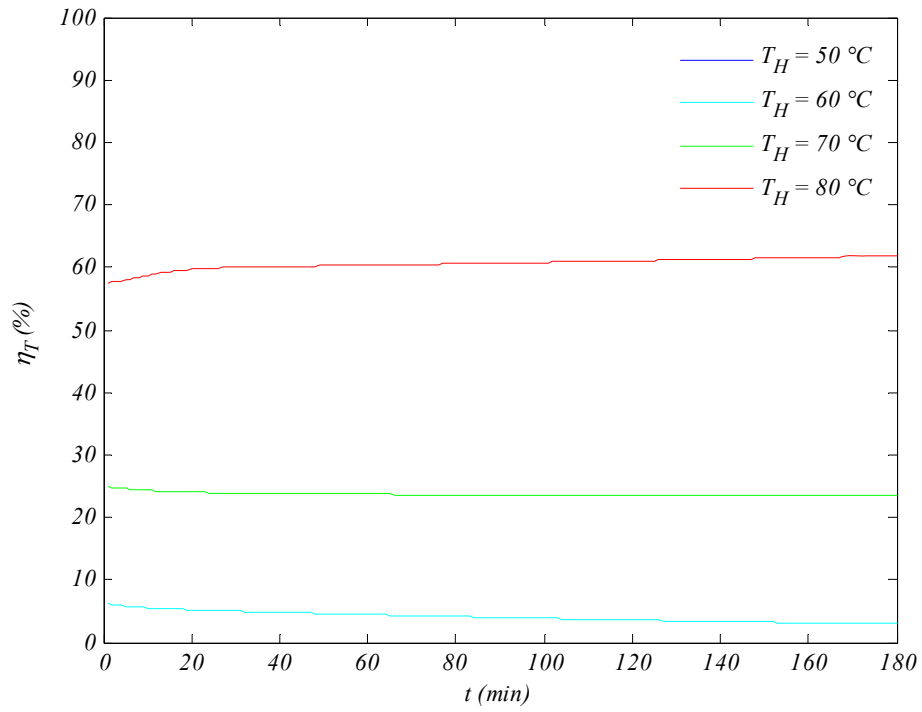
Figure 174. Modeled thermal efficiency profiles at lower flow
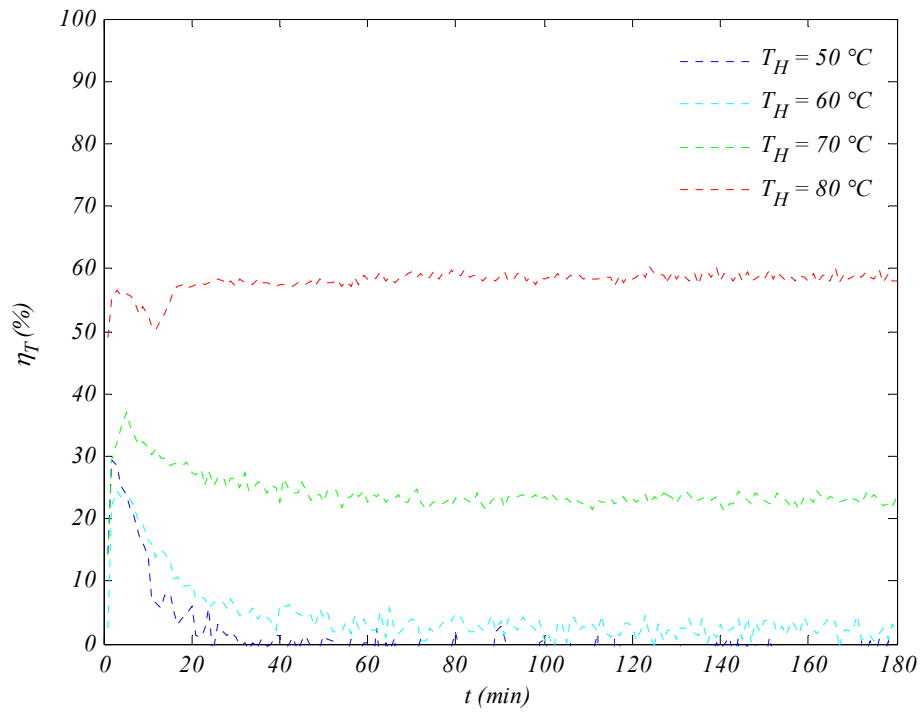
Figure 175. Mined thermal efficiency profiles at lower flow

168
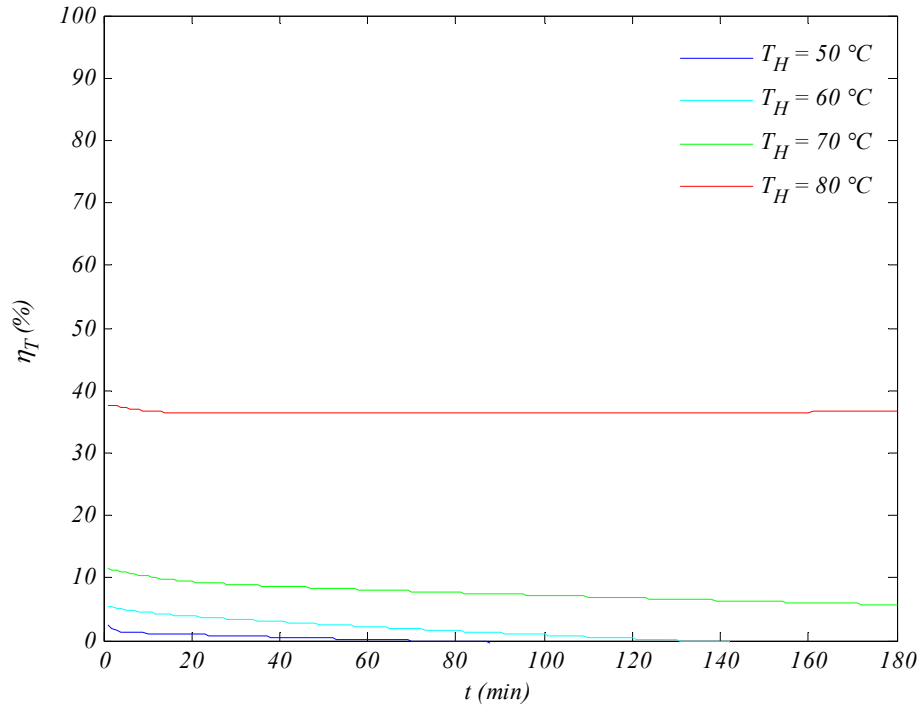
Figure 176. Modeled thermal efficiency profiles at higher flow
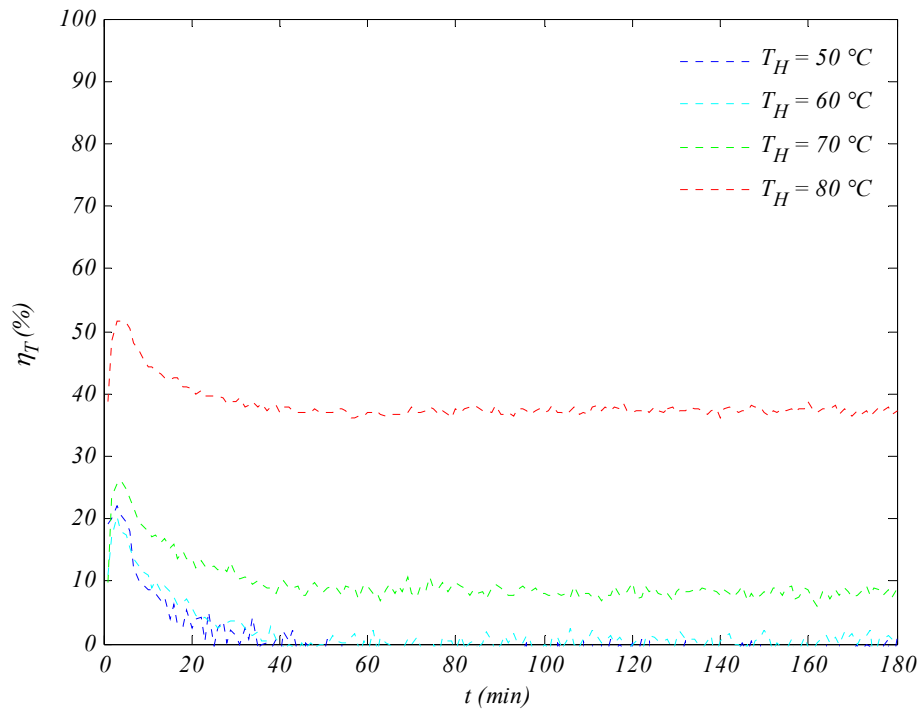
Figure 177. Mined thermal efficiency profiles at higher flow

169
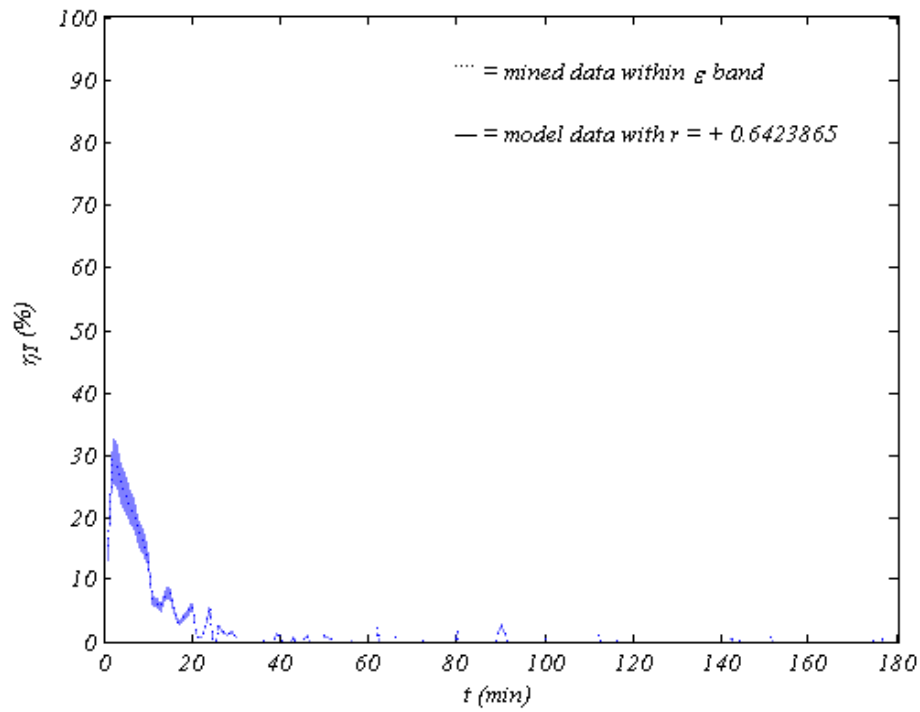
Figure 178. Thermal efficiency at 50°C flash and lower flow
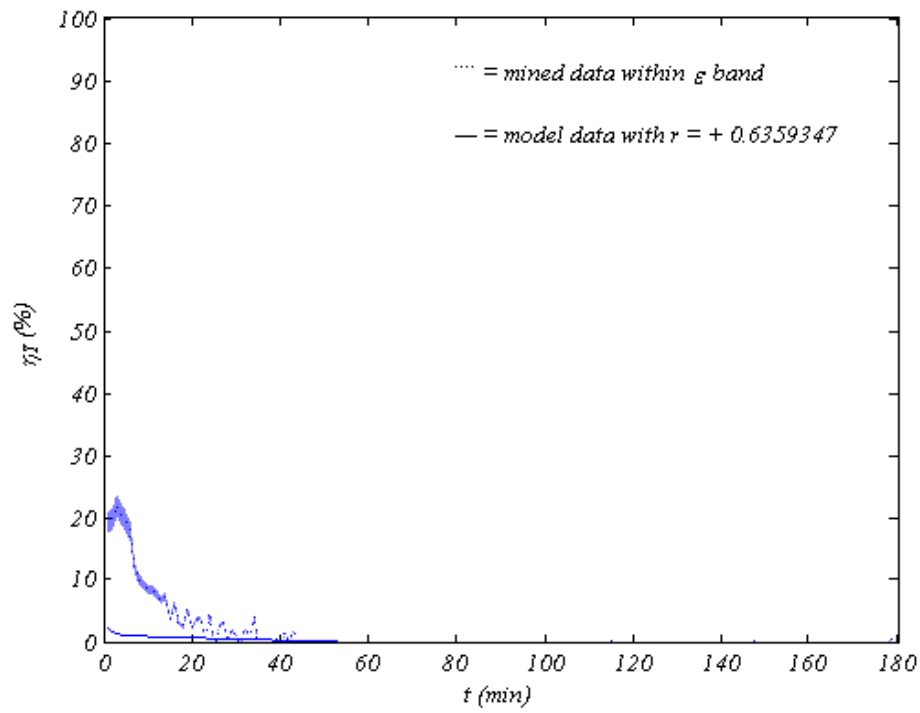
Figure 179. Thermal efficiency at 50°C flash and higher flow

170
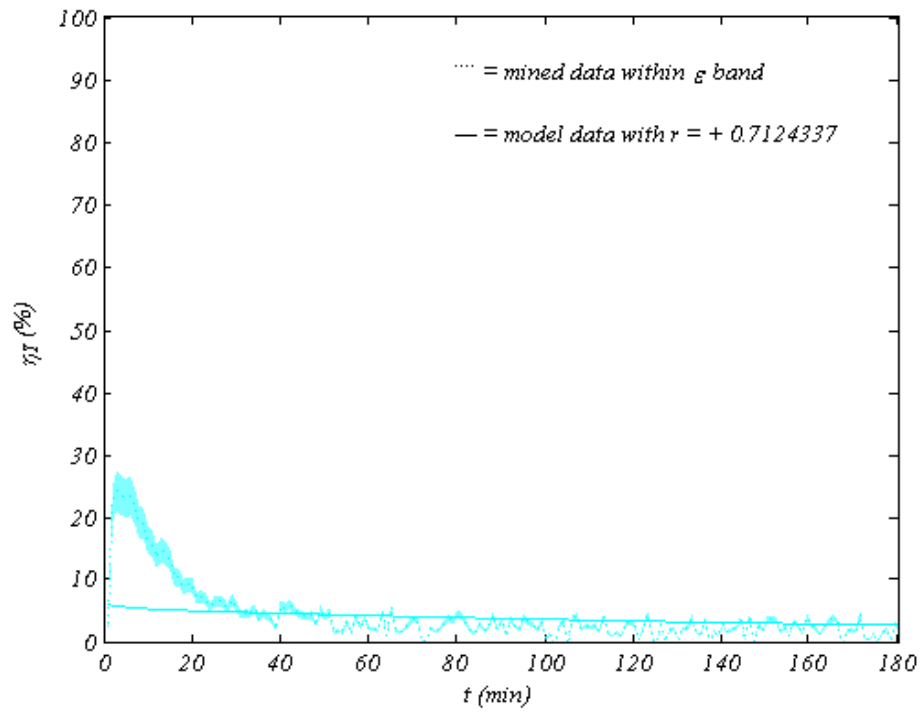
Figure 180. Thermal efficiency at 60°C flash and lower flow
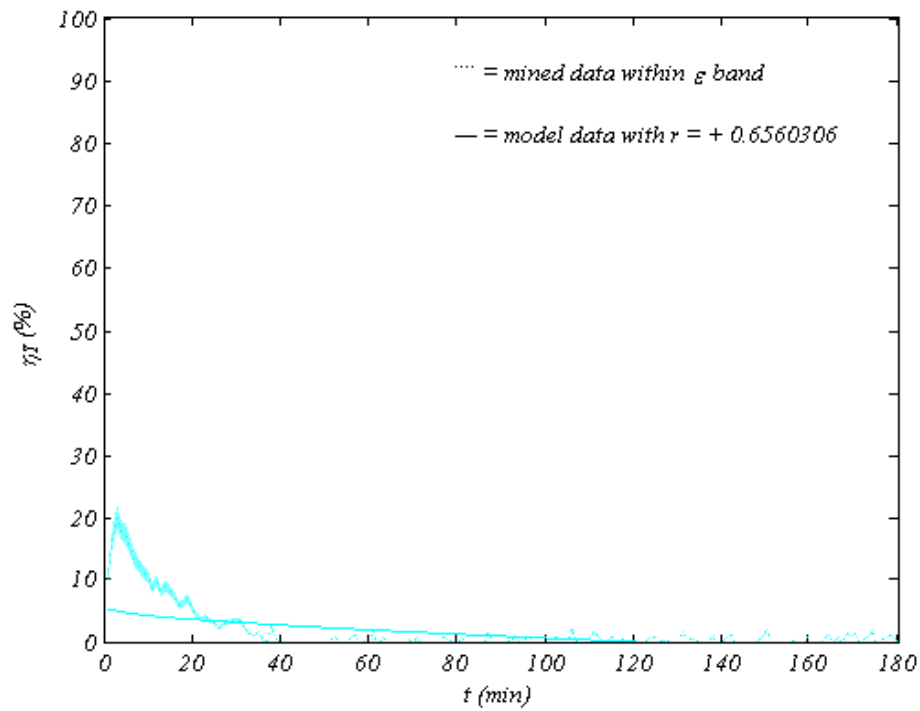
Figure 181. Thermal efficiency at 60°C flash and higher flow

171
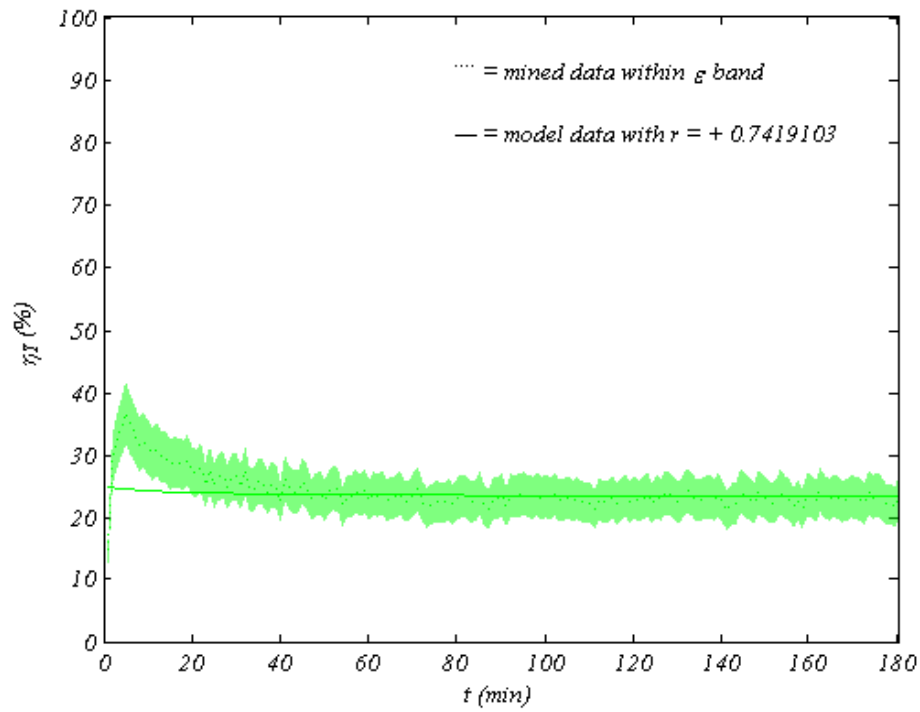
Figure 182. Thermal efficiency at 70°C flash and lower flow
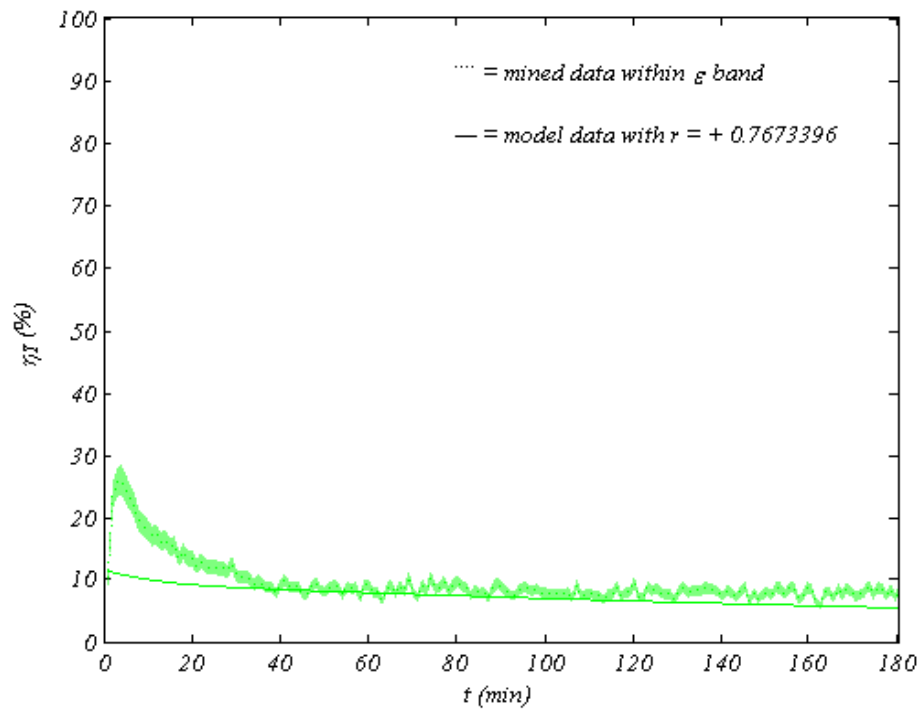
Figure 183. Thermal efficiency at 70°C flash and higher flow

172
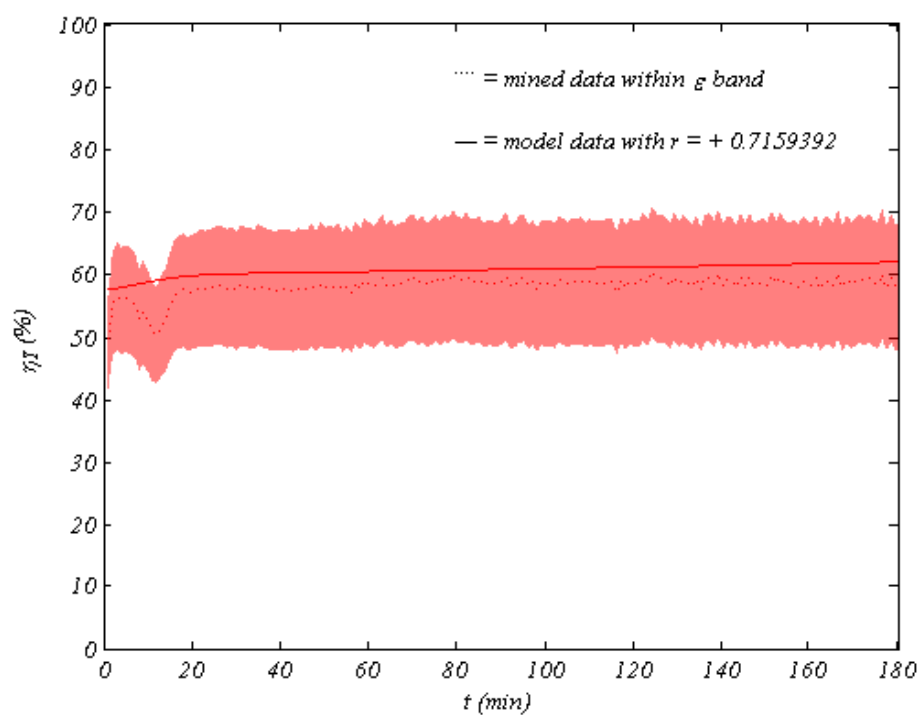
Figure 184. Thermal efficiency at 80°C flash and lower flow
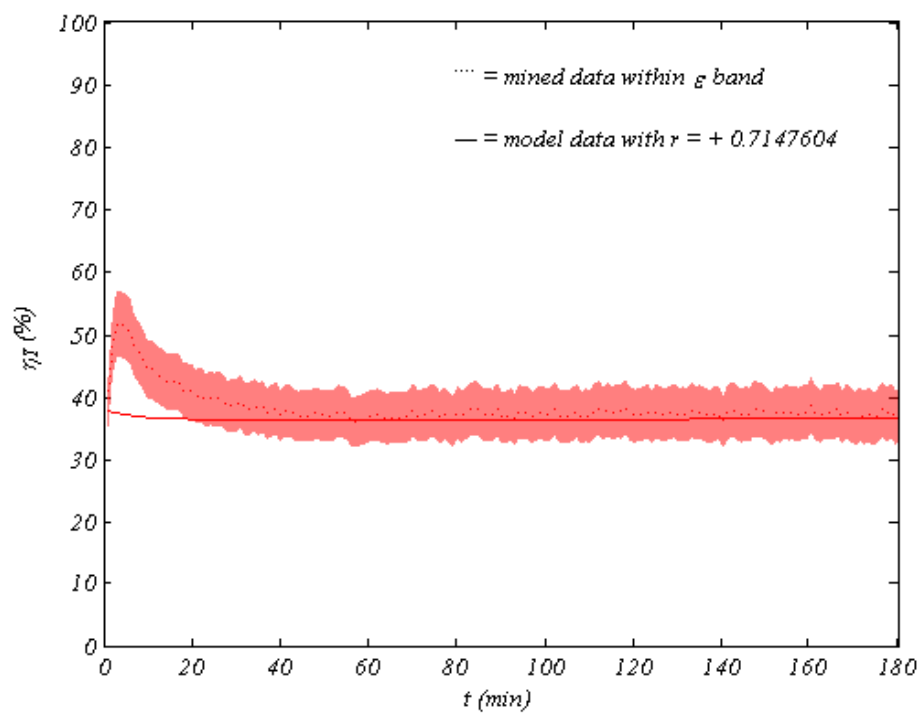
Figure 185. Thermal efficiency at 80°C flash and higher flow

173

7.14 Disambiguation

The preceding discussion included references to three different types of data as it examined profiles of twelve time–varying system variables. Model data refer to data obtained by running the developed model with its alternate equations and adjusted parameter values and expressions. Experimental data refer to averaged temperature and pressure values recorded by the data acquisition system of three matching experiments; furthermore, experimental data also include observed values for seawater flow rate and fresh water amount. Pseudo–experimental data refer to results generated by a computer code composed of the developed model with its alternate equations but without adjusted parameter values and expressions; moreover, energy balance relations were deactivated, while experimental temperature and pressure, as well as recorded seawater flow rate and produced fresh water amount, were supplied to the computer code. The entire data mining procedure is illustrated in Figure 186.
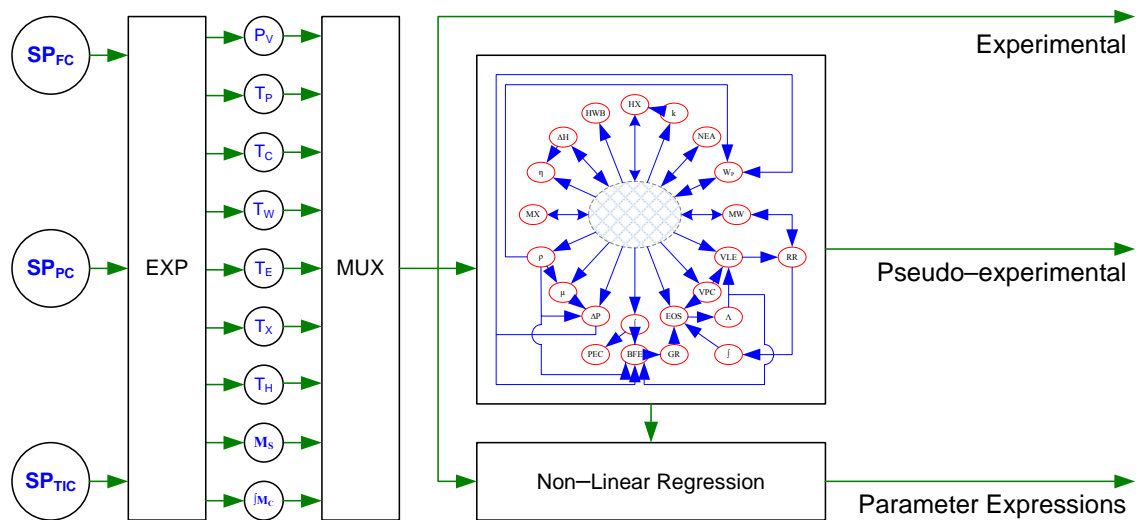
Figure 186. Experimental and pseudo–experimental data acquisition

CHAPTER 8. CONCLUSION

8.1 Summary

A flash desalination process sustainable by natural forces of solar radiation and gravity has been proposed. In addition, experimental and theoretical simulations of the proposed desalination process have been carried out. The process includes a start–up procedure and continuous operation consisting of pumping seawater through a solar heater before flashing it under vacuum in an elevated chamber. The vacuum is passively created and subsequently maintained by hydrostatic balance between pressure inside the elevated flash chamber and outdoor atmospheric pressure.

Experimental simulations were carried out by a pilot unit depicting the proposed system but emulating solar heating and passive vacuum operations. Theoretical simulations were performed using a computer code comprising fundamental physical and thermodynamic laws plus numerous correlations and parameters. Experimental data were fed to an adapted computer code generating pseudo–experimental data; moreover, experimental and pseudo–experimental data were regressed, generating parametric values and correlations that were included in the developed computer model.

Experimental and theoretical simulations were run at varying operating conditions but at analogous circumstances, and their results were compared and analyzed to validate the developed model. Feasibility of the proposed system rapidly increased with flash temperature due to increased fresh water production and improved heat recovery.

8.2 Outcome

Experimental and pseudo–experimental data were regressed, generating four correlations given in CHAPTER 6 that were included in the model. In addition, a dataset of K–values was regressed to adjust parameter values of Henry's constant and vapor pressure correlations for non–condensable gases and water, respectively.

The developed correlation for the counter–current departure correction factor for the condenser tube yielded acceptable results as was seen in CHAPTER 6; however, preheat temperature computed by the model using that developed correlation yielded poor predictions as was seen in CHAPTER 7. The data mining code used the log mean temperature difference scheme to generate pseudo–experimental data of F_{CT} that were regressed to generate the aforementioned correlation. This observation suggests that the log mean temperature difference scheme is probably not the best option to model the heat transfer operation across the condenser tube. Modeling a heat transfer operation with a phase change is extremely complex, especially in the presence of non–condensable gases. Precision of the model in predicting preheat temperature affects the quality of its evaluation of system performance as was seen in CHAPTER 7.

The developed correlation for the non–equilibrium allowance yielded average results as was seen in CHAPTER 6; consequently, equilibrium and concentrated brine temperatures computed by the model also yielded average predictions as was seen in CHAPTER 7. Heat loss of the evaporator was ignored, while non–equilibrium allowance correlation and energy balance around the evaporator were used to find equilibrium and the concentrated brine temperatures. This observation suggests that heat loss from the evaporator may need to be accounted for in the model.

The developed correlation for the activity coefficient of water yielded excellent results as was seen in CHAPTER 6. The data mining code used the Rachford–Rice scheme along with experimental values of equilibrium temperature and system pressure, plus average reported composition of seawater to generate pseudo–experimental data of γ_{H2O} that were regressed to generate the previously mentioned correlation. In addition, the data mining code included parameter values of Henry's constant and vapor pressure correlations for non–condensable gases and water obtained using the SUPERTRAPP™ code from NIST [31] as was mentioned in CHAPTER 4. The Rachford–Rice scheme and SUPERTRAPP™ code, plus the reported composition of seawater, are well recognized in literature for their accuracy; therefore, quality of the developed correlation for the activity coefficient of water is believed to be very high.

The developed correlation for the gas phase molecular content correction factor yielded good results, except for the case of higher seawater flow rates flashing at 50 °C as was seen in CHAPTER 6. The data mining code used the ideal gas law with experimental values of equilibrium temperature and system pressure, plus a straightforward formula for calculating dynamic vacuum volume to generate pseudo–experimental data of ψ that were regressed to generate the previous correlation. This observation suggests that flashing seawater at lower temperatures and higher flow rates rapidly increases the rate of accumulation of non–condensable gases. This phenomenon has been experimentally explored and theoretically modeled by Abtahi [32] via the molecular arrival rate concept. Results for ψ seen in CHAPTER 6 indicate that deviation from ideal behavior increases with decreasing P_V / P_{H2O} values due to rising temperature gradient between the hot and the cold sides of the flash chamber. This observation was also confirmed by Abtahi [32].

The results seen in CHAPTER 7 suggest that the proposed process becomes more feasible if operated at higher temperatures and more moderate flow rates. Higher flash temperatures will result in more evaporation and subsequent condensation, resulting in more fresh water production. In addition, the increased amount of heat reclaimed from condensing vapor reduced overall heater load and thus required less solar collection area. The collective outcome of increased fresh water output and decreased heater load is a significant decrease in prime energy consumption of the desalination unit, making it more economically viable. These observations are quantified in Figure 187 and Figure 188 for seawater conversion efficiency and prime energy consumption, respectively.

The results seen in CHAPTER 7 also suggest that most fresh water production occurs in the beginning of the operation, where vacuum pressure is lowest. The current experimental simulations were launched at a reasonably low vacuum; however, a much lower vacuum can be achieved using less energy if the proposed method of creating a passive vacuum is implemented. The collective outcome of applying passive vacuum and solar heating schemes is a significant decrease in prime energy consumption of the unit due to lower energy input and higher product output, furthering its feasibility.

The efficiency of the unit can also be boosted by exploiting the thermal energy of hot brine by either employing multi–stage schemes or including heat recovery provisions to increase the amount of reclaimed heat, effectively reducing prime energy consumption. The temperature difference manifested in the vapor pressure gradient between the two compartments of the flash chamber is the driving force of vapor transfer from the hot evaporator to the cold condenser; therefore, any attempt to exploit the thermal energy of the hot concentrated brine should be carefully applied as not to compromise that gradient.

178
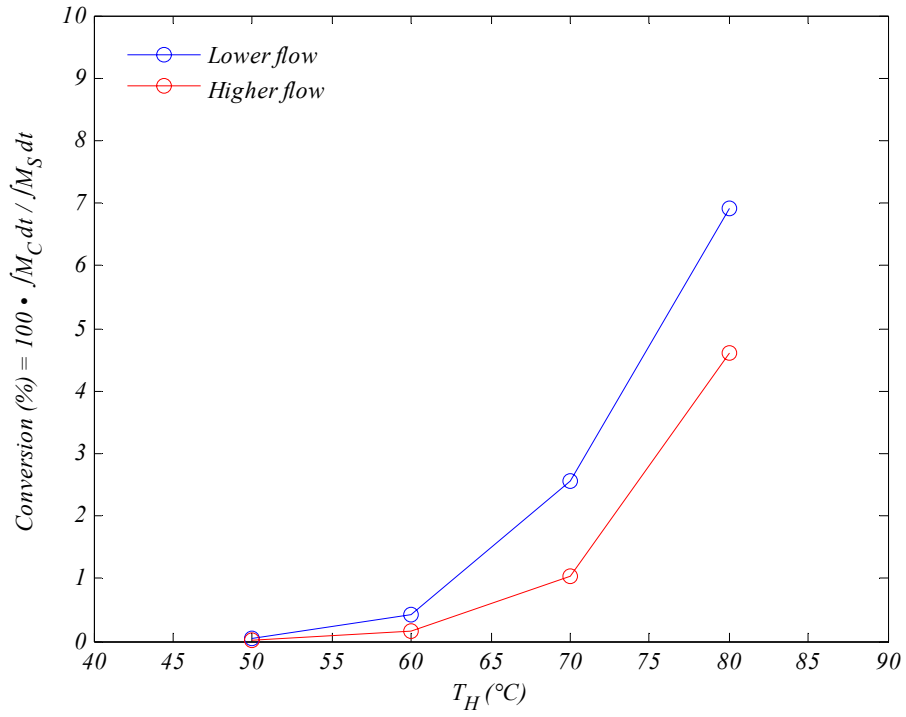
Figure 187. Seawater conversion dependence on flash temperature
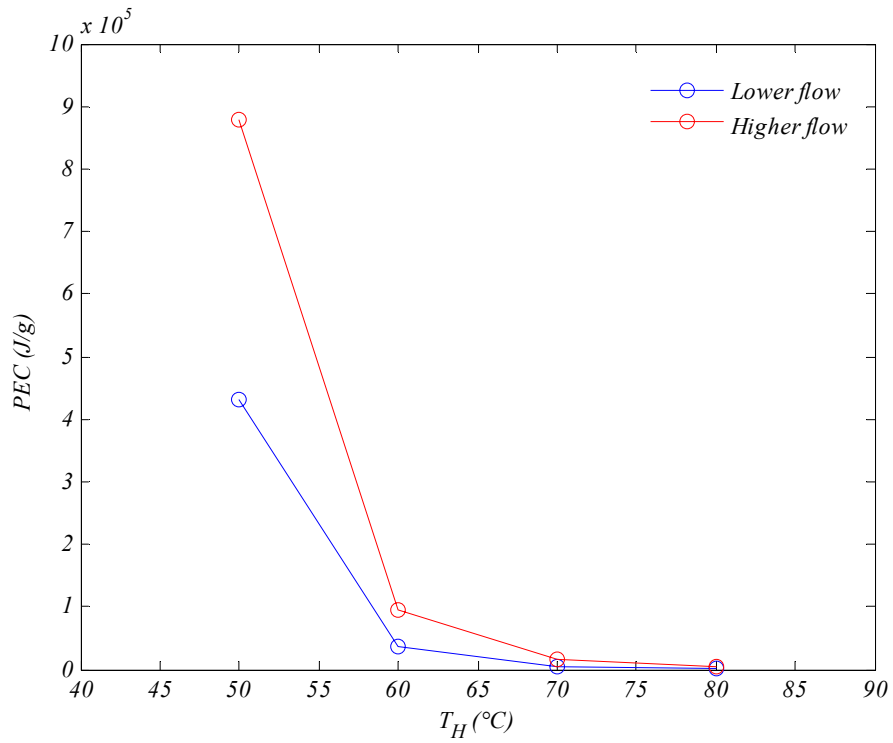
Figure 188. Prime energy consumption dependence on flash temperature

8.3 Prospects

The results of this exploration demonstrate great potential for application of the proposed desalination system, especially in light of growing energy and water demands. This section is aimed at offering recommendations for prospective researchers seeking to optimize and further feasibility of the proposed desalination system.

CHAPTER 2 includes a brief overview of the most common conventional and solar desalination methods. An immense number of renewable energy driven desalination systems have been proposed and examined but never commercially materialized. The current study did not present those systems; nevertheless, including them in the literature review of future research would be supportive of the novelty of the current system. In addition, corrosion and scaling are major challenges to all desalination systems; however, they were overlooked in this study to keep the focus on simulation of the proposed desalination system, but they should be addressed in future investigations.

Moving the experimental unit to an outdoor setting would enhance replication of the proposed system. An outdoor unit can be furnished with a real solar heater and will enable the proposed passive vacuum generation by elevating the flash chamber to at least ten meters above ground. Implementing the proposed passive vacuum generation will also allow for much lower vacuums to be achieved using less energy, which translates to more fresh water production. In addition, vacuum erosion will be slower in an outdoor unit because vacuum volume will be increasing as system pressure increases due to the hydrostatic balance between the levels of the ground tanks and the flash chamber, which translates to more fresh water production due to lower pressures. Also, an outdoor unit will enable automatic flow control via a throttling valve or a variable–frequency drive.

Accuracy of model output and pseudo–experimental data, as well as the precision of the regression, deeply rely on certainty of their input. There are slight discrepancies in literature when it comes to reporting seawater content; therefore, it is essential to investigate the seawater parameters given in CHAPTER 6 further, explicitly φ_i and α_i, especially those pertaining to carbon dioxide due to its complex kinetics.

Model convergence was difficult at times due to interdependence nature of its equations; therefore, other programming tools may be explored. In addition, the current model executes and integrates using one minute increments, yielding smooth results; however, easier convergence and smoother results can be obtained by decreasing increment size but that will also increase program run time.

Heat transfer relations of the current model did not produce very reliable results; consequently, they should be improved to predict heat loss of the flash chamber accurately as well as heat transfer across the condenser tube. Rigorous heat transfer computations will result in better predictions of equilibrium and brine temperatures resulting in superior flash calculations. More rigorous heat transfer computations will also result in better predictions of preheat temperature, resulting in enhanced performance evaluation due to regression of a more precise mined data.

The log mean temperature difference method should be substituted with a more appropriate heat transfer model capable of handling the complexity of phase change operations. Experimental data should always be used to fine–tune the parameters of the employed heat transfer model. In addition, if heat transfer computations remained imprecise, adjusting local and overall heat transfer coefficients should be explored as an alternative to adjusting the parameters of the heat transfer model.

Abtahi [32] hypothesized that the non–condensable gas molecules accumulating in the condenser tend to amass around the cold surface of the condenser tube, in essence forming an insulation layer that hampers heat transfer from the condensing water vapor. In addition, some heat transfer texts include mass transfer parameters within heat transfer coefficient correlations in condensers as they try to model the diffusion of water vapor molecules through the non–condensable gas layer.

The current model assumes the total condensation of flashed water vapor and uses a regressed molecular content correction factor to account for rate of accumulation of non–condensable gases. Alternately, the distribution of non-condensable gases among flashed vapor, concentrated brine, and condensed water in the flash chamber can be estimated by assuming equilibrium among the three phases [33]. This approach may be more valid, but will exacerbate computations and hinder convergence.

A more accurate version of the correlation for the activity coefficient of water can be obtained by using a suitable activity coefficient model to write the activity coefficient formula, then adjusting its parameters using the data mining code mentioned earlier in CHAPTER 6 and found in the APPENDICES section.

The diffusion correlation developed in CHAPTER 4 includes two parameters that serve as conductance and resistance terms. In its current form, the model considers resistance to water vapor transfer to be pertinent only to diffusing and not flashing vapor. It would be more prudent to remove the resistance term, then readjust the conductance term in accordance with reported values [14]. Afterward, a resistance term pertaining to diffusing and flashing water vapor should be included in the model and adjusted using the data mining code mentioned in CHAPTER 6 and found in the APPENDICES section.

The diffusion correlation development should be carried out alongside the above mentioned molecular arrival rate concept modeled by Abtahi [32]. This approach will make the adjusted conductance and resistance terms more consistent with the complex mass and heat transfer operations, which will ultimately result in improved vacuum pressure and preheat temperature predictions.

Feasibility of the proposed desalination process should be simply investigated via prime energy consumption, $PEC = (\int Q_H + \int W_P) / \int M_C$, and not via unnecessarily meticulous economic analyses. Process optimization is synonymous with prime energy consumption mitigation that is realized via minimizing the amount of energy exhausted or maximizing the amount of fresh water produced. Most of the exhausted energy of all thermal desalination processes is due to heat and not to power input as was seen earlier in CHAPTER 2 and as confirmed by the current experimental and theoretical simulations; therefore, optimizing the proposed desalination system should specifically revolve around reducing heater load and amplifying fresh water production rate. Detailed economic analyses can be performed by properly estimating capital and operating costs; however, these analyses can be quite cumbersome and should be carefully employed.

Seawater flash temperature is a set parameter; therefore, reducing heater load should be aimed for by increasing preheat temperature achieved via improved heat recovery in the condenser. Improving heat recovery in the condenser can be accomplished by improving the geometry of the condenser tube to harness the most of the latent heat of the condensing steam. Thermally insulating the condenser should be investigated to see its consequences on directing condensing steam away from the condenser wall and more towards the condenser tube.

Amplifying the fresh water production rate is thermodynamically controlled via increasing equilibrium temperature and lowering system pressure. With the exception of increasing flash temperature set point, increasing equilibrium temperature is accomplished by minimizing heat loss of the evaporator via enhanced thermal insulation. System pressure is always increasing because of the eroding vacuum due to build up of non–condensable gases in the flash chamber; however, initial system pressure is a controlled variable, and lowering it would lower system pressure all through the desalination process. The proposed method of passively creating vacuums should accomplish very low vacuum pressures, in effect equaling ambient water vapor pressure. In addition, fresh water production rate can be significantly enhanced by employing the multi–stage scheme outlined earlier in CHAPTER 4. The current model should be extended from simulating single–stage to multi–stage desalination schemes. In addition, a qualitative sensitivity analysis of model parameters should be executed to evaluate the outcome of their variation on model results.

The proposed desalination system is meant to be driven by solar energy and average values for a generic solar collector were used to estimate solar collection area. Detailed solar computations should be used instead of the average values to broaden the applicability of the model to different geographies and different collectors. This would involve including several solar calculations that are widely available in literature [8].

Finally, experimental results discussed earlier have proven that some of the flashed vapor condenses prematurely in the evaporator before making it to the condenser; therefore, resistance to vapor transfer from the evaporator to condenser should be reduced to increase fresh water production and improve heat recovery.

REFERENCES

1. National Atlas of the United States. *Water Resources of the United States*; U. S. Geological Survey: Reston, VA, 2005.

2. Minton, P. E. *Handbook of Evaporation Technology*; Noyes Publications: Westwood, NJ, 1986.

3. Maxwell, E., George R., Wilcox S. *Climatological Solar Radiation Model*; the National Climatic Data Center: Asheville, NC, 1998.

4. Culp, A. *Principles of Energy Conversion*; McGraw Hill: New York, NY, 1991.

5. Wangnick, K. *Worldwide Desalting Plants Inventory*; Report Number 15; International Desalination Association: Topsfield, MA, 1998.

6. Miller, J. E. *Review of Water Resources and Desalination Technologies*; Materials Chemistry Department; Sandia National Laboratories: Albuquerque, NM, 2003.

7. Kalogirou, S. A. Seawater Desalination Using Renewable Energy Sources, *Progress in Energy and Combustion Science* 2005, 31(3), pp 242–281.

8. Goswami, D. Y., Kreith, F., Kreider, J. F. *Principles of Solar Engineering*, second edition; Taylor & Francis: Philadelphia, PA, 2000.

9. Delyannis, E. Historic Background of Desalination and Renewable Energies, *Solar Energy* 2003, 75(5), pp 357–366.

10. Tzen, E., Morris, R. Renewable Energy Sources for Desalination, *Solar Energy* 2003, 75(5), pp 375–379.

11. Al–Kharabsheh, S. *Theoretical and Experimental Analysis of Water Desalination System Using Low Grade Solar Heat*, Doctoral Dissertation; University of Florida: Gainesville, Florida, 2003.

12. Maroo, S. C. *Theoretical Analysis of Solar Driven Flash Desalination System Based on Passive Vacuum Generation*, Master Thesis; University of Florida: Gainesville, Florida, 2006.

13. Rachford, H. H., Rice J. D. Procedure for Use of Electronic Digital Computers in Calculation Flash Vaporization Hydrocarbon Equilibrium, *Petroleum Technology* 1952, 4, 9.

14. Bemporad, G. A. Basic Thermodynamic Aspects of a Solar Energy Based Desalination Process, *Solar Energy* 1995, 54 (2), pp 125–134.

15. Geankoplis, C. J. *Transport Processes and Separation Process Principles*; Prentice Hall: Englewood Cliffs, NJ, 2003.

16. Turekian, K. K. *Oceans*; Prentice Hall: Englewood Cliffs, NJ, 1968.

17. Sander, R. *Compilation of Henry's Law Constants for Inorganic and Organic Species of Potential Importance in Environmental Chemistry*, www.henrys–law.org, 1999.

18. Perry, R. H., Green, D. *Perry's Chemical Engineers' Handbook*; McGraw–Hill: New York, NY, 1984.

19. Thibodeaux, L. J. *Environmental Chemodynamics*; John Wiley & Sons: New York, NY, 1996.

20. Sinnott, R. K. *Coulson and Richardson's Chemical Engineering*; Butterworth–Heinemann: Oxford, UK, 1996.

21. E1–Nashar, A. M., Qamhiyeh, A. A. Simulation of the Steady–State Operation of a Multi–Effect Stack Seawater Distillation Plant, *Desalination* 1995, 101(3), pp 231–243.

22. Miyatake, O., Murakami, K., Kawata, Y., Fujii, T. Fundamental Experiments with Flash Evaporation, *Heat Transfer – Japan Research* 1973, 2(4), pp 89–100.

23. Coker, A. K. *Chemical Process Design, Analysis, and Simulation*; Gulf Publishing: Houston, TX, 1995.

24. Hermann M., Koschikowski J., Rommel M. Corrosion–Free Solar Collectors for Thermally Driven Seawater Desalination, *Solar Energy* 2002, 72(5), pp 415–426.

25. Granet, I. *Fluid Mechanics*; Prentice Hall: Englewood Cliffs, NJ, 1996.

26. Caldwell, D. R. The Thermal Conductivity of Seawater, *Deep–Sea Research* 1974, 21, 131–138.

27. Chopey, N. P. *Handbook of Chemical Engineering Calculations*; McGraw–Hill: New York, NY, 1994.

28. Millero, F. J., Poisson, A. International One Atmosphere Equation of State of Seawater, *Deep–Sea Research* 1981, 28, pp 625–629.

29. Sündermann, J. Numerical Data and Functional Relationships in Science and Technology – New Series Group V: Geophysics and Space Research, *Oceanography* 1986, 3(A), Springer–Verlag, Berlin, Germany.

30. Mamaev, O. I. *Temperature–Salinity Analysis of World Ocean Waters*; translation from Russian by Burton, R. J.; Elsevier Scientific Publishing: Amsterdam, Netherlands, 1975.

31. Chase, M. W. *NIST–JANAF Themochemical Tables*. Journal of Physical and Chemical Reference, Number 9; American Chemical Society: Washington, DC, 1998.

32. Abtahi, H. Investigation of local pressure characteristics in gas–loaded heat pipes, *Proceedings of the ASME National Heat Transfer Conference*, Houston, TX, 1988; American Society of Mechanical Engineers: New York, NY, 1988, A89 53251 23 34, pp 347–352.

33. Abutayeh, M., Goswami, D. Y. Passive Vacuum Solar Flash Desalination, *American Institute of Chemical Engineers* [Online] 2009, pp 1547–5905.

APPENDICES

Appendix A. The operating procedure
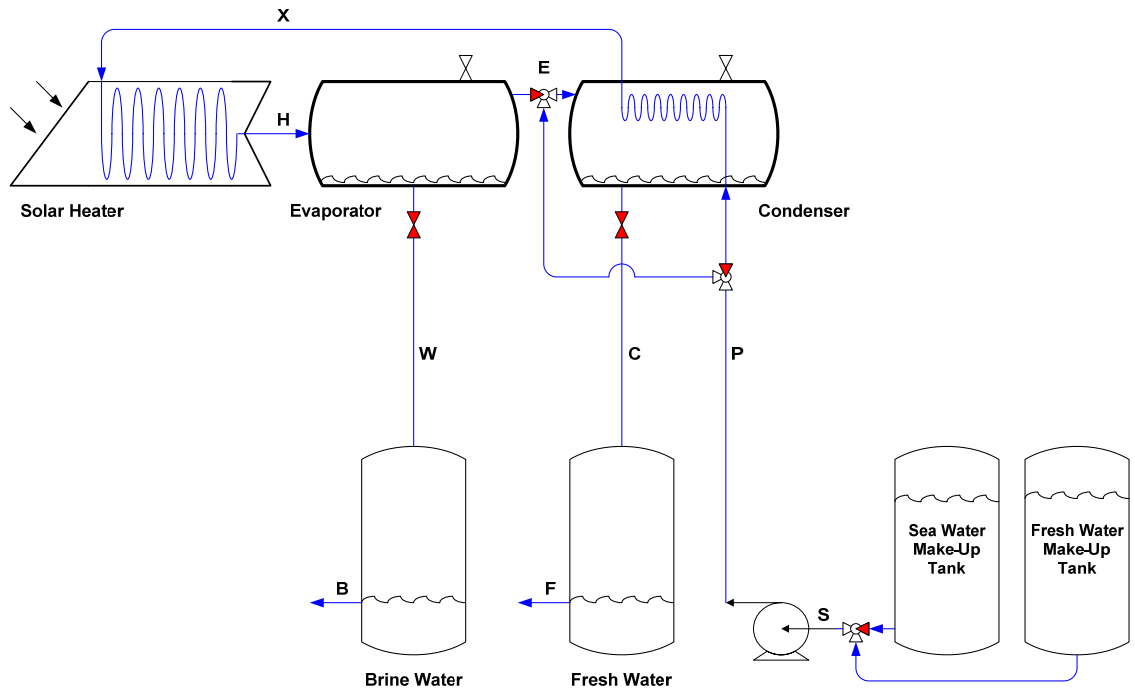
Figure 189. Preparing to fill up the condenser
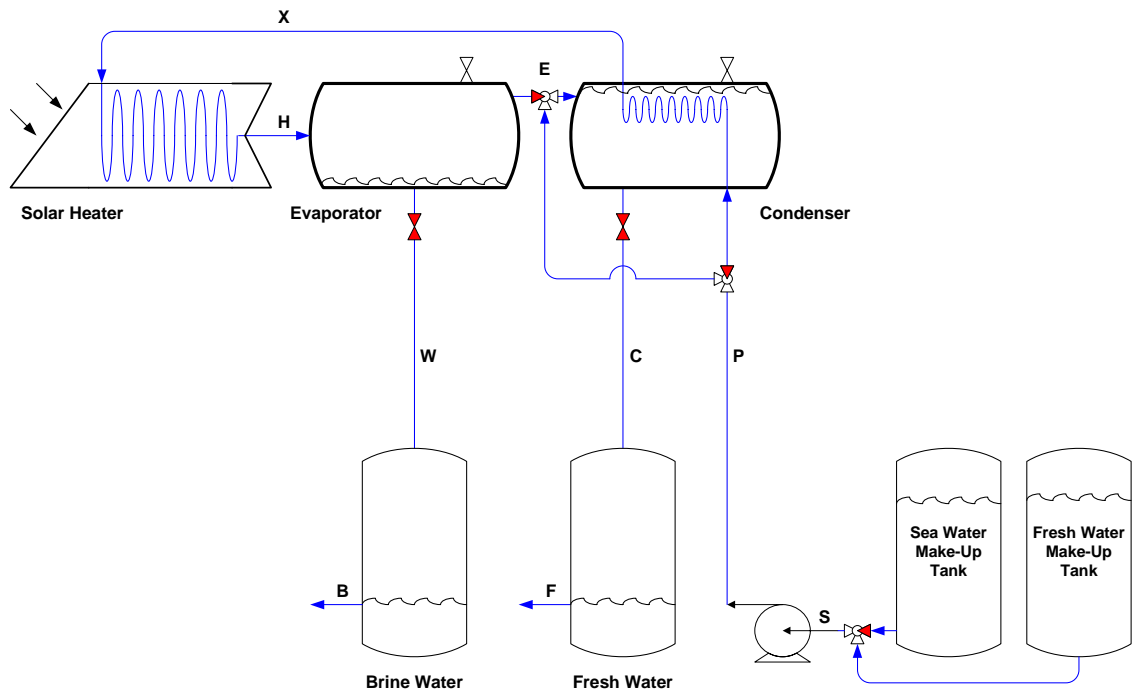
Figure 190. Condenser full of fresh water
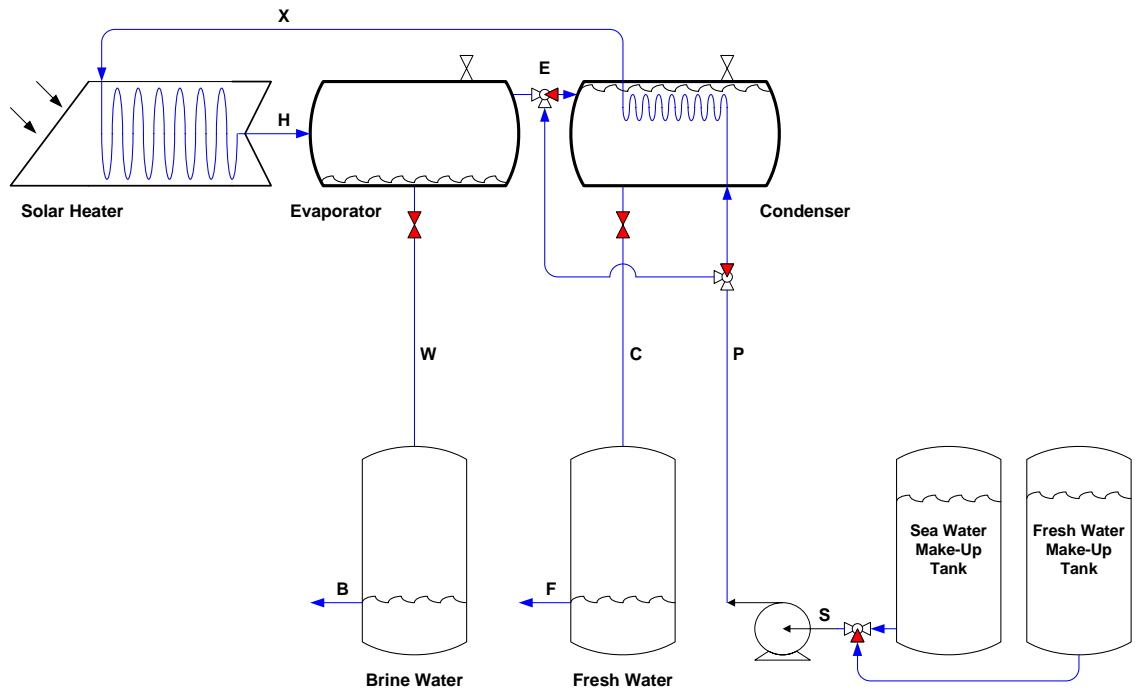
Figure 191. Preparing to fill up the evaporator
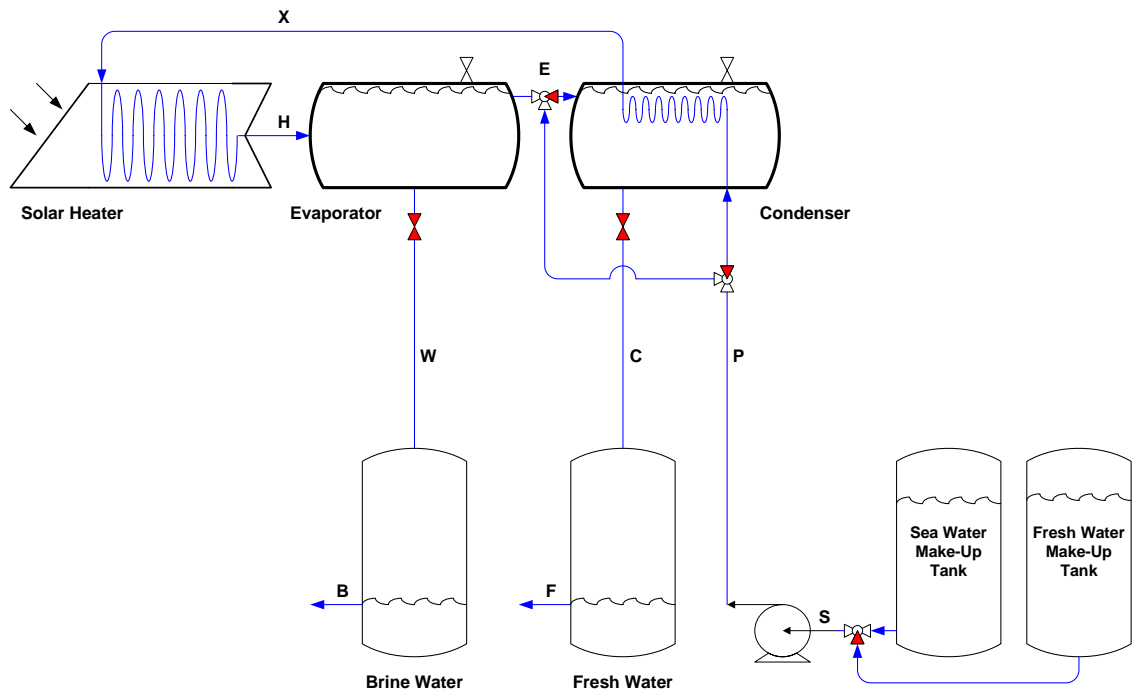
Figure 192. Evaporator full of seawater

191
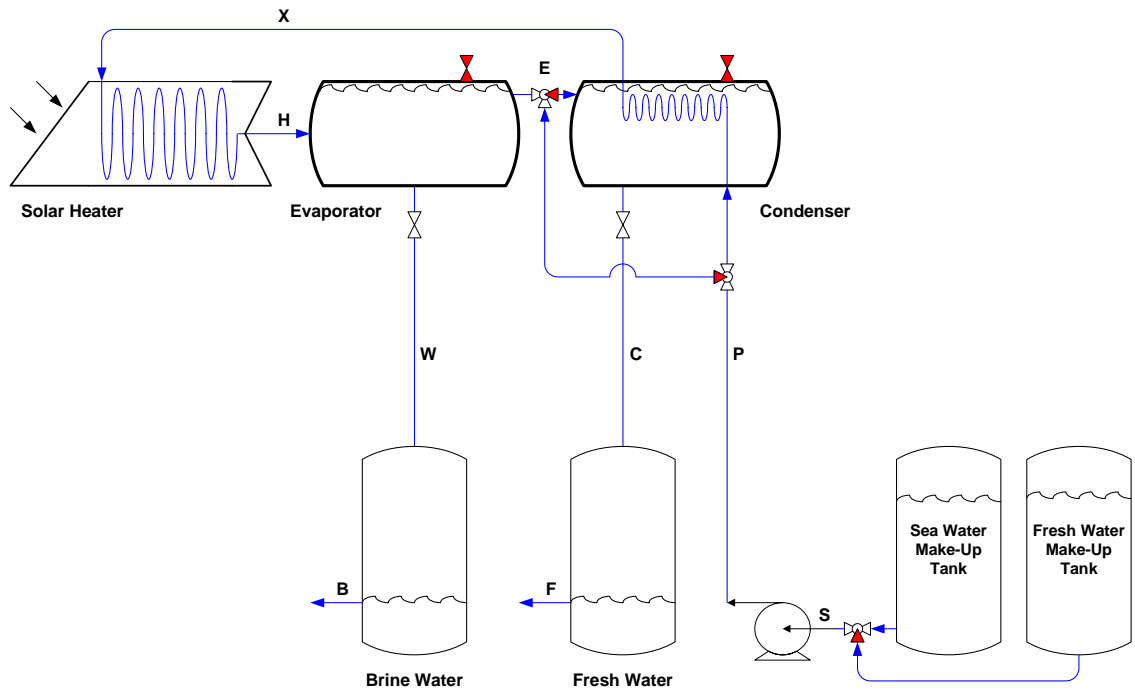
Figure 193. Switching the valve positions of the flash chamber
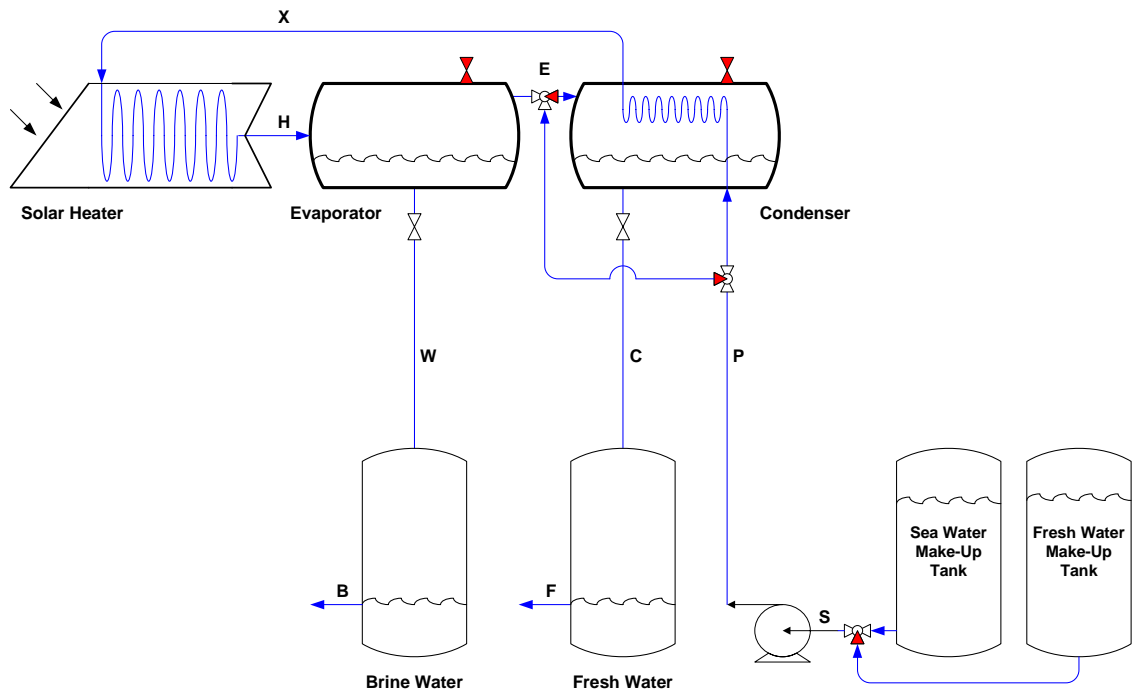
Figure 194. Flash chamber passively vacuumed
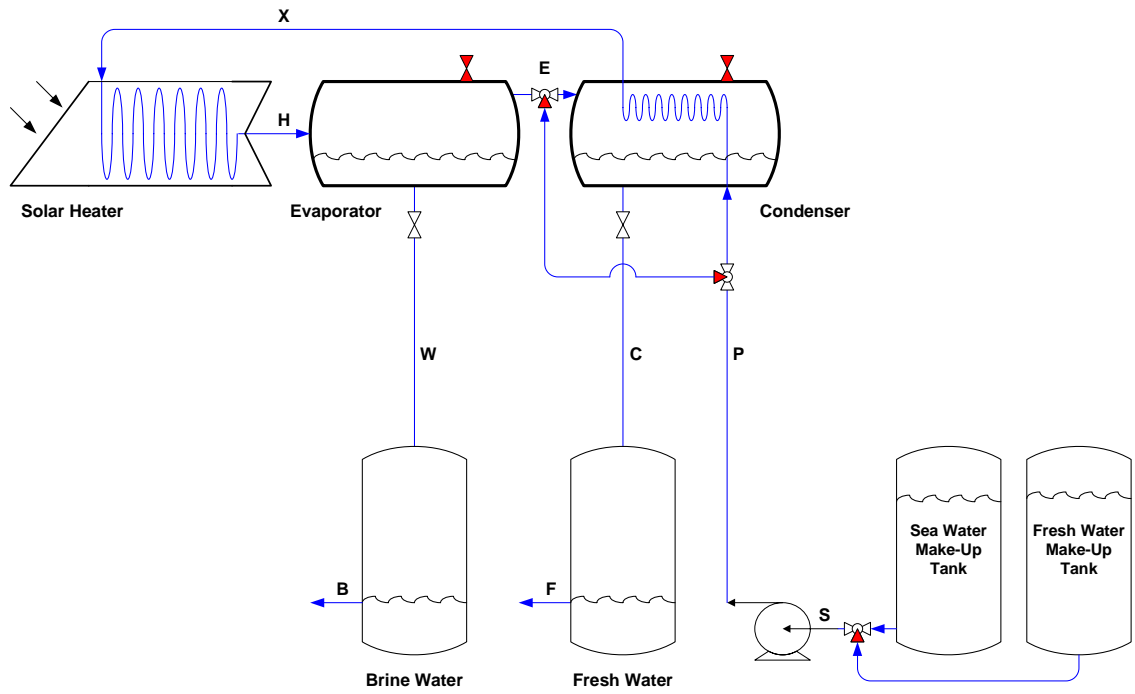
Figure 195. Preparing to start the desalination process
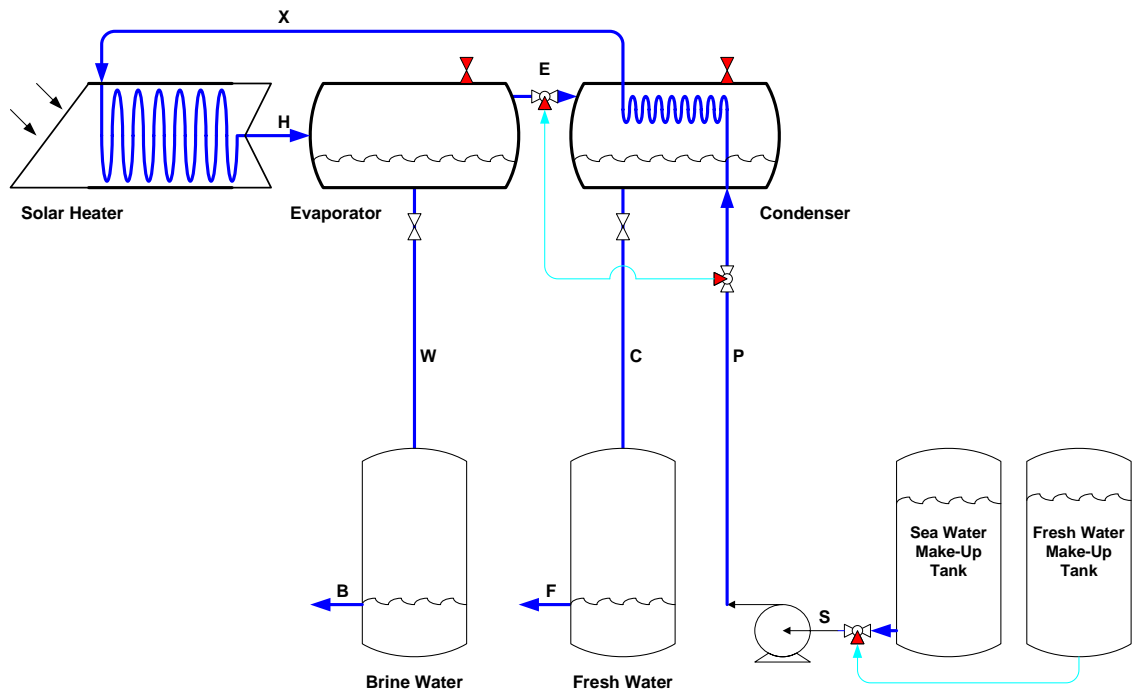
Figure 196. Desalination process taking place
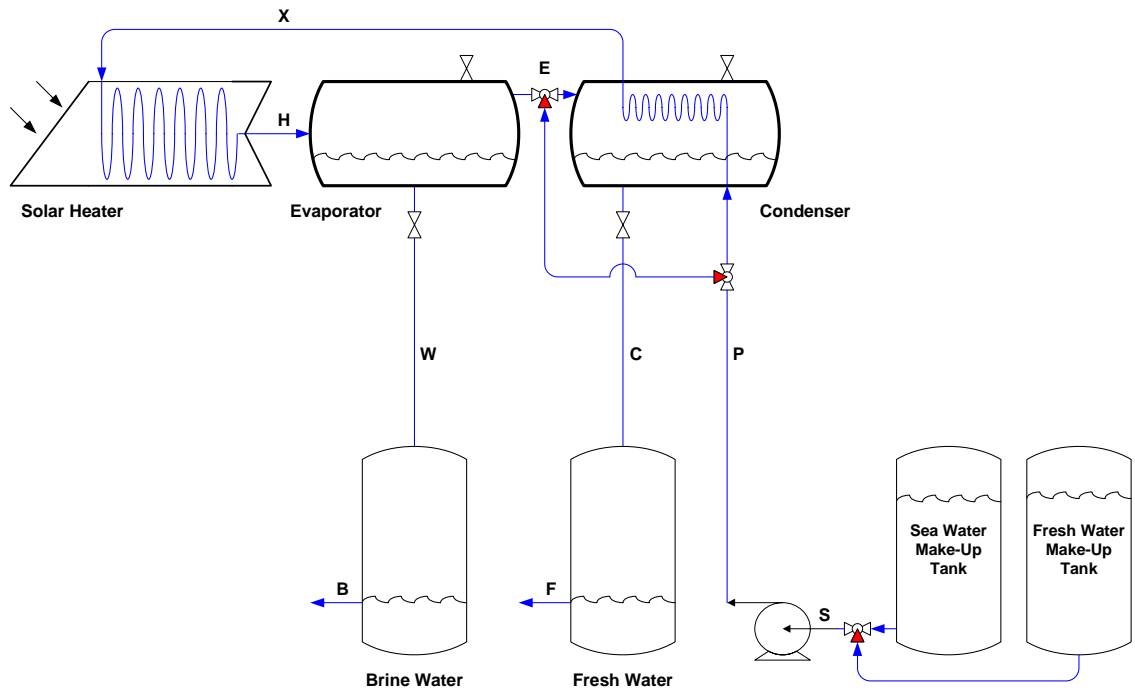
Figure 197. Flash chamber vented to terminate vacuum
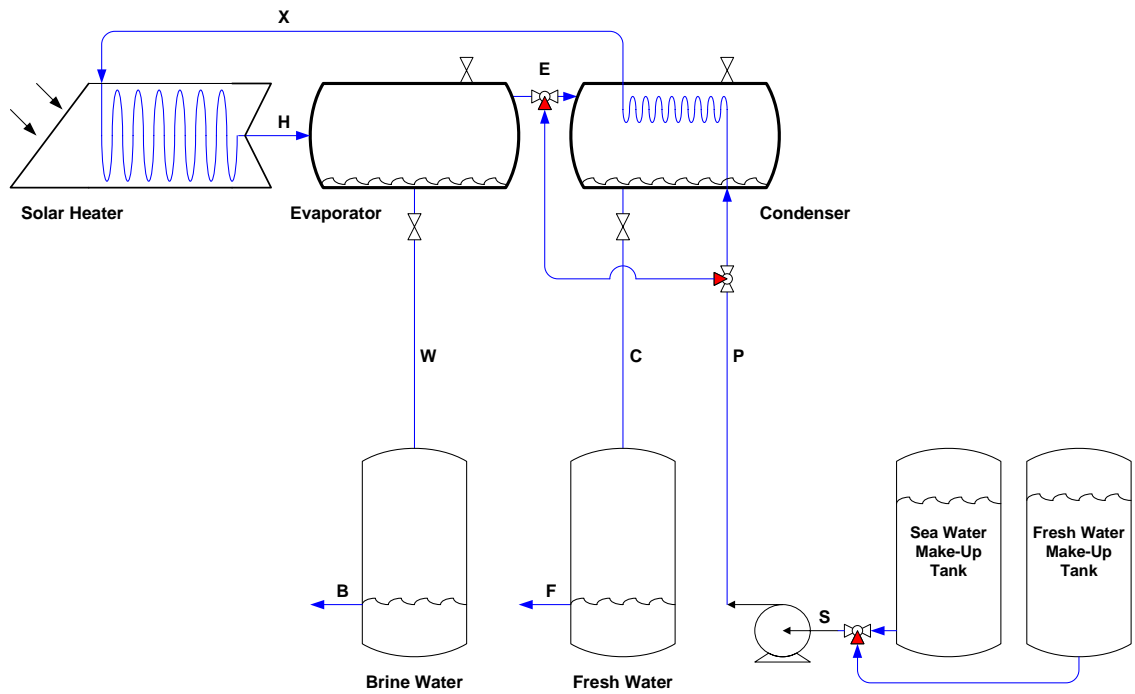
Figure 198. Flash chamber drained

194

Appendix B. SUPERTRAPP™ code to generate K–values

```
**************************************************************
*              NIST Standard Reference Database 4            *
*    NIST THERMOPHYSICAL PROPERTIES OF HYDROCARBON MIXTURES  *
*              Program SUPERTRAPP - Version 3.1, beta 1      *
*                                                            *
*                  Based on research sponsored by            *
*                  the NASA Lewis Research Center,           *
*          the NIST Supercritical Fluid Property Consortium  *
*                  and Standard Reference Data               *
*                                                            *
*                      Marcia L. Huber                       *
*         Physical and Chemical Properties Division          *
*                                                            *
*            Distributed by Standard Reference Data          *
*         National Institute of Standards and Technology     *
*                  Gaithersburg, MD 20899 USA                *
*                                                            *
*         Copyright 2002 by the U.S. Secretary of Commerce   *
*             on behalf of the United States of America      *
*                     All rights reserved.                   *
**************************************************************

For help in response to any question, enter "?".
For a brief description of SUPERTRAPP, enter "?".
Press enter to continue.

Do you want to use default settings? (Y/N)
(The default settings are whatever you last selected for units and file I/O.)


How many components (maximum is 20, enter 0 to stop) ? 5
Enter the name of component  1 ? N2
Enter the name of component  2 ? O2
Enter the name of component  3 ? Ar
Enter the name of component  4 ? CO2
Enter the name of component  5 ? H2O
Enter the moles of nitrogen? 0.000892430051332573
Enter the moles of oxygen? 0.00043752734545909
Enter the moles of argon? 0.0000200300450676013
Enter the moles of carbon dioxide? 0.00409007248517348
Enter the moles of water? 107.121933077247

For a list of available options, type ? Otherwise
enter command or, if you wish to do a flash calculation,
enter T(K) and P(bar) separated by a comma.
288.15,1


2-Phase Flash results at T =  288.150 K and P =  1.00000      bar

----Component------ ---Feed--- --Liquid-- --Vapor--- ---Phi---- --K--
nitrogen           0.833055E-05 0.344128E-07 0.427495   0.427528   .12E+08
oxygen             0.408418E-05 0.409242E-06 0.189368   0.189267   .46E+06
argon              0.186974E-06 0.175174E-07 0.873203E-02 0.872798E-02 .50E+06
carbon dioxide     0.381795E-04 0.312301E-04 0.358131   0.356581   .11E+05
water              0.999949     0.999968     0.162738E-01 0.161498E-01 .16E-01
Molar Basis
                   1.00000      0.999981     0.194064E-04 Feed Fraction
                   18.0211      18.0208      34.4373      Molar Mass
                   0.762087E-03 0.742729E-03 0.998250     Comp. Factor, Z
                   54.7708      56.1983      0.418133E-01 D, mol/liter
                   -287.426     -287.429     -145.202     H, kJ/mol
                   64.9348      64.9320      210.196      S, J/mol.K
                   76.7500      76.7509      32.3969      Cp, J/mol.K
                                1.26448      1.34988      Cp/Cv
                                3410.20      305.911      Sound Speed, m/s
                                -0.193114E-01 0.496588    JT, K/bar
                                11292.3      171.639      Visc., uP
                                579.549      22.0159      Th. Cond.,mW/m.K

(VLE=PRS,PROPS=EXCST)
For a list of available options, type ? Otherwise
enter command or, if you wish to do a flash calculation,
enter T(K) and P(bar) separated by a comma.
293.15,1
```

Appendix B (Continued)

```
2-Phase Flash results at T =  293.150 K and P =  1.00000     bar

----Component------ ---Feed--- --Liquid-- --Vapor--- ---Phi---- --K--
nitrogen           0.833055E-05 0.427090E-07 0.429025    0.429076    .10E+08
oxygen             0.408418E-05 0.460568E-06 0.187579    0.187490    .41E+06
argon              0.186974E-06 0.198371E-07 0.865197E-02 0.864843E-02 .44E+06
carbon dioxide     0.381795E-04 0.313748E-04 0.352284    0.350834    .11E+05
water              0.999949    0.999968    0.224604E-01 0.222965E-01 .22E-01
Molar Basis
                      1.00000     0.999981    0.193178E-04 Feed Fraction
                      18.0211     18.0208     34.2739     Molar Mass
                      0.754310E-03 0.735038E-03 0.998342   Comp. Factor, Z
                      54.3917     55.8178     0.410963E-01 D, mol/liter
                      -286.753    -286.755    -144.235    H, kJ/mol
                      67.1288     67.1260     210.722     S, J/mol.K
                      75.6292     75.6301     32.4522     Cp, J/mol.K
                                  1.19949     1.34891     Cp/Cv
                                  3277.46     309.206     Sound Speed, m/s
                                  -0.201080E-01 0.483944  JT, K/bar
                                  10054.1     173.823     Visc., uP
                                  588.761     22.4243     Th. Cond.,mW/m.K
(VLE=PRS,PROPS=EXCST)
For a list of available options, type ? Otherwise
enter command or, if you wish to do a flash calculation,
enter T(K) and P(bar) separated by a comma.
298.15,1


2-Phase Flash results at T =  298.150 K and P =  1.00000     bar

----Component------ ---Feed--- --Liquid-- --Vapor--- ---Phi---- --K--
nitrogen           0.833055E-05 0.525191E-07 0.429422    0.429493    .82E+07
oxygen             0.408418E-05 0.514592E-06 0.185172    0.185096    .36E+06
argon              0.186974E-06 0.222940E-07 0.854277E-02 0.853976E-02 .38E+06
carbon dioxide     0.381795E-04 0.315055E-04 0.346245    0.344888    .11E+05
water              0.999949    0.999968    0.306178E-01 0.304033E-01 .31E-01
Molar Basis
                      1.00000     0.999981    0.192772E-04 Feed Fraction
                      18.0211     18.0208     34.0849     Molar Mass
                      0.746899E-03 0.727667E-03 0.998416   Comp. Factor, Z
                      54.0102     55.4377     0.404041E-01 D, mol/liter
                      -286.086    -286.089    -143.669    H, kJ/mol
                      69.2517     69.2490     211.245     S, J/mol.K
                      74.5180     74.5188     32.5133     Cp, J/mol.K
                                  1.14872     1.34788     Cp/Cv
                                  3164.64     312.599     Sound Speed, m/s
                                  -0.209314E-01 0.474132  JT, K/bar
                                  9000.45     175.802     Visc., uP
                                  597.672     22.8360     Th. Cond.,mW/m.K
(VLE=PRS,PROPS=EXCST)
For a list of available options, type ? Otherwise
enter command or, if you wish to do a flash calculation,
enter T(K) and P(bar) separated by a comma.
303.15,1


2-Phase Flash results at T =  303.150 K and P =  1.00000     bar

----Component------ ---Feed--- --Liquid-- --Vapor--- ---Phi---- --K--
nitrogen           0.833055E-05 0.639249E-07 0.428310    0.428401    .67E+07
oxygen             0.408418E-05 0.570542E-06 0.182049    0.181984    .32E+06
argon              0.186974E-06 0.248543E-07 0.839976E-02 0.839729E-02 .34E+06
carbon dioxide     0.381795E-04 0.316181E-04 0.339991    0.338717    .11E+05
water              0.999949    0.999968    0.412514E-01 0.409730E-01 .41E-01
Molar Basis
                      1.00000     0.999981    0.193005E-04 Feed Fraction
                      18.0211     18.0208     33.8644     Molar Mass
                      0.739394E-03 0.720137E-03 0.998470   Comp. Factor, Z
                      53.6585     55.0934     0.397356E-01 D, mol/liter
                      -285.463    -285.465    -143.617    H, kJ/mol
                      71.2038     71.2010     211.762     S, J/mol.K
                      73.5538     73.5546     32.5823     Cp, J/mol.K
                                  1.11477     1.34678     Cp/Cv
```

196

Appendix B (Continued)

```
                                    3076. 35         316. 121      Sound Speed, m/s
                                 -0. 216544E-01 0. 467549      JT,  K/bar
                                    8098. 85         177. 528      Visc.,  uP
                                     606. 261         23. 2528      Th.  Cond., mW/m. K
(VLE=PRS, PROPS=EXCST)
For a list of available options, type ? Otherwise
enter command or, if you wish to do a flash calculation,
enter T(K) and P(bar) separated by a comma.
308. 15, 1
```

2-Phase Flash results at T = 308. 150 K and P = 1. 00000   bar

----Component------	---Feed---	--Liquid--	--Vapor---	---Phi----	--K--
nitrogen	0. 833055E-05	0. 769946E-07	0. 425229	0. 425343	. 55E+07
oxygen	0. 408418E-05	0. 627324E-06	0. 178100	0. 178049	. 28E+06
argon	0. 186974E-06	0. 274689E-07	0. 821784E-02	0. 821594E-02	. 30E+06
carbon dioxide	0. 381795E-04	0. 317072E-04	0. 333489	0. 332291	. 11E+05
water	0. 999949	0. 999968	0. 549638E-01	0. 546051E-01	. 55E-01

```
Molar Basis
                    1. 00000         0. 999981       0. 194096E-04  Feed Fraction
                   18. 0211           18. 0208          33. 6055        Molar Mass
            0. 729280E-03 0. 709913E-03 0. 998501         Comp. Factor, Z
                   53. 5200           54. 9800        0. 390896E-01  D,  mol/liter
                 -285. 087          -285. 089        -144. 212        H,  kJ/mol
                   72. 4338           72. 4311          212. 268        S,  J/mol. K
                   73. 5108           73. 5116           32. 6618        Cp,  J/mol. K
                                         1. 12424           1. 34556        Cp/Cv
                                       3052. 71          319. 808        Sound Speed, m/s
                                  -0. 215396E-01 0. 464722         JT,  K/bar
                                      7323. 15          178. 947        Visc.,  uP
                                       614. 421           23. 6766        Th.  Cond., mW/m. K
(VLE=PRS, PROPS=EXCST)
For a list of available options, type ? Otherwise
enter command or, if you wish to do a flash calculation,
enter T(K) and P(bar) separated by a comma.
313. 15, 1
```

2-Phase Flash results at T = 313. 150 K and P = 1. 00000   bar

----Component------	---Feed---	--Liquid--	--Vapor---	---Phi----	--K--
nitrogen	0. 833055E-05	0. 916537E-07	0. 419638	0. 419776	. 46E+07
oxygen	0. 408418E-05	0. 683483E-06	0. 173211	0. 173173	. 25E+06
argon	0. 186974E-06	0. 300721E-07	0. 799164E-02	0. 799034E-02	. 27E+06
carbon dioxide	0. 381795E-04	0. 317661E-04	0. 326694	0. 325564	. 10E+05
water	0. 999949	0. 999967	0. 724650E-01	0. 720057E-01	. 72E-01

```
Molar Basis
                    1. 00000         0. 999980       0. 196333E-04  Feed Fraction
                   18. 0211           18. 0208          33. 2997        Molar Mass
            0. 719666E-03 0. 700076E-03 0. 998506         Comp. Factor, Z
                   53. 3690           54. 8624        0. 384653E-01  D,  mol/liter
                 -284. 712          -284. 715        -145. 607        H,  kJ/mol
                   73. 6397           73. 6369          212. 756        S,  J/mol. K
                   73. 4833           73. 4841           32. 7550        Cp,  J/mol. K
                                         1. 13444           1. 34419        Cp/Cv
                                       3029. 90          323. 706        Sound Speed, m/s
                                  -0. 214130E-01 0. 466334         JT,  K/bar
                                      6652. 37          179. 992        Visc.,  uP
                                       622. 271           24. 1101        Th.  Cond., mW/m. K
(VLE=PRS, PROPS=EXCST)
For a list of available options, type ? Otherwise
enter command or, if you wish to do a flash calculation,
enter T(K) and P(bar) separated by a comma.
318. 15, 1
```

2-Phase Flash results at T = 318. 150 K and P = 1. 00000   bar

----Component------	---Feed---	--Liquid--	--Vapor---	---Phi----	--K--
nitrogen	0. 833055E-05	0. 107669E-06	0. 410902	0. 411067	. 38E+07
oxygen	0. 408418E-05	0. 737106E-06	0. 167256	0. 167232	. 23E+06
argon	0. 186974E-06	0. 325762E-07	0. 771537E-02	0. 771471E-02	. 24E+06
carbon dioxide	0. 381795E-04	0. 317855E-04	0. 319543	0. 318473	. 10E+05

```
water                   0.999949     0.999967       0.945847E-01 0.939993E-01 .95E-01
Molar Basis
                        1.00000      0.999980       0.200118E-04 Feed Fraction
                        18.0211      18.0208        32.9372      Molar Mass
                        0.710577E-03 0.690609E-03 0.998482       Comp. Factor, Z
                        53.2022      54.7404        0.378617E-01 D, mol/liter
                        -284.339     -284.341       -147.979     H, kJ/mol
                        74.8225      74.8197        213.214      S, J/mol.K
                        73.4714      73.4722        32.8654      Cp, J/mol.K
                                     1.14539        1.34263      Cp/Cv
                                     3007.94        327.872      Sound Speed, m/s
                                     -0.212745E-01 0.473293      JT, K/bar
                                     6069.52        180.587      Visc., uP
                                     629.807        24.5568      Th. Cond.,mW/m.K
(VLE=PRS,PROPS=EXCST)
For a list of available options, type ? Otherwise
enter command or, if you wish to do a flash calculation,
enter T(K) and P(bar) separated by a comma.
323.15,1


2-Phase Flash results at T =   323.150 K and P =   1.00000      bar

----Component------  ---Feed---   --Liquid--   --Vapor---   ---Phi----   --K--
nitrogen             0.833055E-05 0.124565E-06 0.398291     0.398487     .32E+07
oxygen               0.408418E-05 0.785728E-06 0.160097     0.160088     .20E+06
argon                0.186974E-06 0.348681E-07 0.738275E-02 0.738280E-02 .21E+06
carbon dioxide       0.381795E-04 0.317532E-04 0.311946     0.310930     .98E+04
water                0.999949     0.999967     0.122284     0.121540     .12E+00
Molar Basis
                     1.00000      0.999979       0.206030E-04 Feed Fraction
                     18.0211      18.0208        32.5064      Molar Mass
                     0.702055E-03 0.681498E-03 0.998424       Comp. Factor, Z
                     53.0148      54.6139        0.372780E-01 D, mol/liter
                     -283.966     -283.969       -151.523     H, kJ/mol
                     75.9832      75.9804        213.624      S, J/mol.K
                     73.4754      73.4762        32.9972      Cp, J/mol.K
                                  1.15716        1.34083      Cp/Cv
                                  2986.83        332.379      Sound Speed, m/s
                                  -0.211239E-01 0.486828      JT, K/bar
                                  5560.75        180.639      Visc., uP
                                  637.027        25.0208      Th. Cond.,mW/m.K
(VLE=PRS,PROPS=EXCST)
For a list of available options, type ? Otherwise
enter command or, if you wish to do a flash calculation,
enter T(K) and P(bar) separated by a comma.
328.15,1


2-Phase Flash results at T =   328.150 K and P =   1.00000      bar

----Component------  ---Feed---   --Liquid--   --Vapor---   ---Phi----   --K--
nitrogen             0.833055E-05 0.141527E-06 0.380999     0.381229     .27E+07
oxygen               0.408418E-05 0.826198E-06 0.151580     0.151589     .18E+06
argon                0.186974E-06 0.368027E-07 0.698684E-02 0.698769E-02 .19E+06
carbon dioxide       0.381795E-04 0.316511E-04 0.303770     0.302803     .96E+04
water                0.999949     0.999967     0.156664     0.155721     .16E+00
Molar Basis
                     1.00000      0.999979       0.214936E-04 Feed Fraction
                     18.0211      18.0208        31.9935      Molar Mass
                     0.694172E-03 0.672728E-03 0.998326       Comp. Factor, Z
                     52.7999      54.4829        0.367137E-01 D, mol/liter
                     -283.595     -283.598       -156.454     H, kJ/mol
                     77.1229      77.1200        213.961      S, J/mol.K
                     73.4953      73.4962        33.1549      Cp, J/mol.K
                                  1.16979        1.33875      Cp/Cv
                                  2966.57        337.320      Sound Speed, m/s
                                  -0.209608E-01 0.508656      JT, K/bar
                                  5114.70        180.042      Visc., uP
                                  643.930        25.5071      Th. Cond.,mW/m.K
(VLE=PRS,PROPS=EXCST)
For a list of available options, type ? Otherwise
enter command or, if you wish to do a flash calculation,
enter T(K) and P(bar) separated by a comma.
```

333.15,1

2-Phase Flash results at T = 333.150 K and P = 1.00000   bar

----Component------	---Feed---	--Liquid--	--Vapor---	---Phi----	--K--
nitrogen	0.833055E-05	0.157290E-06	0.358158	0.358430	.23E+07
oxygen	0.408418E-05	0.854500E-06	0.141528	0.141557	.17E+06
argon	0.186974E-06	0.381947E-07	0.651966E-02	0.652142E-02	.17E+06
carbon dioxide	0.381795E-04	0.314525E-04	0.294815	0.293892	.94E+04
water	0.999949	0.999967	0.198979	0.197782	.20E+00

Molar Basis

1.00000	0.999977	0.228202E-04	Feed Fraction
18.0211	18.0208	31.3818	Molar Mass
0.687051E-03	0.664287E-03	0.998177	Comp. Factor, Z
52.5465	54.3471	0.361680E-01	D, mol/liter
-283.225	-283.228	-162.995	H, kJ/mol
78.2425	78.2394	214.188	S, J/mol.K
73.5315	73.5324	33.3432	Cp, J/mol.K
	1.18333	1.33636	Cp/Cv
	2947.16	342.819	Sound Speed, m/s
	-0.207850E-01	0.541296	JT, K/bar
	4722.05	178.677	Visc., uP
	650.515	26.0218	Th. Cond.,mW/m.K

(VLE=PRS,PROPS=EXCST)
For a list of available options, type ? Otherwise
enter command or, if you wish to do a flash calculation,
enter T(K) and P(bar) separated by a comma.
338.15,1

2-Phase Flash results at T = 338.150 K and P = 1.00000   bar

----Component------	---Feed---	--Liquid--	--Vapor---	---Phi----	--K--
nitrogen	0.833055E-05	0.170017E-06	0.328901	0.329223	.19E+07
oxygen	0.408418E-05	0.865497E-06	0.129726	0.129778	.15E+06
argon	0.186974E-06	0.388077E-07	0.597171E-02	0.597455E-02	.15E+06
carbon dioxide	0.381795E-04	0.311150E-04	0.284758	0.283878	.92E+04
water	0.999949	0.999968	0.250644	0.249120	.25E+00

Molar Basis

1.00000	0.999975	0.248116E-04	Feed Fraction
18.0211	18.0208	30.6511	Molar Mass
0.680907E-03	0.656162E-03	0.997966	Comp. Factor, Z
52.2366	54.2065	0.356408E-01	D, mol/liter
-282.856	-282.858	-171.361	H, kJ/mol
79.3429	79.3396	214.254	S, J/mol.K
73.5839	73.5849	33.5673	Cp, J/mol.K
	1.19785	1.33363	Cp/Cv
	2928.60	349.043	Sound Speed, m/s
	-0.205963E-01	0.588638	JT, K/bar
	4375.04	176.560	Visc., uP
	656.778	26.5724	Th. Cond.,mW/m.K

(VLE=PRS,PROPS=EXCST)
For a list of available options, type ? Otherwise
enter command or, if you wish to do a flash calculation,
enter T(K) and P(bar) separated by a comma.
343.15,1

2-Phase Flash results at T = 343.150 K and P = 1.00000   bar

----Component------	---Feed---	--Liquid--	--Vapor---	---Phi----	--K--
nitrogen	0.833055E-05	0.177209E-06	0.292456	0.292840	.17E+07
oxygen	0.408418E-05	0.852608E-06	0.115916	0.115996	.14E+06
argon	0.186974E-06	0.383384E-07	0.533152E-02	0.533568E-02	.14E+06
carbon dioxide	0.381795E-04	0.305679E-04	0.273056	0.272223	.89E+04
water	0.999949	0.999968	0.313241	0.311289	.31E+00

Molar Basis

1.00000	0.999972	0.278789E-04	Feed Fraction
18.0211	18.0208	29.7758	Molar Mass
0.676138E-03	0.648342E-03	0.997674	Comp. Factor, Z
51.8386	54.0610	0.351317E-01	D, mol/liter
-282.487	-282.490	-181.721	H, kJ/mol
80.4252	80.4215	214.085	S, J/mol.K

Appendix B (Continued)

```
                      73.6530         73.6541     33.8314     Cp, J/mol.K
                                      1.21342     1.33058     Cp/Cv
                                      2910.91     356.232     Sound Speed, m/s
                                     -0.203943E-01 0.657058   JT, K/bar
                                      4067.22     173.651     Visc., uP
                                      662.720     27.1684     Th. Cond.,mW/m.K
(VLE=PRS,PROPS=EXCST)
For a list of available options, type ? Otherwise
enter command or, if you wish to do a flash calculation,
enter T(K) and P(bar) separated by a comma.
348.15,1


2-Phase Flash results at T =  348.150 K and P =  1.00000     bar

----Component------ ---Feed---   --Liquid--   --Vapor---   ---Phi----   --K--
nitrogen           0.833055E-05 0.175706E-06 0.248355     0.248816     .14E+07
oxygen             0.408418E-05 0.807485E-06 0.997923E-01 0.999089E-01 .12E+06
argon              0.186974E-06 0.364031E-07 0.458567E-02 0.459148E-02 .13E+06
carbon dioxide     0.381795E-04 0.296847E-04 0.258740     0.257968     .87E+04
water              0.999949     0.999969     0.388527     0.386000     .39E+00
Molar Basis
                    1.00000      0.999967     0.328354E-04 Feed Fraction
                    18.0211      18.0208      28.7214      Molar Mass
                    0.673540E-03 0.640815E-03 0.997272     Comp. Factor, Z
                    51.2911      53.9105      0.346411E-01 D, mol/liter
                   -282.119     -282.122     -194.119      H, kJ/mol
                    81.4902      81.4859      213.573      S, J/mol.K
                    73.7388      73.7401      34.1379      Cp, J/mol.K
                                 1.23010      1.32728      Cp/Cv
                                 2894.09      364.745      Sound Speed, m/s
                                -0.201789E-01 0.757657     JT, K/bar
                                 3793.21      169.625      Visc., uP
                                 668.338      27.8239      Th. Cond.,mW/m.K
(VLE=PRS,PROPS=EXCST)
For a list of available options, type ? Otherwise
enter command or, if you wish to do a flash calculation,
enter T(K) and P(bar) separated by a comma.
353.15,1


2-Phase Flash results at T =  353.150 K and P =  1.00000     bar

----Component------ ---Feed---   --Liquid--   --Vapor---   ---Phi----   --K--
nitrogen           0.833055E-05 0.161986E-06 0.196831     0.197385     .12E+07
oxygen             0.408418E-05 0.720114E-06 0.810616E-01 0.812226E-01 .11E+06
argon              0.186974E-06 0.325409E-07 0.372127E-02 0.372913E-02 .11E+06
carbon dioxide     0.381795E-04 0.282225E-04 0.239954     0.239281     .85E+04
water              0.999949     0.999971     0.478432     0.475112     .48E+00
Molar Basis
                    1.00000      0.999958     0.415005E-04 Feed Fraction
                    18.0211      18.0207      27.4376      Molar Mass
                    0.674910E-03 0.633572E-03 0.996706     Comp. Factor, Z
                    50.4623      53.7548      0.341701E-01 D, mol/liter
                   -281.751     -281.754     -208.291      H, kJ/mol
                    82.5390      82.5336      212.554      S, J/mol.K
                    73.8415      73.8432      34.4836      Cp, J/mol.K
                                 1.24796      1.32396      Cp/Cv
                                 2878.14      375.167      Sound Speed, m/s
                                -0.199497E-01 0.910718     JT, K/bar
                                 3548.48      164.386      Visc., uP
                                 673.632      28.5632      Th. Cond.,mW/m.K
(VLE=PRS,PROPS=EXCST)
For a list of available options, type ? Otherwise
enter command or, if you wish to do a flash calculation,
enter T(K) and P(bar) separated by a comma.
358.15,1


2-Phase Flash results at T =  358.150 K and P =  1.00000     bar

----Component------ ---Feed---   --Liquid--   --Vapor---   ---Phi----   --K--
nitrogen           0.833055E-05 0.133193E-06 0.139622     0.140262     .10E+07
oxygen             0.408418E-05 0.580861E-06 0.596710E-01 0.598798E-01 .10E+06
```

Appendix B (Continued)

```
argon               0.186974E-06 0.263063E-07 0.273661E-02 0.274667E-02 .10E+06
carbon dioxide      0.381795E-04 0.256809E-04 0.212908     0.212416     .83E+04
water               0.999949     0.999974     0.585062     0.580665     .59E+00
Molar Basis
                    1.00000      0.999941     0.587112E-04 Feed Fraction
                    18.0211      18.0207      25.8425      Molar Mass
                    0.685034E-03 0.626603E-03 0.995858     Comp. Factor, Z
                    49.0224      53.5938      0.337217E-01 D, mol/liter
                    -281.383     -281.387     -223.258     H, kJ/mol
                    83.5729      83.5654      210.774      S, J/mol.K
                    73.9614      73.9637      34.8491      Cp, J/mol.K
                                 1.26709      1.32111      Cp/Cv
                                 2863.07      388.563      Sound Speed, m/s
                                 -0.197064E-01 1.15016     JT, K/bar
                                 3329.19      157.890      Visc., uP
                                 678.600      29.4386      Th. Cond.,mW/m.K
(VLE=PRS,PROPS=EXCST)
For a list of available options, type ? Otherwise
enter command or, if you wish to do a flash calculation,
enter T(K) and P(bar) separated by a comma.
stop
```

Appendix C. Matlab code for F_{CT} data regression

```
% Non-Linear Least-Squares Regression of Condenser Tube Counter Current Departure
Correction Factor

a = 0.0293;
b = 0.1655;
c = 2.9102;
d = 6.1629;
e = 4.2518;

T_P = Parameters(:,2);
T_E = Parameters(:,5);
T_X = Parameters(:,6);
F_CT = Parameters(:,10);

S_CT = ( T_X - T_P ) ./ ( T_E - T_P );

% Global Variables, Initial Guesses, & Options

global S_CT F_CT;
parameters =[a b c d e];
OPTIONS(1)=0;

% The Fun Function ( An m-File )

    % function f=fun(parameters);
    % global S_CT F_CT;
    % a = parameters(1,1);
    % b = parameters(1,2);
    % c = parameters(1,3);
    % d = parameters(1,4);
    % e = parameters(1,5);
    % Fc_CT = a + b .* S_CT + c .* S_CT .^ 2 - d .* S_CT .^ 3 + e .* S_CT .^ 4;
    % f = sum ( ( Fc_CT - F_CT ) .^ 2 );

% Regression & Results, Fc_CT = Calculated Condenser Tube Counter Current Departure Correction Factor

x=fminsearch('fun(x)',parameters,OPTIONS);
a=x(1,1);
b=x(1,2);
c=x(1,3);
d=x(1,4);
e=x(1,5);
a = 0.021965104279624;
b = 0.275138363079761;
c = 2.449155721049220;
d = 5.436838343831495;
e = 3.869806028493753;

Fc_CT = a + b .* S_CT + c .* S_CT .^ 2 - d .* S_CT .^ 3 + e .* S_CT .^ 4;
r = corr2(F_CT,Fc_CT);
r = 0.995860313403891;

plot(S_CT(1:170),F_CT(1:170),'m:',S_CT(171:340),F_CT(171:340),'m:',S_CT(341:510),F_CT(341
:510),'m:',S_CT(511:680),F_CT(511:680),'m:',S_CT(681:850),F_CT(681:850),'m:',S_CT(851:102
0),F_CT(851:1020),'m:',S_CT(1021:1190),F_CT(1021:1190),'m:',S_CT(1191:1360),F_CT(1191:136
0),'m:',S_CT(1:170),Fc_CT(1:170),'k-',S_CT(171:340),Fc_CT(171:340),'k-
',S_CT(341:510),Fc_CT(341:510),'k-',S_CT(511:680),Fc_CT(511:680),'k-
',S_CT(681:850),Fc_CT(681:850),'k-',S_CT(851:1020),Fc_CT(851:1020),'k-
',S_CT(1021:1190),Fc_CT(1021:1190),'k-',S_CT(1191:1360),Fc_CT(1191:1360),'k-'),...
axis([0 1 0 1]),xlabel('S_C_T'),ylabel('F_C_T'),gtext('^.^.^.^. = mined data'),gtext('– =
regression'),gtext('r = +0.9958603')
```

Appendix D. Matlab code for *NEA* data regression

```
% Non-Linear Least-Squares Regression of Non-Equilibrium Allowance Ratio

a = 1.6836;
b = 3.3898;
c = 2.7785;
d = 0.1399;
e = 5.9154;
f = 29.3208;

T0 = 273.15;
Tr = 298.15;
T_H = Parameters(:,7);
T_E = Parameters(:,5);
T_W = Parameters(:,4);

R1 = ( T_H + T0 ) ./ Tr;
R2 = ( T_W + T0 ) ./ ( T_E + T0 );

% Global Variables, Initial Guesses, & Options

global R1 R2;
parameters =[a b c d e f];
OPTIONS(1)=0;

% The Fun Function ( An m-File )

    % function f=fun(parameters);
    % global R1 R2;
    % a = parameters(1,1);
    % b = parameters(1,2);
    % c = parameters(1,3);
    % d = parameters(1,4);
    % e = parameters(1,5);
    % f = parameters(1,6);
    % R2c = a .* R1 .^ 2 - b .* R1 + c - d .* exp ( - e .* R1 .^ - f );
    % f = sum ( ( R2c - R2 ) .^ 2 );

% Regression & Results, R2c = Calculated Non-Equilibrium Allowance Ratio

x=fminsearch('fun(x)',parameters,OPTIONS);
a=x(1,1);
b=x(1,2);
c=x(1,3);
d=x(1,4);
e=x(1,5);
f=x(1,6);
a = 1.346445189163027;
b = 2.976010121977662;
c = 2.674925159910569;
d = 0.099408245751382;
e = 11.939078418864948;
f = 28.250917259494326;

R2c = a .* R1 .^ 2 - b .* R1 + c - d .* exp ( - e .* R1 .^ - f );
r = corr2(R2,R2c);
r = 0.948793730491143;

plot(R1(1:170),R2(1:170),'m:',R1(171:340),R2(171:340),'m:',R1(341:510),R2(341:510),'m:',R
1(511:680),R2(511:680),'m:',R1(681:850),R2(681:850),'m:',R1(851:1020),R2(851:1020),'m:',R
1(1021:1190),R2(1021:1190),'m:',R1(1191:1360),R2(1191:1360),'m:',R1(1:170),R2c(1:170),'k-
',R1(171:340),R2c(171:340),'k-',R1(341:510),R2c(341:510),'k-
',R1(511:680),R2c(511:680),'k-',R1(681:850),R2c(681:850),'k-
',R1(851:1020),R2c(851:1020),'k-',R1(1021:1190),R2c(1021:1190),'k-
',R1(1191:1360),R2c(1191:1360),'k-'),...
axis([1.05 1.20 0.92 1.02]),xlabel('( T_H + 273.15 ) / ( 25 + 273.15 )'),ylabel('( T_W +
273.15 ) / ( T_E + 273.15 )'),gtext('^.^.^.^. = experiment'),gtext('- =
regression'),gtext('r = +0.9487937')
```

Appendix E. Matlab code for γ_{H2O} data regression

```
% Non-Linear Least-Squares Regression of Water Activity Coefficient

b = 0.0020;
m = 1.0385;

PA = 12.762946317344;
PB = 4391.12942196166;
PC = 245.367016018802;

T_E = Parameters(:,5);
P_V = Parameters(:,1);
gamma_H2O = Parameters(:,8);

P_H2O = exp ( PA - PB ./ ( T_E + PC ) );
PoP = P_V ./ P_H2O;

% Global Variables, Initial Guesses, & Options

global PoP gamma_H2O;
parameters =[b m];
OPTIONS(1)=0;

% The Fun Function ( An m-File )

    % function f=fun(parameters);
    % global PoP gamma_H2O;
    % b = parameters(1,1);
    % m = parameters(1,2);
    % gammac_H2O = b + m .* PoP;
    % f = sum ( ( gammac_H2O - gamma_H2O ) .^ 2 );

% Regression & Results, gammac_H2O = Calculated Water Activity Coefficient

x=fminsearch('fun(x)',parameters,OPTIONS);
b=x(1,1);
m=x(1,2);
b = 0.002040679931641;
m = 1.038442953491211;

gammac_H2O = b + m .* PoP;
r = corr2(gamma_H2O,gammac_H2O);
r = 0.999999864855922;

plot(PoP(1:170),gamma_H2O(1:170),'m:',PoP(171:340),gamma_H2O(171:340),'m:',PoP(341:510),g
amma_H2O(341:510),'m:',PoP(511:680),gamma_H2O(511:680),'m:',PoP(681:850),gamma_H2O(681:85
0),'m:',PoP(851:1020),gamma_H2O(851:1020),'m:',PoP(1021:1190),gamma_H2O(1021:1190),'m:',P
oP(1191:1360),gamma_H2O(1191:1360),'m:',PoP(1:170),gammac_H2O(1:170),'k-
',PoP(171:340),gammac_H2O(171:340),'k-',PoP(341:510),gammac_H2O(341:510),'k-
',PoP(511:680),gammac_H2O(511:680),'k-',PoP(681:850),gammac_H2O(681:850),'k-
',PoP(851:1020),gammac_H2O(851:1020),'k-',PoP(1021:1190),gammac_H2O(1021:1190),'k-
',PoP(1191:1360),gammac_H2O(1191:1360),'k-'),...
axis([1 5 1 5]),xlabel('P_V / P_H_2_O'),ylabel('\gamma_H_2_O'),gtext('^.^.^.^. = mined
data'),gtext('- = regression'),gtext('r = +0.9999999')
```

Appendix F. Matlab code for ψ data regression

```
% Non-Linear Least-Squares Regression of Fraction of NCG Molecules Accumulating

a = 2.29;

PA = 12.762946317344;
PB = 4391.12942196166;
PC = 245.367016018802;

T_E = Parameters(:,5);
P_V = Parameters(:,1);
psi = Parameters(:,9);

P_H2O = exp ( PA - PB ./ ( T_E + PC ) );
PoP = P_V ./ P_H2O;

% Global Variables, Initial Guesses, & Options

global PoP psi;
parameters =[a];
OPTIONS(1)=0;

% The Fun Function ( An m-File )

    % function f=fun(parameters);
    % global PoP psi;
    % a = parameters(1,1);
    % psic = 1 - a .* exp ( - PoP );
    % f = sum ( ( psic - psi ) .^ 2 );

% Regression & Results, psic = Calculated Fraction of NCG Molecules Accumulating

x=fminsearch('fun(x)',parameters,OPTIONS);
a=x(1,1);
a = 2.276134765625000;

psic = 1 - a .* exp ( - PoP );
r = corr2(psi,psic);
r = 0.991470128181259;

plot(PoP(1:170),psi(1:170),'m:',PoP(171:340),psi(171:340),'m:',PoP(341:510),psi(341:510),
'm:',PoP(511:680),psi(511:680),'m:',PoP(681:850),psi(681:850),'m:',PoP(851:1020),psi(851:
1020),'m:',PoP(1021:1190),psi(1021:1190),'m:',PoP(1191:1360),psi(1191:1360),'m:',PoP(1:17
0),psic(1:170),'k-',PoP(171:340),psic(171:340),'k-',PoP(341:510),psic(341:510),'k-
',PoP(511:680),psic(511:680),'k-',PoP(681:850),psic(681:850),'k-
',PoP(851:1020),psic(851:1020),'k-',PoP(1021:1190),psic(1021:1190),'k-
',PoP(1191:1360),psic(1191:1360),'k-'),...
axis([1 5 0 1.5]),xlabel('P_V / P_H_2_0'),ylabel('\psi'),gtext('^.^.^.^. = mined
data'),gtext('— = regression'),gtext('r = +0.9914701')
```

Appendix G. Matlab code for HC_{N2} data regression

```
% Non-Linear Least-Squares Regression of Temperature-Henry's Constant
% Data for Nitrogen Obtained from NIST's SUPERTRAPP Program at 1 bar

T0 = 273.15;
Tr = 298.15;
HRI_N2 = 91973;
HFI_N2 = 1300;
T = [15 20 25 30 35 40 45 50 55 60 65 70 75 80 85]';
HC_N2 = [1.20E+07 1.00E+07 8.20E+06 6.70E+06 5.50E+06 4.60E+06 3.80E+06 3.20E+06 ...
         2.70E+06 2.30E+06 1.90E+06 1.70E+06 1.40E+06 1.20E+06 1.00E+06]';

% Global Variables, Initial Guesses, & Options

global T HC_N2;
parameters =[HRI_N2 HFI_N2];
OPTIONS(1)=0;

% The Fun Function ( An m-File )

    % function f=fun(parameters);
    % global T HC_N2;
    % HR_N2 = parameters(1,1);
    % HF_N2 = parameters(1,2);
    % HCc_N2 = HR_N2 .* exp ( - HF_N2 .* ( ( 1 ./ ( T + 273.15 ) ) - ( 1 ./ 298.15 ) ) );
    % f = sum ( ( HCc_N2 - HC_N2 ) .^ 2 );

% Regression & Results, HCc_N2 = Calculated Henry's Constant

x=fminsearch('fun(x)',parameters,OPTIONS);
HR_N2=x(1,1);
HF_N2=x(1,2);
HR_N2 = 8.0676e+006;
HF_N2 = -3.5456e+003;

HCc1_N2 = HR_N2 .* exp ( - HF_N2 .* ( ( 1 ./ ( T + T0 ) ) - ( 1 ./ Tr ) ) );
HCc2_N2 = HRI_N2 .* exp ( - HFI_N2 .* ( ( 1 ./ ( T + T0 ) ) - ( 1 ./ Tr ) ) );

r = corr2(HC_N2,HCc1_N2);
r = 0.999717396687485;

plot(T,HC_N2,'mo',T,HCc1_N2,'k-',T,HCc2_N2,'m:'),xlabel('Temperature
(°C)'),ylabel('HC_N_2 (bar)'),...
axis([0 100 0 14e6]),gtext('o  = NIST'),gtext('- = regression'),gtext('^.^.^.^. =
Sander'),gtext('r = +0.9997174')
```

Appendix H. Matlab code for HC_{O2} data regression

```
% Non-Linear Least-Squares Regression of Temperature-Henry's Constant
% Data for Oxygen Obtained from NIST's SUPERTRAPP Program at 1 bar

TO = 273.15;
Tr = 298.15;
HRI_O2 = 43154;
HFI_O2 = 1700;
T = [15 20 25 30 35 40 45 50 55 60 65 70 75 80 85]';
HC_O2 = [4.60E+05 4.10E+05 3.60E+05 3.20E+05 2.80E+05 2.50E+05 2.30E+05 2.00E+05 ...
         1.80E+05 1.70E+05 1.50E+05 1.40E+05 1.20E+05 1.10E+05 1.00E+05]';

% Global Variables, Initial Guesses, & Options

global T HC_O2;
parameters =[HRI_O2 HFI_O2];
OPTIONS(1)=0;

% The Fun Function ( An m-File )

    % function f=fun(parameters);
    % global T HC_O2;
    % HR_O2 = parameters(1,1);
    % HF_O2 = parameters(1,2);
    % HCc_O2 = HR_O2 .* exp ( - HF_O2 .* ( ( 1 ./ ( T + 273.15 ) ) - ( 1 ./ 298.15 ) ) );
    % f = sum ( ( HCc_O2 - HC_O2 ) .^ 2 );

% Regression & Results, HCc_O2 = Calculated Henry's Constant

x=fminsearch('fun(x)',parameters,OPTIONS);
HR_O2=x(1,1);
HF_O2=x(1,2);
HR_O2 = 3.5881e+005;
HF_O2 = -2.2088e+003;

HCc1_O2 = HR_O2 .* exp ( - HF_O2 .* ( ( 1 ./ ( T + TO ) ) - ( 1 ./ Tr ) ) );
HCc2_O2 = HRI_O2 .* exp ( - HFI_O2 .* ( ( 1 ./ ( T + TO ) ) - ( 1 ./ Tr ) ) );

r = corr2(HC_O2,HCc1_O2);
r = 0.999564809550137;

plot(T,HC_O2,'mo',T,HCc1_O2,'k-',T,HCc2_O2,'m:'),xlabel('Temperature
(°C)'),ylabel('HC_O_2 (bar)'),...
axis([0 100 0 5e5]),gtext('o  = NIST'),gtext('- = regression'),gtext('^.^.^.^. =
Sander'),gtext('r = +0.9995648')
```

Appendix I. Matlab code for HC_{Ar} data regression

```
% Non-Linear Least-Squares Regression of Temperature-Henry's Constant
% Data for Argon Obtained from NIST's SUPERTRAPP Program at 1 bar

T0 = 273.15;
Tr = 298.15;
HRI_Ar = 40074;
HFI_Ar = 1300;
T = [15 20 25 30 35 40 45 50 55 60 65 70 75 80 85]';
HC_Ar = [5.00E+05 4.40E+05 3.80E+05 3.40E+05 3.00E+05 2.70E+05 2.40E+05 2.10E+05 ...
         1.90E+05 1.70E+05 1.50E+05 1.40E+05 1.30E+05 1.10E+05 1.00E+05]';

% Global Variables, Initial Guesses, & Options

global T HC_Ar;
parameters =[HRI_Ar HFI_Ar];
OPTIONS(1)=0;

% The Fun Function ( An m-File )

    % function f=fun(parameters);
    % global T HC_Ar;
    % HR_Ar = parameters(1,1);
    % HF_Ar = parameters(1,2);
    % HCc_Ar = HR_Ar .* exp ( - HF_Ar .* ( ( 1 ./ ( T + 273.15 ) ) - ( 1 ./ 298.15 ) ) );
    % f = sum ( ( HCc_Ar - HC_Ar ) .^ 2 );

% Regression & Results, HCc_Ar = Calculated Henry's Constant

x=fminsearch('fun(x)',parameters,OPTIONS);
HR_Ar=x(1,1);
HF_Ar=x(1,2);
HR_Ar = 3.8407e+005;
HF_Ar = -2.3080e+003;

HCc1_Ar = HR_Ar .* exp ( - HF_Ar .* ( ( 1 ./ ( T + T0 ) ) - ( 1 ./ Tr ) ) );
HCc2_Ar = HRI_Ar .* exp ( - HFI_Ar .* ( ( 1 ./ ( T + T0 ) ) - ( 1 ./ Tr ) ) );

r = corr2(HC_Ar,HCc1_Ar);
r = 0.999658097432208;

plot(T,HC_Ar,'mo',T,HCc1_Ar,'k-',T,HCc2_Ar,'m:'),xlabel('Temperature
(°C)'),ylabel('HC_A_r (bar)'),...
axis([0 100 0 6e5]),gtext('o  = NIST'),gtext('- = regression'),gtext('^.^.^.^. =
Sander'),gtext('r = +0.9996581')
```

208

Appendix J. Matlab code for HC_{CO_2} data regression

```
% Non-Linear Least-Squares Regression of Temperature-Henry's Constant
% Data for Carbon Dioxide Obtained from NIST's SUPERTRAPP Program at 1 bar

T0 = 273.15;
Tr = 298.15;
HRI_CO2 = 1652;
HFI_CO2 = 2400;
T = [15 20 25 30 35 40 45 50 55 60 65 70 75 80 85]';
HC_CO2 = [1.10E+04 1.10E+04 1.10E+04 1.10E+04 1.10E+04 1.00E+04 1.00E+04 9.80E+03 ...
          9.60E+03 9.40E+03 9.20E+03 8.90E+03 8.70E+03 8.50E+03 8.30E+03]';

% Global Variables, Initial Guesses, & Options

global T HC_CO2;
parameters =[HRI_CO2 HFI_CO2];
OPTIONS(1)=0;

% The Fun Function ( An m-File )

    % function f=fun(parameters);
    % global T HC_CO2;
    % HR_CO2 = parameters(1,1);
    % HF_CO2 = parameters(1,2);
    % HCc_CO2 = HR_CO2 .* exp ( - HF_CO2 .* ( ( 1 ./ ( T + 273.15 ) ) - ( 1 ./ 298.15 ) ) );
    % f = sum ( ( HCc_CO2 - HC_CO2 ) .^ 2 );

% Regression & Results, HCc_CO2 = Calculated Henry's Constant

x=fminsearch('fun(x)',parameters,OPTIONS);
HR_CO2=x(1,1);
HF_CO2=x(1,2);
HR_CO2 = 1.0915e+004;
HF_CO2 = -445.1906;

HCc1_CO2 = HR_CO2 .* exp ( - HF_CO2 .* ( ( 1 ./ ( T + T0 ) ) - ( 1 ./ Tr ) ) );
HCc2_CO2 = HRI_CO2 .* exp ( - HFI_CO2 .* ( ( 1 ./ ( T + T0 ) ) - ( 1 ./ Tr ) ) );

r = corr2(HC_CO2,HCc1_CO2);
r = 0.966663199694565;

plot(T,HC_CO2,'mo',T,HCc1_CO2,'k-',T,HCc2_CO2,'m:'),xlabel('Temperature
(°C)'),ylabel('HC_C_O_2 (bar)'),...
axis([0 100 0 1.2e4]),gtext('o  = NIST'),gtext('— = regression'),gtext('^.^.^.^. =
Sander'),gtext('r = +0.9666632')
```

Appendix K. Matlab code for $P_{H2O}{}^{sat}$ data regression

```
% Non-Linear Least-Squares Regression of Temperature-Saturated Pressure
% Data for Water Obtained from NIST's SUPERTRAPP Program at 1 bar

PAI  = 12;
PBI  = 3993;
PCI  = 234;

T = [15 20 25 30 35 40 45 50 55 60 65 70 75 80 85]';
P_H2O = [1.60E-02 2.20E-02 3.10E-02 4.10E-02 5.50E-02 7.20E-02 9.50E-02 1.20E-01 ...
            1.60E-01 2.00E-01 2.50E-01 3.10E-01 3.90E-01 4.80E-01 5.90E-01]';

% Global Variables, Initial Guesses, & Options

global T P_H2O;
parameters =[PAI PBI PCI];
OPTIONS(1)=0;

% The Fun Function ( An m-File )

    % function f=fun(parameters);
    % global T P_H2O;
    % PA = parameters(1,1);
    % PB = parameters(1,2);
    % PC = parameters(1,3);
    % PPC = exp ( PA - ( PB ./ ( T + PC )));
    % f = sum ( ( PPC - P_H2O ) .^ 2 );

% Regression & Results, PsatPC = Calculated Saturated Pressure

x=fminsearch('fun(x)',parameters,OPTIONS);
PA=x(1,1);
PB=x(1,2);
PC=x(1,3);
PA = 12.7629;
PB = 4.3911e+003;
PC = 245.3670;

Pc1_H2O = exp ( PA - ( PB ./ ( T + PC )));
Pc2_H2O = exp ( PAI - ( PBI ./ ( T + PCI )));

r = corr2(P_H2O,Pc1_H2O);
r = 0.999963505331023;

plot(T,P_H2O,'mo',T,Pc1_H2O,'k-',T,Pc2_H2O,'m:'),xlabel('Temperature
(°C)'),ylabel('P^s^a^t_H_2_O (bar)'),...
axis([0  100  0  0.7]),gtext('o   =  NIST'),gtext('- =  regression'),gtext('^.^.^.^.  =
Geankoplis'),gtext('r = +0.9999635')
```

Appendix L. Sample TK Solver code for data mining

Rules Sheet

Rules

; Material Balance

$$SG\_H = \frac{1000 \cdot \rho\_H}{\rho C\_H}$$

$$FI = CV \cdot \left[\frac{P - P\_V}{SG\_H}\right]^{0.5}$$

$V\_V = Vi\_V - 1000 \cdot FI \cdot t$

$M\_P = 1000 \cdot \rho \cdot FI$

$M\_X = M\_P$

$M\_H = M\_X$

$\Sigma M = \rho \cdot QE$

$N\_H = N\_E + N\_W$

$N\_E = N\_C + Na\_C$

$Na\_C = (1 - y\_H2O) \cdot N\_E$

$M\_H = M\_E + M\_W$

$M\_E = M\_C + Ma\_C$

$\Phi\_H \cdot M\_H = \Phi\_W \cdot M\_W$

$M\_H = N\_H \cdot MW\_H$

$$Md\_E = \sigma \cdot XA\_E \cdot \left[\frac{(1 - 0.54 \cdot \Phi\_W) \cdot \left[e^{\left[PA - \frac{PB}{T\_W + PC}\right]}\right]}{\sqrt{T\_W + 273.15}} - \frac{e^{\left[PA - \frac{PB}{T\_C + PC}\right]}}{\sqrt{T\_C + 273.15}} + \Omega\right]$$

$\Sigma Md\_E = \text{INTEGRAL}(" Md\_E , t ", \text{ELT}('t , \text{ELT}() - 1 , ti) , t) + \text{ELT}('\Sigma Md\_E , \text{ELT}() - 1 , 0)$

$M\_W = N\_W \cdot MW\_W - Md\_E$

$M\_E = N\_E \cdot MW\_E + Md\_E$

$Ma\_C = Na\_C \cdot MWa\_C$

; Parameters

$$hi\_CT = 0.0003052505007075309 \cdot \left[\frac{1.35 + 0.02 \cdot T\_X}{D\_CT}\right] \cdot \left[\frac{M\_X}{\rho\_X \cdot D\_CT}\right]^{0.8}$$

$$ho\_CT = 0.725 \cdot \left[\frac{g \cdot HL\_E \cdot \rho\_X^2 \cdot k\_X^3}{N\_CT \cdot \mu\_X \cdot (D\_CT + \delta\_CT) \cdot (T\_E - T\_X)}\right]^{0.25}$$

Appendix L (Continued)

Rules

$$\frac{1}{U\_CT} = \frac{1}{ho\_CT} + \frac{1}{hod\_CT} + \frac{D\_CT + \delta\_CT}{D\_CT \cdot hi\_CT} + \frac{D\_CT + \delta\_CT}{D\_CT \cdot hid\_CT} + \frac{D\_CT + \delta\_CT}{2 \cdot kw\_CT} \cdot LN\left[\frac{D\_CT + \delta\_CT}{D\_CT}\right]$$

$$\Delta Tm\_CT = \frac{T\_X - T\_P}{LN\left[\frac{T\_E - T\_P}{T\_E - T\_X}\right]}$$

$$A\_CT = \pi \cdot D\_CT \cdot L\_CT$$

$$M\_X \cdot H\_X - M\_P \cdot H\_P = 60 \cdot U\_CT \cdot A\_CT \cdot F\_CT \cdot \Delta Tm\_CT$$

$$hi\_C = 1.13 \cdot \left[\frac{g \cdot HL\_E \cdot \rho\_C^2 \cdot k\_C^3}{\mu\_C \cdot L\_C \cdot (T\_E - T)}\right]^{0.25}$$

$$ho\_C = 0.04477637899495253 \cdot \left[\frac{T\_E - T}{L\_C}\right]^{0.25}$$

$$\frac{1}{U\_C} = \frac{1}{ho\_C} + \frac{1}{hod\_C} + \frac{D\_C + \delta\_C}{D\_C \cdot hi\_C} + \frac{D\_C + \delta\_C}{D\_C \cdot hid\_C} + \frac{D\_C + \delta\_C}{2 \cdot kw\_C} \cdot LN\left[\frac{D\_C + \delta\_C}{D\_C}\right]$$

$$\Delta Tm\_C = \frac{T\_C - T}{LN\left[\frac{T\_E - T}{T\_E - T\_C}\right]}$$

$$A\_C = \pi \cdot D\_C \cdot L\_C$$

$$-Q\_C = 60 \cdot U\_C \cdot A\_C \cdot F\_C \cdot \Delta Tm\_C$$

$$hi\_E = 1.13 \cdot \left[\frac{g \cdot HL\_E \cdot \rho\_W^2 \cdot k\_W^3}{\mu\_W \cdot L\_E \cdot (T\_E - T)}\right]^{0.25}$$

$$ho\_E = 0.04477637899495253 \cdot \left[\frac{T\_E - T}{L\_E}\right]^{0.25}$$

$$\frac{1}{U\_E} = \frac{1}{ho\_E} + \frac{1}{hod\_E} + \frac{D\_E + \delta\_E}{D\_E \cdot hi\_E} + \frac{D\_E + \delta\_E}{D\_E \cdot hid\_E} + \frac{D\_E + \delta\_E}{2 \cdot kw\_E} \cdot LN\left[\frac{D\_E + \delta\_E}{D\_E}\right]$$

$$\Delta Tm\_E = \frac{T\_W - T}{LN\left[\frac{T\_E - T}{|T\_E - T\_W|}\right]}$$

$$A\_E = \pi \cdot D\_E \cdot L\_E$$

$$-Q\_E = 60 \cdot U\_E \cdot A\_E \cdot F\_E \cdot \Delta Tm\_E$$

$$Q\_C - W\_C + Ein\_C - Eout\_C = Ea\_C$$

$$Ein\_C = M\_P \cdot H\_P + M\_E \cdot (H\_E + HL\_E)$$

$$Eout\_C = M\_X \cdot H\_X + M\_C \cdot H\_C$$

$$Ea\_C = Ma\_C \cdot Ha\_C$$

$$Q\_E - W\_E + Ein\_E - Eout\_E = Ed\_E$$

$$Ein\_E = M\_H \cdot H\_H$$

$$Eout\_E = M\_W \cdot H\_W + M\_E \cdot (H\_E + HL\_E)$$

212

Rules

$Ed\_E = Md\_E \cdot (H\_W - H\_E - HL\_E)$

$k\_X = 0.00571116 + 0.00001713348 \cdot T\_X - 0.00000005853939 \cdot T\_X^2 - 0.0016562364 \cdot \Phi\_X$

$k\_W = 0.00571116 + 0.00001713348 \cdot T\_W - 0.00000005853939 \cdot T\_W^2 - 0.0016562364 \cdot \Phi\_W$

$k\_C = 0.00571116 + 0.00001713348 \cdot T\_C - 0.00000005853939 \cdot T\_C^2 - 0.0016562364 \cdot \Phi\_C$

$$\Delta P\_E = \frac{6.7906109052542E\text{-}07 \cdot \mu\_E \cdot PL\_E \cdot M\_E}{\rho\_E \cdot PD\_E^4}$$

$$\rho\_E = e^{\left[-13.4579133153846 + 4.1055E\text{-}2 \cdot (1.8 \cdot T\_E + 32) - 7.1159E\text{-}5 \cdot (1.8 \cdot T\_E + 32)^2 + 5.7039E\text{-}8 \cdot (1.8 \cdot T\_E + 32)^3\right]}$$

$\mu\_E = 7.23123710739283E\text{-}5 + 2.37506847313357E\text{-}07 \cdot (1.8 \cdot T\_E + 32) - 5.67031837890055E\text{-}11 \cdot (1.8 \cdot T\_E + 32)^2$

$\mu A\_X = 1.0675E\text{-}4 + 5.185E\text{-}5 \cdot T\_X$

$\mu B\_X = 2.591E\text{-}3 + 3.3E\text{-}5 \cdot T\_X$

$\mu C\_X = 553.541280340981 \cdot \rho\_X \cdot \Phi\_X$

$$\mu D\_X = 0.01002 \cdot 10^{\left[\frac{1.1709 \cdot (20 - T\_X) - 1.827E\text{-}3 \cdot (T\_X - 20)^2}{T\_X + 89.93}\right]}$$

$$\mu\_X = \left[1 + \mu A\_X \cdot \mu C\_X^{0.5} + \mu B\_X \cdot \mu C\_X\right] \cdot \mu D\_X$$

$\rho A\_X = 0.824493 + T\_X \cdot (-0.0040899 + T\_X \cdot (0.000076438 + T\_X \cdot (-0.00000082467 + T\_X \cdot 0.0000000053875)))$

$\rho B\_X = -0.00572466 + T\_X \cdot (0.00010227 - 0.0000016546 \cdot T\_X)$

$\rho C\_X = 999.842594 + T\_X \cdot (0.06793952 + T\_X \cdot (-0.009095290 + T\_X \cdot (0.0001001685 + T\_X \cdot (-0.000001120083 +$

$$\rho\_X = \frac{\rho C\_X}{1000} + \Phi\_X \cdot \left[\rho A\_X + \rho B\_X \cdot (1000 \cdot \Phi\_X)^{0.5} + 0.48314 \cdot \Phi\_X\right]$$

$\mu A\_W = 1.0675E\text{-}4 + 5.185E\text{-}5 \cdot T\_W$

$\mu B\_W = 2.591E\text{-}3 + 3.3E\text{-}5 \cdot T\_W$

$\mu C\_W = 553.541280340981 \cdot \rho\_W \cdot \Phi\_W$

$$\mu D\_W = 0.01002 \cdot 10^{\left[\frac{1.1709 \cdot (20 - T\_W) - 1.827E\text{-}3 \cdot (T\_W - 20)^2}{T\_W + 89.93}\right]}$$

$$\mu\_W = \left[1 + \mu A\_W \cdot \mu C\_W^{0.5} + \mu B\_W \cdot \mu C\_W\right] \cdot \mu D\_W$$

$\rho A\_W = 0.824493 + T\_W \cdot (-0.0040899 + T\_W \cdot (0.000076438 + T\_W \cdot (-0.00000082467 + T\_W \cdot 0.0000000053875$

$\rho B\_W = -0.00572466 + T\_W \cdot (0.00010227 - 0.0000016546 \cdot T\_W)$

$\rho C\_W = 999.842594 + T\_W \cdot (0.06793952 + T\_W \cdot (-0.009095290 + T\_W \cdot (0.0001001685 + T\_W \cdot (-0.00000112000$

$$\rho\_W = \frac{\rho C\_W}{1000} + \Phi\_W \cdot \left[\rho A\_W + \rho B\_W \cdot (1000 \cdot \Phi\_W)^{0.5} + 0.48314 \cdot \Phi\_W\right]$$

Appendix L (Continued)

$\mu A\_C = 1.0675E\text{-}4 + 5.185E\text{-}5 \cdot T\_C$

$\mu B\_C = 2.591E\text{-}3 + 3.3E\text{-}5 \cdot T\_C$

$\mu C\_C = 553.541280340981 \cdot \rho\_C \cdot \Phi\_C$

$\mu D\_C = 0.01002 \cdot 10^{\left[\dfrac{1.1709 \cdot (20 - T\_C) - 1.827E\text{-}3 \cdot (T\_C - 20)^2}{T\_C + 89.93}\right]}$

$\mu\_C = \left[1 + \mu A\_C \cdot \mu C\_C^{0.5} + \mu B\_C \cdot \mu C\_C\right] \cdot \mu D\_C$

$\rho A\_C = 0.824493 + T\_C \cdot (-0.0040899 + T\_C \cdot (0.000076438 + T\_C \cdot (-0.00000082467 + T\_C \cdot 0.0000000053875)))$

$\rho B\_C = -0.00572466 + T\_C \cdot (0.00010227 - 0.0000016546 \cdot T\_C)$

$\rho C\_C = 999.842594 + T\_C \cdot (0.06793952 + T\_C \cdot (-0.009095290 + T\_C \cdot (0.0001001685 + T\_C \cdot (-0.000001120083$

$\rho\_C = \dfrac{\rho C\_C}{1000} + \Phi\_C \cdot \left[\rho A\_C + \rho B\_C \cdot (1000 \cdot \Phi\_C)^{0.5} + 0.48314 \cdot \Phi\_C\right]$

$\rho A\_H = 0.824493 + T\_H \cdot (-0.0040899 + T\_H \cdot (0.000076438 + T\_H \cdot (-0.00000082467 + T\_H \cdot 0.0000000053875)))$

$\rho B\_H = -0.00572466 + T\_H \cdot (0.00010227 - 0.0000016546 \cdot T\_H)$

$\rho C\_H = 999.842594 + T\_H \cdot (0.06793952 + T\_H \cdot (-0.009095290 + T\_H \cdot (0.0001001685 + T\_H \cdot (-0.000001120083$

$\rho\_H = \dfrac{\rho C\_H}{1000} + \Phi\_H \cdot \left[\rho A\_H + \rho B\_H \cdot (1000 \cdot \Phi\_H)^{0.5} + 0.48314 \cdot \Phi\_H\right]$

$\Sigma M\_C = \text{INTEGRAL}(\text{" } M\_C \text{ , t "} , \text{ELT('t , ELT() - 1 , ti) , t)} + \text{ELT('}\Sigma M\_C \text{ , ELT() - 1 , 0)}$

$\Sigma Na\_C = \text{INTEGRAL}(\text{" } Na\_C \text{ , t "} , \text{ELT('t , ELT() - 1 , ti) , t)} + \text{ELT('}\Sigma Na\_C \text{ , ELT() - 1 , } \Sigma Nai\_C)$

$Pi\_V = \dfrac{\Sigma Nai\_C \cdot R \cdot (T + 273.15)}{Vi\_V}$

$P\_V = \dfrac{\Psi \cdot \Sigma Na\_C \cdot R \cdot (T\_E + 273.15)}{V\_V} + (P\_H2O - Pi\_H2O)$

$Pi\_H2O = e^{\left[PA - \dfrac{PB}{T + PC}\right]}$

$P\_H2O = e^{\left[PA - \dfrac{PB}{T\_E + PC}\right]}$

; Flash

$H\_P = 4.204501 \cdot T\_P - 6.78226 \cdot \Phi\_P \cdot T\_P + 14.7532 \cdot \Phi\_P^2 \cdot T\_P - \left[0.00068002552 - 0.03095114 \cdot \Phi\_P + 0.162443\right.$

$H\_X = 4.204501 \cdot T\_X - 6.78226 \cdot \Phi\_X \cdot T\_X + 14.7532 \cdot \Phi\_X^2 \cdot T\_X - \left[0.00068002552 - 0.03095114 \cdot \Phi\_X + 0.1624438 \cdot\right.$

$H\_W = 4.204501 \cdot T\_W - 6.78226 \cdot \Phi\_W \cdot T\_W + 14.7532 \cdot \Phi\_W^2 \cdot T\_W - \left[0.00068002552 - 0.03095114 \cdot \Phi\_W + 0.16\right.$

$H\_C = 4.204501 \cdot T\_C - 6.78226 \cdot \Phi\_C \cdot T\_C + 14.7532 \cdot \Phi\_C^2 \cdot T\_C - \left[0.00068002552 - 0.03095114 \cdot \Phi\_C + 0.162443\right.$

$H\_E = 4.204501 \cdot T\_E - 6.78226 \cdot \Phi\_E \cdot T\_E + 14.7532 \cdot \Phi\_E^2 \cdot T\_E - \left[0.00068002552 - 0.03095114 \cdot \Phi\_E + 0.162443\right.$

214

Rules

$$HL\_E = 2496.21010517215 - 1.9534839865599 \cdot T\_E - 0.00417809176330114 \cdot T\_E^2$$

$$H\_H = 4.204501 \cdot T\_H - 6.78226 \cdot \Phi\_H \cdot T\_H + 14.7532 \cdot \Phi\_H^2 \cdot T\_H - \left[0.00068002552 - 0.03095114 \cdot \Phi\_H + 0.162443\ldots\right.$$

$$H\_N2 = A\_N2 \cdot (T\_E + 273.15) + \left[\frac{B\_N2}{2000}\right] \cdot (T\_E + 273.15)^2 + \left[\frac{C\_N2}{3000000}\right] \cdot (T\_E + 273.15)^3 + \left[\frac{D\_N2}{4000000000}\right] \cdot (T\ldots$$

$$H\_O2 = A\_O2 \cdot (T\_E + 273.15) + \left[\frac{B\_O2}{2000}\right] \cdot (T\_E + 273.15)^2 + \left[\frac{C\_O2}{3000000}\right] \cdot (T\_E + 273.15)^3 + \left[\frac{D\_O2}{4000000000}\right] \cdot (T\ldots$$

$$H\_Ar = A\_Ar \cdot (T\_E + 273.15) + \left[\frac{B\_Ar}{2000}\right] \cdot (T\_E + 273.15)^2 + \left[\frac{C\_Ar}{3000000}\right] \cdot (T\_E + 273.15)^3 + \left[\frac{D\_Ar}{4000000000}\right] \cdot (T\_E\ldots$$

$$H\_CO2 = A\_CO2 \cdot (T\_E + 273.15) + \left[\frac{B\_CO2}{2000}\right] \cdot (T\_E + 273.15)^2 + \left[\frac{C\_CO2}{3000000}\right] \cdot (T\_E + 273.15)^3 + \left[\frac{D\_CO2}{4000000000}\right]\ldots$$

$$H\_H2O = A\_H2O \cdot (T\_E + 273.15) + \left[\frac{B\_H2O}{2000}\right] \cdot (T\_E + 273.15)^2 + \left[\frac{C\_H2O}{3000000}\right] \cdot (T\_E + 273.15)^3 + \left[\frac{D\_H2O}{4000000000}\right]\ldots$$

$$Ha\_C = \frac{y\_N2 \cdot H\_N2 + y\_O2 \cdot H\_O2 + y\_Ar \cdot H\_Ar + y\_CO2 \cdot H\_CO2}{(1 - y\_H2O) \cdot MWa\_C}$$

$$MW\_H = z\_N2 \cdot MW\_N2 + z\_O2 \cdot MW\_O2 + z\_Ar \cdot MW\_Ar + z\_CO2 \cdot MW\_CO2 + z\_Salt \cdot MW\_Salt + z\_H2O \cdot M\ldots$$

$$MW\_W = x\_N2 \cdot MW\_N2 + x\_O2 \cdot MW\_O2 + x\_Ar \cdot MW\_Ar + x\_CO2 \cdot MW\_CO2 + x\_Salt \cdot MW\_Salt + x\_H2O \cdot M\ldots$$

$$MW\_E = y\_N2 \cdot MW\_N2 + y\_O2 \cdot MW\_O2 + y\_Ar \cdot MW\_Ar + y\_CO2 \cdot MW\_CO2 + y\_H2O \cdot MW\_H2O$$

$$MW\_C = MW\_H2O$$

$$MWa\_C = \frac{y\_N2 \cdot MW\_N2 + y\_O2 \cdot MW\_O2 + y\_Ar \cdot MW\_Ar + y\_CO2 \cdot MW\_CO2}{1 - y\_H2O}$$

$$K\_N2 = \frac{HC\_N2 \cdot e^{\left[-HF\_N2 \cdot \left[\frac{1}{T\_E + 273.15} - \frac{1}{298.15}\right]\right]}}{P\_V}$$

$$K\_O2 = \frac{HC\_O2 \cdot e^{\left[-HF\_O2 \cdot \left[\frac{1}{T\_E + 273.15} - \frac{1}{298.15}\right]\right]}}{P\_V}$$

$$K\_Ar = \frac{HC\_Ar \cdot e^{\left[-HF\_Ar \cdot \left[\frac{1}{T\_E + 273.15} - \frac{1}{298.15}\right]\right]}}{P\_V}$$

$$K\_CO2 = \frac{HC\_CO2 \cdot e^{\left[-HF\_CO2 \cdot \left[\frac{1}{T\_E + 273.15} - \frac{1}{298.15}\right]\right]}}{P\_V}$$

$$K\_H2O = \frac{y\_H2O \cdot P\_H2O}{P\_V}$$

Appendix L (Continued)

Rules

$$z\_N2 = \frac{\dfrac{\Phi\_N2}{MW\_N2}}{\dfrac{\Phi\_N2}{MW\_N2} + \dfrac{\Phi\_O2}{MW\_O2} + \dfrac{\Phi\_Ar}{MW\_Ar} + \dfrac{\Phi\_CO2}{MW\_CO2} + \dfrac{\Phi\_H}{MW\_Salt} + \dfrac{\Phi\_H2O}{MW\_H2O}}$$

$$z\_O2 = \frac{\dfrac{\Phi\_O2}{MW\_O2}}{\dfrac{\Phi\_N2}{MW\_N2} + \dfrac{\Phi\_O2}{MW\_O2} + \dfrac{\Phi\_Ar}{MW\_Ar} + \dfrac{\Phi\_CO2}{MW\_CO2} + \dfrac{\Phi\_H}{MW\_Salt} + \dfrac{\Phi\_H2O}{MW\_H2O}}$$

$$z\_Ar = \frac{\dfrac{\Phi\_Ar}{MW\_Ar}}{\dfrac{\Phi\_N2}{MW\_N2} + \dfrac{\Phi\_O2}{MW\_O2} + \dfrac{\Phi\_Ar}{MW\_Ar} + \dfrac{\Phi\_CO2}{MW\_CO2} + \dfrac{\Phi\_H}{MW\_Salt} + \dfrac{\Phi\_H2O}{MW\_H2O}}$$

$$z\_CO2 = \frac{\dfrac{\Phi\_CO2}{MW\_CO2}}{\dfrac{\Phi\_N2}{MW\_N2} + \dfrac{\Phi\_O2}{MW\_O2} + \dfrac{\Phi\_Ar}{MW\_Ar} + \dfrac{\Phi\_CO2}{MW\_CO2} + \dfrac{\Phi\_H}{MW\_Salt} + \dfrac{\Phi\_H2O}{MW\_H2O}}$$

$$z\_Salt = \frac{\dfrac{\Phi\_H}{MW\_Salt}}{\dfrac{\Phi\_N2}{MW\_N2} + \dfrac{\Phi\_O2}{MW\_O2} + \dfrac{\Phi\_Ar}{MW\_Ar} + \dfrac{\Phi\_CO2}{MW\_CO2} + \dfrac{\Phi\_H}{MW\_Salt} + \dfrac{\Phi\_H2O}{MW\_H2O}}$$

$$x\_N2 = \frac{z\_N2 \cdot N\_H}{N\_W + N\_E \cdot \alpha\_N2 \cdot K\_N2}$$

$$x\_O2 = \frac{z\_O2 \cdot N\_H}{N\_W + N\_E \cdot \alpha\_O2 \cdot K\_O2}$$

$$x\_Ar = \frac{z\_Ar \cdot N\_H}{N\_W + N\_E \cdot \alpha\_Ar \cdot K\_Ar}$$

$$x\_CO2 = \frac{z\_CO2 \cdot N\_H}{N\_W + N\_E \cdot \alpha\_CO2 \cdot K\_CO2}$$

$$x\_Salt = \frac{z\_Salt \cdot N\_H}{N\_W}$$

$$x\_H2O = \frac{z\_H2O \cdot N\_H}{N\_W + N\_E \cdot \alpha\_H2O \cdot K\_H2O}$$

$$y\_N2 = x\_N2 \cdot \alpha\_N2 \cdot K\_N2$$

$$y\_O2 = x\_O2 \cdot \alpha\_O2 \cdot K\_O2$$

$$y\_Ar = x\_Ar \cdot \alpha\_Ar \cdot K\_Ar$$

$$y\_CO2 = x\_CO2 \cdot \alpha\_CO2 \cdot K\_CO2$$

$$y\_H2O = x\_H2O \cdot \alpha\_H2O \cdot K\_H2O$$

$$\Phi\_N2 + \Phi\_O2 + \Phi\_Ar + \Phi\_CO2 + \Phi\_H + \Phi\_H2O = 1$$

$$z\_N2 + z\_O2 + z\_Ar + z\_CO2 + z\_Salt + z\_H2O = 1$$

$$x\_N2 + x\_O2 + x\_Ar + x\_CO2 + x\_Salt + x\_H2O = 1$$

$$y\_N2 + y\_O2 + y\_Ar + y\_CO2 + y\_H2O = 1$$

; Performance

Appendix L (Continued)

$$A\_SC = \frac{Q\_H}{60 \cdot F\_SC \cdot (\tau\_SC \cdot \alpha\_SC \cdot I - U\_SC \cdot (T\_X - T))}$$

$$\eta\_T = \frac{100 \cdot M\_E \cdot (H\_E + HL\_E)}{M\_H \cdot H\_H}$$

$$\eta\_R = \frac{100 \cdot (H\_X - H\_P)}{H\_H - H\_P}$$

$$\eta\_C = \frac{100 \cdot (T\_X - T\_P)}{T\_E - T\_C}$$

$\Sigma Q\_H = INTEGRAL("\ Q\_H\ ,\ t\ ",\ ELT('t\ ,\ ELT() - 1\ ,\ ti)\ ,\ t) + ELT('\Sigma Q\_H\ ,\ ELT() - 1\ ,\ 0)$

$\Sigma W\_P = INTEGRAL("\ W\_P\ ,\ t\ ",\ ELT('t\ ,\ ELT() - 1\ ,\ ti)\ ,\ t) + ELT('\Sigma W\_P\ ,\ ELT() - 1\ ,\ 0)$

$$PEC = \frac{\Sigma Q\_H + \Sigma W\_P}{\Sigma M\_C}$$

$Q\_H - W\_H + Ein\_H - Eout\_H = 0$

$Ein\_H = M\_X \cdot H\_X$

$Eout\_H = M\_H \cdot H\_H$

$W\_P = 0$

; Error

$\varepsilon P\_V = \varepsilon P$

$\varepsilon T\_X = \varepsilon T$

$\varepsilon T\_E = \varepsilon T$

$\varepsilon T\_W = \varepsilon T$

$\varepsilon \rho\_P = \varepsilon \rho$

$\varepsilon \rho\_H = \varepsilon \rho$

$\varepsilon \rho\_C = \varepsilon \rho$

$\varepsilon \rho\_E = \varepsilon \rho$

$$\varepsilon \Delta T = \sqrt{2} \cdot \varepsilon T$$

$$\varepsilon \Delta H = \sqrt{2} \cdot \varepsilon H$$

$$\varepsilon M\_P = \left[M\_P^2 \cdot \left[\left[\frac{\varepsilon \rho\_P}{\rho} \right]^2 + \left[\frac{\varepsilon Fl}{Fl} \right]^2 \right] \right]^{0.5}$$

$$\varepsilon M\_H = \left[M\_H^2 \cdot \left[\left[\frac{\varepsilon \rho\_H}{\rho\_H} \right]^2 + \left[\frac{\varepsilon Fl}{Fl} \right]^2 \right] \right]^{0.5}$$

$\varepsilon M\_E = \varepsilon M\_C$

Appendix L (Continued)

$$\varepsilon M\_C = \left[M\_C^2 \cdot \left[\left[\frac{\varepsilon \rho\_C}{\rho\_C} \right]^2 + \left[\frac{\varepsilon FI}{FI} \right]^2 \right] \right]^{0.5}$$

$$\varepsilon \Sigma M\_C = \left[\Sigma M\_C^2 \cdot \left[\left[\frac{\varepsilon \rho\_C}{\rho\_C} \right]^2 + \left[\frac{\varepsilon QE}{QE} \right]^2 \right] \right]^{0.5}$$

$$\varepsilon Q\_H = \left[Q\_H^2 \cdot \left[\left[\frac{\varepsilon M\_P}{M\_P} \right]^2 + \left[\frac{\varepsilon \Delta H}{H\_H - H\_X} \right]^2 \right] \right]^{0.5}$$

$$\varepsilon \Sigma Q\_H = \varepsilon Q\_H$$

$$\varepsilon A\_SC = \left[A\_SC^2 \cdot \left[\left[\frac{\varepsilon Q\_H}{Q\_H} \right]^2 + \left[\frac{U\_SC \cdot \varepsilon T\_X}{\tau\_SC \cdot \alpha\_SC \cdot I - U\_SC \cdot (T\_X - T)} \right]^2 \right] \right]^{0.5}$$

$$\varepsilon PEC = \left[PEC^2 \cdot \left[\left[\frac{\varepsilon \Sigma Q\_H}{\Sigma Q\_H} \right]^2 + \left[\frac{\varepsilon \Sigma M\_C}{\Sigma M\_C} \right]^2 \right] \right]^{0.5}$$

$$\varepsilon \eta\_C = 100 \cdot \left[\left[\frac{\eta\_C}{100} \right]^2 \cdot \left[\left[\frac{\varepsilon \Delta T}{T\_X - T\_P} \right]^2 + \left[\frac{\varepsilon \Delta T}{T\_E - T\_C} \right]^2 \right] \right]^{0.5}$$

$$\varepsilon \eta\_R = 100 \cdot \left[\left[\frac{\eta\_R}{100} \right]^2 \cdot \left[\left[\frac{\varepsilon \Delta H}{H\_X - H\_P} \right]^2 + \left[\frac{\varepsilon \Delta H}{H\_H - H\_P} \right]^2 \right] \right]^{0.5}$$

$$\varepsilon \eta\_T = 100 \cdot \left[\left[\frac{\eta\_T}{100} \right]^2 \cdot \left[\left[\frac{\varepsilon M\_E}{M\_E} \right]^2 + \left[\frac{\varepsilon H}{H\_E} \right]^2 + \left[\frac{\varepsilon M\_H}{M\_H} \right]^2 + \left[\frac{\varepsilon H}{H\_H} \right]^2 \right] \right]^{0.5}$$

218

Appendix L (Continued)

Variables Sheet

Input	Name	Output	Unit	Comment
0	ti		min	Initial Time
1	t		min	Run Time
83.14472	R		(bar - cm ^ 3) / (mol - °C)	Universal Gas Constant
980.0665	g		cm / s ^ 2	Gravity Acceleration
310922.658770	Vi_V		cm ^ 3	Initial Total Vacuum Volume
	V_V	310418.662453	cm ^ 3	Total Vacuum Volume
	ΣNai_C	1.785895	moles	Initial NCG Molar Amount
	ΣNa_C	1.786259	mol	NCG Amount
	Na_C	0.000364	mol / min	NCG Molar Accumulation Rate
	Ma_C	0.010799	g / min	NCG Molar Accumulation Rate
	ΣM	27.653921	g	Actual Product Amount
	ΣM_C	5.071088	g	Calculated Product Amount
	FI	0.503996	L / min	Average Flow Indicator Value
27	QE		cm ^ 3	Average Quantitative Element Value
0.546461	CV			Ball Valve Flow Coefficient
20	T		°C	Ambient Temperature
1.01325	P		bar	Ambient Pressure
1.024219	ρ		g / cm ^ 3	Stream Density
	k_X	0.005988	W / (cm - °C)	Stream Thermal Conductivity
	k_W	0.005990	W / (cm - °C)	Stream Thermal Conductivity
	k_C	0.006043	W / (cm - °C)	Stream Thermal Conductivity
.035	Φ_P			Stream Salt Mass Fraction
.035	Φ_X			Stream Salt Mass Fraction
.035	Φ_H			Stream Salt Mass Fraction
	Φ_W	0.035348		Stream Salt Mass Fraction
0	Φ_C			Stream Salt Mass Fraction
0	Φ_E			Stream Salt Mass Fraction
20	T_P		°C	Stream Temperature
21.022222	T_X		°C	Stream Temperature
43.078889	T_H		°C	Stream Temperature
24.241111	T_E		°C	Stream Temperature

219

Appendix L (Continued)

Input	Name	Output	Unit	Comment
21.240556	T_W		°C	Stream Temperature
20.850556	T_C		°C	Stream Temperature
	Pi_H2O	0.022722	bar	Initial Vapor Pressure
	P_H2O	0.029477	bar	Vapor Pressure
.14	Pi_V		bar	Initial Vacuum Pressure
0.140585	P_V		bar	Vacuum Pressure
35	D_E		cm	Evaporator Nominal Diameter
160	L_E		cm	Evaporator Length
35	D_C		cm	Condenser Nominal Diameter
160	L_C		cm	Condenser Length
26.092	A_N2			Nitrogen Molar Enthalpy Parameter
8.218801	B_N2			Nitrogen Molar Enthalpy Parameter
-1.976141	C_N2			Nitrogen Molar Enthalpy Parameter
.159274	D_N2			Nitrogen Molar Enthalpy Parameter
.044434	E_N2			Nitrogen Molar Enthalpy Parameter
-7.98923	F_N2			Nitrogen Molar Enthalpy Parameter
29.659	A_O2			Oxygen Molar Enthalpy Parameter
6.137261	B_O2			Oxygen Molar Enthalpy Parameter
-1.186521	C_O2			Oxygen Molar Enthalpy Parameter
.09578	D_O2			Oxygen Molar Enthalpy Parameter
-.219663	E_O2			Oxygen Molar Enthalpy Parameter
-9.861391	F_O2			Oxygen Molar Enthalpy Parameter
20.786	A_Ar			Argon Molar Enthalpy Parameter
0.000000	B_Ar			Argon Molar Enthalpy Parameter
0.000000	C_Ar			Argon Molar Enthalpy Parameter
0.000000	D_Ar			Argon Molar Enthalpy Parameter
0.000000	E_Ar			Argon Molar Enthalpy Parameter
-6.19735	F_Ar			Argon Molar Enthalpy Parameter
24.99735	A_CO2			Carbon Dioxide Molar Enthalpy Parameter
55.18696	B_CO2			Carbon Dioxide Molar Enthalpy Parameter
-33.69137	C_CO2			Carbon Dioxide Molar Enthalpy Parameter
7.948387	D_CO2			Carbon Dioxide Molar Enthalpy Parameter
-.136638	E_CO2			Carbon Dioxide Molar Enthalpy Parameter
-10.0851	F_CO2			Carbon Dioxide Molar Enthalpy Parameter
30.092	A_H2O			Water Molar Enthalpy Parameter

Appendix L (Continued)

Input	Name	Output	Unit	Comment
6.832514	B_H2O			Water Molar Enthalpy Parameter
6.793435	C_H2O			Water Molar Enthalpy Parameter
-2.53448	D_H2O			Water Molar Enthalpy Parameter
.082139	E_H2O			Water Molar Enthalpy Parameter
-9.054600	F_H2O			Water Molar Enthalpy Parameter
	H_N2	-32.686204	J / mol	Nitrogen Molar Enthalpy
	H_O2	-41.255674	J / mol	Oxygen Molar Enthalpy
	H_Ar	-15.778230	J / mol	Argon Molar Enthalpy
	H_CO2	-31.084062	J / mol	Carbon Dioxide Molar Enthalpy
	H_H2O	-24.962916	J / mol	Water Molar Enthalpy
	H_P	79.740379	J / g	Stream Enthalpy
	H_X	83.823279	J / g	Stream Enthalpy
	H_H	172.043899	J / g	Stream Enthalpy
	H_W	84.655639	J / g	Stream Enthalpy
	H_E	101.548881	J / g	Stream Enthalpy
	HL_E	2446.400305	J / g	Stream Enthalpy of Vaporization
	H_C	87.369790	J / g	Stream Enthalpy
	Ha_C	-1.192302	J / g	NCG Enthalpy
	MW_H	18.287997	g / mol	Stream Molecular Weight
	MW_W	18.298045	g / mol	Stream Molecular Weight
	MW_E	18.018971	g / mol	Stream Molecular Weight
	MW_C	18.0148	g / mol	Stream Molecular Weight
	MWa_C	29.655264	g / mol	Stream Molecular Weight
	N_H	28.226315	mol / min	Stream Molar Flow Rate
	N_W	27.210002	mol / min	Stream Molar Flow Rate
	N_E	1.016312	mol / min	Stream Molar Flow Rate
	N_C	1.015948	mol / min	Stream Molar Flow Rate
	M_P	516.202756	g / min	Stream Mass Flow Rate
	M_X	516.202756	g / min	Stream Mass Flow Rate
	M_H	516.202756	g / min	Stream Mass Flow Rate
	M_W	511.120869	g / min	Stream Mass Flow Rate
	M_E	5.081887	g / min	Stream Mass Flow Rate
	M_C	5.071088	g / min	Stream Mass Flow Rate
	Ein_E	88809.534752	J / min	Evaporator Energy Input
	Eout_E	56217.653939	J / min	Evaporator Energy Output
0	Q_E		J / min	Evaporator Heat Input

Appendix L (Continued)

Input	Name	Output	Unit	Comment
0	W_E		J / min	Evaporator Work Output
	Ea_C	-0.012876	J / min	NCG Energy Accumulation
	Ein_C	54110.593734	J / min	Condenser Energy Input
	Eout_C	43712.867337	J / min	Condenser Energy Output
	Q_C	-10397.739273	J / min	Condenser Heat Input
0	W_C		J / min	Condenser Work Output
0.000013	Φ_N2			Nitrogen Mass Fraction in Ambient Seawater
0.000008	Φ_O2			Oxygen Mass Fraction in Ambient Seawater
0.000000	Φ_Ar			Argon Mass Fraction in Ambient Seawater
0.000000	Φ_CO2			Carbon Dioxide Mass Fraction in Ambient Seawater
	Φ_H2O	0.964979		Water Mass Fraction in Ambient Seawater
	z_N2	0.000008		Nitrogen Mole Fraction in Ambient Seawater
	z_O2	0.000004		Oxygen Mole Fraction in Ambient Seawater
	z_Ar	0.000000		Argon Mole Fraction in Ambient Seawater
	z_CO2	0.000000		Carbon Dioxide Mole Fraction in Ambient Seawater
	z_Salt	0.020374		Salt Mole Fraction in Ambient Seawater
	z_H2O	0.979613		Water Mole Fraction in Ambient Seawater
	x_N2	0.000000		Nitrogen Mole Fraction in Brine Water
	x_O2	0.000000		Oxygen Mole Fraction in Brine Water
	x_Ar	0.000000		Argon Mole Fraction in Brine Water
	x_CO2	0.000000		Carbon Dioxide Mole Fraction in Brine Water
	x_Salt	0.021135		Salt Mole Fraction in Brine Water
	x_H2O	0.978865		Water Mole Fraction in Brine Water
	y_N2	0.000228		Nitrogen Mole Fraction in Vaporized Water
	y_O2	0.000122		Oxygen Mole Fraction in Vaporized Water
	y_Ar	0.000005		Argon Mole Fraction in Vaporized Water
	y_CO2	0.000003		Carbon Dioxide Mole Fraction in Vaporized Water
	y_H2O	0.999642		Water Mole Fraction in Vaporized Water
28.0134	MW_N2		g / mol	Nitrogen Molecular Weight
31.998	MW_O2		g / mol	Oxygen Molecular Weight
39.94	MW_Ar		g / mol	Argon Molecular Weight
44.009	MW_CO2		g / mol	Carbon Dioxide Molecular Weight
31.416538	MW_Salt		g / mol	Approximated Seawater Salt Molecular Weight
18.0148	MW_H2O		g / mol	Water Molecular Weight
8067573.136086	HC_N2		bar	Nitrogen Reference State Henry's Constant

Input	Name	Output	Unit	Comment
358814.929481	HC_O2		bar	Oxygen Reference State Henry's Constant
384073.329688	HC_Ar		bar	Argon Reference State Henry's Constant
10914.952753	HC_CO2		bar	Carbon Dioxide Reference State Henry's Constant
-3545.567207	HF_N2		°C	Nitrogen Henry's Coefficient
-2208.812178	HF_O2		°C	Oxygen Henry's Coefficient
-2308.046425	HF_Ar		°C	Argon Henry's Coefficient
-445.190581	HF_CO2		°C	Carbon Dioxide Henry's Coefficient
12.762946	PA			Water Vapor Pressure Coefficient
4391.129422	PB		°C	Water Vapor Pressure Coefficient
245.367016	PC		°C	Water Vapor Pressure Coefficient
1.21	α_N2			Nitrogen Relative Solubility
1.22	α_O2			Oxygen Relative Solubility
1.23	α_Ar			Argon Relative Solubility
1.17	α_CO2			Carbon Dioxide Relative Solubility
.9816	α_H2O			Water Relative Vapor Pressure
	K_N2	59153990.173289		Evaporator-Based Nitrogen VLE Distribution Coefficient
	K_O2	2601014.888961		Evaporator-Based Oxygen VLE Distribution Coefficient
	K_Ar	2786476.236923		Evaporator-Based Argon VLE Distribution Coefficient
	K_CO2	77936.106242		Evaporator-Based Carbon Dioxide VLE Distribution Coefficient
	K_H2O	1.040368		Evaporator-Based Water VLE Distribution Coefficient
	ρA_X	0.765685		Stream Density Coefficient
	ρA_H	0.742783		Stream Density Coefficient
	ρA_W	0.765301		Stream Density Coefficient
	ρA_C	0.765990		Stream Density Coefficient
	ρB_X	-0.004306		Stream Density Coefficient
	ρB_H	-0.004390		Stream Density Coefficient
	ρB_W	-0.004299		Stream Density Coefficient
	ρB_C	-0.004312		Stream Density Coefficient
	ρC_X	997.990004		Stream Density Coefficient
	ρC_H	991.010632		Stream Density Coefficient
	ρC_W	997.942402		Stream Density Coefficient
	ρC_C	998.027088		Stream Density Coefficient
	ρ_X	1.024489	g / cm ^ 3	Stream Density

Appendix L (Continued)

Input	Name	Output	Unit	Comment
	ρ_H	1.016691	g / cm ^ 3	Stream Density
	ρ_W	1.024694	g / cm ^ 3	Stream Density
	ρ_C	0.998027	g / cm ^ 3	Stream Density
	μA_X	0.001197		Stream Viscosity Coefficient
	μA_W	0.001208		Stream Viscosity Coefficient
	μA_C	0.001188		Stream Viscosity Coefficient
	μB_X	0.003285		Stream Viscosity Coefficient
	μB_W	0.003292		Stream Viscosity Coefficient
	μB_C	0.003279		Stream Viscosity Coefficient
	μC_X	19.848398		Stream Viscosity Coefficient
	μC_W	20.049759		Stream Viscosity Coefficient
	μC_C	0		Stream Viscosity Coefficient
	μD_X	0.009774		Stream Viscosity Coefficient
	μD_W	0.009722		Stream Viscosity Coefficient
	μD_C	0.009814		Stream Viscosity Coefficient
	μ_X	0.010463	P	Stream Viscosity
	μ_W	0.010417	P	Stream Viscosity
	μ_C	0.009814	P	Stream Viscosity
1.27	D_CT		cm	Condenser Tube Diameter
475	L_CT		cm	Condenser Tube Length
.2	hid_CT		W / (cm ^ 2 - ℃)	Condenser Tube Inside Dirt Coefficient
.5	hod_CT		W / (cm ^ 2 - ℃)	Condenser Tube Outside Dirt Coefficient
	hi_CT	0.051020	W / (cm ^ 2 - ℃)	Condenser Tube Inside Fluid Film Coefficient
	ho_CT	0.943999	W / (cm ^ 2 - ℃)	Condenser Tube Outside Fluid Film Coefficient
.5	hid_E		W / (cm ^ 2 - ℃)	Evaporator Inside Dirt Coefficient
.75	hod_E		W / (cm ^ 2 - ℃)	Evaporator Outside Dirt Coefficient
	hi_E	0.594382	W / (cm ^ 2 - ℃)	Evaporator Inside Fluid Film Coefficient
	ho_E	0.018067	W / (cm ^ 2 - ℃)	Evaporator Outside Fluid Film Coefficient
.5	hid_C		W / (cm ^ 2 - ℃)	Condenser Inside Dirt Coefficient
.75	hod_C		W / (cm ^ 2 - ℃)	Condenser Outside Dirt Coefficient
	hi_C	0.599330	W / (cm ^ 2 - ℃)	Condenser Inside Fluid Film Coefficient
	ho_C	0.018067	W / (cm ^ 2 - ℃)	Condenser Outside Fluid Film Coefficient
4	N_CT			Number of Condenser Tube Vertical Rows

Appendix L (Continued)

Input	Name	Output	Unit	Comment
.125	δ_CT		cm	Condenser Tube Thickness
3.81	kw_CT		W / (cm - °C)	Condenser Tube Thermal Conductivity
.25	δ_C		cm	Condenser Thickness
.45	kw_C		W / (cm - °C)	Condenser Thermal Conductivity
.25	δ_E		cm	Evaporator Thickness
.001	kw_E		W / (cm - °C)	Evaporator Thermal Conductivity
	U_CT	0.033225	W / (cm ^ 2 - °C)	Condenser Tube Overall Heat Transfer Coefficient
	A_CT	1895.165768	cm ^ 2	Condenser Tube Surface Area
	ΔTm_CT	3.706537	°C	Condenser Tube Logarithmic Mean Temperature Difference
	U_E	0.005381	W / (cm ^ 2 - °C)	Evaporator Overall Heat Transfer Coefficient
	A_E	17592.918860	cm ^ 2	Evaporator Surface Area
	ΔTm_E	3.585132	°C	Evaporator Logarithmic Mean Temperature Difference
	U_C	0.016486	W / (cm ^ 2 - °C)	Condenser Overall Heat Transfer Coefficient
	A_C	17592.918860	cm ^ 2	Condenser Surface Area
	ΔTm_C	3.799981	°C	Condenser Logarithmic Mean Temperature Difference
	γ_H2O	4.961777		Evaporator-Based Water Activity Coefficient
	Ψ	0.940570		Fraction of NCG Molecules Accumulating
	F_CT	0.150507		Condenser Tube Counter Current Departure Correction Factor
	F_E	0		Evaporator Counter Current Departure Correction Factor
	F_C	0.157232		Condenser Counter Current Departure Correction Factor
	μ_E	0.000090	P	Stream Viscosity
	ρ_E	0.000022	g / cm ^ 3	Stream Density
5.08	PD_E		cm	Stream Nominal Pipe Diameter
180	PL_E		cm	Stream Equivalent Pipe Length
962.112750	XA_E		cm ^ 2	Evaporator Cross Sectional Area
	ΔP_E	0.000004	bar	Stream Pressure Drop
	SG_H	1.025913		Stream Specific Gravity
.118	Ω		bar	Steam Diffusion Resistance
2	σ		(g - °C ^ 0.5) / (bar - min - cm ^ 2)	Steam Diffusion Coefficient
	Md_E	-13.231018	g / min	Steam Diffusion Rate
	ΣMd_E	-13.231018	g	Total Steam Diffused
	Ed_E	32591.880813	J / min	Steam Diffusion Energy
0	W_H		J / min	Heater Work Output
	Q_H	45539.727333	J / min	Heater Heat Input
	Ein_H	43269.807420	J / min	Heater Energy Input

225

Appendix L (Continued)

Input	Name	Output	Unit	Comment
	Eout_H	88809.534752	J / min	Heater Energy Output
0	W_P		J / min	Pump Work Output
	ΣW_P	0	J	Power Input
	ΣQ_H	45539.727333	J	Heat Input
	PEC	8980.267181	J / g	Prime Energy Consumption
	η_R	4.423341	%	Recovery Efficiency
	η_T	14.579955	%	Thermal Efficiency
	η_C	30.149107	%	Condenser Efficiency
.92	α_SC			Solar Collector Absorptance
.9	τ_SC			Solar Collector Transmittance
.000092	U_SC		W / (cm ^ 2 - °C)	Solar Collector Heat Loss Conductance
.82	F_SC			Solar Collector Heat Removal Factor
.06	I		W / cm ^ 2	Incident Insolation On Solar Collector
	A_SC	18666.660826	cm ^ 2	Solar Collector Area
.005	εP		bar	Pressure Transducer Error
1	εT		°C	Thermocouple Error
.045	εFI		L / min	Flow Indicator Error
.2	εQE		cm ^ 3	Quantitative Element Error
.000035	ερ		g / cm ^ 3	Density Correlation Error
.045	εH		J / g	Enthalpy Correlation Error
	εP_V	.005	bar	Vacuum Pressure Error
	εT_E	1	°C	Stream Temperature Error
	εT_W	1	°C	Stream Temperature Error
	εT_X	1	°C	Stream Temperature Error
	ερ_P	.000035	g / cm ^ 3	Stream Density Error
	ερ_H	.000035	g / cm ^ 3	Stream Density Error
	ερ_E	.000035	g / cm ^ 3	Stream Density Error
	ερ_C	.000035	g / cm ^ 3	Stream Density Error
	εΔT	1.414214	°C	Temperature Gradient Error
	εΔH	0.063640	J / g	Enthalpy Gradient Error
	εM_P	46.089872	g / min	Stream Mass Flow Rate Error
	εM_H	46.089872	g / min	Stream Mass Flow Rate Error
	εM_E	0.452779	g / min	Stream Mass Flow Rate Error
	εM_C	0.452779	g / min	Stream Mass Flow Rate Error
	εΣM_C	0.037564	g	Product Amount Error
	εQ_H	4066.209798	J / min	Heater Heat Input Error
	εΣQ_H	4066.209798	J	Heat Input Error
	εA_SC	1667.092631	cm ^ 2	Solar Collector Area Error
	εPEC	804.596245	J / g	Prime Energy Consumption Error
	εη_C	43.564826	%	Condenser Efficiency Error
	εη_R	0.069013	%	Recovery Efficiency Error

226

Appendix L (Continued)

Input	Name	Output	Unit	Comment
	εη_T	1.839071	%	Thermal Efficiency Error

Appendix M. Sample TK Solver code for model simulation

Rules Sheet

Rules

; Phenomenological Equations

$\Phi\_S = \Phi\_P$

$\Phi\_P = \Phi\_X$

$\Phi\_X = \Phi\_H$

$\Phi\_E = \Phi\_C$

; Salt Balance

$\Phi\_S \cdot M\_S = \Phi\_P \cdot M\_P$

$\Phi\_P \cdot M\_P = \Phi\_X \cdot M\_X$

$\Phi\_X \cdot M\_X = \Phi\_H \cdot M\_H$

$\Phi\_H \cdot M\_H = \Phi\_W \cdot M\_W$

; Energy Balance

$Q\_P - W\_P + Ein\_P - Eout\_P = 0$

$Q\_C - W\_C + Ein\_C - Eout\_C = Ea\_C$

$Q\_H - W\_H + Ein\_H - Eout\_H = 0$

$Q\_E - W\_E + Ein\_E - Eout\_E = Ed\_E$

; Energy Inputs

$Ein\_P = M\_S \cdot H\_S$

$Ein\_C = M\_P \cdot H\_P + M\_E \cdot (H\_E + HL\_E)$

$Ein\_H = M\_X \cdot H\_X$

$Ein\_E = M\_H \cdot H\_H$

; Energy Outputs

$Eout\_P = M\_P \cdot H\_P$

$Eout\_C = M\_X \cdot H\_X + M\_C \cdot H\_C$

$Eout\_H = M\_H \cdot H\_H$

$Eout\_E = M\_W \cdot H\_W + M\_E \cdot (H\_E + HL\_E)$

; Energy Accumulation & Diffusion

$Ea\_C = Ma\_C \cdot Ha\_C$

$Ed\_E = Md\_E \cdot (H\_W - H\_E - HL\_E)$

; Quasi Steady State

$N\_H = N\_E + N\_W$

$N\_E = N\_C + Na\_C$

$Na\_C = (1 - y\_H2O) \cdot N\_E$

Rules

$$Md\_E = \sigma \cdot XA\_E \cdot \left[\frac{(1 - 0.54 \cdot \Phi\_W) \cdot \left[e^{\left[PA - \frac{PB}{T\_W + PC} \right]} \right]}{\sqrt{T\_W + 273.15}} - \frac{e^{\left[PA - \frac{PB}{T\_C + PC} \right]} + \Omega}{\sqrt{T\_C + 273.15}} \right]$$

; Average Molecular Weights

$$\frac{1}{MW\_Salt} = \frac{\omega\_Cl}{MW\_Cl} + \frac{\omega\_Na}{MW\_Na} + \frac{\omega\_SO4}{MW\_SO4} + \frac{\omega\_Mg}{MW\_Mg} + \frac{\omega\_Ca}{MW\_Ca} + \frac{\omega\_K}{MW\_K} + \frac{\omega\_HCO3}{MW\_HCO3} + \frac{\omega\_Br}{MW\_Br} +$$

$MW\_H = z\_N2 \cdot MW\_N2 + z\_O2 \cdot MW\_O2 + z\_Ar \cdot MW\_Ar + z\_CO2 \cdot MW\_CO2 + z\_Salt \cdot MW\_Salt + z\_H2O \cdot M$

$MW\_W = x\_N2 \cdot MW\_N2 + x\_O2 \cdot MW\_O2 + x\_Ar \cdot MW\_Ar + x\_CO2 \cdot MW\_CO2 + x\_Salt \cdot MW\_Salt + x\_H2O \cdot N$

$MW\_E = y\_N2 \cdot MW\_N2 + y\_O2 \cdot MW\_O2 + y\_Ar \cdot MW\_Ar + y\_CO2 \cdot MW\_CO2 + y\_H2O \cdot MW\_H2O$

$MW\_C = MW\_H2O$

$$MWa\_C = \frac{y\_N2 \cdot MW\_N2 + y\_O2 \cdot MW\_O2 + y\_Ar \cdot MW\_Ar + y\_CO2 \cdot MW\_CO2}{1 - y\_H2O}$$

$MW\_S = MW\_P$

$MW\_P = MW\_X$

$MW\_X = MW\_H$

; Mass & Molar Flows

$M\_S = N\_S \cdot MW\_S$

$M\_P = N\_P \cdot MW\_P$

$M\_X = N\_X \cdot MW\_X$

$M\_H = N\_H \cdot MW\_H$

$M\_W = N\_W \cdot MW\_W - Md\_E$

$M\_E = N\_E \cdot MW\_E + Md\_E$

$M\_C = N\_C \cdot MW\_C + Md\_E$

$Ma\_C = Na\_C \cdot MWa\_C$

; VLE Distribution Coefficients

$$K\_N2 = \frac{HC\_N2 \cdot e^{\left[-HF\_N2 \cdot \left[\frac{1}{T\_E + 273.15} - \frac{1}{298.15} \right] \right]}}{P\_V}$$

$$K\_O2 = \frac{HC\_O2 \cdot e^{\left[-HF\_O2 \cdot \left[\frac{1}{T\_E + 273.15} - \frac{1}{298.15} \right] \right]}}{P\_V}$$

$$K\_Ar = \frac{HC\_Ar \cdot e^{\left[-HF\_Ar \cdot \left[\frac{1}{T\_E + 273.15} - \frac{1}{298.15} \right] \right]}}{P\_V}$$

Rules

$$K\_CO2 = \frac{HC\_CO2 \cdot e^{\left[-HF\_CO2 \cdot \left[\frac{1}{T\_E + 273.15} - \frac{1}{298.15}\right]\right]}}{P\_V}$$

$$K\_H2O = \frac{\gamma\_H2O \cdot P\_H2O}{P\_V}$$

$$\gamma\_H2O = 0.0019583973 + \frac{1.038491 \cdot P\_V}{P\_H2O}$$

; Flash Calculations

$$z\_N2 = \frac{\dfrac{\Phi\_N2}{MW\_N2}}{\dfrac{\Phi\_N2}{MW\_N2} + \dfrac{\Phi\_O2}{MW\_O2} + \dfrac{\Phi\_Ar}{MW\_Ar} + \dfrac{\Phi\_CO2}{MW\_CO2} + \dfrac{\Phi\_H}{MW\_Salt} + \dfrac{\Phi\_H2O}{MW\_H2O}}$$

$$z\_O2 = \frac{\dfrac{\Phi\_O2}{MW\_O2}}{\dfrac{\Phi\_N2}{MW\_N2} + \dfrac{\Phi\_O2}{MW\_O2} + \dfrac{\Phi\_Ar}{MW\_Ar} + \dfrac{\Phi\_CO2}{MW\_CO2} + \dfrac{\Phi\_H}{MW\_Salt} + \dfrac{\Phi\_H2O}{MW\_H2O}}$$

$$z\_Ar = \frac{\dfrac{\Phi\_Ar}{MW\_Ar}}{\dfrac{\Phi\_N2}{MW\_N2} + \dfrac{\Phi\_O2}{MW\_O2} + \dfrac{\Phi\_Ar}{MW\_Ar} + \dfrac{\Phi\_CO2}{MW\_CO2} + \dfrac{\Phi\_H}{MW\_Salt} + \dfrac{\Phi\_H2O}{MW\_H2O}}$$

$$z\_CO2 = \frac{\dfrac{\Phi\_CO2}{MW\_CO2}}{\dfrac{\Phi\_N2}{MW\_N2} + \dfrac{\Phi\_O2}{MW\_O2} + \dfrac{\Phi\_Ar}{MW\_Ar} + \dfrac{\Phi\_CO2}{MW\_CO2} + \dfrac{\Phi\_H}{MW\_Salt} + \dfrac{\Phi\_H2O}{MW\_H2O}}$$

$$z\_Salt = \frac{\dfrac{\Phi\_H}{MW\_Salt}}{\dfrac{\Phi\_N2}{MW\_N2} + \dfrac{\Phi\_O2}{MW\_O2} + \dfrac{\Phi\_Ar}{MW\_Ar} + \dfrac{\Phi\_CO2}{MW\_CO2} + \dfrac{\Phi\_H}{MW\_Salt} + \dfrac{\Phi\_H2O}{MW\_H2O}}$$

$$x\_N2 = \frac{z\_N2 \cdot N\_H}{N\_W + N\_E \cdot \alpha\_N2 \cdot K\_N2}$$

$$x\_O2 = \frac{z\_O2 \cdot N\_H}{N\_W + N\_E \cdot \alpha\_O2 \cdot K\_O2}$$

$$x\_Ar = \frac{z\_Ar \cdot N\_H}{N\_W + N\_E \cdot \alpha\_Ar \cdot K\_Ar}$$

$$x\_CO2 = \frac{z\_CO2 \cdot N\_H}{N\_W + N\_E \cdot \alpha\_CO2 \cdot K\_CO2}$$

$$x\_Salt = \frac{z\_Salt \cdot N\_H}{N\_W}$$

$$x\_H2O = \frac{z\_H2O \cdot N\_H}{N\_W + N\_E \cdot \alpha\_H2O \cdot K\_H2O}$$

$$y\_N2 = x\_N2 \cdot \alpha\_N2 \cdot K\_N2$$

$$y\_O2 = x\_O2 \cdot \alpha\_O2 \cdot K\_O2$$

$$y\_Ar = x\_Ar \cdot \alpha\_Ar \cdot K\_Ar$$

Appendix M (Continued)

Rules

y_CO2 = x_CO2 · α_CO2 · K_CO2

y_H2O = x_H2O · α_H2O · K_H2O

; Flash Fractions Summation

Φ_N2 + Φ_O2 + Φ_Ar + Φ_CO2 + Φ_H + Φ_H2O = 1

z_N2 + z_O2 + z_Ar + z_CO2 + z_Salt + z_H2O = 1

x_N2 + x_O2 + x_Ar + x_CO2 + x_Salt + x_H2O = 1

y_N2 + y_O2 + y_Ar + y_CO2 + y_H2O = 1

; System Throughput

$$SG\_H = \frac{1000 \cdot \rho\_H}{\rho C\_H}$$

$$FI = CV \cdot \left[\frac{P - P\_V}{SG\_H}\right]^{0.5}$$

FI = 0.483691505733334

M_S = 1000 · ρ_S · FI

ΣM = ρ_S · QE

; Totalized Variables

ΣM_S = INTEGRAL(" M_S , t " , ELT('t , ELT() - 1 , ti) , t) + ELT('ΣM_S , ELT() - 1 , 0)

ΣM_W = INTEGRAL(" M_W , t " , ELT('t , ELT() - 1 , ti) , t) + ELT('ΣM_W , ELT() - 1 , 0)

ΣM_C = INTEGRAL(" M_C , t " , ELT('t , ELT() - 1 , ti) , t) + ELT('ΣM_C , ELT() - 1 , 0)

ΣNa_C = INTEGRAL(" Na_C , t " , ELT('t , ELT() - 1 , ti) , t) + ELT('ΣNa_C , ELT() - 1 , ΣNai_C)

; Vessel Capacities

$$XA\_S = \frac{\pi \cdot D\_S^2}{4}$$

$$XA\_B = \frac{\pi \cdot D\_B^2}{4}$$

$$XA\_F = \frac{\pi \cdot D\_F^2}{4}$$

$$XA\_E = \frac{\pi \cdot D\_E^2}{4}$$

$$XA\_C = \frac{\pi \cdot D\_C^2}{4}$$

V_S = XA_S · L_S

V_B = XA_B · L_B

V_F = XA_F · L_F

V_E = XA_E · L_E

V_C = XA_C · L_C

Appendix M (Continued)

Rules

; Vessel Levels

$Zi\_S = 24$

$Z\_S = Zi\_S - \dfrac{\Sigma M\_S}{\rho\_S \cdot XA\_S}$

$Zi\_C = 0$

$Z\_C = Zi\_C + \dfrac{\Sigma M\_C}{\rho\_C \cdot XA\_C}$

$Zi\_C = \dfrac{1000000 \cdot (P - Pi\_V - \Delta P\_C)}{\rho\_C \cdot g} - PL\_C + Z\_F$

$Z\_C = \dfrac{1000000 \cdot (P - P\_V - \Delta P\_C)}{\rho\_C \cdot g} - PL\_C + Z\_F$

$Zi\_E = 0$

$Z\_E = Zi\_E + \dfrac{\Sigma M\_W}{\rho\_W \cdot XA\_E}$

$Zi\_E = \dfrac{1000000 \cdot (P - Pi\_V - \Delta P\_W)}{\rho\_W \cdot g} - PL\_W + Z\_B$

$Z\_E = \dfrac{1000000 \cdot (P - P\_V - \Delta P\_W)}{\rho\_W \cdot g} - PL\_W + Z\_B$

; Vacuum Volume

$Vi\_CV = XA\_C \cdot (L\_C - Zi\_C)$

$V\_CV = XA\_C \cdot (L\_C - Z\_C)$

$Vi\_CV = L\_C \cdot \left[\dfrac{\pi \cdot D\_C^2}{8} + \dfrac{D\_C^2}{4} \cdot ASIN\left[1 - \dfrac{2 \cdot Zi\_C}{D\_C}\right] + \left[\dfrac{D\_C}{2} - Zi\_C\right] \cdot (Zi\_C \cdot (D\_C - Zi\_C))^{0.5} \right]$

$V\_CV = L\_C \cdot \left[\dfrac{\pi \cdot D\_C^2}{8} + \dfrac{D\_C^2}{4} \cdot ASIN\left[1 - \dfrac{2 \cdot Z\_C}{D\_C}\right] + \left[\dfrac{D\_C}{2} - Z\_C\right] \cdot (Z\_C \cdot (D\_C - Z\_C))^{0.5} \right]$

$Vi\_EV = XA\_E \cdot (L\_E - Zi\_E)$

$V\_EV = XA\_E \cdot (L\_E - Z\_E)$

$Vi\_EV = L\_E \cdot \left[\dfrac{\pi \cdot D\_E^2}{8} + \dfrac{D\_E^2}{4} \cdot ASIN\left[1 - \dfrac{2 \cdot Zi\_E}{D\_E}\right] + \left[\dfrac{D\_E}{2} - Zi\_E\right] \cdot (Zi\_E \cdot (D\_E - Zi\_E))^{0.5} \right]$

$V\_EV = L\_E \cdot \left[\dfrac{\pi \cdot D\_E^2}{8} + \dfrac{D\_E^2}{4} \cdot ASIN\left[1 - \dfrac{2 \cdot Z\_E}{D\_E}\right] + \left[\dfrac{D\_E}{2} - Z\_E\right] \cdot (Z\_E \cdot (D\_E - Z\_E))^{0.5} \right]$

$Vi\_V = Vi\_CV + Vi\_EV + \dfrac{\pi}{4} \cdot \left[PL\_E \cdot PD\_E^2 - L\_CT \cdot D\_CT^2 \right]$

$V\_V = V\_CV + V\_EV + \dfrac{\pi}{4} \cdot \left[PL\_E \cdot PD\_E^2 - L\_CT \cdot D\_CT^2 \right]$

; Vacuum Pressure

Rules

$$Pi\_H2O = e^{\left[PA - \frac{PB}{T + PC} \right]}$$

$$P\_H2O = e^{\left[PA - \frac{PB}{T\_E + PC} \right]}$$

$$Pi\_V = 0.14$$

$$Pi\_V = Pi\_H2O$$

$$Pi\_V = \frac{\Sigma Nai\_C \cdot R \cdot (T + 273.15)}{Vi\_V}$$

$$Pt\_V = \frac{\Psi \cdot \Sigma Na\_C \cdot R \cdot (T\_E + 273.15)}{V\_V} + (P\_H2O - Pi\_H2O)$$

$$\Psi = 1 - 2.2860837 \cdot e^{\left[\frac{-P\_V}{P\_H2O} \right]}$$

$$P\_V = ELT('Pt\_V , ELT() - 1 , Pi\_V)$$

$$\frac{P\_BP}{P\_V} = z\_N2 \cdot \alpha\_N2 \cdot K\_N2 + z\_O2 \cdot \alpha\_O2 \cdot K\_O2 + z\_Ar \cdot \alpha\_Ar \cdot K\_Ar + z\_CO2 \cdot \alpha\_CO2 \cdot K\_CO2 + z\_H2O \cdot \alpha\_H2$$

$$\frac{P\_V}{P\_DP} = \frac{z\_N2}{\alpha\_N2 \cdot K\_N2} + \frac{z\_O2}{\alpha\_N2 \cdot K\_O2} + \frac{z\_Ar}{\alpha\_N2 \cdot K\_Ar} + \frac{z\_CO2}{\alpha\_N2 \cdot K\_CO2} + \frac{z\_H2O}{\alpha\_H2O \cdot K\_H2O}$$

; Heat Transfer

$$hi\_CT = 0.00030525050070753090 \cdot \left[\frac{1.35 + 0.02 \cdot T\_X}{D\_CT} \right] \cdot \left[\frac{M\_X}{\rho\_X \cdot D\_CT} \right]^{0.8}$$

$$ho\_CT = 0.725 \cdot \left[\frac{g \cdot HL\_E \cdot \rho\_X^2 \cdot k\_X^3}{N\_CT \cdot \mu\_X \cdot (D\_CT + \delta\_CT) \cdot (T\_E - T\_X)} \right]^{0.25}$$

$$\frac{1}{U\_CT} = \frac{1}{ho\_CT} + \frac{1}{hod\_CT} + \frac{D\_CT + \delta\_CT}{D\_CT \cdot hi\_CT} + \frac{D\_CT + \delta\_CT}{D\_CT \cdot hid\_CT} + \frac{D\_CT + \delta\_CT}{2 \cdot kw\_CT} \cdot LN\left[\frac{D\_CT + \delta\_CT}{D\_CT} \right]$$

$$A\_CT = \pi \cdot D\_CT \cdot L\_CT$$

$$S\_CT = \frac{T\_X - T\_P}{T\_E - T\_P}$$

$$F\_CT = 0.029277821 + 0.16549348 \cdot S\_CT + 2.9101541 \cdot S\_CT^2 - 6.1629393 \cdot S\_CT^3 + 4.251837 \cdot S\_CT^4$$

$$\Delta Tm\_CT = \frac{T\_X - T\_P}{LN\left[\frac{T\_E - T\_P}{T\_E - T\_X} \right]}$$

$$M\_X \cdot H\_X - M\_P \cdot H\_P = 60 \cdot U\_CT \cdot A\_CT \cdot F\_CT \cdot \Delta Tm\_CT$$

$$hi\_C = 1.13 \cdot \left[\frac{g \cdot HL\_E \cdot \rho\_C^2 \cdot k\_C^3}{\mu\_C \cdot L\_C \cdot (T\_E - T)} \right]^{0.25}$$

Appendix M (Continued)

Rules

$$ho\_C = 0.04477637899495253 \cdot \left[\frac{T\_E - T}{L\_C} \right]^{0.25}$$

$$\frac{1}{U\_C} = \frac{1}{ho\_C} + \frac{1}{hod\_C} + \frac{D\_C + \delta\_C}{D\_C \cdot hi\_C} + \frac{D\_C + \delta\_C}{D\_C \cdot hid\_C} + \frac{D\_C + \delta\_C}{2 \cdot kw\_C} \cdot LN\left[\frac{D\_C + \delta\_C}{D\_C} \right]$$

$$A\_C = \pi \cdot D\_C \cdot L\_C$$

$$S\_C = \frac{T\_C - T}{T\_E - T}$$

$$;F\_C = f(S\_C)$$

$$\Delta Tm\_C = \frac{T\_C - T}{LN\left[\frac{T\_E - T}{T\_E - T\_C} \right]}$$

$$-Q\_C = 60 \cdot U\_C \cdot A\_C \cdot F\_C \cdot \Delta Tm\_C$$

$$hi\_E = 1.13 \cdot \left[\frac{g \cdot HL\_E \cdot \rho\_W^2 \cdot k\_W^3}{\mu\_W \cdot L\_E \cdot (T\_E - T)} \right]^{0.25}$$

$$ho\_E = 0.04477637899495253 \cdot \left[\frac{T\_E - T}{L\_E} \right]^{0.25}$$

$$\frac{1}{U\_E} = \frac{1}{ho\_E} + \frac{1}{hod\_E} + \frac{D\_E + \delta\_E}{D\_E \cdot hi\_E} + \frac{D\_E + \delta\_E}{D\_E \cdot hid\_E} + \frac{D\_E + \delta\_E}{2 \cdot kw\_E} \cdot LN\left[\frac{D\_E + \delta\_E}{D\_E} \right]$$

$$A\_E = \pi \cdot D\_E \cdot L\_E$$

$$S\_E = \frac{T\_W - T}{T\_E - T}$$

$$;F\_E = f(S\_E)$$

$$\Delta Tm\_E = \frac{T\_W - T}{LN\left[\frac{T\_E - T}{|T\_E - T\_W|} \right]}$$

$$-Q\_E = 60 \cdot U\_E \cdot A\_E \cdot F\_E \cdot \Delta Tm\_E$$

; Equipment Sizing

$$HP\_P = \frac{-W\_P}{44741.994}$$

$$NPSH = \frac{1000000 \cdot (P - Pi\_H2O - \Delta P\_S)}{\rho\_S \cdot g} + \frac{\left[\frac{M\_S}{15 \cdot \pi \cdot \rho\_S \cdot PD\_S^2} \right]^2}{2 \cdot g} + Z\_S - Z\_P$$

$$\Delta P = \Delta P\_S + \Delta P\_P + \Delta P\_X + \Delta P\_H + \Delta P\_HT + \Delta P\_CT$$

$$P\_O - P = \frac{-\rho\_P \cdot \eta\_P \cdot W\_P}{10 \cdot M\_P} - \frac{\rho\_P \cdot g \cdot (Z\_O - Z\_P)}{1000000} - \Delta P$$

$$C\_O = \left[\frac{41318.7502427578}{M\_H} \right] \cdot (\rho\_H \cdot (P\_O - Pi\_V))^{0.5}$$

234

Appendix M (Continued)

Rules

$$D\_O = \left[\frac{PD\_H^4}{1 + PD\_H^4 \cdot C\_O^2} \right]^{0.25}$$

$$Mmax\_O = 14416.2942558703 \cdot CV\_O \cdot \rho\_H \cdot \left[\frac{P\_O - Pi\_V}{SG\_H} \right]^{0.5}$$

$$A\_SC = \frac{Q\_H}{60 \cdot F\_SC \cdot (\tau\_SC \cdot \alpha\_SC \cdot I - U\_SC \cdot (T\_X - T))}$$

; System Performance

$$W\_P = 0$$

$$W\_P = M\_P \cdot \left[\frac{g \cdot (Z\_S - Z\_O)}{10000000} + \frac{P\_V - P - \Delta P}{10 \cdot \rho\_P} \right]$$

$$T\_S = T$$

$$T\_C = 22$$

$$BPE = 8.77 \cdot \Phi\_H \cdot \left[0.9576 + 0.8189E\text{-}2 \cdot T\_E + 0.1647E\text{-}4 \cdot T\_E^2 \right] - 0.05$$

$$NEA = \frac{33 \cdot (T\_H - T\_E)^{0.55}}{T\_E - BPE}$$

$$T\_W = T\_E + BPE + NEA$$

$$\frac{T\_W + 273.15}{T\_E + 273.15} = 1.683590 \cdot \left[\frac{T\_H + 273.15}{298.15} \right]^2 - 3.389767 \cdot \left[\frac{T\_H + 273.15}{298.15} \right] + 2.778541 - 0.13986184 \cdot e^{\left[-5.9153673 \cdot \right.}$$

$$\eta\_T = \frac{100 \cdot M\_E \cdot (H\_E + HL\_E)}{M\_H \cdot H\_H}$$

$$\eta\_R = \frac{100 \cdot (H\_X - H\_P)}{H\_H - H\_P}$$

$$\eta\_C = \frac{100 \cdot (T\_X - T\_P)}{T\_E - T\_C}$$

$$\Sigma Q\_H = INTEGRAL(\text{" } Q\_H , t \text{ "}, ELT(\text{'}t , ELT() - 1 , ti) , t) + ELT(\text{'}\Sigma Q\_H , ELT() - 1 , 0)$$

$$\Sigma W\_P = INTEGRAL(\text{" } W\_P , t \text{ "}, ELT(\text{'}t , ELT() - 1 , ti) , t) + ELT(\text{'}\Sigma W\_P , ELT() - 1 , 0)$$

$$PEC = \frac{\Sigma Q\_H + \Sigma W\_P}{\Sigma M\_C}$$

; Pressure Drops

$$\Delta P\_S = \frac{6.7906109052542E\text{-}07 \cdot \mu\_S \cdot PL\_S \cdot M\_S}{\rho\_S \cdot PD\_S^4}$$

$$\Delta P\_P = \frac{6.7906109052542E\text{-}07 \cdot \mu\_P \cdot PL\_P \cdot M\_P}{\rho\_P \cdot PD\_P^4}$$

Appendix M (Continued)

Rules

$$\Delta P\_X = \frac{6.7906109052542\text{E-}07 \cdot \mu\_X \cdot PL\_X \cdot M\_X}{\rho\_X \cdot PD\_X^4}$$

$$\Delta P\_H = \frac{6.7906109052542\text{E-}07 \cdot \mu\_H \cdot PL\_H \cdot M\_H}{\rho\_H \cdot PD\_H^4}$$

$$\Delta P\_W = \frac{6.7906109052542\text{E-}07 \cdot \mu\_W \cdot PL\_W \cdot M\_W}{\rho\_W \cdot PD\_W^4}$$

$$\Delta P\_C = \frac{6.7906109052542\text{E-}07 \cdot \mu\_C \cdot PL\_C \cdot M\_C}{\rho\_C \cdot PD\_C^4}$$

$$\Delta P\_E = \frac{6.7906109052542\text{E-}07 \cdot \mu\_E \cdot PL\_E \cdot M\_E}{\rho\_E \cdot PD\_E^4}$$

$$\Delta P\_HT = \frac{6.7906109052542\text{E-}07 \cdot \mu\_H \cdot L\_HT \cdot M\_H}{\rho\_H \cdot D\_HT^4}$$

$$\Delta P\_CT = \frac{6.7906109052542\text{E-}07 \cdot \mu\_X \cdot L\_CT \cdot M\_X}{\rho\_X \cdot D\_CT^4}$$

; Enthalpies

$$H\_S = 4.204501 \cdot T\_S - 6.78226 \cdot \Phi\_S \cdot T\_S + 14.7532 \cdot \Phi\_S^2 \cdot T\_S - \left[0.00068002552 - 0.03095114 \cdot \Phi\_S + 0.162443\ldots\right.$$

$$H\_P = 4.204501 \cdot T\_P - 6.78226 \cdot \Phi\_P \cdot T\_P + 14.7532 \cdot \Phi\_P^2 \cdot T\_P - \left[0.00068002552 - 0.03095114 \cdot \Phi\_P + 0.162443\ldots\right.$$

$$H\_X = 4.204501 \cdot T\_X - 6.78226 \cdot \Phi\_X \cdot T\_X + 14.7532 \cdot \Phi\_X^2 \cdot T\_X - \left[0.00068002552 - 0.03095114 \cdot \Phi\_X + 0.1624438 \cdot\right.$$

$$H\_H = 4.204501 \cdot T\_H - 6.78226 \cdot \Phi\_H \cdot T\_H + 14.7532 \cdot \Phi\_H^2 \cdot T\_H - \left[0.00068002552 - 0.03095114 \cdot \Phi\_H + 0.162443\ldots\right.$$

$$H\_W = 4.204501 \cdot T\_W - 6.78226 \cdot \Phi\_W \cdot T\_W + 14.7532 \cdot \Phi\_W^2 \cdot T\_W - \left[0.00068002552 - 0.03095114 \cdot \Phi\_W + 0.16\ldots\right.$$

$$H\_C = 4.204501 \cdot T\_C - 6.78226 \cdot \Phi\_C \cdot T\_C + 14.7532 \cdot \Phi\_C^2 \cdot T\_C - \left[0.00068002552 - 0.03095114 \cdot \Phi\_C + 0.162443\ldots\right.$$

$$H\_E = 4.204501 \cdot T\_E - 6.78226 \cdot \Phi\_E \cdot T\_E + 14.7532 \cdot \Phi\_E^2 \cdot T\_E - \left[0.00068002552 - 0.03095114 \cdot \Phi\_E + 0.162443\ldots\right.$$

$$HL\_E = 2496.21010517215 - 1.9534839865599 \cdot T\_E - 0.00417809176330114 \cdot T\_E^2$$

$$H\_N2 = A\_N2 \cdot (T\_E + 273.15) + \left[\frac{B\_N2}{2000}\right] \cdot (T\_E + 273.15)^2 + \left[\frac{C\_N2}{3000000}\right] \cdot (T\_E + 273.15)^3 + \left[\frac{D\_N2}{4000000000}\right] \cdot (T\ldots$$

$$H\_O2 = A\_O2 \cdot (T\_E + 273.15) + \left[\frac{B\_O2}{2000}\right] \cdot (T\_E + 273.15)^2 + \left[\frac{C\_O2}{3000000}\right] \cdot (T\_E + 273.15)^3 + \left[\frac{D\_O2}{4000000000}\right] \cdot (T\ldots$$

$$H\_Ar = A\_Ar \cdot (T\_E + 273.15) + \left[\frac{B\_Ar}{2000}\right] \cdot (T\_E + 273.15)^2 + \left[\frac{C\_Ar}{3000000}\right] \cdot (T\_E + 273.15)^3 + \left[\frac{D\_Ar}{4000000000}\right] \cdot (T\_E\ldots$$

Appendix M (Continued)

Rules

$$H\_CO2 = A\_CO2 \cdot (T\_E + 273.15) + \left[\frac{B\_CO2}{2000}\right] \cdot (T\_E + 273.15)^2 + \left[\frac{C\_CO2}{3000000}\right] \cdot (T\_E + 273.15)^3 + \left[\frac{D\_CO2}{4000000000}\right].$$

$$H\_H2O = A\_H2O \cdot (T\_E + 273.15) + \left[\frac{B\_H2O}{2000}\right] \cdot (T\_E + 273.15)^2 + \left[\frac{C\_H2O}{3000000}\right] \cdot (T\_E + 273.15)^3 + \left[\frac{D\_H2O}{4000000000}\right].$$

$$Ha\_C = \frac{y\_N2 \cdot H\_N2 + y\_O2 \cdot H\_O2 + y\_Ar \cdot H\_Ar + y\_CO2 \cdot H\_CO2}{(1 - y\_H2O) \cdot MWa\_C}$$

; Densities

ρA_S = 0.824493 + T_S · (-0.0040899 + T_S · (0.000076438 + T_S · (-0.00000082467 + T_S · 0.0000000053875)))

ρA_P = 0.824493 + T_P · (-0.0040899 + T_P · (0.000076438 + T_P · (-0.00000082467 + T_P · 0.0000000053875)))

ρA_X = 0.824493 + T_X · (-0.0040899 + T_X · (0.000076438 + T_X · (-0.00000082467 + T_X · 0.0000000053875)))

ρA_H = 0.824493 + T_H · (-0.0040899 + T_H · (0.000076438 + T_H · (-0.00000082467 + T_H · 0.0000000053875)))

ρA_W = 0.824493 + T_W · (-0.0040899 + T_W · (0.000076438 + T_W · (-0.00000082467 + T_W · 0.0000000053875

ρA_C = 0.824493 + T_C · (-0.0040899 + T_C · (0.000076438 + T_C · (-0.00000082467 + T_C · 0.0000000053875)))

ρB_S = -0.00572466 + T_S · (0.00010227 - 0.0000016546 · T_S)

ρB_P = -0.00572466 + T_P · (0.00010227 - 0.0000016546 · T_P)

ρB_X = -0.00572466 + T_X · (0.00010227 - 0.0000016546 · T_X)

ρB_H = -0.00572466 + T_H · (0.00010227 - 0.0000016546 · T_H)

ρB_W = -0.00572466 + T_W · (0.00010227 - 0.0000016546 · T_W)

ρB_C = -0.00572466 + T_C · (0.00010227 - 0.0000016546 · T_C)

ρC_S = 999.842594 + T_S · (0.06793952 + T_S · (-0.009095290 + T_S · (0.0001001685 + T_S · (-0.000001120083

ρC_P = 999.842594 + T_P · (0.06793952 + T_P · (-0.009095290 + T_P · (0.0001001685 + T_P · (-0.000001120083

ρC_X = 999.842594 + T_X · (0.06793952 + T_X · (-0.009095290 + T_X · (0.0001001685 + T_X · (-0.000001120083 +

ρC_H = 999.842594 + T_H · (0.06793952 + T_H · (-0.009095290 + T_H · (0.0001001685 + T_H · (-0.000001120083

ρC_W = 999.842594 + T_W · (0.06793952 + T_W · (-0.009095290 + T_W · (0.0001001685 + T_W · (-0.000001120C

ρC_C = 999.842594 + T_C · (0.06793952 + T_C · (-0.009095290 + T_C · (0.0001001685 + T_C · (-0.000001120083

$$\rho\_S = \frac{\rho C\_S}{1000} + \Phi\_S \cdot \left[\rho A\_S + \rho B\_S \cdot (1000 \cdot \Phi\_S)^{0.5} + 0.48314 \cdot \Phi\_S\right]$$

$$\rho\_P = \frac{\rho C\_P}{1000} + \Phi\_P \cdot \left[\rho A\_P + \rho B\_P \cdot (1000 \cdot \Phi\_P)^{0.5} + 0.48314 \cdot \Phi\_P\right]$$

$$\rho\_X = \frac{\rho C\_X}{1000} + \Phi\_X \cdot \left[\rho A\_X + \rho B\_X \cdot (1000 \cdot \Phi\_X)^{0.5} + 0.48314 \cdot \Phi\_X\right]$$

$$\rho\_H = \frac{\rho C\_H}{1000} + \Phi\_H \cdot \left[\rho A\_H + \rho B\_H \cdot (1000 \cdot \Phi\_H)^{0.5} + 0.48314 \cdot \Phi\_H\right]$$

$$\rho\_W = \frac{\rho C\_W}{1000} + \Phi\_W \cdot \left[\rho A\_W + \rho B\_W \cdot (1000 \cdot \Phi\_W)^{0.5} + 0.48314 \cdot \Phi\_W\right]$$

$$\rho\_C = \frac{\rho C\_C}{1000} + \Phi\_C \cdot \left[\rho A\_C + \rho B\_C \cdot (1000 \cdot \Phi\_C)^{0.5} + 0.48314 \cdot \Phi\_C\right]$$

Appendix M (Continued)

$$\rho\_E = e^{\left[-13.4579133153846 + 4.1055E\text{-}2 \cdot (1.8 \cdot T\_E + 32) - 7.1159E\text{-}5 \cdot (1.8 \cdot T\_E + 32)^2 + 5.7039E\text{-}8 \cdot (1.8 \cdot T\_E + 32)^3\right]}$$

; Viscosities

$\mu A\_S = 1.0675E\text{-}4 + 5.185E\text{-}5 \cdot T\_S$

$\mu A\_P = 1.0675E\text{-}4 + 5.185E\text{-}5 \cdot T\_P$

$\mu A\_X = 1.0675E\text{-}4 + 5.185E\text{-}5 \cdot T\_X$

$\mu A\_H = 1.0675E\text{-}4 + 5.185E\text{-}5 \cdot T\_H$

$\mu A\_W = 1.0675E\text{-}4 + 5.185E\text{-}5 \cdot T\_W$

$\mu A\_C = 1.0675E\text{-}4 + 5.185E\text{-}5 \cdot T\_C$

$\mu B\_S = 2.591E\text{-}3 + 3.3E\text{-}5 \cdot T\_S$

$\mu B\_P = 2.591E\text{-}3 + 3.3E\text{-}5 \cdot T\_P$

$\mu B\_X = 2.591E\text{-}3 + 3.3E\text{-}5 \cdot T\_X$

$\mu B\_H = 2.591E\text{-}3 + 3.3E\text{-}5 \cdot T\_H$

$\mu B\_W = 2.591E\text{-}3 + 3.3E\text{-}5 \cdot T\_W$

$\mu B\_C = 2.591E\text{-}3 + 3.3E\text{-}5 \cdot T\_C$

$\mu C\_S = 553.541280340981 \cdot \rho\_S \cdot \Phi\_S$

$\mu C\_P = 553.541280340981 \cdot \rho\_P \cdot \Phi\_P$

$\mu C\_X = 553.541280340981 \cdot \rho\_X \cdot \Phi\_X$

$\mu C\_H = 553.541280340981 \cdot \rho\_H \cdot \Phi\_H$

$\mu C\_W = 553.541280340981 \cdot \rho\_W \cdot \Phi\_W$

$\mu C\_C = 553.541280340981 \cdot \rho\_C \cdot \Phi\_C$

$$\mu D\_S = 0.01002 \cdot 10^{\left[\frac{1.1709 \cdot (20 - T\_S) - 1.827E\text{-}3 \cdot (T\_S - 20)^2}{T\_S + 89.93}\right]}$$

$$\mu D\_P = 0.01002 \cdot 10^{\left[\frac{1.1709 \cdot (20 - T\_P) - 1.827E\text{-}3 \cdot (T\_P - 20)^2}{T\_P + 89.93}\right]}$$

$$\mu D\_X = 0.01002 \cdot 10^{\left[\frac{1.1709 \cdot (20 - T\_X) - 1.827E\text{-}3 \cdot (T\_X - 20)^2}{T\_X + 89.93}\right]}$$

$$\mu D\_H = 0.01002 \cdot 10^{\left[\frac{1.1709 \cdot (20 - T\_H) - 1.827E\text{-}3 \cdot (T\_H - 20)^2}{T\_H + 89.93}\right]}$$

$$\mu D\_W = 0.01002 \cdot 10^{\left[\frac{1.1709 \cdot (20 - T\_W) - 1.827E\text{-}3 \cdot (T\_W - 20)^2}{T\_W + 89.93}\right]}$$

Appendix M (Continued)

$$\mu D\_C = 0.01002 \cdot 10^{\left[\frac{1.1709 \cdot (20 - T\_C) - 1.827\text{E-3} \cdot (T\_C - 20)^2}{T\_C + 89.93}\right]}$$

$$\mu\_S = \left[1 + \mu A\_S \cdot \mu C\_S^{0.5} + \mu B\_S \cdot \mu C\_S\right] \cdot \mu D\_S$$

$$\mu\_P = \left[1 + \mu A\_P \cdot \mu C\_P^{0.5} + \mu B\_P \cdot \mu C\_P\right] \cdot \mu D\_P$$

$$\mu\_X = \left[1 + \mu A\_X \cdot \mu C\_X^{0.5} + \mu B\_X \cdot \mu C\_X\right] \cdot \mu D\_X$$

$$\mu\_H = \left[1 + \mu A\_H \cdot \mu C\_H^{0.5} + \mu B\_H \cdot \mu C\_H\right] \cdot \mu D\_H$$

$$\mu\_W = \left[1 + \mu A\_W \cdot \mu C\_W^{0.5} + \mu B\_W \cdot \mu C\_W\right] \cdot \mu D\_W$$

$$\mu\_C = \left[1 + \mu A\_C \cdot \mu C\_C^{0.5} + \mu B\_C \cdot \mu C\_C\right] \cdot \mu D\_C$$

$$\mu\_E = 7.23123710739283\text{E-5} + 2.37506847313357\text{E-07} \cdot (1.8 \cdot T\_E + 32) - 5.67031837890055\text{E-11} \cdot (1.8 \cdot T\_E + 32)^2$$

; Thermal Conductivities

$$k\_S = 0.00571116 + 0.00001713348 \cdot T\_S - 0.00000005853939 \cdot T\_S^2 - 0.0016562364 \cdot \Phi\_S$$

$$k\_P = 0.00571116 + 0.00001713348 \cdot T\_P - 0.00000005853939 \cdot T\_P^2 - 0.0016562364 \cdot \Phi\_P$$

$$k\_X = 0.00571116 + 0.00001713348 \cdot T\_X - 0.00000005853939 \cdot T\_X^2 - 0.0016562364 \cdot \Phi\_X$$

$$k\_H = 0.00571116 + 0.00001713348 \cdot T\_H - 0.00000005853939 \cdot T\_H^2 - 0.0016562364 \cdot \Phi\_H$$

$$k\_W = 0.00571116 + 0.00001713348 \cdot T\_W - 0.00000005853939 \cdot T\_W^2 - 0.0016562364 \cdot \Phi\_W$$

$$k\_C = 0.00571116 + 0.00001713348 \cdot T\_C - 0.00000005853939 \cdot T\_C^2 - 0.0016562364 \cdot \Phi\_C$$

$$ka\_C = 1.5207\text{E-13} \cdot (T\_E + 273.15)^3 - 4.8574\text{E-10} \cdot (T\_E + 273.15)^2 + 1.0184\text{E-06} \cdot (T\_E + 273.15) - 3.9333\text{E-06}$$

$$k\_E = 1.69430023512008\text{E-4} + 3.89120840469752\text{E-7} \cdot (1.8 \cdot T\_E + 32) - 5.8517701472412\text{E-10} \cdot (1.8 \cdot T\_E + 32)^2 +$$

; Reynolds Numbers

$$Re\_S = \frac{M\_S}{15 \cdot \pi \cdot PD\_S \cdot \mu\_S}$$

$$Re\_P = \frac{M\_P}{15 \cdot \pi \cdot PD\_P \cdot \mu\_P}$$

$$Re\_X = \frac{M\_X}{15 \cdot \pi \cdot PD\_X \cdot \mu\_X}$$

$$Re\_H = \frac{M\_H}{15 \cdot \pi \cdot PD\_H \cdot \mu\_H}$$

Appendix M (Continued)

Rules

$$Re\_W = \frac{M\_W}{15 \cdot \pi \cdot PD\_W \cdot \mu\_W}$$

$$Re\_C = \frac{M\_C}{15 \cdot \pi \cdot PD\_C \cdot \mu\_C}$$

$$Re\_E = \frac{M\_E}{15 \cdot \pi \cdot PD\_E \cdot \mu\_E}$$

; Prandtl Numbers

$$Pr\_S = \frac{H\_S \cdot \mu\_S}{(T\_S + 273.15) \cdot k\_S}$$

$$Pr\_P = \frac{H\_P \cdot \mu\_P}{(T\_P + 273.15) \cdot k\_P}$$

$$Pr\_X = \frac{H\_X \cdot \mu\_X}{(T\_X + 273.15) \cdot k\_X}$$

$$Pr\_H = \frac{H\_H \cdot \mu\_H}{(T\_H + 273.15) \cdot k\_H}$$

$$Pr\_W = \frac{H\_W \cdot \mu\_W}{(T\_W + 273.15) \cdot k\_W}$$

$$Pr\_C = \frac{H\_C \cdot \mu\_C}{(T\_C + 273.15) \cdot k\_C}$$

$$Pr\_E = \frac{H\_E \cdot \mu\_E}{(T\_E + 273.15) \cdot k\_E}$$

; Nusselt Numbers

$$Nu\_S = 1.86 \cdot \left[\frac{Re\_S \cdot Pr\_S \cdot PD\_S}{PL\_S} \right]^{0.33}$$

$$Nu\_P = 1.86 \cdot \left[\frac{Re\_P \cdot Pr\_P \cdot PD\_P}{PL\_P} \right]^{0.33}$$

$$Nu\_X = 1.86 \cdot \left[\frac{Re\_X \cdot Pr\_X \cdot PD\_X}{PL\_X} \right]^{0.33}$$

$$Nu\_H = 1.86 \cdot \left[\frac{Re\_H \cdot Pr\_H \cdot PD\_H}{PL\_H} \right]^{0.33}$$

$$Nu\_W = 1.86 \cdot \left[\frac{Re\_W \cdot Pr\_W \cdot PD\_W}{PL\_W} \right]^{0.33}$$

$$Nu\_C = 1.86 \cdot \left[\frac{Re\_C \cdot Pr\_C \cdot PD\_C}{PL\_C} \right]^{0.33}$$

$$Nu\_E = 1.86 \cdot \left[\frac{Re\_E \cdot Pr\_E \cdot PD\_E}{PL\_E} \right]^{0.33}$$

Appendix M (Continued)

Variables Sheet

Input	Name	Output	Unit	Comment
0	ti		min	Initial Time
1	t		min	Run Time
20	T		°C	Ambient Temperature
1.01325	P		bar	Ambient Pressure
	FI	0.483692	L / min	Average Flow Indicator Value
27	QE		cm ^ 3	Average Quantitative Element Value
	ΣM	27.668601	g	Actual Product Amount
83.14472	R		(bar - cm ^ 3) / (mol - °C)	Universal Gas Constant
980.0665	g		cm / s ^ 2	Gravity Acceleration
	P_BP	47.803156	bar	Bubble Point Pressure
	P_DP	0.145822	bar	Dew Point Pressure
	ΣM_S	495.669161	g	Total Seawater Amount
	ΣM_W	495.911874	g	Total Brine Amount
	ΣM_C	-0.253082	g	Total Condensed Steam Amount
	ΣNa_C	1.786244	mol	Total NCG Amount
	ΣQ_H	41983.941375	J	Heat Input
	ΣW_P	0	J	Power Input
	PEC	-165890.373805	J / g	Prime Energy Consumption
.5503	ω_Cl			Chloride Mass Fraction in Seawater Salt
.3059	ω_Na			Sodium Mass Fraction in Seawater Salt
.0768	ω_SO4			Sulfate Mass Fraction in Seawater Salt
.0368	ω_Mg			Magnesium Mass Fraction in Seawater Salt
.0118	ω_Ca			Calcium Mass Fraction in Seawater Salt
.0111	ω_K			Potassium Mass Fraction in Seawater Salt
.0041	ω_HCO3			Bicarbonate Mass Fraction in Seawater Salt
.0019	ω_Br			Bromide Mass Fraction in Seawater Salt
.0008	ω_BO3			Borate Mass Fraction in Seawater Salt
.0004	ω_Sr			Strontium Mass Fraction in Seawater Salt
.00003	ω_F			Fluoride Mass Fraction in Seawater Salt
35.453	MW_Cl		g / mol	Chloride Molecular Weight
22.99	MW_Na		g / mol	Sodium Molecular Weight
96.062	MW_SO4		g / mol	Sulfate Molecular Weight
24.305	MW_Mg		g / mol	Magnesium Molecular Weight
40.078	MW_Ca		g / mol	Calcium Molecular Weight
39.098	MW_K		g / mol	Potassium Molecular Weight
61.016	MW_HCO3		g / mol	Bicarbonate Molecular Weight
79.904	MW_Br		g / mol	Bromide Molecular Weight
58.808	MW_BO3		g / mol	Borate Molecular Weight
87.62	MW_Sr		g / mol	Strontium Molecular Weight

Input	Name	Output	Unit	Comment
18.998	MW_F		g / mol	Fluoride Molecular Weight
28.0134	MW_N2		g / mol	Nitrogen Molecular Weight
31.998	MW_O2		g / mol	Oxygen Molecular Weight
39.94	MW_Ar		g / mol	Argon Molecular Weight
44.009	MW_CO2		g / mol	Carbon Dioxide Molecular Weight
	MW_Salt	31.416538	g / mol	Approximated Seawater Salt Molecular Weight
18.0148	MW_H2O		g / mol	Water Molecular Weight
0.000013	Φ_N2			Nitrogen Mass Fraction in Ambient Seawater
0.000008	Φ_O2			Oxygen Mass Fraction in Ambient Seawater
0.000000	Φ_Ar			Argon Mass Fraction in Ambient Seawater
0.000000	Φ_CO2			Carbon Dioxide Mass Fraction in Ambient Seawater
	Φ_H2O	0.964979		Water Mass Fraction in Ambient Seawater
	z_N2	0.000008		Nitrogen Mole Fraction in Ambient Seawater
	z_O2	0.000004		Oxygen Mole Fraction in Ambient Seawater
	z_Ar	0.000000		Argon Mole Fraction in Ambient Seawater
	z_CO2	0.000000		Carbon Dioxide Mole Fraction in Ambient Seawater
	z_Salt	0.020374		Salt Mole Fraction in Ambient Seawater
	z_H2O	0.979613		Water Mole Fraction in Ambient Seawater
	x_N2	0.000000		Nitrogen Mole Fraction in Brine Water
	x_O2	0.000000		Oxygen Mole Fraction in Brine Water
	x_Ar	0.000000		Argon Mole Fraction in Brine Water
	x_CO2	0.000000		Carbon Dioxide Mole Fraction in Brine Water
	x_Salt	0.020715		Salt Mole Fraction in Brine Water
	x_H2O	0.979285		Water Mole Fraction in Brine Water
	y_N2	0.000500		Nitrogen Mole Fraction in Vaporized Water
	y_O2	0.000268		Oxygen Mole Fraction in Vaporized Water
	y_Ar	0.000011		Argon Mole Fraction in Vaporized Water
	y_CO2	0.000006		Carbon Dioxide Mole Fraction in Vaporized Water
	y_H2O	0.999216		Water Mole Fraction in Vaporized Water
26.092	A_N2			Nitrogen Molar Enthalpy Parameter
8.218801	B_N2			Nitrogen Molar Enthalpy Parameter
-1.976141	C_N2			Nitrogen Molar Enthalpy Parameter
.159274	D_N2			Nitrogen Molar Enthalpy Parameter
.044434	E_N2			Nitrogen Molar Enthalpy Parameter
-7.98923	F_N2			Nitrogen Molar Enthalpy Parameter
29.659	A_O2			Oxygen Molar Enthalpy Parameter
6.137261	B_O2			Oxygen Molar Enthalpy Parameter

Input	Name	Output	Unit	Comment
-1.186521	C_O2			Oxygen Molar Enthalpy Parameter
.09578	D_O2			Oxygen Molar Enthalpy Parameter
-.219663	E_O2			Oxygen Molar Enthalpy Parameter
-9.861391	F_O2			Oxygen Molar Enthalpy Parameter
20.786	A_Ar			Argon Molar Enthalpy Parameter
0.000000	B_Ar			Argon Molar Enthalpy Parameter
0.000000	C_Ar			Argon Molar Enthalpy Parameter
0.000000	D_Ar			Argon Molar Enthalpy Parameter
0.000000	E_Ar			Argon Molar Enthalpy Parameter
-6.19735	F_Ar			Argon Molar Enthalpy Parameter
24.99735	A_CO2			Carbon Dioxide Molar Enthalpy Parameter
55.18696	B_CO2			Carbon Dioxide Molar Enthalpy Parameter
-33.69137	C_CO2			Carbon Dioxide Molar Enthalpy Parameter
7.948387	D_CO2			Carbon Dioxide Molar Enthalpy Parameter
-.136638	E_CO2			Carbon Dioxide Molar Enthalpy Parameter
-10.0851	F_CO2			Carbon Dioxide Molar Enthalpy Parameter
30.092	A_H2O			Water Molar Enthalpy Parameter
6.832514	B_H2O			Water Molar Enthalpy Parameter
6.793435	C_H2O			Water Molar Enthalpy Parameter
-2.53448	D_H2O			Water Molar Enthalpy Parameter
.082139	E_H2O			Water Molar Enthalpy Parameter
-9.054600	F_H2O			Water Molar Enthalpy Parameter
	H_N2	408.621886	J / mol	Nitrogen Molar Enthalpy
	H_O2	402.549078	J / mol	Oxygen Molar Enthalpy
	H_Ar	301.655669	J / mol	Argon Molar Enthalpy
	H_CO2	540.860997	J / mol	Carbon Dioxide Molar Enthalpy
	H_H2O	488.461223	J / mol	Water Molar Enthalpy
	H_S	79.740379	J / g	Stream Enthalpy
	H_P	79.740379	J / g	Stream Enthalpy
	H_X	115.076142	J / g	Stream Enthalpy
	H_H	199.777682	J / g	Stream Enthalpy
	H_W	160.594502	J / g	Stream Enthalpy
	H_C	92.177531	J / g	Stream Enthalpy
	H_E	165.347464	J / g	Stream Enthalpy
	HL_E	2412.499766	J / g	Stream Enthalpy of Vaporization
8067573.136086	HC_N2		bar	Nitrogen Reference State Henry's Constant

243

Appendix M (Continued)

Input	Name	Output	Unit	Comment
358814.929481	HC_O2		bar	Oxygen Reference State Henry's Constant
384073.329688	HC_Ar		bar	Argon Reference State Henry's Constant
10914.952753	HC_CO2		bar	Carbon Dioxide Reference State Henry's Constant
-3545.567207	HF_N2		°C	Nitrogen Henry's Coefficient
-2208.812178	HF_O2		°C	Oxygen Henry's Coefficient
-2308.046425	HF_Ar		°C	Argon Henry's Coefficient
-445.190581	HF_CO2		°C	Carbon Dioxide Henry's Coefficient
12.762946	PA			Water Vapor Pressure Coefficient
4391.129422	PB		°C	Water Vapor Pressure Coefficient
245.367016	PC		°C	Water Vapor Pressure Coefficient
1.21	α_N2			Nitrogen Relative Solubility
1.22	α_O2			Oxygen Relative Solubility
1.23	α_Ar			Argon Relative Solubility
1.17	α_CO2			Carbon Dioxide Relative Solubility
.9816	α_H2O			Water Relative Vapor Pressure
	K_N2	33181360.195354		Evaporator-Based Nitrogen VLE Distribution Coefficient
	K_O2	1817195.406546		Evaporator-Based Oxygen VLE Distribution Coefficient
	K_Ar	1915296.044397		Evaporator-Based Argon VLE Distribution Coefficient
	K_CO2	72743.446749		Evaporator-Based Carbon Dioxide VLE Distribution Coefficient
	K_H2O	1.039478		Evaporator-Based Water VLE Distribution Coefficient
	T_S	20	°C	Stream Temperature
	T_P	20	°C	Stream Temperature
	T_X	28.842820	°C	Stream Temperature
50	T_H		°C	Stream Temperature
	T_W	40.218905	°C	Stream Temperature
	T_C	22	°C	Stream Temperature
	T_E	39.512635	°C	Stream Temperature
.035	Φ_S			Stream Salt Mass Fraction
	Φ_P	.035		Stream Salt Mass Fraction
	Φ_X	.035		Stream Salt Mass Fraction
	Φ_H	.035		Stream Salt Mass Fraction
	Φ_W	0.034983		Stream Salt Mass Fraction
0	Φ_C			Stream Salt Mass Fraction
	Φ_E	0		Stream Salt Mass Fraction
	MW_S	18.287997	g / mol	Stream Molecular Weight
	MW_P	18.287997	g / mol	Stream Molecular Weight

Appendix M (Continued)

Input	Name	Output	Unit	Comment
	MW_X	18.287997	g / mol	Stream Molecular Weight
	MW_H	18.287997	g / mol	Stream Molecular Weight
	MW_W	18.292413	g / mol	Stream Molecular Weight
	MW_C	18.0148	g / mol	Stream Molecular Weight
	MW_E	18.023930	g / mol	Stream Molecular Weight
	M_S	495.669161	g / min	Stream Mass Flow Rate
	M_P	495.669161	g / min	Stream Mass Flow Rate
	M_X	495.669161	g / min	Stream Mass Flow Rate
	M_H	495.669161	g / min	Stream Mass Flow Rate
	M_W	495.911874	g / min	Stream Mass Flow Rate
	M_C	-0.253082	g / min	Stream Mass Flow Rate
	M_E	-0.242713	g / min	Stream Mass Flow Rate
	N_S	27.103524	mol / min	Stream Molar Flow Rate
	N_P	27.103524	mol / min	Stream Molar Flow Rate
	N_X	27.103524	mol / min	Stream Molar Flow Rate
	N_H	27.103524	mol / min	Stream Molar Flow Rate
	N_W	26.657744	mol / min	Stream Molar Flow Rate
	N_C	0.445430	mol / min	Stream Molar Flow Rate
	N_E	0.445779	mol / min	Stream Molar Flow Rate
	ρA_S	0.767535		Stream Density Coefficient
	ρA_P	0.767535		Stream Density Coefficient
	ρA_X	0.754059		Stream Density Coefficient
	ρA_H	0.741681		Stream Density Coefficient
	ρA_W	0.744091		Stream Density Coefficient
	ρA_C	0.763992		Stream Density Coefficient
	ρB_S	-0.004341		Stream Density Coefficient
	ρB_P	-0.004341		Stream Density Coefficient
	ρB_X	-0.004151		Stream Density Coefficient
	ρB_H	-0.004748		Stream Density Coefficient
	ρB_W	-0.004288		Stream Density Coefficient
	ρB_C	-0.004276		Stream Density Coefficient
	ρC_S	998.206319		Stream Density Coefficient
	ρC_P	998.206319		Stream Density Coefficient
	ρC_X	995.994512		Stream Density Coefficient
	ρC_H	988.064493		Stream Density Coefficient
	ρC_W	992.136617		Stream Density Coefficient
	ρC_C	997.773037		Stream Density Coefficient

Appendix M (Continued)

Input	Name	Output	Unit	Comment
	ρ_S	1.024763	g / cm ^ 3	Stream Density
	ρ_P	1.024763	g / cm ^ 3	Stream Density
	ρ_X	1.022119	g / cm ^ 3	Stream Density
	ρ_H	1.013632	g / cm ^ 3	Stream Density
	ρ_W	1.017871	g / cm ^ 3	Stream Density
	ρ_C	0.997773	g / cm ^ 3	Stream Density
	ρ_E	0.000049	g / cm ^ 3	Stream Density
	μA_S	0.001144		Stream Viscosity Coefficient
	μA_P	0.001144		Stream Viscosity Coefficient
	μA_X	0.001602		Stream Viscosity Coefficient
	μA_H	0.002699		Stream Viscosity Coefficient
	μA_W	0.002192		Stream Viscosity Coefficient
	μA_C	0.001247		Stream Viscosity Coefficient
	μB_S	.003251		Stream Viscosity Coefficient
	μB_P	.003251		Stream Viscosity Coefficient
	μB_X	0.003543		Stream Viscosity Coefficient
	μB_H	.004241		Stream Viscosity Coefficient
	μB_W	0.003918		Stream Viscosity Coefficient
	μB_C	.003317		Stream Viscosity Coefficient
	μC_S	19.853702		Stream Viscosity Coefficient
	μC_P	19.853702		Stream Viscosity Coefficient
	μC_X	19.802474		Stream Viscosity Coefficient
	μC_H	19.638053		Stream Viscosity Coefficient
	μC_W	19.710527		Stream Viscosity Coefficient
	μC_C	0		Stream Viscosity Coefficient
	μD_S	.01002		Stream Viscosity Coefficient
	μD_P	.01002		Stream Viscosity Coefficient
	μD_X	0.008175		Stream Viscosity Coefficient
	μD_H	0.005471		Stream Viscosity Coefficient
	μD_W	0.006505		Stream Viscosity Coefficient
	μD_C	0.009547		Stream Viscosity Coefficient
	μ_S	0.010718	P	Stream Viscosity
	μ_P	0.010718	P	Stream Viscosity
	μ_X	0.008807	P	Stream Viscosity
	μ_H	0.005992	P	Stream Viscosity
	μ_W	0.007070	P	Stream Viscosity
	μ_C	0.009547	P	Stream Viscosity

Appendix M (Continued)

Input	Name	Output	Unit	Comment
	μ_E	0.000096	P	Stream Viscosity
	k_S	0.005972	W / (cm - °C)	Stream Thermal Conductivity
	k_P	0.005972	W / (cm - °C)	Stream Thermal Conductivity
	k_X	0.006099	W / (cm - °C)	Stream Thermal Conductivity
	k_H	0.006364	W / (cm - °C)	Stream Thermal Conductivity
	k_W	0.006248	W / (cm - °C)	Stream Thermal Conductivity
	k_C	0.006060	W / (cm - °C)	Stream Thermal Conductivity
	k_E	0.000206	W / (cm - °C)	Stream Thermal Conductivity
	Re_S	772.754293		Stream Reynolds Number
	Re_P	772.754293		Stream Reynolds Number
	Re_X	940.429542		Stream Reynolds Number
	Re_H	1382.136449		Stream Reynolds Number
	Re_W	1171.973697		Stream Reynolds Number
	Re_C	-1.771727		Stream Reynolds Number
	Re_E	-10.539154		Stream Reynolds Number
	Pr_S	0.488137		Stream Prandtl Number
	Pr_P	0.488137		Stream Prandtl Number
	Pr_X	0.550268		Stream Prandtl Number
	Pr_H	0.582159		Stream Prandtl Number
	Pr_W	0.579965		Stream Prandtl Number
	Pr_C	0.492048		Stream Prandtl Number
	Pr_E	0.247172		Stream Prandtl Number
	Nu_S			Stream Nusselt Number
	Nu_P			Stream Nusselt Number
	Nu_X			Stream Nusselt Number
	Nu_H			Stream Nusselt Number
	Nu_W			Stream Nusselt Number
	Nu_C			Stream Nusselt Number
	Nu_E			Stream Nusselt Number
1.27	PD_S		cm	Stream Nominal Pipe Diameter
1.27	PD_P		cm	Stream Nominal Pipe Diameter
1.27	PD_X		cm	Stream Nominal Pipe Diameter
1.27	PD_H		cm	Stream Nominal Pipe Diameter
1.27	PD_W		cm	Stream Nominal Pipe Diameter
5.08	PD_E		cm	Stream Nominal Pipe Diameter
.3175	PD_C		cm	Stream Nominal Pipe Diameter
95	PL_S		cm	Stream Equivalent Pipe Length
25	PL_P		cm	Stream Equivalent Pipe Length
60	PL_X		cm	Stream Equivalent Pipe Length
75	PL_H		cm	Stream Equivalent Pipe Length

Appendix M (Continued)

Input	Name	Output	Unit	Comment
30	PL_W		cm	Stream Equivalent Pipe Length
180	PL_E		cm	Stream Equivalent Pipe Length
35	PL_C		cm	Stream Equivalent Pipe Length
	ΔP_S	0.000129	bar	Stream Pressure Drop
	ΔP_P	0.000034	bar	Stream Pressure Drop
	ΔP_X	0.000067	bar	Stream Pressure Drop
	ΔP_H	0.000057	bar	Stream Pressure Drop
	ΔP_W	0.000027	bar	Stream Pressure Drop
	ΔP_C	-0.000006	bar	Stream Pressure Drop
	ΔP_E	0.000000	bar	Stream Pressure Drop
	ΔP_CT	0.000530	bar	Condenser Tube Side Pressure Drop
	ΔP_HT	0.000010	bar	Heater Tube Side Pressure Drop
	ΔP	0.000826	bar	Total Pressure Drop From Pump to Valve
90	D_S		cm	Seawater Tank Nominal Diameter
35	D_B		cm	Brine Water Tank Nominal Diameter
35	D_F		cm	Fresh Water Tank Nominal Diameter
35	D_E		cm	Evaporator Nominal Diameter
35	D_C		cm	Condenser Nominal Diameter
30	L_S		cm	Seawater Tank Length
160	L_B		cm	Brine Water Tank Length
160	L_F		cm	Fresh Water Tank Length
160	L_E		cm	Evaporator Length
160	L_C		cm	Condenser Length
	XA_S	6361.725124	cm^2	Seawater Tank Cross Sectional Area
	XA_B	962.112750	cm^2	Brine Water Tank Cross Sectional Area
	XA_F	962.112750	cm^2	Fresh Water Tank Cross Sectional Area
	XA_E	962.112750	cm^2	Evaporator Cross Sectional Area
	XA_C	962.112750	cm^2	Condenser Cross Sectional Area
	V_S	190851.753706	cm^3	Seawater Tank Volume
	V_B	153938.040026	cm^3	Brine Water Tank Volume
	V_F	153938.040026	cm^3	Fresh Water Tank Volume
	V_E	153938.040026	cm^3	Evaporator Volume
	V_C	153938.040026	cm^3	Condenser Volume
	Zi_S	24	cm	Initial Seawater Tank Level
	Zi_E	0	cm	Initial Evaporator Level
	Zi_C	0	cm	Initial Condenser Level
	Z_S	23.923968	cm	Seawater Tank Level
5	Z_B		cm	Brine Water Tank Level
5	Z_F		cm	Fresh Water Tank Level

248

Input	Name	Output	Unit	Comment
	Z_E	0.506391	cm	Evaporator Level
	Z_C	-0.000264	cm	Condenser Level
	Vi_CV	153938.040026	cm ^ 3	Initial Condenser Vacuum Volume
	Vi_EV	153938.040026	cm ^ 3	Initial Evaporator Vacuum Volume
	Vi_V	310922.658770	cm ^ 3	Initial Total Vacuum Volume
	V_CV	153938.293673	cm ^ 3	Condenser Vacuum Volume
	V_EV	153450.835048	cm ^ 3	Evaporator Vacuum Volume
	V_V	310435.707439	cm ^ 3	Total Vacuum Volume
.118	Ω		bar	Steam Diffusion Resistance
2	σ		(g - °C ^ 0.5) / (bar - min - cm ^ 2)	Steam Diffusion Coefficient
	Md_E	-8.277411	g / min	Steam Diffusion Rate
	Ed_E	20008.593395	J / min	Steam Diffusion Energy
	Ψ	0.685501		Fraction of NCG Molecules Accumulating
	ΣNai_C	1.785895	moles	Initial NCG Molar Amount
	γ_H2O	2.061926		Water Activity Coefficient
	Pi_H2O	0.022722	bar	Initial Vapor Pressure
	P_H2O	0.070578	bar	Vapor Pressure
	Pi_V	.14	bar	Initial Vacuum Pressure
	Pt_V	0.150395	bar	Transitional Vacuum Pressure
	P_V	.14	bar	Vacuum Pressure
	Ein_P	39524.846869	J / min	Pump Energy Input
	Ein_C	38899.169216	J / min	Condenser Energy Input
	Ein_H	57039.694651	J / min	Heater Energy Input
	Ein_E	99023.636026	J / min	Evaporator Energy Input
	Eout_P	39524.846869	J / min	Pump Energy Output
	Eout_C	57016.366136	J / min	Condenser Energy Output
	Eout_H	99023.636026	J / min	Heater Energy Output
	Eout_E	79015.042631	J / min	Evaporator Energy Output
0	Q_P		J / min	Pump Heat Input
	Q_C	18117.338871	J / min	Condenser Heat Input
	Q_H	41983.941375	J / min	Heater Heat Input
0	Q_E		J / min	Evaporator Heat Input
	W_P	0	J / min	Pump Work Output
0	W_C		J / min	Condenser Work Output
0	W_H		J / min	Heater Work Output
0	W_E		J / min	Evaporator Work Output
	ka_C	0.000272	W / (cm - °C)	NCG Thermal Conductivity
	Ha_C	13.689610	J / g	NCG Enthalpy

Input	Name	Output	Unit	Comment
	MWa_C	29.655207	g / mol	NCG Molecular Weight
	Ma_C	0.010369	g / min	NCG Mass Accumulation Rate
	Na_C	0.000350	mol / min	NCG Molar Accumulation Rate
	Ea_C	0.141950	J / min	NCG Energy Accumulation
2	Z_P		cm	Pump Center Elevation
250	Z_O		cm	Expansion Orifice Center Elevation
	HP_P	0	HP	Pump Power
	NPSH	1008.068669	cm	Net Positive Suction Head
	P_O	0.763349	bar	Expansion Orifice Inlet Pressure
	C_O	66.261451	1 / cm ^ 2	Expansion Orifice Coefficient
	D_O	0.122846	cm	Expansion Orifice Nominal Diameter
	SG_H	1.025876		Stream Specific Gravity
	Mmax_O	7290.073786	g / min	Maximum Flow Delivered By Needle Valve
.64	CV_O			Needle Valve Flow Coefficient
0.546461	CV			Ball Valve Flow Coefficient
1.27	D_HT		cm	Heater Tube Diameter
13	L_HT		cm	Heater Tube Length
1.27	D_CT		cm	Condenser Tube Diameter
475	L_CT		cm	Condenser Tube Length
.2	hid_CT		W / (cm ^ 2 - °C)	Condenser Tube Inside Dirt Coefficient
.5	hod_CT		W / (cm ^ 2 - °C)	Condenser Tube Outside Dirt Coefficient
	hi_CT	0.053853	W / (cm ^ 2 - °C)	Condenser Tube Inside Fluid Film Coefficient
	ho_CT	0.737128	W / (cm ^ 2 - °C)	Condenser Tube Outside Fluid Film Coefficient
.5	hid_C		W / (cm ^ 2 - °C)	Condenser Inside Dirt Coefficient
.75	hod_C		W / (cm ^ 2 - °C)	Condenser Outside Dirt Coefficient
	hi_C	0.411422	W / (cm ^ 2 - °C)	Condenser Inside Fluid Film Coefficient
	ho_C	0.026460	W / (cm ^ 2 - °C)	Condenser Outside Fluid Film Coefficient
.5	hid_E		W / (cm ^ 2 - °C)	Evaporator Inside Dirt Coefficient
.75	hod_E		W / (cm ^ 2 - °C)	Evaporator Outside Dirt Coefficient
	hi_E	0.458323	W / (cm ^ 2 - °C)	Evaporator Inside Fluid Film Coefficient
	ho_E	0.026460	W / (cm ^ 2 - °C)	Evaporator Outside Fluid Film Coefficient
4	N_CT			Number of Condenser Tube Vertical Rows
.125	δ_CT		cm	Condenser Tube Thickness
3.81	kw_CT		W / (cm - °C)	Condenser Tube Thermal Conductivity
.25	δ_C		cm	Condenser Thickness
.45	kw_C		W / (cm - °C)	Condenser Thermal Conductivity
.25	δ_E		cm	Evaporator Thickness
.001	kw_E		W / (cm - °C)	Evaporator Thermal Conductivity
	U_CT	0.034173	W / (cm ^ 2 - °C)	Condenser Tube Overall Heat Transfer Coefficient
	A_CT	1895.165768	cm ^ 2	Condenser Tube Surface Area
	S_CT	0.453184		Condenser Tube Counter Current Departure Parameter

Appendix M (Continued)

Input	Name	Output	Unit	Comment
	F_CT	0.307688		Condenser Tube Counter Current Departure Correction Factor
	ΔTm_CT	14.649078	°C	Condenser Tube Logarithmic Mean Temperature Difference
	U_C	0.022796	W / (cm ^ 2 - °C)	Condenser Overall Heat Transfer Coefficient
	A_C	17592.918860	cm ^ 2	Condenser Surface Area
	S_C	0.102498		Condenser Counter Current Departure Parameter
	F_C	-0.040709		Condenser Counter Current Departure Correction Factor
	ΔTm_C	18.494616	°C	Condenser Logarithmic Mean Temperature Difference
	U_E	0.005925	W / (cm ^ 2 - °C)	Evaporator Overall Heat Transfer Coefficient
	A_E	17592.918860	cm ^ 2	Evaporator Surface Area
	S_E	1.036195		Evaporator Counter Current Departure Parameter
	F_E	0		Evaporator Counter Current Departure Correction Factor
	ΔTm_E	6.092195	°C	Evaporator Logarithmic Mean Temperature Difference
	BPE		°C	Boiling Point Elevation
	NEA		°C	Non Equilibrium Allowance
75	η_P		%	Pumping Efficiency
	η_R	29.437318	%	Recovery Efficiency
	η_T	-0.631847	%	Thermal Efficiency
	η_C	50.493944	%	Condenser Efficiency
.92	α_SC			Solar Collector Absorptance
.9	τ_SC			Solar Collector Transmittance
.000092	U_SC		W / (cm ^ 2 - °C)	Solar Collector Heat Loss Conductance
.82	F_SC			Solar Collector Heat Removal Factor
.06	I		W / cm ^ 2	Incident Insolation On Solar Collector
	A_SC	17462.532227	cm ^ 2	Solar Collector Area
21.022222	T_Xe		°C	Experimental Value of Stream Temperature
21.240556	T_We		°C	Experimental Value of Stream Temperature
24.241111	T_Ee		°C	Experimental Value of Stream Temperature
0.140585	Pt_Ve		bar	Experimental Value of Vacuum Pressure

251

Appendix N. Experimental record

Number	Date	Start	Stop	t (minutes)	PE^i (bar)	V_S^i (Gallon)	V_S^f (Gallon)	M_S (LPM)	TIC (°C)	QE (ml)
1	4/24/09	3:20:00 PM	6:20:00 PM	180	0.140	40	17	0.48	50	30
2	4/25/09	1:15:00 PM	4:15:00 PM	180	0.140	40	17	0.48	50	15
3	4/26/09	2:09:00 PM	5:09:00 PM	180	0.140	40	17	0.48	50	36
4	4/27/09	12:55:00 PM	3:55:00 PM	180	0.140	40	18	0.46	60	345
5	4/28/09	12:42:00 PM	3:42:00 PM	180	0.140	40	18	0.46	60	350
6	4/29/09	12:37:00 PM	3:37:00 PM	180	0.140	40	18	0.46	60	360
7	4/30/09	1:17:00 PM	4:17:00 PM	180	0.140	40	19	0.44	70	2030
8	5/1/09	2:49:00 PM	5:49:00 PM	180	0.140	40	19	0.44	70	2050
9	5/2/09	1:07:00 PM	4:07:00 PM	180	0.140	40	19	0.44	70	2030
10	5/3/09	1:37:00 PM	4:37:00 PM	180	0.140	40	22	0.38	80	4880
11	5/4/09	1:17:00 PM	4:17:00 PM	180	0.140	40	22	0.38	80	4720
12	5/5/09	1:47:00 PM	4:47:00 PM	180	0.140	40	22	0.38	80	4560
13	5/15/09	1:13:00 PM	4:13:00 PM	180	0.140	40	7	0.69	50	13
14	5/16/09	1:04:00 PM	4:04:00 PM	180	0.140	40	7	0.69	50	25
15	5/17/09	2:24:00 PM	5:24:00 PM	180	0.140	40	7	0.69	50	27
16	5/18/09	12:24:00 PM	3:24:00 PM	180	0.140	40	8	0.67	60	190
17	5/19/09	12:30:00 PM	3:30:00 PM	180	0.140	40	8	0.67	60	205
18	5/20/09	12:59:00 PM	3:59:00 PM	180	0.140	40	8	0.67	60	200
19	5/21/09	12:24:00 PM	3:24:00 PM	180	0.140	40	9	0.65	70	1310
20	5/22/09	1:24:00 PM	4:24:00 PM	180	0.140	40	9	0.65	70	1180
21	5/23/09	1:39:00 PM	4:39:00 PM	180	0.140	40	9	0.65	70	1145
22	5/24/09	2:42:00 PM	5:42:00 PM	180	0.140	40	13	0.57	80	4995
23	5/25/09	1:04:00 PM	4:04:00 PM	180	0.140	40	13	0.57	80	4770
24	5/26/09	1:04:00 PM	4:04:00 PM	180	0.140	40	13	0.57	80	4365

Appendix O. Experimental equipment specifications

1 Seawater Tank – McMaster–Carr

Polyethylene Troughs

Polyethylene troughs are built tough so they won't rust, dent, or leak—even when frozen. All are nestable.
(A) Structural-foam troughs have a heavy-wall construction and a 1 1/4" NPT female plastic drain with plug. Max. temperature is 120° F. Color is black.
(B) FDA-compliant trough is ideal for contents where sanitation is important. Made of FDA-compliant resins and meets USDA requirements. Max. temperature is 156° F. Color is white. *Optional cover* is made of white polyethylene. *Optional mobile base* is made of a galvanized steel angle frame and has four 5" dia. phenolic swivel casters. Base adds 6 7/8" to trough height.

Cap., gal.	O'all Body Size, Lg. x Wd.†	O'all Top Size, Lg. x Wd.	O'all Ht.	Wall Thick.		Each
Structural-Foam Troughs						
50	49 1/2" x 28 5/8"	52" x 31"	12"	1/4"	3673K49	$118.22
100	49 1/2" x 28 1/2"	53" x 31"	25"	1/4"	3673K52	109.36
150	55" x 36 1/8"	58" x 39"	25"	5/16"	3673K53	183.02
300	66 1/4" x 60 1/2"	69" x 63 1/4"	25"	5/16"	3673K54	284.35

† Represents dimensions just below top lip.

1 Condenser – McMaster–Carr

ASME Painted-Steel Tanks

Manufactured in accordance with ASME codes. Maximum pressure is 150 psi. Maximum operating temperature is 450° F. Tanks have a gray enamel finish.
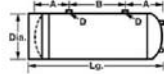
Cap., gal.	Dia.	Lg.	(A)	(B)	(C)	Opening Pipe Size (D)	(E)	Wall Ga		Each
15	12"	34 1/8"	7"	19"	8"	1"	1/2"	13	48075T61	$240.94
30	14"	49 3/8"	8 3/8"	31 1/4"	10"	1"	1/2"	12	48075T63	281.62
40	14"	64 3/8"	8 3/8"	46 1/4"	10"	1"	1/2"	12	48075T64	307.68
80	20"	64 5/16"	10"	42"	16"	1"	1/2"	11	48075T66	405.38

1 Evaporator – McMaster–Carr

Galvanized-Steel Tanks

Maximum pressure is 75 psi. Maximum operating temperature is 450° F. Tanks are hot-dipped for maximum corrosion resistance.
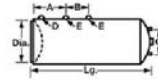
Cap., gal.	Dia.	Lg.	(A)	(B)	(C)	Opening Pipe Size (D)	(E)	(F)	Wall Ga		Each
8	12"	19"	4"	4"	8 13/16"	1 1/4"	1/2"	2"	14	3666K11	$181.95
15	12"	33"	4"	11"	8 13/16"	1 1/4"	1/2"	2"	14	3666K12	225.65
40	14"	63"	4"	26"	8 13/16"	1 1/4"	1/2"	2"	14	3666K16	364.01

End View

1 Electric Heater – McMaster–Carr

Water Heater Replacement Parts

Heater elements are made of zinc-plated copper and must be mounted horizontally. *Screw-in* style have 1" NPSM threads. *Flat flange* and *raised flange* styles have four bolt holes on a 2 1/2" dia. circle (gaskets are included; 5/16" dia. bolts are not). Flange is steel.
Thermostats are for 120 to 480 VAC. Temp. range is 120° to 160° F.
Pilot-light thermocouples include adapter nut. CSA certified.

Screw-In   Flat Flange   Raised Flange

Heater Elements

Watts	VAC (Phase)	Amps	Min. Tank Dia.		Each
Screw-In					
1500	120 (1)	12.5	8 1/2"	36555K31	$9.12
1500	240 (1)	6.25	8 1/2"	36555K34	9.28
4500	240 (1)	18.75	12"	36555K32	8.49
5500	240 (1)	22.92	12"	36555K33	12.81
Flat Flange Bolt-In					
1500	120 (1)	12.5	8 1/2"	36555K21	10.88
4500	240 (1)	18.75	12"	36555K22	11.12
5500	240 (1)	22.92	12"	36555K23	16.65
Raised Flange Bolt-In					
1500	120 (1)	12.5	8 1/2"	36555K41	10.60
4500	240 (1)	18.75	12"	36555K42	9.93

Pilot-Light Thermocouples

O'all Lg.		Each
18"	4148K14	$5.68
24"	4148K15	5.93
36"	4148K17	6.42
48"	4148K19	7.43

Thermostats

		Each
Lower Thermostat for Two-Element Heater	36555K14	$9.09
Upper Thermostat for Two-Element Heater	36555K16	19.88
Thermostat for One-Element Heater	36555K18	17.26

Appendix O (Continued)

CPVC Piping & Fittings – McMaster–Carr

Plastic Pipe Fittings and Pipe
26 products match your selections

Shape	Pipe
Pipe Type	Unthreaded
Pipe to Pipe Connection	Unthreaded (pipe)
System of Measurement	Inch
Schedule	80
Perforation Type	Solid Pipe
Material	CPVC
Color	Gray
Specifications Met	American Society for Testing and Materials (ASTM) and National Sanitation Foundation (NSF)
ASTM Specification	ASTM D1784 and ASTM F441
NSF Specification	NSF 61

Pipe/Thread Size

Pipe size is the accepted industry designation, not the actual measured size. To determine pipe size, first measure the inside diameter (ID) or outside diameter (OD) of a threaded fitting or the OD of unthreaded pipe, as shown at left. Then, round up the measurement to the closest ID or OD listed in the chart and select the corresponding pipe size. For example, if the fitting ID or OD measures 1-3/16", the next highest ID or OD in the chart is 1-3/8", and the corresponding pipe size is 1".

Threaded Fitting ID or OD	3/8"	1/2"	5/8"	3/4"	1"	1-3/8"	1-5/8"	1-7/8"	2-3/8"	2-7/8"	3-1/2"	4-1/2"	
Unthreaded Fitting and Pipe OD	1/2"	5/8"	3/4"	1"	1-1/8"	1-3/8"	1-3/4"	2"	2-1/2"	2-7/8"	3-1/2"	4-1/2"	6-3/4"
Pipe Size	1/8"	1/4"	3/8"	1/2"	3/4"	1"	1-1/4"	1-1/2"	2"	2-1/2"	3"	4"	6"

1/4" | 3/8" | 1/2" | 3/4" | 1" | 1-1/4" | 1-1/2" | 2" | 2-1/2" | 3" | 4" | 6" | 8"

Maximum Pressure (psi)
PSI (pounds per square inch) is the amount of pressure a pipe fitting can endure.

Low Pressure	High Pressure
250	520
280	630
320	690
370	850
400	920
420	1130
470	

Length
5' | 10'

Plastic Pipe Fittings and Pipe

Elbow Tee Coupling Union
Bushing Adapter Cap Plug
Flange Nipple Pipe

254

Appendix O (Continued)

Copper Piping & Fittings – McMaster–Carr

Tubing
126 products match your selections

Metal	Copper
Shape	Single Line
System of Measurement	Inch
Low Temperature Range	0° to +100° F
Metal Construction	Seamless
Fittings Used	Soldered Wrot Copper
Specifications Met	American Society for Testing and Materials (ASTM)

ASTM Specification
ASTM B88 | ASTM B280

Copper Material Type — Copper material comparison chart
Drinking Water Copper (Alloy 122) | General Purpose Copper (Alloy 122)

Dimensions

Outside Diameter
Inside Diameter
Wall Thickness
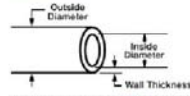
Select Outside Dia.: ▾   Select Inside Dia.: ▾   Select Wall Thickness: ▾

Tube Size
Tube size is the accepted designation for wrot copper tube fittings, not an actual diameter size. Specific diameters can be selected in Dimensions.
1/8" | 1/4" | 3/8" | 1/2" | 5/8" | 3/4" | 1" | 1-1/4" | 1-1/2" | 2" | 2-1/2" | 3"

Maximum Pressure Range, psi
Select the range of maximum pressure ratings (psi) that best approximates your need.
251-500 | 501-750 | 751-1,000 | 1,001-2,000 | 3,001-4,000

Operating Temperature
Select the range of low and/or high temperature resistance that best approximates your need. Before purchasing a product, verify that the Operating Temperature range is suitable for your application. These selections are meant only as a general guide.

High Temperature Range
+101° to +200° F
+301° to +500° F

Copper Tube Fittings

Elbow   Tee   Coupling

Adapter   Union   Reducer Bushing

Flange   Cap   Dissolvable Plug with Insertion Tool

255

Appendix O (Continued)

6 Ball Valves – McMaster–Carr

4 ½" Full Port with Lever Handle

2 ¼" Full Port with Lever Handle

Type 316 Stainless Steel Ball Valves

Full Port
- Max Pressure: W.O.G. (water, oil, inert gas): 1000 psi @ 200° F ; W.S.P. (working steam pressure): 150 psi @ 366° F
- Vacuum Rating: 28" Hg
- Temperature Range: -25° to +450° F

Reduced Port
- Maximum Pressure: W.O.G. (water, oil, inert gas): 800 psi @ 100° F ; W.S.P. (working steam pressure): 50 psi @ 297° F
- Vacuum Rating: 29" Hg
- Temperature Range: -25° to +450° F

Body, ball, and stem are Type 316 stainless steel for use in corrosive environments. Stem is blowout proof. Handle is Type 304 stainless steel with vinyl grip. On full-port models, seats are glass-filled PTFE and seals are PTFE; on reduced-port models, seats and packing are PTFE.
Connections: NPT female.
Valves can be locked in the closed position using a padlock (not included). Those with an **oval handle** prevent accidental snagging.

Pipe Size	End-to-End Lg.	Maximum Padlock Shackle Dia.	w/Lever Handle	Each	w/Oval Handle	Each
Full Port						
1/4"	2"	19/64"	46495K58	$27.02	46495K78	$29.80
3/8"	2"	19/64"	46495K59	27.02	46495K79	29.80
1/2"	2 23/64"	19/64"	46495K61	27.80	46495K81	30.47
3/4"	2 3/4"	19/64"	46495K62	37.15	46495K82	39.49
1"	3 1/4"	19/64"	46495K63	62.90	46495K83	55.48
1 1/4"	3 61/64"	19/64"	46495K64	92.17	46495K84	94.54
1 1/2"	4 21/64"	19/64"	46495K65	102.90	46495K85	102.83
2"	5 17/64"	19/64"	46495K66	137.97	46495K86	137.69
2 1/2"	6 37/64"	3/8"	46495K67	379.08	—	—
3"	7 35/64"	3/8"	46495K68	467.32	—	—
Reduced Port						
1/4"	1 17/32"	19/64"	46325K46	19.27	46325K66	26.41
3/8"	1 47/64"	19/64"	46325K47	19.27	46325K67	23.28
1/2"	2 7/32"	19/64"	46325K48	20.63	46325K68	21.25
3/4"	2 9/32"	19/64"	46325K49	26.75	46325K69	33.44
1"	2 61/64"	19/64"	46325K51	31.78	46325K71	41.84
1 1/4"	3 1/16"	19/64"	46325K52	47.36	46325K72	66.33
1 1/2"	3 47/64"	19/64"	46325K53	70.56	46325K73	81.80
2"	3 15/16"	19/64"	46325K54	81.98	46325K74	94.40

Insulation Material – McMaster–Carr

Plastics
This product matches all of your selections.

Part Number: 85316K303 $387.81 Each

Material	Garolite
Garolite Material	Grade XX Garolite
Backing	Plain Back
Shape	Sheets, Bars, Strips, and Cubes
Sheets, Bars, Strips, and Cubes Type	Rectangular Sheet
Thickness	1"
Thickness Tolerance	±.033"
Length	48"
Length Tolerance	±1"
Width	36"
Width Tolerance	±1"
Opaque	Black
Operating Temperature Range	+32° to +266° F
Performance Characteristic	High Tensile Strength
Tensile Strength	23,900 psi lengthwise, 16,100 psi crosswise
Impact Strength	0.55 ft.-lbs./in. lengthwise; 0.46 ft-lbs./in. crosswise
Tolerance	Standard
Hardness	Barcol 50-65
Specifications Met	Military Specifications (MIL), Underwriters Laboratories (UL)
MIL Specification	MIL-I-24768
UL Rating	UL 94HB

Strut Channels – McMaster–Carr

2 1" Solid 10' bars

7 1" Slotted–Hole 10' bars

2 0.5" Slotted–Hole 10' bars

Strut Channel

About Strut Channel and Accessories

The U-shaped design of strut channel provides connection points in suspending and routing applications. Strut channel can also be used to build structures such as racks.
Slotted-hole and round-hole strut channel allow connections to the channel opening, as well as connections to the back of the channel without drilling.
Solid strut channel allows connections to the channel opening.

Strut channel and accessories are available in a variety of materials:

Zinc-plated steel offers good corrosion resistance in most environments.
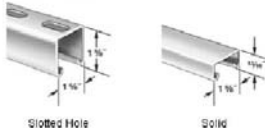**Primed steel** is ready for custom painting with no prep work required. It provides some corrosion resistance and can be welded.
Painted and choose-a-color steel are ideal for color coding your system. The powder-coated finish provides rust protection.
Aluminum is lightweight, yet strong and corrosion resistant.

Galvanized steel has a hot-dipped zinc coating for better corrosion resistance than zinc-plated steel.
Type 304 stainless steel offers excellent corrosion resistance.
Type 316 stainless steel provides maximum corrosion resistance.
Fiberglass (polyester) is nonconductive and maintenance free with good corrosion resistance. Compatible with metal accessories. Temperature range is -35° to +200° F.

Strut Channel

Save time—we have the length you need already cut. Strut channel is great for supporting conduit, pipe, electrical components, and duct.
Slotted-Hole Channel— Holes are 9/16" Wd. x 1 1/8" Lg. except on fiberglass, which has 3/8" Wd. x 1" Lg. holes. All holes are spaced on 2" centers.
Steel and Stainless Steel Channel— 1 5/8" x 1 5/8" channel is 0.105" thick and 13/16" x 1 5/8" channel is 0.079" thick.
Aluminum Channel— 1 5/8" x 1 5/8" channel is 0.08" thick and 13/16" x 1 5/8" channel is 0.084" thick.
Fiberglass Channel— Wall thickness is 0.13" for each side and 0.21" for the bottom. Color is gray.
6'8" length channel is for use with beams spaced 6 ft. apart. The length allows 4" on each end to attach the channel to the beam.
To Order: For 1- to 4-ft. lengths, please specify length: 1, 1 1/2, 2, 3, or 4 ft.
To Order: For choose-a-color steel, please specify color: black, red, white, or yellow.

Material	1- to 4-ft. Lg. Per Ft.	5-ft. Lg.	Each	6-ft. Lg.	Each	6'8" Lg.	Each	8-ft. Lg.	Each	10-ft. Lg.	Each
Slotted-Hole Channel											
1 5/8" x 1 5/8"											
Zinc-Plated Steel	3310T201 $4.11	3310T39	$19.52	3310T212	$22.19	3310T213	$24.66	3310T214	$29.59	3310T4	$34.94
Primed Steel	3310T334 8.82	3310T116	41.90	3310T117	47.63	3310T118	52.92	3310T119	63.50	3310T126	74.97
Green-Painted Steel	3310T107 4.11	3310T481	19.52	3310T172	22.19	3310T173	24.66	3310T174	29.59	3310T483	34.94
Choose- a-Color Steel	3310T285 4.65	3310T286	22.09	3310T287	25.11	3310T288	27.90	3310T289	33.48	3310T290	39.53
Aluminum	3230T81 5.57	3230T47	26.46	3230T82	30.08	3230T83	33.42	3230T84	40.10	3230T48	47.34
Galv. Steel	3310T628 10.41	3310T656	49.45	3310T657	56.21	33107658	62.48	3310T659	74.95	3310T661	88.48
Type 304 SS	33085T531 16.98	33085T22	80.66	33085T541	91.69	33095T542	101.88	33085T543	122.26	33085T43	144.33
Type 316 SS	33085T671 23.70	33085T76	112.58	33085T581	127.98	330985T582	142.20	33085T583	170.64	330857761	201.45
Fiberglass	3261T65 9.80	3261T35	46.55	3261T66	52.92	3261T67	58.80	3261T68	70.58	3261T36	88.20
13/16" x 1 5/8"											
Zinc-Plated Steel	3310T204 3.32	3310T49	15.77	3310T242	17.93	3310T243	19.92	3310T244	23.90	3310T8	28.22
Primed Steel	3310T335 6.32	3310T127	30.02	3310T128	34.13	3310T129	37.92	3310T136	45.50	3310T137	53.72
Green-Painted Steel	3310T202 3.32	3310T621	15.77	3310T222	17.93	3310T223	19.92	3310T224	23.90	3310T623	28.22
Choose- a-Color Steel	3310T291 3.65	3310T292	17.34	3310T293	19.71	3310T294	21.90	3310T295	26.28	3310T296	31.02
Aluminum	3230T85 3.61	3230T55	17.15	3230T86	19.49	3230T87	21.66	3230T88	25.99	3230T56	30.68
Galv. Steel	3310T629 6.96	3310T863	33.08	3310T684	37.58	3310T686	41.78	3310T868	50.11	3310T686	59.16
Type 304 SS	33085T611 12.34	33085T24	58.62	33085T631	66.64	33085T632	74.04	33085T633	86.85	33085T747	104.89
Type 316 SS	33085T681 14.77	330857774	70.16	33085T691	79.76	33085T692	88.62	33085T693	106.34	330857775	125.55
Fiberglass	3261T69 7.73	3261T71	36.72	3261T72	41.74	3261T73	46.38	3261T74	55.66	3261T75	65.70

Material	1- to 4-ft. Lg. Per Ft.	5-ft. Lg.	Each	6-ft. Lg.	Each	6'8" Lg.	Each	8-ft. Lg.	Each	10-ft. Lg.	Each
Solid Channel											
1 5/8" x 1 5/8"											
Zinc-Plated Steel	3310T103 4.55	3310T37	21.61	3310T132	24.57	3310T133	27.30	3310T134	32.78	3310T2	38.67
Primed Steel	3310T336 9.09	3310T149	43.18	3310T156	49.09	3310T157	54.54	3310T158	65.45	3310T159	77.27
Green-Painted Steel	3310T101 4.55	3310T441	21.61	3310T112	24.57	3310T113	27.30	3310T114	32.78	3310T443	38.67
Choose- a-Color Steel	3310T297 5.26	3310T298	24.94	3310T299	28.35	3310T301	31.50	3310T302	37.80	3310T303	44.62
Aluminum	3230T21 5.67	3230T85	26.93	3230T22	30.62	3230T23	34.02	3230T24	40.82	3230T66	48.20
Galv. Steel	3310T631 9.87	3310T972	46.88	3310T673	53.30	3310T674	59.22	3310T675	71.06	3310T676	83.89
Type 304 SS	33085T15 18.35	33085T21	87.16	33085T16	99.09	33085T17	110.10	33085T18	132.12	33085T41	155.98
Type 316 SS	33085T25 25.57	33085T26	121.46	33085T26	138.09	33085T27	153.42	33085T28	184.10	33085T49	217.34
Fiberglass	3261T61 7.95	3261T25	37.76	3261T62	42.93	3261T63	47.70	3261T64	57.24	3261T26	67.50
13/16" x 1 5/8"											
Zinc-Plated Steel	3310T106 3.43	3310T47	16.29	3310T162	18.52	3310T163	20.58	3310T164	24.70	3310T6	29.16
Primed Steel	3310T337 7.06	3310T166	33.53	3310T167	38.12	3310T168	42.36	3310T169	50.83	3310T176	60.01
Green-Painted Steel	3310T104 3.43	3310T581	16.29	3310T142	18.52	3310T143	20.58	3310T144	24.70	3310T583	29.16
Choose- a-Color Steel	3310T304 3.81	3310T305	18.10	3310T306	20.57	3310T307	22.88	3310T308	27.43	3310T306	32.38
Aluminum	3230T31 3.95	3230T75	18.76	3230T32	21.33	3230T33	23.70	3230T34	28.44	3230T76	33.58
Galv. Steel	3310T632 6.82	3310T878	31.45	3310T679	35.76	3310T681	39.72	3310T682	47.66	3310T683	56.27
Type 304 SS	33085T411 12.58	33085T23	59.76	33085T421	67.93	33085T422	75.48	33085T423	90.58	33085T746	106.93
Type 316 SS	33085T461 15.59	33085T59	74.05	33085T471	84.19	33085T472	93.54	330857473	112.25	33085T75	132.51
Fiberglass	3261T76 5.09	3261T77	24.18	3261T78	27.49	3261T79	30.54	3261T81	36.65	3261T82	43.27

15 lbs Sea Salt – Petco

Aquarium Systems Instant Ocean Aquarium Salt

Nitrate-free, phosphate-free, fast-dissolving mix contains every important major, minor and trace element necessary for the health of your aquarium.

12 of 13 (92%) of customers said they would recommend this product to a friend.

Aquarium Systems Instant Ocean Aquarium Salt

15 lbs. - Makes 50 Gallons

SKU: 77780

Instant Ocean salt is the most carefully formulated and most carefully manufactured synthetic sea salt in the world. It's pharmaceutically blended and scientifically analyzed. This complete formula contains every major, minor, and trace element necessary to insure that even the most delicate marine fish, invertebrates, and plants will thrive.

Exceptional solubility provides a clear solution in minutes and can be used immediately after mixing. Reaches and maintains proper pH quickly. The convenient one-part form is easy to use for mixing complete package or small quantities--no special additives to handle. Uniform particle size assures consistency throughout package--no separation during packaging and shipping.

Nitrate-free. Phosphate-free.

Simply put, no other product outperforms Instant Ocean salt. It's the world's most popular brand.

1 Needle Valve – Cole–Parmer

Plastic Needle Valves

EW-03245-70	Qty: 1
PP Needle Valve, 1/2" NPT(F)	Add to Cart

$74.00 / each (USD)   Available in 4 days.

Product Rating ☆☆☆☆☆ (0 Ratings)

PVC and PP valves withstand up to 150 psi; PVDF up to 200 psi. Seats are made of PTFE and O-rings made of Viton®. Pipe thread connections.

Specifications

NPT(F)	1/2"
Max gpm	8
Max temperature	250°F (121°C)
Material	polypropylene

258

Appendix O (Continued)

1 Vacuum Gauge – Cole–Parmer

WIKA Forged-Brass Liquid-Filled Gauge

EW-68051-22
WIKA FORGED BRASS INDUSTRIAL GAUGE ~ 30"HG TO 15 PSI, 1/2" NPT(M)

Qty: 1
Add to Cart

$157.00 / each (USD)   Available in 15 days.

Product Rating ☆☆☆☆☆ (0 Ratings)

- **Accurately measure pressure in heavy industrial environments**
-
- NEMA 4X (IP65) rated

These high-quality gauges are intended for use in adverse service conditions where pulsation or vibration exists. The solid forged-brass case and socket is resistant to shock and vibration, and is suitable for hydraulics and compressors. Liquid fill is glycerine.

1 Pressure Transducer – Cole–Parmer

Cole-Parmer High-Accuracy Pressure Transducers

EW-68075-02
−14.7 to 15 psig Cole-Parmer® ±0.25%-Accuracy Compound Transmitter, 4 to 20 mA Output

Qty: 1
Add to Cart

$149.00 / each (USD)   In stock.

Product Rating ☆☆☆☆☆ (0 Ratings)

Specifications

Output	4 to 20 mA
Accuracy	±0.25% full-scale
Process connection	1/4" NPT(M)
Power	9 to 30 VDC
Electrical connections	2-ft cable
Dimensions	2 3/4"L x 1 1/2" dia
Wetted parts	17-4 PH stainless steel
Range	-14.7 to 15 psig

259

Appendix O (Continued)

1 Flow Meter – Cole–Parmer

Easy-View Acrylic In-Line Flowmeters

EW-32477-02
General-Purpose Acrylic In-Line
Flowmeter for Liquids; 0.025 to
0.25 GPM, 3/8" NPT(F) Adapter

Qty: 1
Add to Cart

$98.00 / each (USD)   In stock.

Product Rating ☆☆☆☆☆ (0 Ratings)

- Choose the high/low level alarm meters to monitor critical flow points.
- Units designed for in-line installation.
- General purpose liquid flowmeters feature easy-to-read dual scales (GPM/LPM).
- Polypropylene-reinforced fittings have aluminum stress rings for added strength.
- Machined high-quality acrylic rod stock, polished to a clear-as-glass finish.
- Flow ranges up to 50 GPM with model 32477-82.

General-Purpose Acrylic Flowmeters are for liquids or air. Models for liquids have both English and metric direct-reading scales; models for air have English direct-reading scales only.
Large-Body Flowmeters are for use with liquids and are direct reading, with PVC floats and 11/2" NPT(M) PVC adapters.
Flowmeters with High/Low Level Alarm are for use with liquids and feature an adjustable aluminum sensor bezel clamp with an enclosed one-watt reed switch. Two lead wires are included for hookup to your own electronics.

Specifications

Flow rate	water	0.025 to 0.25 GPM (0.1 to 1 LPM)
Accuracy		±5% of reading
Repeatability		±1%
Material	Housing	Acrylic
	o-ring	Viton®
	float	316 SS
Max operating temperature		150°F
Max pressure		150 psi
Dimensions		8 3/16"H x 1 1/4" dia.
Scale		English/Metric
fitting	Polypropylene-reinforced with aluminum stress rings	
Connections		3/8" NPT(F), polypropylene reinforced, aluminum stress rings
Media		Liquids

260

1 Temperature Controller – Omega

1/16 DIN Autotune PID/On-Off Controllers with Modular Output Options

CN9000A Series

- 1/16 DIN Cutout
- User Selectable Input from 9 Thermocouple Types or RTD Input
- Clear 3 1/2 Digit High Brightness Green LED Display
- 0.1° Resolution to 200°
- Constant Setpoint Deviation Indication
- Auto/Manual Output Control
- User Select from Autotune PID, PI, PD, P or On/Off Control
- Independent Second Setpoint and Output Models
- Comprehensive Alarm Features Deviation, Full Scale, Loop Break with Latching Option
- Fault Indication for Sensor Burnout, Sensor Short, Heater Break and Process Diagnostics
- Min/Max Data Storage and Autotune Diagnostics Eliminates Need for Chart Recorder
- Optional 24 Vac Power
- Field Replaceable Output Modules

Click here for larger image.

The CN9000A digital temperature controllers feature high accuracy and reliability, and the sophisticated PID with approach control for optimal control during start-up and steady-state operation. These units are well suited for a broad range of applications, and are easy to install and operate. The unique, sophisticated autotune algorithm will calculate the optimum PID values, and additionally recommends the best value for cycle time. For most applications, the user need only select the desired input type, simply by using the front pushbuttons. The autotune parameters can be changed by the operator at any time, allowing the operator to fine tune the controller to an individual process.

The microprocessor holds all data in non-volatile memory, with the ability to retain data for 10 years with no power. The CN9000A has a large, 3 1/2 digit green LED readout, with auxiliary indicators for each output, and 3 LED's to indicate deviation from setpoint.

Selection of all operational controls is made through the keys on the front panel, with the display prompting the user through each step. After the parameters have been set, they can be locked in, simply by removing a jumper located behind the front bezel. The user can select the control mode and parameters, display resolution (1 or 0.1°), and units (°F/°C). The operator can also utilize the ranging feature, which limits the range in which the setpoint may be chosen, or lock out a user from changing the setpoint. The new single setpoint controller has rear termination. The optional second setpoint and output of the CN9000A model can be set for proportional, on-off or latching limit control, and can be set as either a tracking or non-tracking setpoint. Cycle time, proportional band and on-off deadband are all set independently of the primary setpoint.

1 ADC – Omega

Portable Data Acquisition SystemsFor Notebook and Desktop PCs

OMB-DAQBOOK Series

- Links to Notebook or Desktop PCs via a Standard or Enhanced Parallel Port (EPP) or Optional PCMCIA Link
- Operable From ac Adapter, Optional Nickel-Cadmium Power Module, 12 V Car Battery, or Any 9 to 20 Vdc Source
- Two 12-bit Analog Outputs
- 24 General-purpose Digital O Lines, Expandable to 192
- Five Programmable 16-bit Counter/timers
- DOS and Windows Drivers

Click here for larger image.

OMB-DAQBOOK portable data acquisition systems for notebook and desktop PCs offer 12- or 16-bit, 100 kHz data acquisition. The OMB-DAQBOOK models provide >700 Kbyte/s bidirectional data communication to the PC via an enhanced parallel port (EPP) or PCMCIA link interfaces. Operable from ac or dc power sources, OMB-DAQBOOK series products are ideal for a variety of portable, field, and benchtop applications. The OMB-DAQBOOKs' high performance A/D conversion and 100 kHz sampling make them particularly useful for applications with high accuracy and speed requirements. Their extensive I/O and signal conditioning capabilities, and low cost per channel also make them an effective alternative to more expensive stand-alone data loggers, less portable strip-chart recorders, and less versatile dedicated handheld devices. The OMB-DAQBOOKs are supplied with DaqView, a Windows-based data logging application that allows you to set up your acquisition applications and save acquired data directly to disk. The package includes thermocouple linearization for direct readout of temperatures when used with an OMB-DBK19 thermocouple card. The OMB-DAQBOOK products include drivers for Visual Basic, Quick Basic, C, and Pascal; they also include DOS drivers that are compatible with DAS-16, PIO-12, and CTM-05 boards. Several graphical analysis and control software packages also support the OMB-DAQBOOKs..

5 Single–Output Thermocouples – Omega

Quick Disconnect Thermocouples with Miniature Connectors

☐MQSS Series -JMQSS, KMQSS, EMQSS, TMQSS,NMQIN

MADE IN USA | RoHS BY PART®

$ **48.00** JMQSS-010G-6

- 6" and 12" Lengths in StocK
- Sheath Diameters from 0.010" to 0.125"
- 304SS or 321SS Sheath
- Grounded, Ungrounded or Exposed Junction
- Color-Coded SMP Miniature Connector Termination
- Mating Connector and Cable Clamp Included FREE!
- Custom Lengths Available
- Made from Special Limits of Error Material
- Glass Filled Nylon Connector Body Rated to 220°C (425°F)

Click here for larger image.

Alloy/ANSI Color Code	Sheath Dia. inches	Model No. 6" Length	Model No. 12" Length
J Iron-Constantan 304 SS Sheath	0.010	JMQSS-010(*)-6	JMQSS-010(*)-12
	0.020	JMQSS-020(*)-6	JMQSS-020(*)-12
	0.032	JMQSS-032(*)-6	JMQSS-032(*)-12
	0.040	JMQSS-040(*)-6	JMQSS-040(*)-12
	0.062	JMQSS-062(*)-6	JMQSS-062(*)-12
	0.125	JMQSS-125(*)-6	JMQSS-125(*)-12
K CHROMEGA®-ALOMEGA® 304 SS Sheath	0.010	KMQSS-010(*)-6	KMQSS-010(*)-12
	0.020	KMQSS-020(*)-6	KMQSS-020(*)-12
	0.032	KMQSS-032(*)-6	KMQSS-032(*)-12
	0.040	KMQSS-040(*)-6	KMQSS-040(*)-12
	0.062	KMQSS-062(*)-6	KMQSS-062(*)-12
	0.125	KMQSS-125(*)-6	KMQSS-125(*)-12
K CHROMEGA®-ALOMEGA® Super OMEGACLAD® XL Sheath Sheath	0.010	KMQXL-010(*)-6	KMQXL-010(*)-12
	0.020	KMQXL-020(*)-6	KMQXL-020(*)-12
	0.032	KMQXL-032(*)-6	KMQXL-032(*)-12
	0.040	KMQXL-040(*)-6	KMQXL-040(*)-12
	0.062	KMQXL-062(*)-6	KMQXL-062(*)-12
	0.125	KMQXL-125(*)-6	KMQXL-125(*)-12
N OMEGA-P®-OMEGA-N® Super OMEGACLAD® XL Sheath	0.020	NMQXL-020(*)-6	NMQXL-020(*)-12
	0.032	NMQXL-032(*)-6	NMQXL-032(*)-12
	0.040	NMQXL-040(*)-6	NMQXL-040(*)-12
	0.062	NMQXL-062(*)-6	NMQXL-062(*)-12
	0.125	NMQXL-125(*)-6	NMQXL-125(*)-12
E CHROMEGA®-Constantan 304 SS Sheath	0.010	EMQSS-010(*)-6	EMQSS-010(*)-12
	0.020	EMQSS-020(*)-6	EMQSS-020(*)-12
	0.032	EMQSS-032(*)-6	EMQSS-032(*)-12
	0.040	EMQSS-040(*)-6	EMQSS-040(*)-12
	0.062	EMQSS-062(*)-6	EMQSS-062(*)-12
	0.125	EMQSS-125(*)-6	EMQSS-125(*)-12
T Copper-Constantan 304 SS Sheath	0.020	TMQSS-020(*)-6	TMQSS-020(*)-12
	0.032	TMQSS-032(*)-6	TMQSS-032(*)-12
	0.040	TMQSS-040(*)-6	TMQSS-040(*)-12
	0.062	TMQSS-062(*)-6	TMQSS-062(*)-12
	0.125	TMQSS-125(*)-6	TMQSS-125(*)-12
N OMEGALLOY® Inconel 600 Sheath	0.010	NMQIN-010(*)-6	NMQIN-010(*)-12
	0.020	NMQIN-020(*)-6	NMQIN-020(*)-12
	0.032	NMQIN-032(*)-6	NMQIN-032(*)-12
	0.040	NMQIN-040(*)-6	NMQIN-040(*)-12
	0.062	NMQIN-062(*)-6	NMQIN-062(*)-12
	0.125	NMQIN-125(*)-6	NMQIN-125(*)-12

1 Dual–Output Thermocouple – Omega

Dual Element Thermocouple Assemblies with Standard Size Dual TC Connector

(*)XL or SS Series and (*)IN Dual Element

MADE IN USA

Click here for larger image.

$ **57.50** ICIN-116E-12-DUAL

- Two Sensor Readings
- Allows Two Readings of a Single Point
- Continuous Monitor and Control
- Built-in Backup
- Made from Special Limits of Error Material
- Glass Filled Nylon Connector Rated to 220°C (425°F)
- 12" Length Standard
- 1/16, 1/8, 3/16 and 1/4" Diameters Available
- Omegaclad XL , SS or Inconel Sheath
- DTC Type Dual Connector— Mating Connector Included

Thermocouple Alloy	Sheath Dia. mm (in.)	Grounded Junction	Ungrounded Junction	Exposed Junction
J IRON-CONSTANTAN Inconel Sheath	1.5 (1/16") 3.0 (1/8") 4.5 (3/16") 6.0 (1/4")	ICIN-116G-12-DUAL ICIN-18G-12-DUAL ICIN-316G-12-DUAL ICIN-14G-12-DUAL	ICIN-116U-12-DUAL ICIN-18U-12-DUAL ICIN-316U-12-DUAL ICIN-14U-12-DUAL	ICIN-116E-12-DUAL ICIN-18E-12-DUAL ICIN-316E-12-DUAL ICIN-14E-12-DUAL
J IRON-CONSTANTAN 304 SS Sheath	1.5 (1/16") 3.0 (1/8") 4.5 (3/16") 6.0 (1/4")	ICSS-116G-12-DUAL ICSS-18G-12-DUAL ICSS-316G-12-DUAL ICSS-14G-12-DUAL	ICSS-116U-12-DUAL ICSS-18U-12-DUAL ICSS-316U-12-DUAL ICSS-14U-12-DUAL	ICSS-116E-12-DUAL ICSS-18E-12-DUAL ICSS-316E-12-DUAL ICSS-14E-12-DUAL
K CHROMEGA®-ALOMEGA® Inconel Sheath	1.5 (1/16") 3.0 (1/8") 4.5 (3/16") 6.0 (1/4")	CAIN-116G-12-DUAL CAIN-18G-12-DUAL CAIN-316G-12-DUAL CAIN-14G-12-DUAL	CAIN-116U-12-DUAL CAIN-18U-12-DUAL CAIN-316U-12-DUAL CAIN-14U-12-DUAL	CAIN-116E-12-DUAL CAIN-18E-12-DUAL CAIN-316E-12-DUAL CAIN-14E-12-DUAL
K CHROMEGA®-ALOMEGA® 304 SS Sheath	1.5 (1/16") 3.0 (1/8") 4.5 (3/16") 6.0 (1/4")	CASS-116G-12-DUAL CASS-18G-12-DUAL CASS-316G-12-DUAL CASS-14G-12-DUAL	CASS-116U-12-DUAL CASS-18U-12-DUAL CASS-316U-12-DUAL CASS-14U-12-DUAL	CASS-116E-12-DUAL CASS-18E-12-DUAL CASS-316E-12-DUAL CASS-14E-12-DUAL
E CHROMEGA®-CONSTANTAN Inconel Sheath	1.5 (1/16") 3.0 (1/8") 4.5 (3/16") 6.0 (1/4")	CXIN-116G-12-DUAL CXIN-18G-12-DUAL CXIN-316G-12-DUAL CXIN-14G-12-DUAL	CXIN-116U-12-DUAL CXIN-18U-12-DUAL CXIN-316U-12-DUAL CXIN-14U-12-DUAL	CXIN-116E-12-DUAL CXIN-18E-12-DUAL CXIN-316E-12-DUAL CXIN-14E-12-DUAL
E CHROMEGA®-CONSTANTAN 304 SS Sheath	1.5 (1/16") 3.0 (1/8") 4.5 (3/16") 6.0 (1/4")	CXSS-116G-12-DUAL CXSS-18G-12-DUAL CXSS-316G-12-DUAL CXSS-14G-12-DUAL	CXSS-116U-12-DUAL CXSS-18U-12-DUAL CXSS-316U-12-DUAL CXSS-14U-12-DUAL	CXSS-116E-12-DUAL CXSS-18E-12-DUAL CXSS-316E-12-DUAL CXSS-14E-12-DUAL
T COPPER-CONSTANTAN Inconel Sheath	1.5 (1/16") 3.0 (1/8") 4.5 (3/16") 6.0 (1/4")	CPIN-116G-12-DUAL CPIN-18G-12-DUAL CPIN-316G-12-DUAL CPIN-14G-12-DUAL	CPIN-116U-12-DUAL CPIN-18U-12-DUAL CPIN-316U-12-DUAL CPIN-14U-12-DUAL	CPIN-116E-12-DUAL CPIN-18E-12-DUAL CPIN-316E-12-DUAL CPIN-14E-12-DUAL
T COPPER-CONSTANTAN 304 SS Sheath	1.5 (1/16") 3.0 (1/8") 4.5 (3/16") 6.0 (1/4")	CPSS-116G-12-DUAL CPSS-18G-12-DUAL CPSS-316G-12-DUAL CPSS-14G-12-DUAL	CPSS-116U-12-DUAL CPSS-18U-12-DUAL CPSS-316U-12-DUAL CPSS-14U-12-DUAL	CPSS-116E-12-DUAL CPSS-18E-12-DUAL CPSS-316E-12-DUAL CPSS-14E-12-DUAL

263

Appendix O (Continued)

1 Vacuum Pump – Robin Air

Model	Free Air Displacement	Factory Micron Rating	No. of Stages	Intake Fitting	Oil Capacity	Motor Size	Voltage	Approvals	Weight	Dimensions
Domestic Models										
15234	1.2 CFM	50 microns	2	1/4" MFL and 1/2" ACME	5 oz. (148ml)	1/8 hp	115V 50/60 Hz	UL	10 lbs. (4.5kg)	8.5" H x 4.3" W x 9.5" L 215mm x 108mm x 240mm
15400	4 CFM	20 microns	2	1/4" MFL and 1/2" MFL	16 oz. (445ml)	1/3 hp	115V 60 Hz	UL	27 lbs. (12.2 kg)	9.5" H x 5.5" W x 15" L 247mm x 142mm x 381mm
15434	4 CFM	20 microns	2	1/4" MFL and 1/2" ACME	16 oz. (445ml)	1/3 hp	115V 60 Hz	UL	27 lbs. (12.2 kg)	9.5" H x 5.5" W x 15" L 247mm x 142mm x 381mm
15600	6 CFM	20 microns	2	1/4" MFL and 1/2" MFL	16 oz. (445ml)	1/2 hp	115V 60 Hz	UL	27 lbs. (12.2 kg)	9.5" H x 5.5" W x 15" L 247mm x 142mm x 381mm
15120A	10 CFM	20 microns	2	1/4" MFL and 1/2" MFL	17 oz. (500ml)	1/2 hp	115V 60 Hz	UL	38 lbs. (17.2 kg)	10" H x 5.5" W x 16" L 272mm x 142mm x 419mm
International Models										
15226	28 liters/minute	50 microns	2	1/4" MFL and 1/2" ACME	5 oz. (148ml)	1/8 hp	220V 50/60 Hz	CE	10 lbs. (4.5kg)	8.5" H x 4.5" W x 9.5" L 215mm x 108mm x 240mm
15401	93 liters/minute	20 microns	2	1/4" MFL and 1/2" MFL	16 oz. (445ml)	1/3 hp	115V/220-250V 60/60 Hz	CE	27 lbs. (12.2 kg)	9.5" H x 5.5" W x 15" L 247mm x 142mm x 381mm
15424	93 liters/minute	20 microns	2	1/4" MFL and 1/2" ACME	16 oz. (445ml)	1/3 hp	115V/220-250V 50/60 Hz	CE	27 lbs. (12.2 kg)	9.5" H x 5.5" W x 15" L 247mm x 142mm x 381mm
15601	142 liters/minute	20 microns	2	1/4" MFL and 1/2" MFL	16 oz. (445ml)	1/3 hp	115V/220-250V 50/60 Hz	CE	27 lbs. (12.2 kg)	9.5" H x 5.5" W x 15" L 247mm x 142mm x 381mm
15121A	236 liters/minute	20 microns	2	1/4" MFL and 1/2" MFL	17 oz. (500ml)	1/2 hp	115V/220V 50/60 Hz	CE	38 lbs. (17.2 kg)	10" H x 5.5" W x 16" L 272mm x 142mm x 419mm

Appendix O (Continued)

1 FBM1 – IO Tech

DBK15
Universal Current/Voltage Input Card

The DBK15 provides 16 channels
of current or voltage input

Features

- Ideally suited for 4 to 20 mA measurements
- Can measure up to ±30V*
- Provides 16 differential input channels
- Offers user-configurable current or voltage input

* ±10V to 30V input signals can be measured by installing <10K Ohms attenuation resistors on the card. For 1% or greater accuracy, the output impedance of the measured signal should be <100 Ohms. To accurately measure high-voltage signals with >100 Ohms of output impedance, the DBK8 high-voltage input card should be used rather than the DBK15. The DBK8 has very high-input impedance, which is ideal for measuring high-voltage input signals

1 FBM2 – IO Tech

DBK81, DBK82, DBK83, and DBK84
7- & 14-Channel, Low-Noise, High-Accuracy, Thermocouple/mV Expansion Options

Features

- Measures type J, K, S, T, E, B, R, and N thermocouples as well as voltage up to ±100 mV
- Low noise, high accuracy, high stability
- 200-kHz maximum scan rate
- High noise immunity
- Open thermocouple detection per channel
- Over-voltage protection
- Available in four form-factors:
  - 7-channel card with on-board screw terminals (DBK81)
  - 14-channel card with on-board screw terminals (DBK82)
  - 14-channel card with external signal connection "pod" (DBK83)
  - 14-channel module, housed in a metal package with mini TC connections (DBK84)

DBK81: 7-channel card with on-board screw terminals

DBK82: 14-channel card with on-board screw terminals

DBK83: 14-channel card with external signal connection pod

DBK84: 14-channel module, housed in a metal package with mini TC connections

265

Appendix P. Error analysis

Experimental data are directly measured and entail specific errors provided by the manufacture of the measuring devices. In addition, physical properties determined by empirical relations also entail certain errors given by the developers of those correlations. Pseudo–experimental data are generated using the experimental data and the empirically determined physical properties; consequently, they entail indirect errors that are propagations of the direct errors of the experimental data and the physical properties.

The errors associated with the previously mentioned devices and correlations are given in Table 12 while formulas to calculate the propagation of error as functions of directly measured errors are given in Table 13. The rules of Table 13 can be multiplexed to represent the error of other variations as will be seen shortly.

Table 12. Device and correlation errors

	Correlation		Device			
	ρ (g/cm^3)	H (J/g)	TE $(°C)$	PE (bar)	FI (LPM)	QE (cm^3)
Error	$\pm 35 \cdot 10^{-6}$	± 0.045	± 1.000	± 0.005	± 0.045	± 0.200

Table 13. Propagation of error rules

Relationship	Compounded Error
$Z = X + Y$	$\varepsilon_Z^2 = \varepsilon_X^2 + \varepsilon_Y^2$
$Z = X - Y$	$\varepsilon_Z^2 = \varepsilon_X^2 + \varepsilon_Y^2$
$Z = X \cdot Y$	$(\varepsilon_Z/Z)^2 = (\varepsilon_X/X)^2 + (\varepsilon_Y/Y)^2$
$Z = X/Y$	$(\varepsilon_Z/Z)^2 = (\varepsilon_X/X)^2 + (\varepsilon_Y/Y)^2$
$Z = X^n$	$(\varepsilon_Z/Z) = n \cdot (\varepsilon_X/X)$
$Z = ln(X)$	$\varepsilon_Z = (\varepsilon_X/X)$
$Z = exp(X)$	$(\varepsilon_Z/Z) = \varepsilon_X$

Many elements contribute to error in measurements; however, the average error values given above in Table 12 are considered inclusive of all errors since experiments were conducted at matching laboratory conditions and because a true measurement can never be claimed. The dynamic errors of the time–varying system variables that were graphically presented in CHAPTER 7 as error bands were computed using the values of Table 12 and the rules of Table 13 to generate the following perturbations

$$\varepsilon_{FI} = \pm 0.045 \tag{144}$$

$$\varepsilon_{QE} = \pm 0.2 \tag{145}$$

$$\varepsilon_{P_V} = \varepsilon_{PE} = \pm 0.005 \tag{146}$$

$$\varepsilon_{T_E} = \varepsilon_{T_W} = \varepsilon_{T_X} = \varepsilon_{TE} = \pm 1 \tag{147}$$

$$\varepsilon_{\rho_P} = \varepsilon_{\rho_H} = \varepsilon_{\rho_C} = \varepsilon_{\rho_E} = \varepsilon_\rho = \pm 35 \cdot 10^{-6} \tag{148}$$

$$\varepsilon_{H_P} = \varepsilon_{H_X} = \varepsilon_{H_H} = \varepsilon_{H_E} = \varepsilon_H = \pm 0.045 \tag{149}$$

$$\varepsilon_{AT} = \pm\sqrt{2} \cdot \varepsilon_{TE} \tag{150}$$

$$\varepsilon_{AH} = \pm\sqrt{2} \cdot \varepsilon_H \tag{151}$$

$$\varepsilon_{M_P} = \pm\left[M_P{}^2 \cdot \left(\left[\frac{\varepsilon_{\rho_P}}{\rho_P}\right]^2 + \left[\frac{\varepsilon_{FI}}{FI}\right]^2 \right) \right]^{\frac{1}{2}} \tag{152}$$

$$\varepsilon_{M_H} = \pm\left[M_H{}^2 \cdot \left(\left[\frac{\varepsilon_{\rho_H}}{\rho_H}\right]^2 + \left[\frac{\varepsilon_{FI}}{FI}\right]^2 \right) \right]^{\frac{1}{2}} \tag{153}$$

$$\varepsilon_{M_E} = \varepsilon_{M_C} = \pm\left[M_C{}^2 \cdot \left(\left[\frac{\varepsilon_{\rho_C}}{\rho_C}\right]^2 + \left[\frac{\varepsilon_{FI}}{FI}\right]^2 \right) \right]^{\frac{1}{2}} \tag{154}$$

$$\varepsilon_{\int M_C} = \pm \left[\left(\int M_C \right)^2 \cdot \left(\left[\frac{\varepsilon_{\rho_C}}{\rho_C} \right]^2 + \left[\frac{\varepsilon_{QE}}{QE} \right]^2 \right) \right]^{\frac{1}{2}} \qquad (155)$$

$$\varepsilon_{\int Q_H} = \varepsilon_{Q_H} = \pm \left[Q_H^2 \cdot \left(\left[\frac{\varepsilon_{M_P}}{M_P} \right]^2 + \left[\frac{\varepsilon_{\Delta H}}{H_H - H_X} \right]^2 \right) \right]^{\frac{1}{2}} \qquad (156)$$

$$\varepsilon_{A_{SC}} = \pm \left[A_{SC}^2 \cdot \left(\left[\frac{\varepsilon_{Q_H}}{Q_H} \right]^2 + \left[\frac{U_{SC} \cdot \varepsilon_{T_X}}{\tau_{SC} \cdot \alpha_{SC} \cdot I - U_{SC} \cdot (T_X - T)} \right]^2 \right) \right]^{\frac{1}{2}} \qquad (157)$$

$$\varepsilon_{PEC} = \pm \left[PEC^2 \cdot \left(\left[\frac{\varepsilon_{\int Q_H}}{\int Q_H} \right]^2 + \left[\frac{\varepsilon_{\int M_C}}{\int M_C} \right]^2 \right) \right]^{\frac{1}{2}} \qquad (158)$$

$$\varepsilon_{\eta_C} = \pm 100 \cdot \left[\left(\frac{\eta_C}{100} \right)^2 \cdot \left(\left[\frac{\varepsilon_{\Delta T}}{T_X - T_P} \right]^2 + \left[\frac{\varepsilon_{\Delta T}}{T_E - T_C} \right]^2 \right) \right]^{\frac{1}{2}} \qquad (159)$$

$$\varepsilon_{\eta_R} = \pm 100 \cdot \left[\left(\frac{\eta_R}{100} \right)^2 \cdot \left(\left[\frac{\varepsilon_{\Delta H}}{H_X - H_P} \right]^2 + \left[\frac{\varepsilon_{\Delta H}}{H_H - H_P} \right]^2 \right) \right]^{\frac{1}{2}} \qquad (160)$$

$$\varepsilon_{\eta_T} = \pm 100 \cdot \left[\left(\frac{\eta_R}{100} \right)^2 \cdot \left(\left[\frac{\varepsilon_{M_E}}{M_E} \right]^2 + \left[\frac{\varepsilon_{H_E}}{H_E} \right]^2 + \left[\frac{\varepsilon_{M_H}}{M_H} \right]^2 + \left[\frac{\varepsilon_{H_H}}{H_H} \right]^2 \right) \right]^{\frac{1}{2}} \qquad (161)$$

The above perturbations were included in the data mining code presented earlier to generate static error values for the primary variables and dynamic error values for the derived variables. The error values were then linked to their prospective variables to generate a translucent patch of error bars, or error bands, around their profiles as was presented earlier in CHAPTER 7.

ABOUT THE AUTHOR

Mohammad Abutayeh is originally from Kafr Sur, Palestine: a small West Bank village approximately thirty miles north of Jerusalem. He came to America in search of a better life almost twenty years ago and has been calling it home since.

He received a Bachelor of Science in Chemical Engineering from the University of South Florida in 1997 with Cum Laude distinction. He continued on obtaining his Master of Science in Chemical Engineering from the University of South Florida in 1999 where he wrote a thesis on predicting the citrate soluble–loss of the dihydrate process.

He then worked in several engineering areas designing process control systems, optimizing unit operations, customizing process equipment, administering US patent laws, and many other functions. In addition, he successfully completed the Fundamentals of Engineering examination of the Florida Board of Professional Engineers, attended numerous seminars, and acquired several other certifications.

He published several journal articles and presented his thesis and dissertation research findings at national and international venues. He graduated with a Doctor of Philosophy in Chemical Engineering from the University of South Florida in 2010 where he wrote a dissertation on simulating the passive vacuum solar flash desalination.